COMPENDUM OF FLIGHT VEHICLE BASE PRESSURE AND BASE DRAG PREDICTION TECHNIQUES

FINAL REPORT

August 1983

Contract NAS8–34976

NATIONAL AERONAUTICS AND SPACE ADMINISTRATION MARSHALL SPACE FLIGHT CENTER, AL 35812
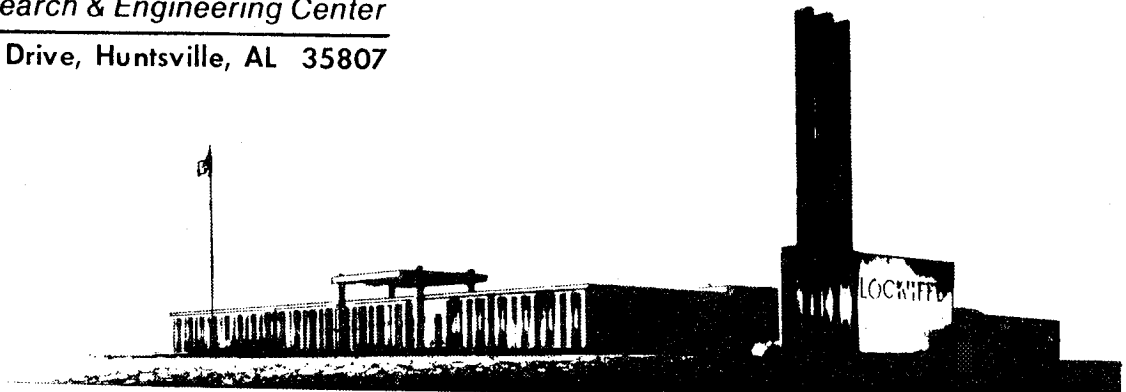
by Wayne W. Boyle and James P. Pace

≡⚡*Lockheed*
Missiles & Space Company, Inc.
Huntsville Research & Engineering Center

4800 Bradford Drive, Huntsville, AL 35807

FOREWORD

This report documents the results of a literature survey to assemble a compendium of launch vehicle flight measured base pressure data and analyses techniques to correlate the data and develop math model and base drag prediction techniques. This study was performed by personnel of the Systems Analysis & Simulation Section of the Lockheed-Huntsville Research & Engineering Center for the NASA-George C. Marshall Space Flight Center under Contract NAS8-34976. The technical monitor for the contract was Mr. Charlie C. Dill, Jr.

LOCKHEED-HUNTSVILLE RESEARCH & ENGINEERING CENTER

SUMMARY

This report documents the results of a literature survey to assemble a compendium of launch vehicle flight measured base pressure data and base drag prediction techniques. The flight base pressure data have been assembled into tables that include trajectory data, thrust characteristics and the flight measured base pressure data. Data are presented for single engine vehicles that include the Redstone, Jupiter, and Thor, multi-engine vehicles including the Atlas and Saturn series, and multi-body vehicles including the Thor Delta, Titan 3C and Space Shuttle. A survey of base pressure and base drag prediction techniques was also conducted from which significant, easily evaluated, variables were identified and used to correlate the base pressure data into a math model. Methods for predicting the base drag using the math model of base pressure and effective base area are also developed.

LOCKHEED-HUNTSVILLE RESEARCH & ENGINEERING CENTER

CONTENTS

LIST OF ILLUSTRATIONS

LOCKHEED-HUNTSVILLE RESEARCH & ENGINEERING CENTER

ILLUSTRATIONS (Concluded)

LIST OF TABLES

LOCKHEED-HUNTSVILLE RESEARCH & ENGINEERING CENTER

NOMENCLATURE

Symbol	Definition
A_{Base}	base area
A_{Nozzle}	nozzle exit plane area
C_D	base drag coefficient
C_{P_B}	base pressure coefficient $(P_B - P_\infty)/q_\infty$
C_T	thrust coefficient
D_B	base diameter
D_N	nozzle exit diameter
$\dot{m}$	mass flow
M_E	nozzle exit Mach number
M_j	jet plume boundary Mach number
M_∞	freestream Mach number
P_∞	freestream static pressure
P_B	base pressure
$P_{B_{Cyl}}$	base pressure for cylindrical forebody
$P_{B_{Non-Cyl}}$	base pressure for non-cylindrical forebody
P_c	jet chamber pressure
P_j, P_E	jet exit pressure
q_∞	freestream dynamic pressure
R_M	momentum flux ratio
S_{REF}	reference area
T_o	total temperature
V	flow velocity

NOMENCLATURE (Cont'd)

Symbol	Definition
X_j	axial position of nozzle exit plane with respect to base
ϵ	nozzle expansion ratio
j	jet initial expansion angle
γ	ratio of specific heats
L	nozzle internal wall angle at exit plane

Subscripts

E	nozzle exit
j	jet exit
∞	freestream

DATA PLOT NOMENCLATURE

Single Nozzle Vehicles

R	Redstone
J	Jupiter
T	THOR
N_{A1} = A1 config.	NACA Vehicles
SR_1 = STS-1	Space Shuttle SRB

Multiple Nozzle Vehicles

A	ATLAS
S1 = SA1	Saturn 1, Block 1
S5 = SA5	Saturn 1, Block 2

LOCKHEED-HUNTSVILLE RESEARCH & ENGINEERING CENTER

NOMENCLATURE (Cont'd)

Symbol	Definition

SB_1 = SA-201   Saturn 1B

V_1 = SA-501   Saturn V

O_1 = STS-1   Space Shuttle Orbiter

Multiple Body Vehicles

TD   THOR DELTA

E_1 = STS-1   Space Shuttle External Tank

3C   TITAN IIIC

1. INTRODUCTION

The application of flight measured power-on base pressure from one vehicle to another vehicle is questionable because of vehicle/engine configuration differences. The application is not straightforward in many cases because of the lack of documentation of all the variations in the affecting parameters from flight to flight and vehicle to vehicle. However, a useful tool - based on flight experience - can be developed to provide a quick reliable source of preliminary design data. Compiling a compendium of flight measured base pressure environments from all applicable launch vehicles into one source with substantiated application techniques for other vehicles would provide the engineering community, in general, a useful tool for estimating future launch vehicle base pressure/drag in the early definition/optimization phases. Data generally available for use in the early definition phase would include the configuration geometry, engine thrust characteristics and preliminary trajectory data. These data will generally be sufficient to develop preliminary power-on drag characteristics using this report. The purpose of this report is to provide such a handbook.

Flight measured power-on base pressure from a variety of launch vehicles during ascent flight has been collected and evaluated for correlation of the data. Flight data for the following vehicles was used in the analysis:

Single Nozzle Vehicles	Multiple Nozzle Vehicles	Multiple Body Vehicles
Redstone	Atlas	Thor Delta
Jupiter	Saturn 1, Block 1	Titan IIIC
Thor	Saturn 1, Block 2	Space Shuttle
NACA Vehicles	Saturn 1B	
	Saturn V	

The flight measured base pressure data have been correlated and developed into a math model for use in predicting the base pressure and base drag characteristics of any flight vehicle.

LOCKHEED-HUNTSVILLE RESEARCH & ENGINEERING CENTER

2. DATA BASE DEVELOPMENT

A literature survey was conducted to develop the ascent flight measured base pressure data base. An effort was made to include only unclassified data to enable a broader distribution of the results. Flight base pressure data was obtained on the following generic types of vehicles -- single engine, multi-engine, and multi-body configurations. A description of each vehicle including the vehicle configuration, engine characteristics, base configurations, trajectory data, base pressure data, and references is contained in the Appendix.

Summary flight characteristics of the complete vehicle data base are presented in Figs. 2-1 and 2-2. These figures show the ascent altitude and dynamic pressure versus Mach number, respectively. Figure 2-1 shows that the flight altitude corridor to Mach 2.0 is on the order of 10,000 to 15,000 ft. At the higher Mach numbers the flight altitude corridor increases significantly to approximately 40,000 ft. Thus, at the lower Mach numbers all the vehicles have a narrow flight corridor. The flight dynamic pressure, however, varies considerably in this corridor as shown in Fig. 2-2. The maximum flight dynamic pressure varies from 500 psf for early Shuttle flights to over 1300 psf for the Thor Delta vehicle. Thus, the small flight corridor has sufficient variation in altitude to significantly influence the flight dynamic pressure environment and thus complicate the data correlation.

The development of the aerodynamic characteristics of a vehicle involves two types of tests or analyses as shown in Fig. 2-3. The total drag coefficient is comprised of forebody and base characteristics.
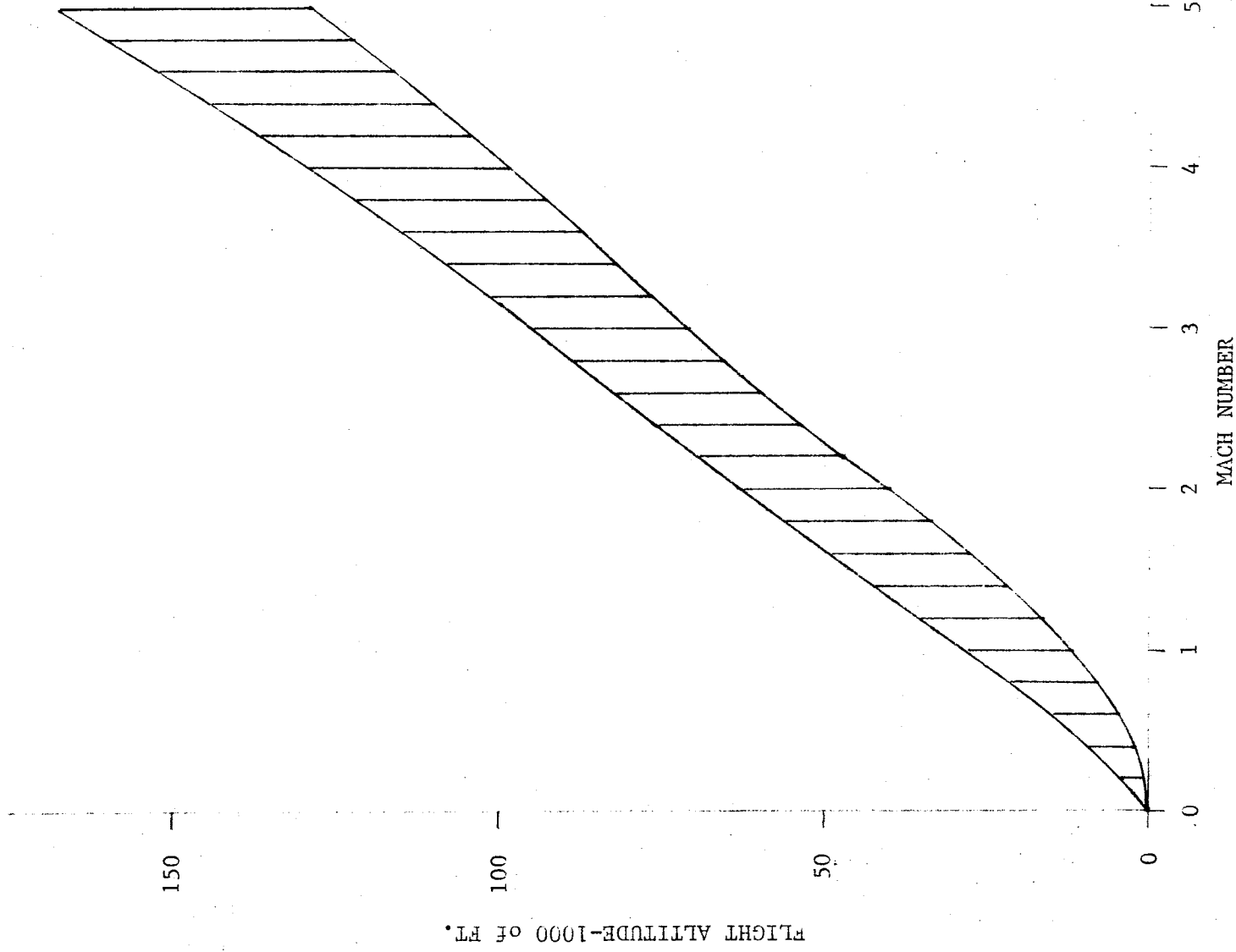
Fig. 2-1 – Summary Altitude versus Mach Number

2-2
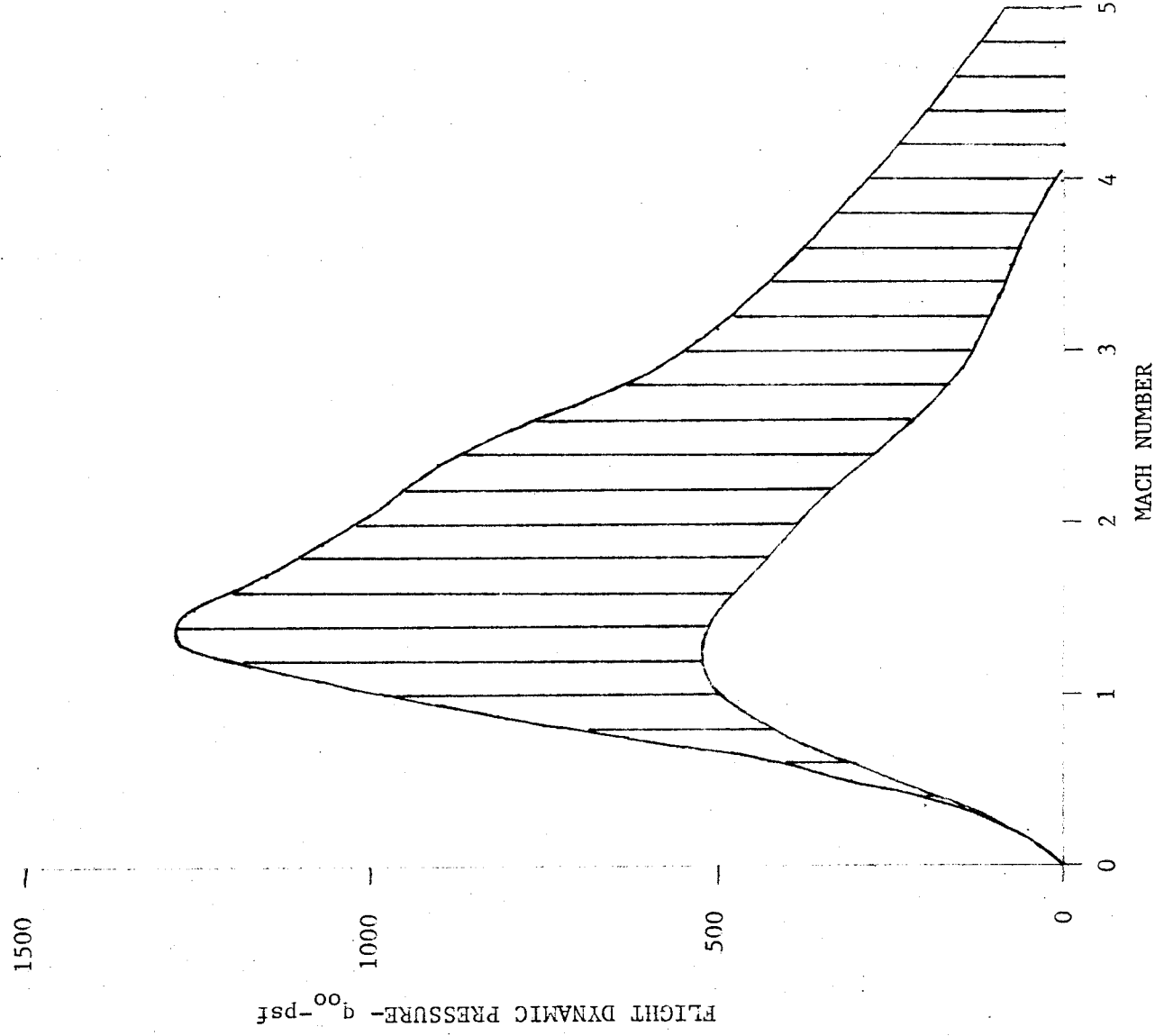
Fig. 2-2 - Summary Dynamic Pressure versus Mach Number

LOCKHEED-HUNTSVILLE RESEARCH & ENGINEERING CENTER
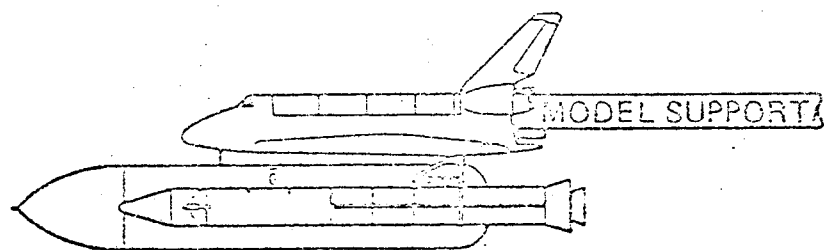
Ⓐ FOREBODY DRAG
·WIND TUNNEL TEST
·ANALYSIS

MODEL SUPPORT
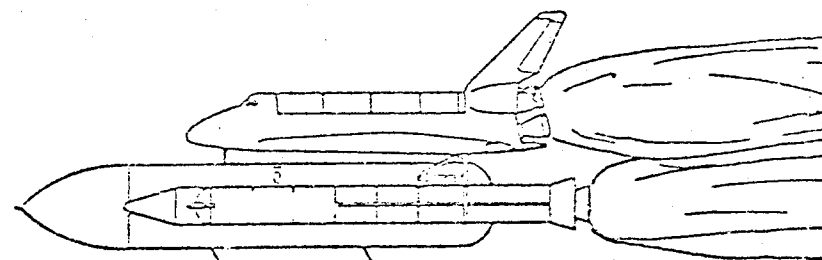
Ⓑ BASE DRAG
·COLD FLOW TEST
·HOT FLOW TEST
·ANALYSIS

IN GENERAL,

$$C_{D_{TOTAL}} = \left(C_{D_{FP-OFF}} + C_{D_{BASE}}_{P-ON} \right)$$

Ⓐ $C_{D_{FP-OFF}} = \left(C_{D_{TOTAL}} - C_{D_{BASE}} \right)_{P-OFF}$

$C_{D_{BASE}}_{P-OFF} = \frac{1}{q_{oo} S_{ref}} \int (P_B - P_\infty) \, d(A_B)$

$C_{D_{B_{P-ON}}} = \frac{1}{q_{oo} S_{ref}} \int_{P-ON} (P_B - P_\infty) \, d(A_B)$

Ⓑ

FIG. 2-3 Aerodynamic Coefficient Formulation.

This formulation generally permits the determination of the most significant aerodynamic characteristics, the power-off forebody data, from one test or analysis (A in Fig. 2-3) and the plume effects from an independent test or analysis (B in Fig. 2-3). Plume-off base environments on wind tunnel models can be removed from the total measured data results to create power-off forebody data. These base environments are irrelevant to the data base because of model support system interference and the changes created by the exhaust plumes. The base characteristics are determined generally from a plume test or analysis techniques. The addition of the estimated/measured power-off base pressures (Fig. 2-3B) adequately includes the effects of the plumes on the base pressure environment. This report addresses the methods for prediction of the base or B term in Figure 2-3 utilizing the analysis of flight measured base pressure data.

The base aerodynamic characteristics are generally required in two forms. Base aerodynamic coefficients are generally required for loads analysis. Base aerodynamic forces versus altitude are generally required for vehicle performance evaluation. In the flight regime of maximum dynamic pressure (M < 2.0, altitude < 70,000 ft) the base drag characteristics are a function of Mach number, dynamic pressure, and to a lesser extent on altitude. This is generally due to the smaller variation in launch vehicle ascent corridors (see Fig. 2-1) at lower altitudes. At higher Mach numbers and altitudes the base drag characteristics are a stronger function of altitude than Mach number. Thus the base aerodynamic characteristics are usually developed in terms of both base drag coefficients versus Mach number and base drag forces versus altitude.

The relationship between base pressure coefficient and base drag coefficient is the following:

$$C_D = - 1/S_{Ref} \int C_{p_B} \, dA \qquad (2.1)$$

This equation must be used if the base pressure varies over the base of the vehicle. This generally occurs for multi-nozzle vehicles.

The base pressure coefficient is defined by the following:

$$C_{p_B} = \frac{P_B - P_\infty}{q_\infty} = \frac{P_B - P_\infty}{\frac{\gamma}{2} P_\infty M^2} = \frac{P_B/P_\infty - 1}{\frac{\gamma}{2} M^2} \qquad (2.2)$$

Thus a base pressure that is lower than ambient produces a negative base pressure coefficient and a positive drag force. A base pressure environment that is higher than the local ambient pressure will produce a positive base pressure coefficient and a negative drag in thrust terms. A positive base pressure coefficient creates a negative drag or an effective thrust. These relationships are shown in Fig. 2-4

If the base pressure or base pressure coefficient is relatively constant over the base then the base drag coefficient has a simpler form:

$$C_{D_{Base}} = - C_{p_{Base}} A_{Base}/S_{Ref} \qquad (2.3)$$

The base area is not the geometric base area but an effective base area. The effective base area is the total base area minus the engine exit area. Thus for base drag considerations the base area is the following:

$$A_{Base} = A_{Base} - A_{Nozzles} \qquad (2.4)$$

This is described by referring to Fig. 2-5.

The base pressure acting on the nozzles is generally the same as the base pressure acting on the base of the vehicle. Thus the integral of the base pressure over the portion of the nozzle forward of the nozzle exit plane is equal and opposite to the base pressure acting over the base directly under the nozzle, thus these two components cancel. The nozzle exit area itself is not considered in the aerodynamic description of the vehicle, but is included in the thrust term.

P_B/P_{oo}

1.0

POWER ON TREND

0

MACH NUMBER ──────▷

C_{PB}

+.1

POWER ON TREND

0

-.1

MACH NUMBER ──────▷

q_{oo}

MACH NUMBER ──────▷

BASE DRAG

+

0

-

+BASE DRAG

-BASE DRAG (EFFECTIVE THRUST)

MACH NUMBER ──────▷
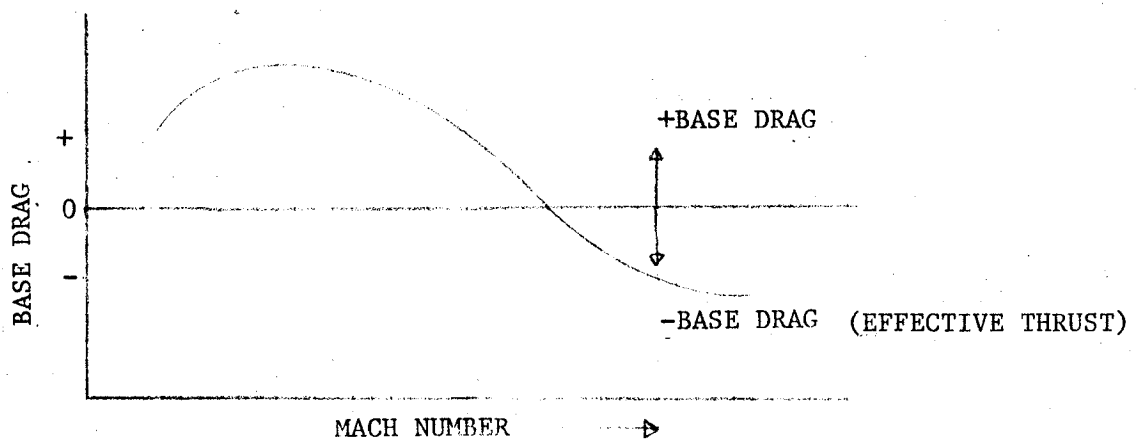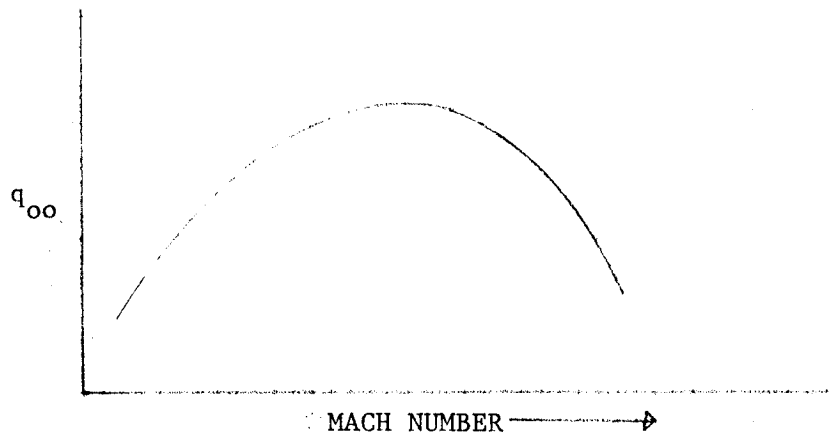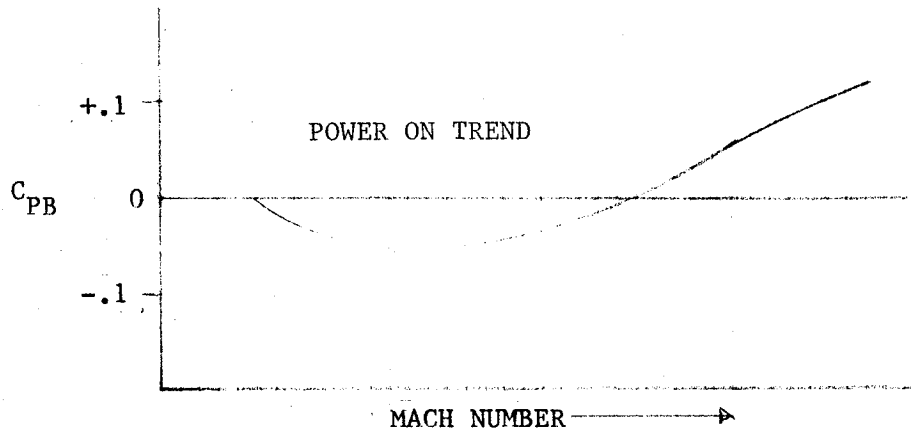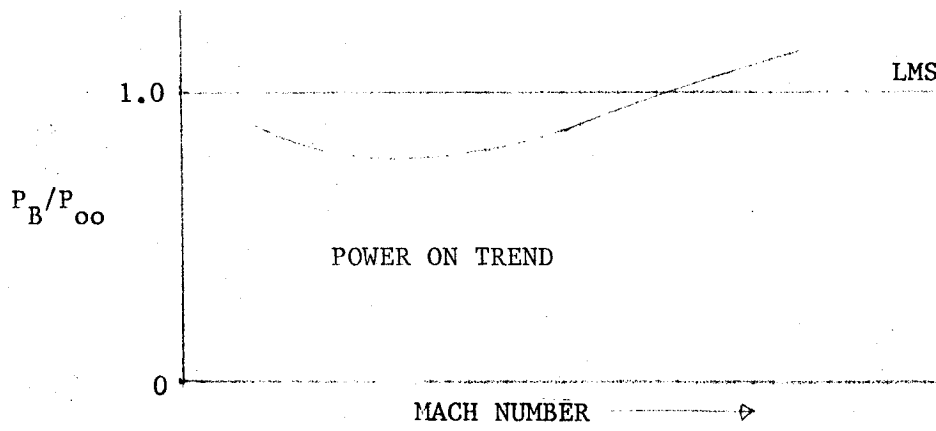
FIGURE 2-4 BASE PRESSURE RATIO AND BASE DRAG RELATIONSHIP

2-7

$$A_{effective} = A_{base} - A_{all\ nozzles}$$
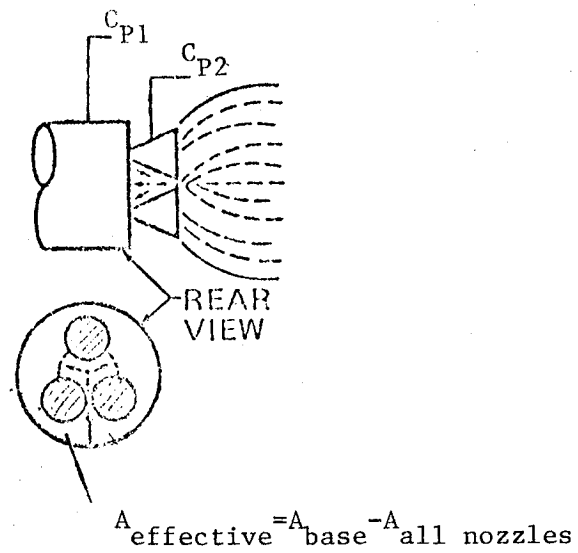
Fig. 2-5 – Effective Base Area for Drag Calculation

LOCKHEED-HUNTSVILLE RESEARCH & ENGINEERING CENTER

The engine operating conditions have an influence on the base pressure coefficient and consequently on the base drag as shown in Fig. 2-6. At moderate power levels and generally low altitudes, the engine exhaust plume aspirates the base of the vehicle. Initially the plume is small and the high velocity gases of the viscous layer of the jet entrain the local surrounding air and thus reduce the local pressure in the base. As the power levels increase the base pressure and base pressure coefficient reaches a lower limit where the mass flow being aspirated is supplemented with additional mass flow into the base. At this point the plume is beginning to act as blockage to the flow. At higher power levels the mass flow recirculation into the base can increase the base pressure to a level higher than ambient resulting in positive base pressure coefficients and negative drag or base thrust.

A summary plot of the flight extracted base pressure coefficient versus Mach number for several flight vehicles is presented in Fig. 2-7. Note in this figure that there is a large variation in the flight base pressure coefficient with Mach number and with vehicle configuration. At certain Mach numbers some vehicles would experience base drag ($-Cp_B$) and some vehicles would experience a base thrust ($+Cp_B$).

The objective of this study is to correlate the flight base pressure data in such a manner that prediction of the base pressure environment of a new vehicle configuration can be made with confidence. The prediction of base pressure environments should also be of such a nature that complex gas-dynamic equations and analysis techniques will not be needed.

A survey of base pressure prediction techniques has identified several important variables that significantly influence the base pressure environment. These variables are thrust coefficient (C_T), base configuration (boattail-flare), base thrust loading (T/A_B), plume size to base area, nozzle position to the base, and fins. The following section discusses each of these variables and the methods used to correlate the influence of each variable on the base pressure environment.
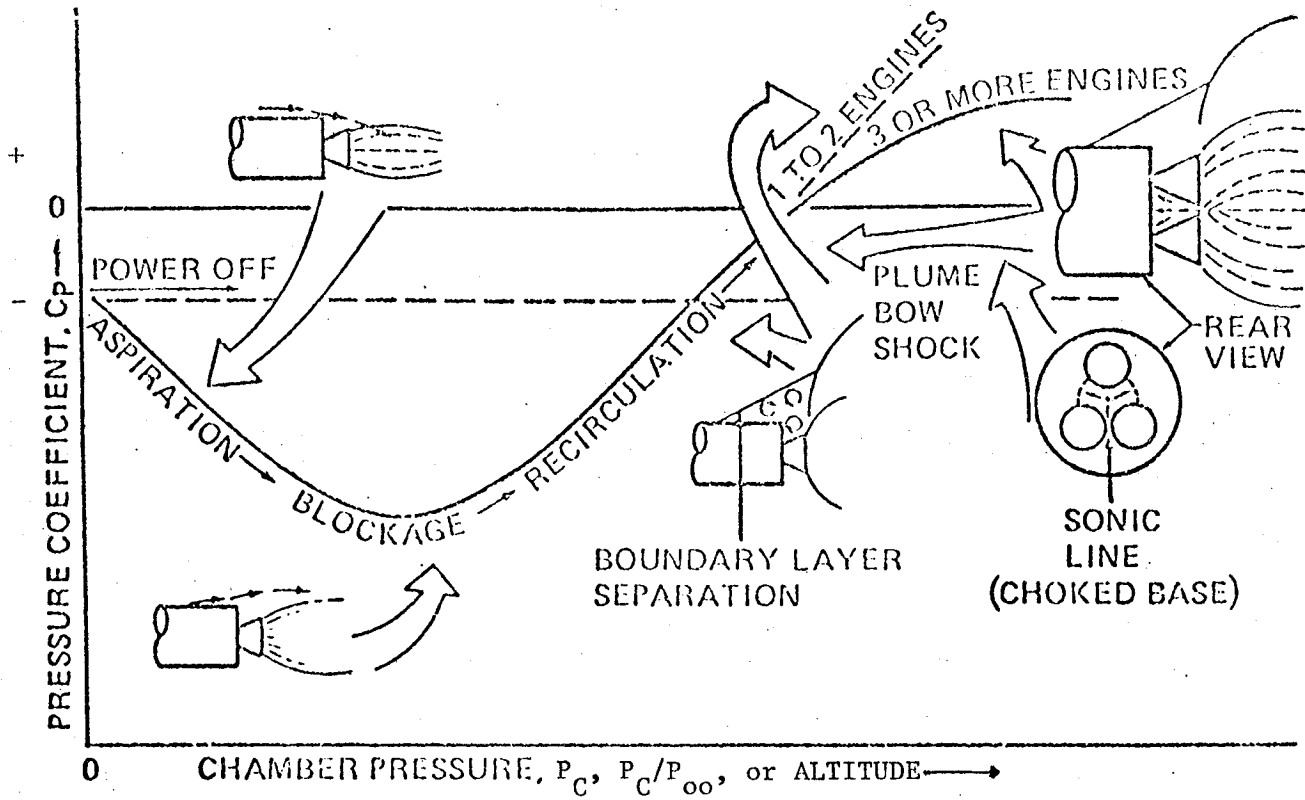
Fig. 2-6 – Base Flow-Exhaust Plume Phenomena

LOCKHEED-HUNTSVILLE RESEARCH & ENGINEERING CENTER
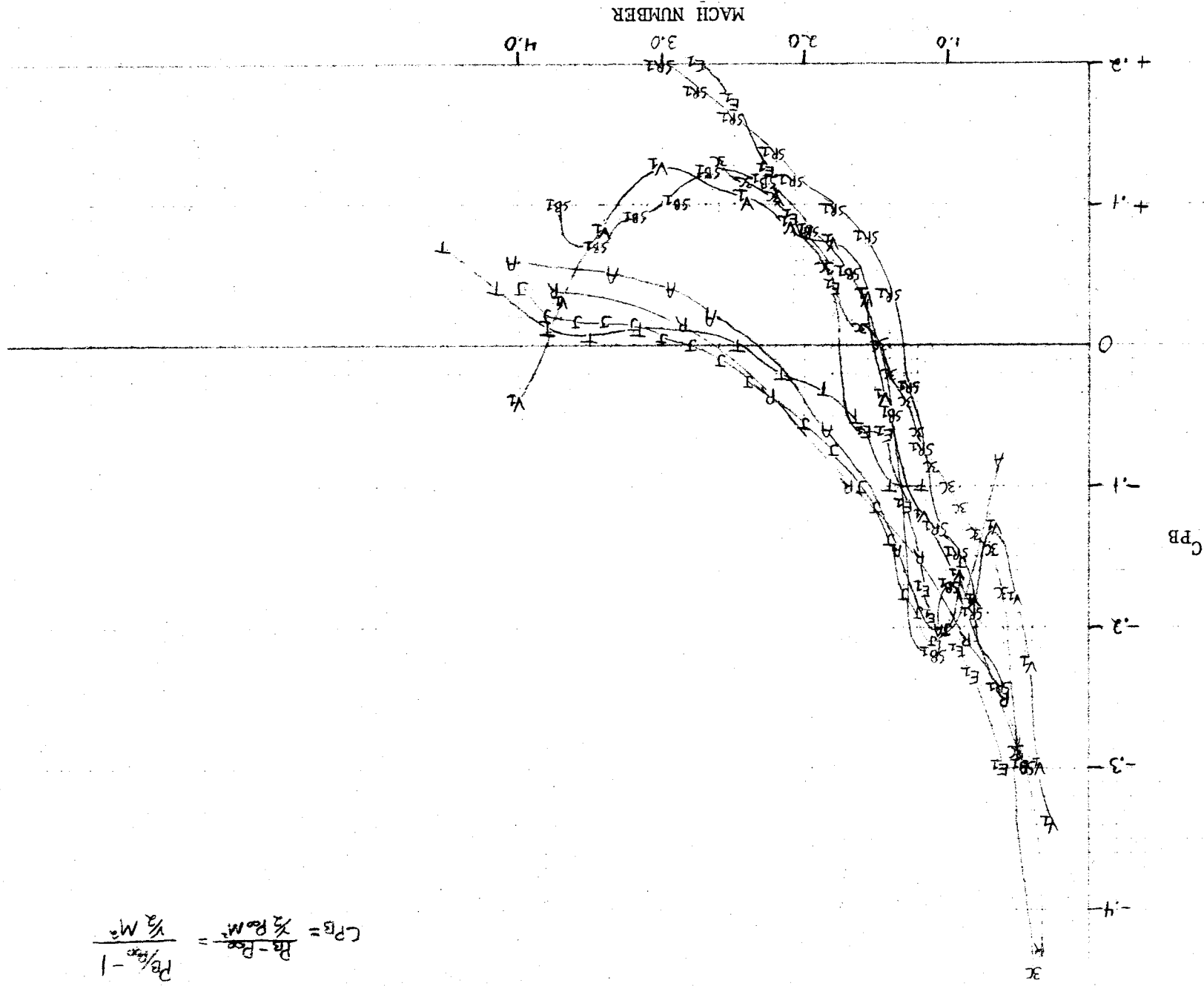
FIGURE 2-7 SUMMARY FLIGHT BASE PRESSURE COEFFICIENT VERSUS MACH NUMBER

$$CP_B = \frac{P_B - P_\infty}{\frac{1}{2}\rho_\infty M_\infty^2} = \frac{P_B/P_\infty - 1}{\frac{1}{2}\gamma M^2}$$

2.1 CORRELATION OF BASE PRESSURE DATA WITH AFFECTING PARAMETERS

A literature survey was conducted to assemble and evaluate various base pressure prediction techniques and identify significant variables that influence the base pressure environment. The significant variables were then screened to include only those that would be available in the preliminary design environment. These significant variables were then used to develop correlation techniques for the flight data base. A discussion of these variables and their influence on the base pressure environment is presented below.

Two variables that significantly influence the base pressure environment are the thrust and the base area. The influence of both of these variables on the base pressure ratio is shown in Fig. 2-8a. The figure shows that increasing the thrust increases the base pressure raio for configurations that have a recirculation base flow environment. It is noted that for a recirculation base flow environment, that increasing the base area decreases the base pressure ratio, while for an aspiration base flow environment, it increases the base pressure ratio. The two variables, thrust and base area, can be combined into a single variable, thrust coefficient (CT), to correlate the base pressure ratio for similar nozzle configurations. The thrust coefficient correlation is presented below.

Thrust Coefficient Correlation

The thrust coefficient correlation of base pressure was developed by Messrs. Brazzel and Henderson in the 1966 - 1967 time period (Refs. 1 and 2). The original correlation used the momentum flux ratio defined as

$$R_{m_f} = \frac{(mV)_j}{(mV)_\infty} = \frac{V_j P_j A_j M_j^2}{V_\infty P_\infty A_B M_\infty^2} \tag{2.5}$$

LOCKHEED-HUNTSVILLE RESEARCH & ENGINEERING CENTER

defining the jet thrust as

$$\text{Thrust} = (mV)_j + A_j (P_j - P_\infty) \tag{2.6}$$

The thrust coefficient is

$$C_T = \frac{\text{Thrust}}{q_\infty A_B} = 2 \times R_{m_f} \tag{2.7}$$

The thrust coefficient was found to correlate base pressure for jet
conditions above the minimum base pressure level. Referring to Fig. 2-6,
the thrust coefficient correlates data for the recirculation portion of the
curve only. The thrust coefficient inherently also correlates the influence
of nozzle to base area since this ratio is in the thrust coeffcient (see Eq.
2-5). A correlation of cold flow wind tunnel data using the thrust coeffi-
cient (Ref. 1) is shown in Fig. 2-8. Figure 2-8a presents the results of
experiments by Reid and Hastings (Ref. 3) showing the effects of nozzle size
on base pressure ratio for various values of jet pressure ratio. The figure
shows that the base pressure ratio is significantly influenced by the size
of the nozzle. The recirculation portion of the curves is shown in Figure
2-8b to correlate with the jet momentum ratio and/or thrust coefficient.
The thrust coefficient correlation presented in Fig. 2-8 is for geometri-
cally similar nozzles. Thus, the thrust coefficient correlates the thrust
level and nozzle to base area. This correlation is for geometrically simi-
lar nozzles that use air as a jet simulant gas. The aspiration portion of
the curve cannot be correlated with thrust coefficient.

Different nozzle configurations have an influence on the base pressure
that cannot be correlated with the thrust coefficient. The influence of
nozzle configuration is shown in Fig. 2-9. Figure 2-9 presents the correla-
tion of base pressure ratio with thrust coefficient for three different
nozzle configurations. The three nozzles have different area ratios which
develop different nozzle exit Mach numbers. The nozzle area

2-13
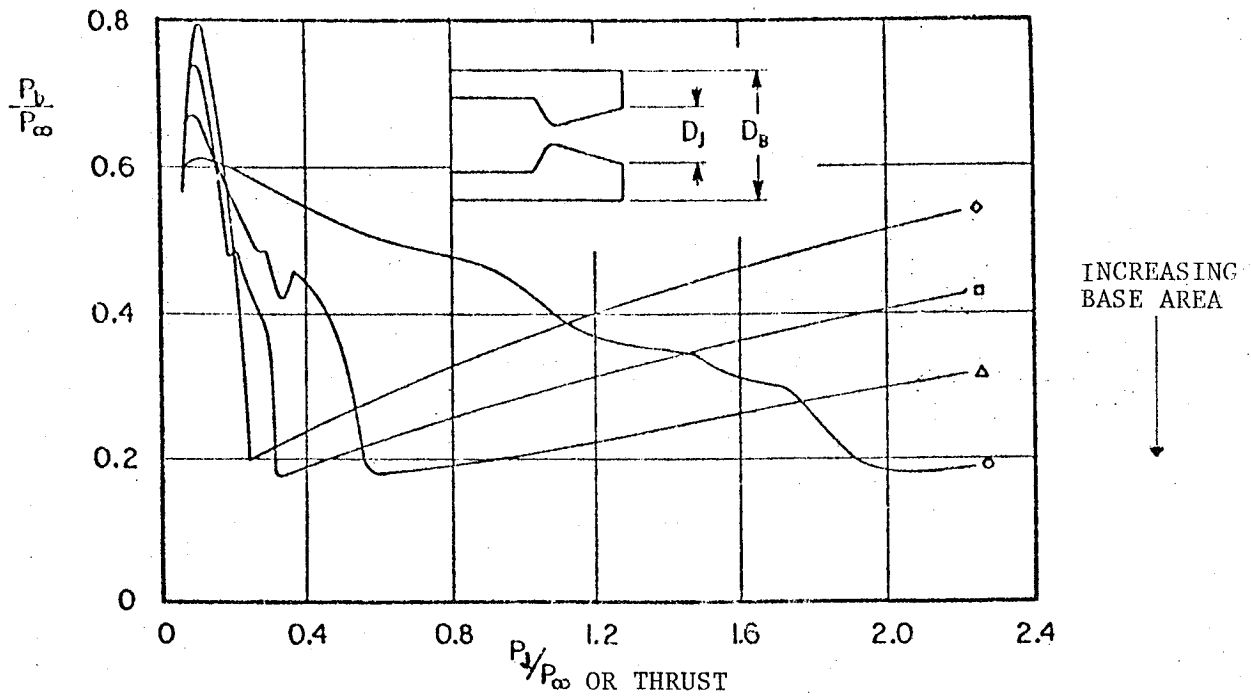
(a)   Base Pressure Variation with Jet Pressure Ratio
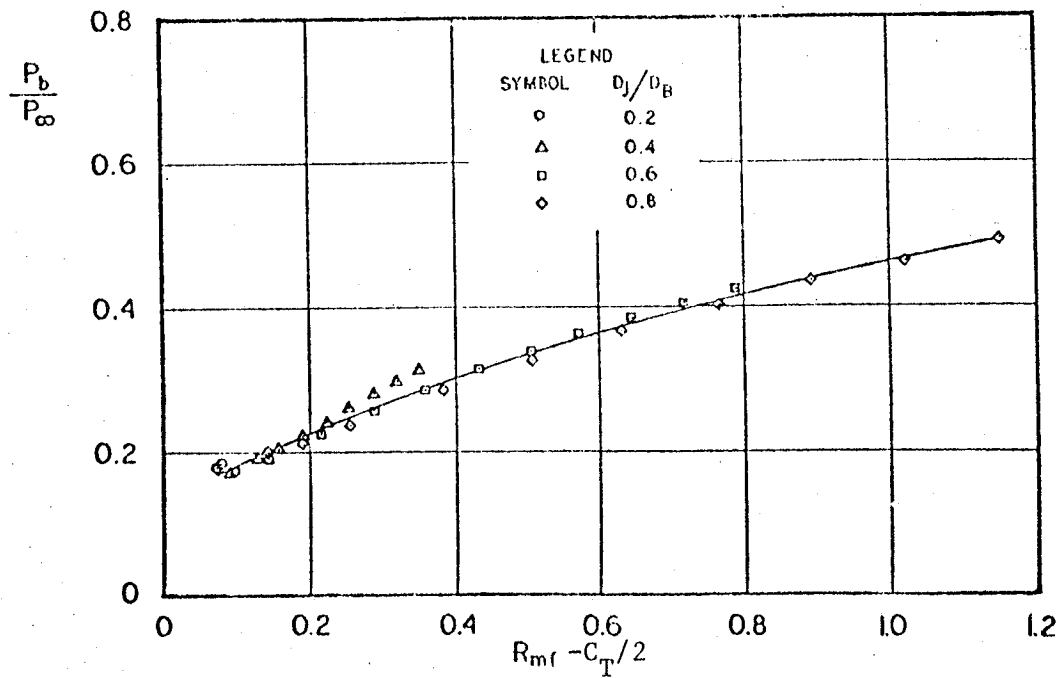
(b) Base pressure variation with jet momentum flux ratio

Fig. 2-8 – Effect of Nozzle Exit Diameter on Base Pressure
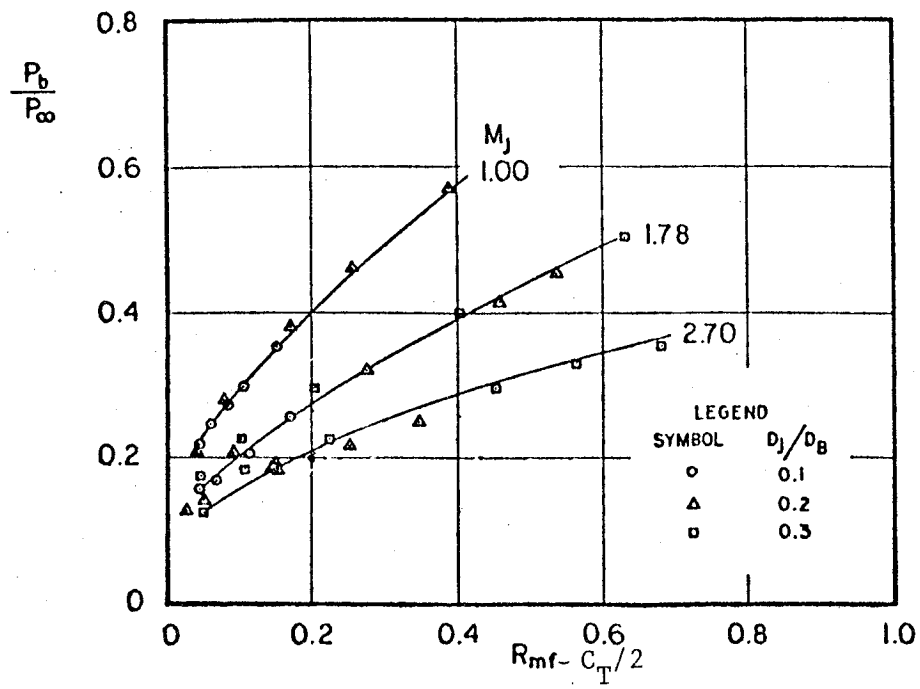
Fig. 2-9 - Effect of Nozzle Configuration on Base Pressure Correlation

ratios for the flight data base are presented in the appendix for each vehicle configuration. The nozzle area ratios for the flight vehicles range from 3.61 for the Redstone to 77.5 for the Space Shuttle SSME.

The influence of nozzle exit Mach number on the flight data could not be determined because of the difficulty of determining the exit Mach number for the flight vehicle nozzles. Experimental studies and data correlations (Ref. 4) for a vehicle configuration with a single nozzle have shown that the base pressure ratio is a stronger function of the plume expansion angle, δ_j, than the exit Mach number. Estimates of the values of the plume expansion angle for the various flight vehicles are presented in Figure 2-10. The figure shows that the plume angle for a large portion of the flight vehicles is within a band of approximately 20 degrees. Exceptions to this band are the large plume angles for several of the NACA test vehicles.

A compilation of data from several references (Refs. 3, 5 and 6) has been formulated into a math model to predict the change in base pressure ratio due to a change in plume angle. The plume angle influence curves are presented in Fig. 2-11. The curves are for boattail and cylinder configurations with a single nozzle. The curves are satisfactory for flared skirt configurations up to Mach 1.2. After Mach 1.2, flared skirt configurations have a different trend. The curves are not applicable to multi-nozzle and multi-body configurations. The curves presented in Fig. 2-11 are used to develop increments in base pressure ratio due to an increment in plume angle from baseline values. The baseline plume angles for the flight vehicles are considered to cover the band of data presented in Fig. 2-10. This is a large data band and refinements to this are recommended for future work.

The only flight vehicles that have plume angles outside of this band are the NACA vehicles. The significance of this and the need for the curves in Fig. 2-11 will be discussed later.
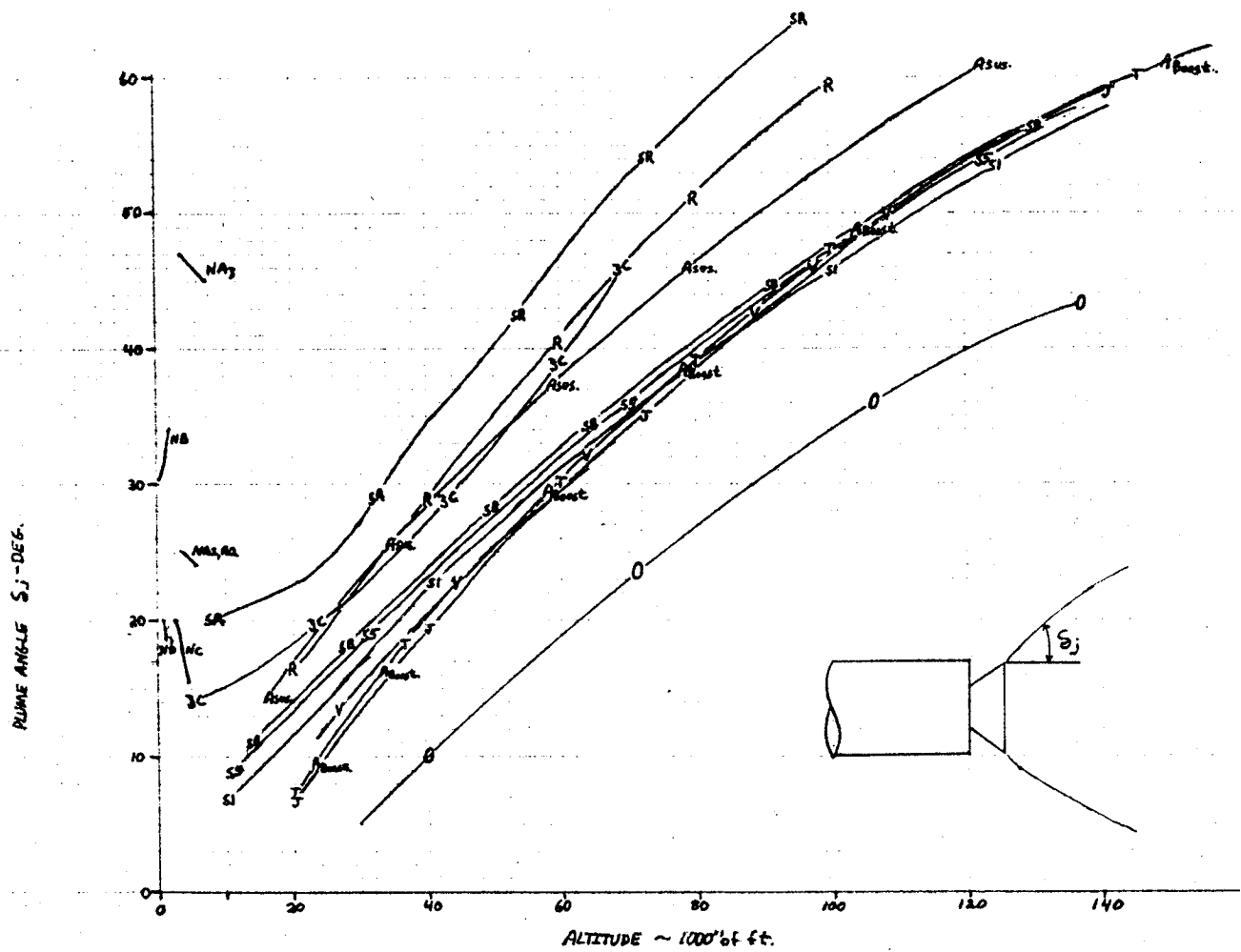
Fig. 2-10 - Jet Plume Angle versus Altitude

LOCKHEED-HUNTSVILLE RESEARCH & ENGINEERING CENTER
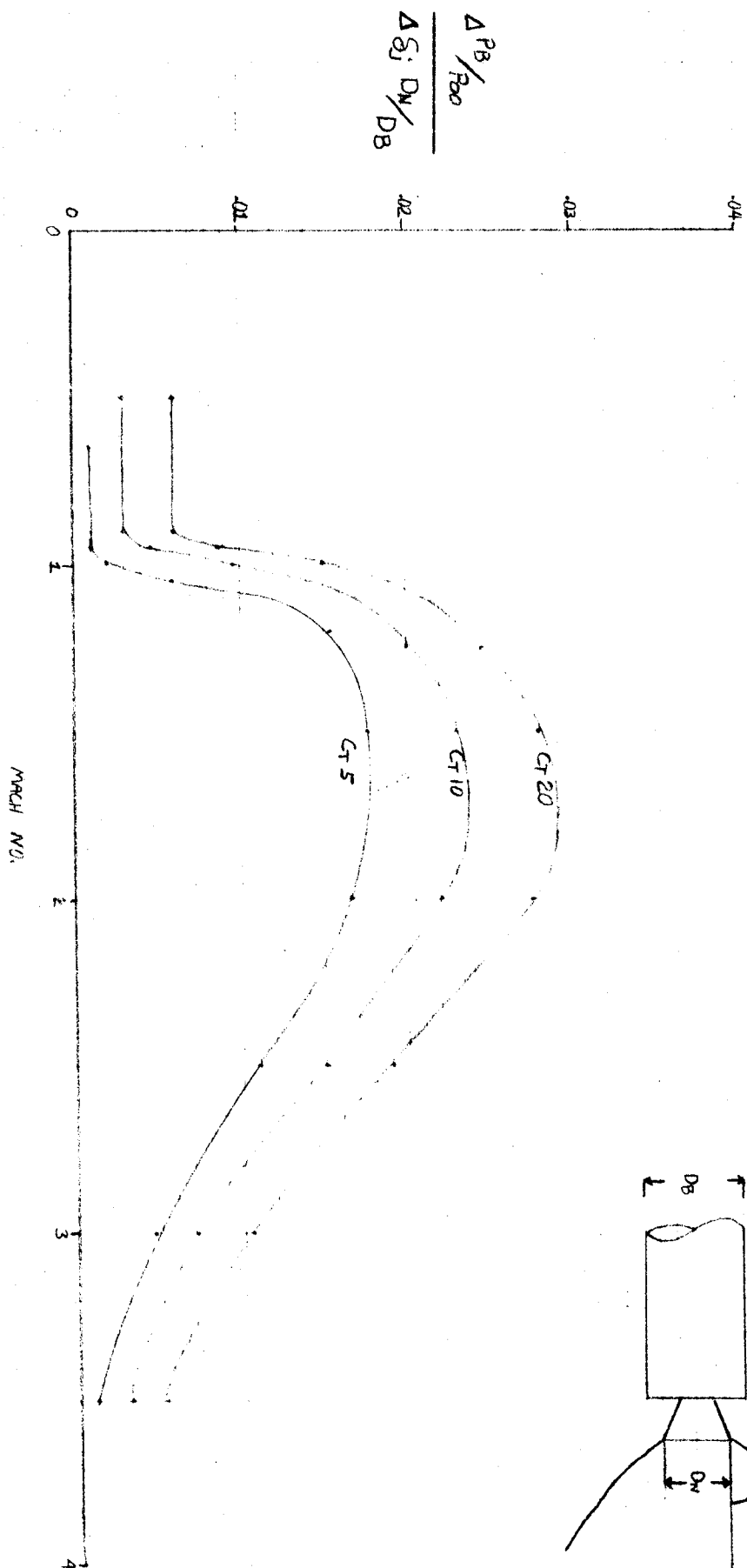
FIGURE 2-11 JET PLUME CORRECTION TO BASE PRESSURE

The result of the thrust coefficient correlation is that it will only correlate the recirculation portion of the base pressure curve for similar nozzle configurations. An approximation (Fig. 2-11) for different nozzle configurations has been developed for use if the plume angle (the major influence of different nozzle configurations) falls outside a certain band of the flight data. Figure 2-11 results are of limited use, however, since it does not cover all vehicle configurations.

Jet Nozzle Position

The influence of jet nozzle position on the base pressure ratio is shown in Fig. 2-12. These results are from Ref. 1 and are based on cold flow test data. Figure 12-a shows that the base pressure ratio is increased as the nozzle exit plane is moved aft of the forebody . These data are developed into a math model (Ref. 1) as shown in Fig. 2-12b. The correlation of the flight data indicate that the effects of nozzle position are approximately half the values shown in Fig. 2-12 . The flight data correlation developed the trends shown in Fig. 2-13. The flight vehicle data base had a variety of nozzle axial positions as shown in Table 2-1. Since all of the vehicles had a nozzle extension aft of the base except the Redstone, a base- line nozzle extension of 0.34 was used in the data correlation and a form of the curve in Figure 2-13 is used to develop increments in the base pressure ratio for vehicles with a nozzle extension different than 0.34.

Flare - Boattail Configurations

A flare or boattail has a major influence on the base pressure as shown in Fig. 2-14 (Ref. 1). Figure 2-14 shows the ratio of the base pressure on a cylinder to the base pressure on a non-cylinder body for supersonic Mach numbers. Flight data on boattail vehicles and vehicles with a flared base have been evaluated. The change in base pressure due to the base area ratio was found to be much less than the Fig. 2-14 results show. The flight data correlation for an equivalent base area ratio of 2.0 is presented versus
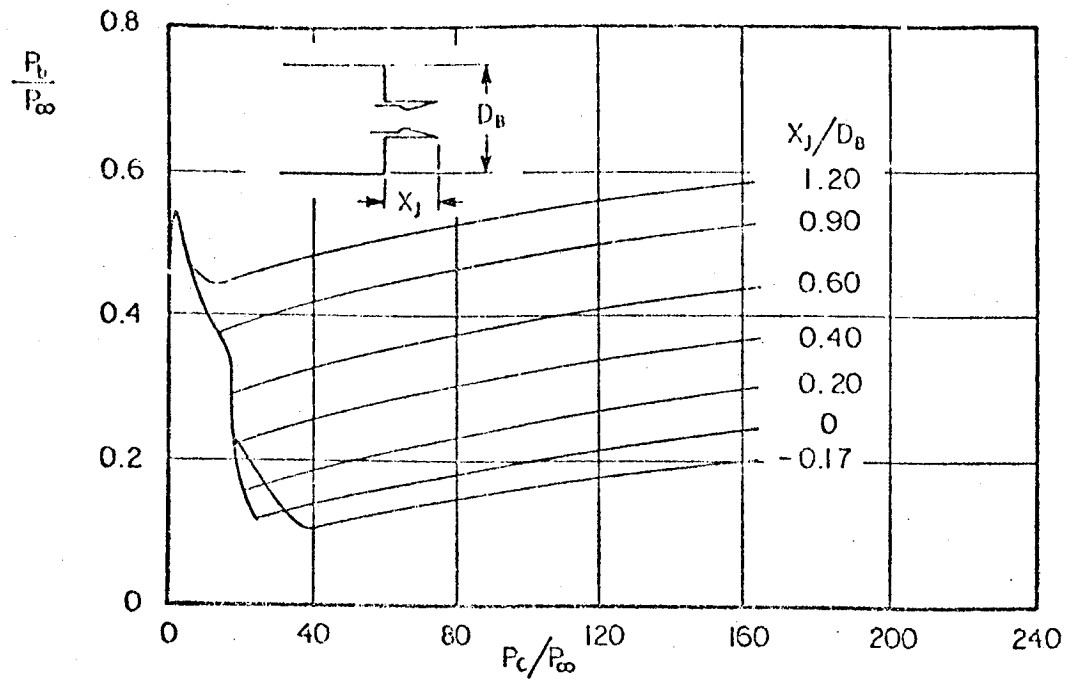
(a) Base Pressure as a Function of Jet Pressure Ratio, M = 2.5
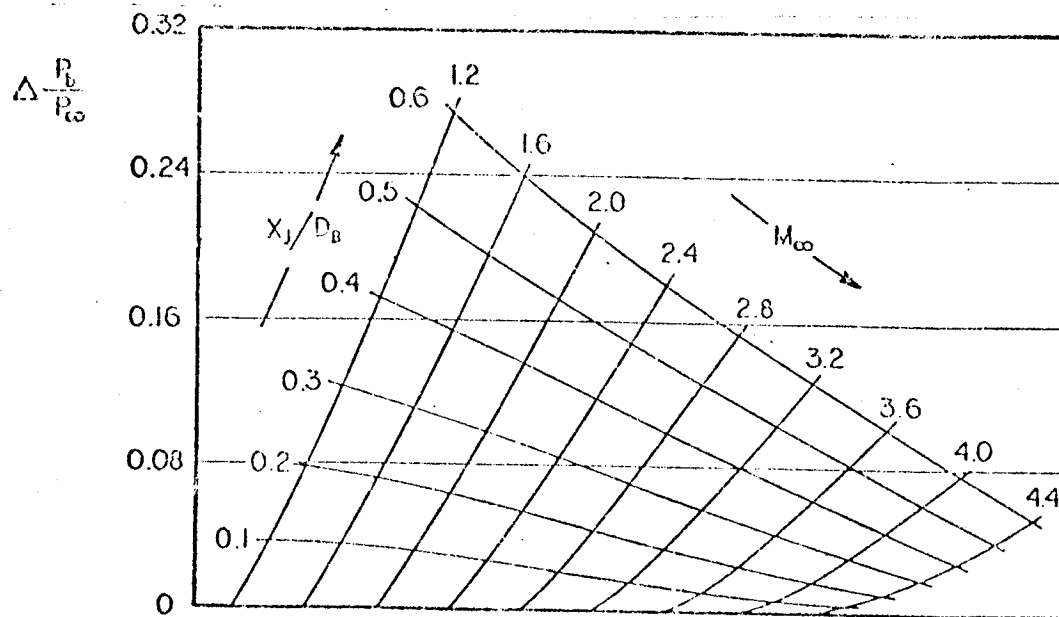
(b) Incremental Effects of Nozzle Position as a Function of Mach Number

Fig. 2-12 – Effects of Nozzle Position on Base Pressure (Cold Flow)

LOCKHEED-HUNTSVILLE RESEARCH & ENGINEERING CENTER

Table 2-1   NOZZLE AXIAL POSITION

Configuration	X_J/D_B
Redstone	0
Jupiter	.33
THOR	.58
Space Shuttle SRB	.28
Atlas	.39
Saturn I BK I	.257
Saturn I BK II	.20
Saturn IB	.20
Saturn V	.467
Space Shuttle Orbiter	.39
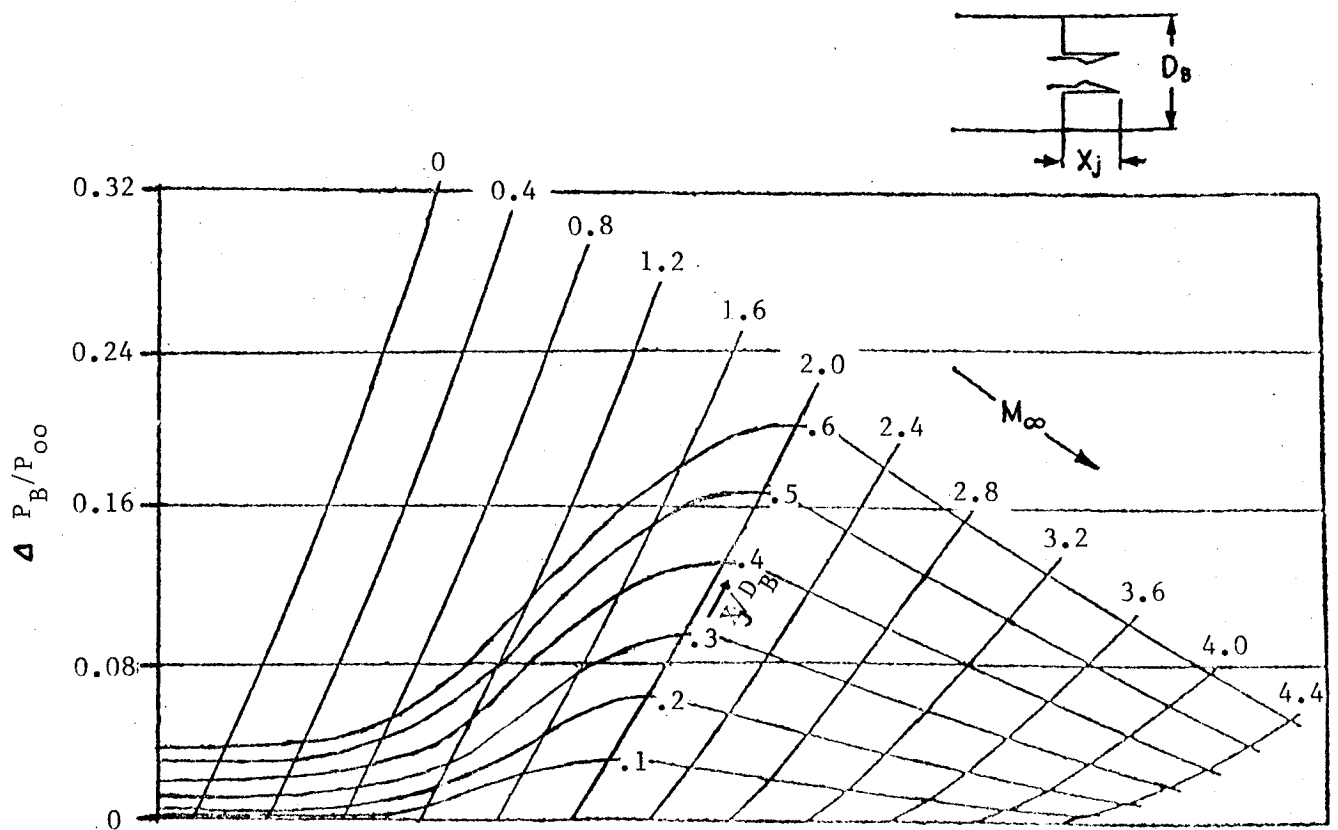
Fig. 2-13 - Effects of Nozzle Position on Base Pressure
(Flight Data)

LOCKHEED-HUNTSVILLE RESEARCH & ENGINEERING CENTER
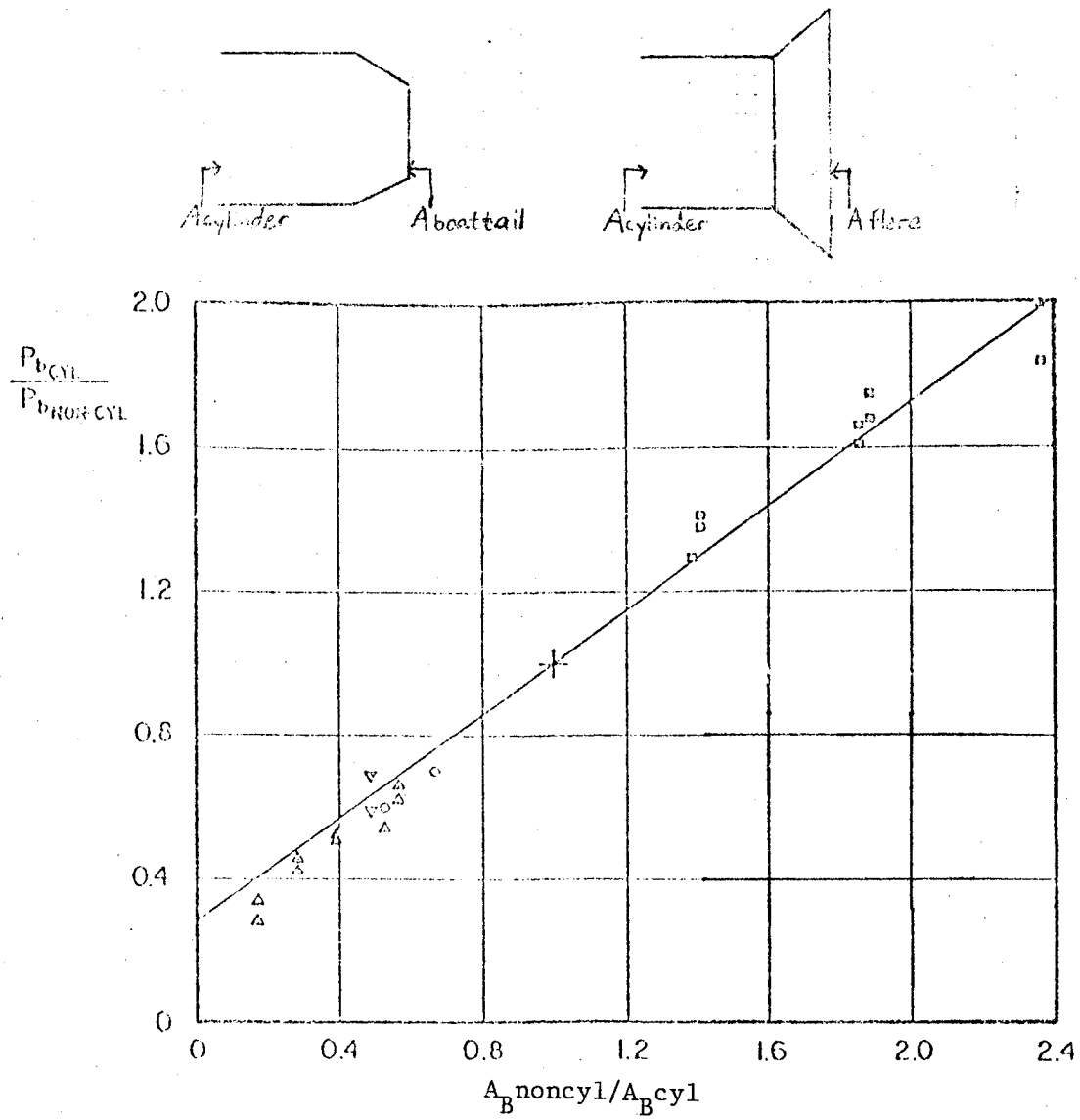
Fig. 2-14 - Effects of Conical Afterbody Geometry on Base Pressure

Mach number in Fig. 2-15. The flight data presented in Fig. 2-15 for an equivalent area ratio of 2.0 assumes a linear curve of base pressure ratio versus area ratio similar to Fig. 2-14. Additional transonic cold flow data from Reference 4 is also presented in Fig. 2-15. It is noted in the figure that the flight data correlation shows only about 10 percent of the effectiveness of the cold flow data. These data trends were developed using the NACA vehicle data and the SRB data (see Appendix A). A faring through the flight data was used to develop a math model.

It is noted that almost all the flight vehicles have fairings around outboard engines that can be evaluated as partial flares. The effectiveness of this type of configuration is unknown but it appears from the data to have much less influence on the base pressure than a full base flare. The influence of engine fairings appears to be only about 25 percent of the full flare effectiveness.

Multi-Nozzle Configurations

Multi-nozzle configurations and multi-body configurations have variations in base pressure due to the nozzle arrangement that require special consideration. Configurations with three and four nozzles experience high pressures in the center compared with other locations as shown in Fig. 2-16 (Ref. 5). Three and four nozzle configurations that are closely spaced will experience extremely high local pressure environments. Engine nozzles that are laterally positioned within 1.2 exit diameter will have high local base pressure environments that are a function of the spacing and plume expansion angle. The base pressure variation with plume angle is presented in Fig. 2-17. The data presented in Fig. 2-17 consists of flight data (Ref. 7) and cold flow data (Ref. 5). Both data sets follow the same trends. These data trends generally occur only above Mach 2.0. The high rise in the base pressure with plume angle is only applicable for the area within the nozzle envelope. The base pressure outside the nozzle envelope does not increase nearly as fast as shown in Fig. 2-16. This phenomenon generally creates two distinct levels of base pressure that must be considered in evaluating the integral of base pressure shown in Eq. 2.1.

LOCKHEED-HUNTSVILLE RESEARCH & ENGINEERING CENTER
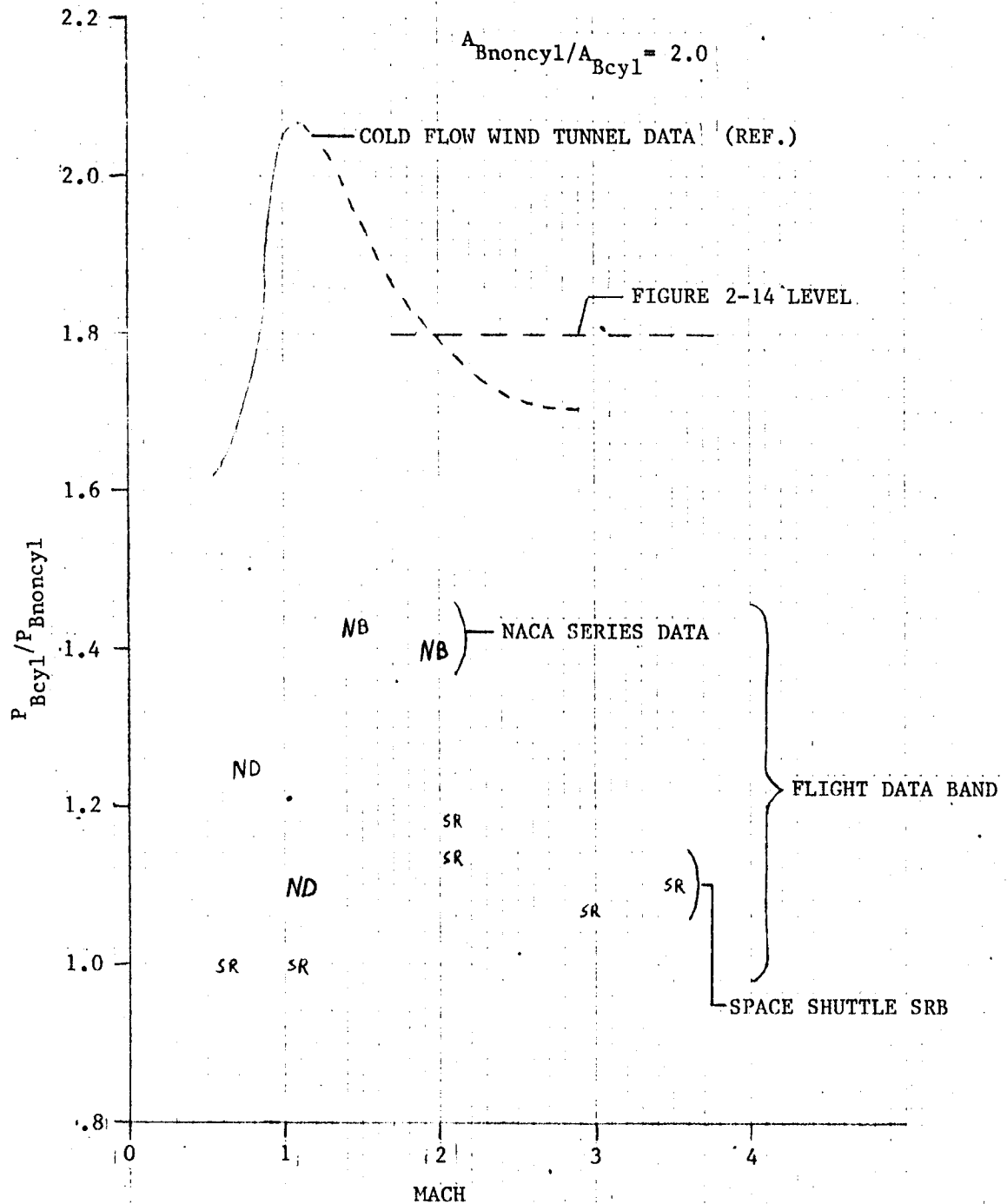
Fig. 2-15 - Effects of Base Geometry on Base Pressure Ratio-Cold
Flow and Flight Results

MULTI–NOZZLES

$M_{oo} = 2.3$

CENTER TAP 4 NOZZLE

CENTER TAP 3 NOZZLE

DATA BAND ALL OTHER TAPS

$$\frac{A_{ETOTAL}}{A_{BASE}} = CONSTANT$$

C_{PB}

P_j/P_{oo}
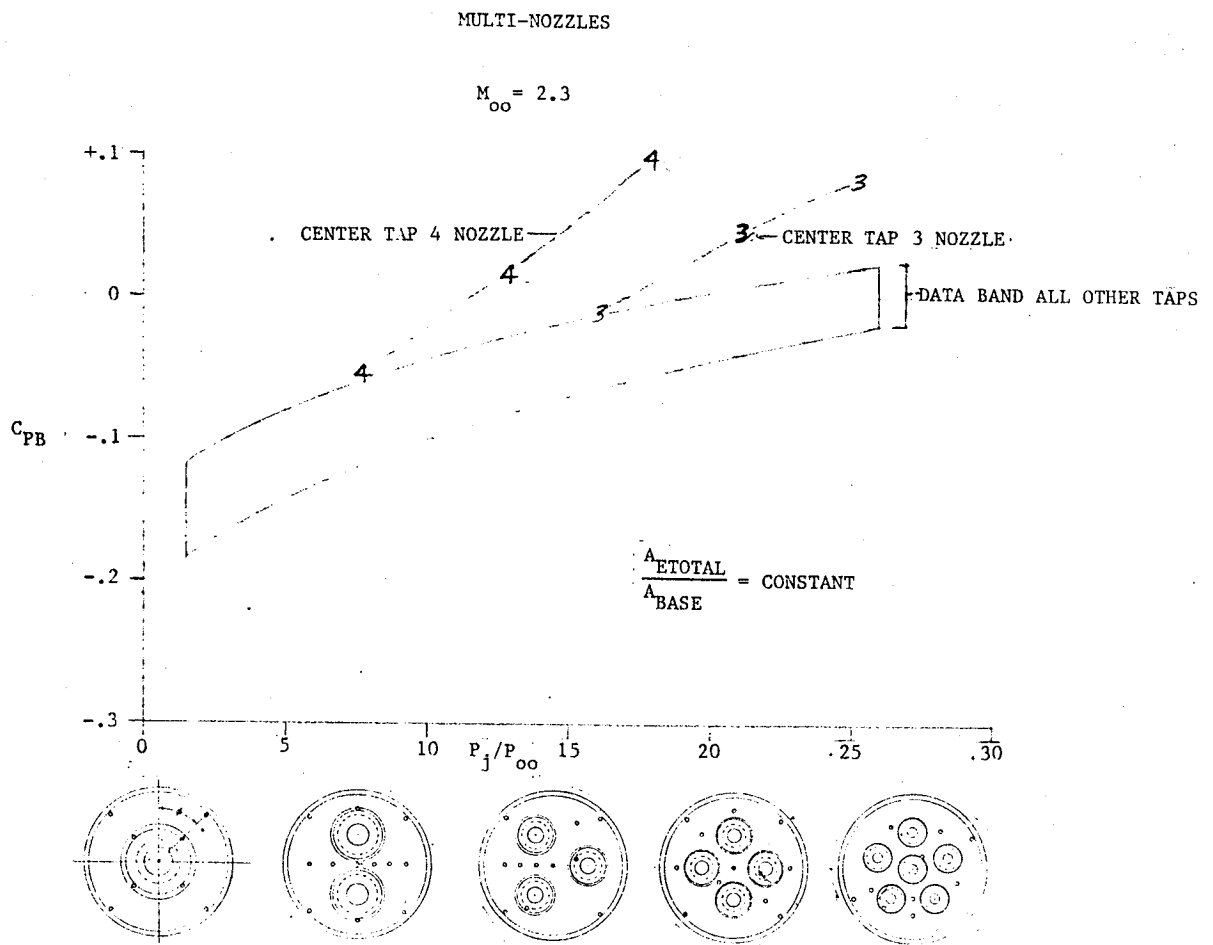
Fig. 2-16 – Base Pressure Rise Due to Three and Four Nozzles

Fig. 2-17 - Base Pressure Ratio versus Plume Angle and Spacing

θ_j

0   10   20   30   40   50   60   70

P_B/P_{∞}

0   1.0   2.0   3.0   4.0   5.0

FLT.

ET2

X/DN=30

FLT.

X/DN=13

FLT.

X/DN=22

X/DN=48

X/DN=35

X/DN=42

ENGINE

EFFECTIVE AREA

$\frac{P_B}{P_\infty}$ ET2

$\frac{P_B}{P_\infty}$ EFFECTIVE AREA

ENGINE

SB

FLT.

SB

COLD FLOW TEST

$M_\infty < 2.0$
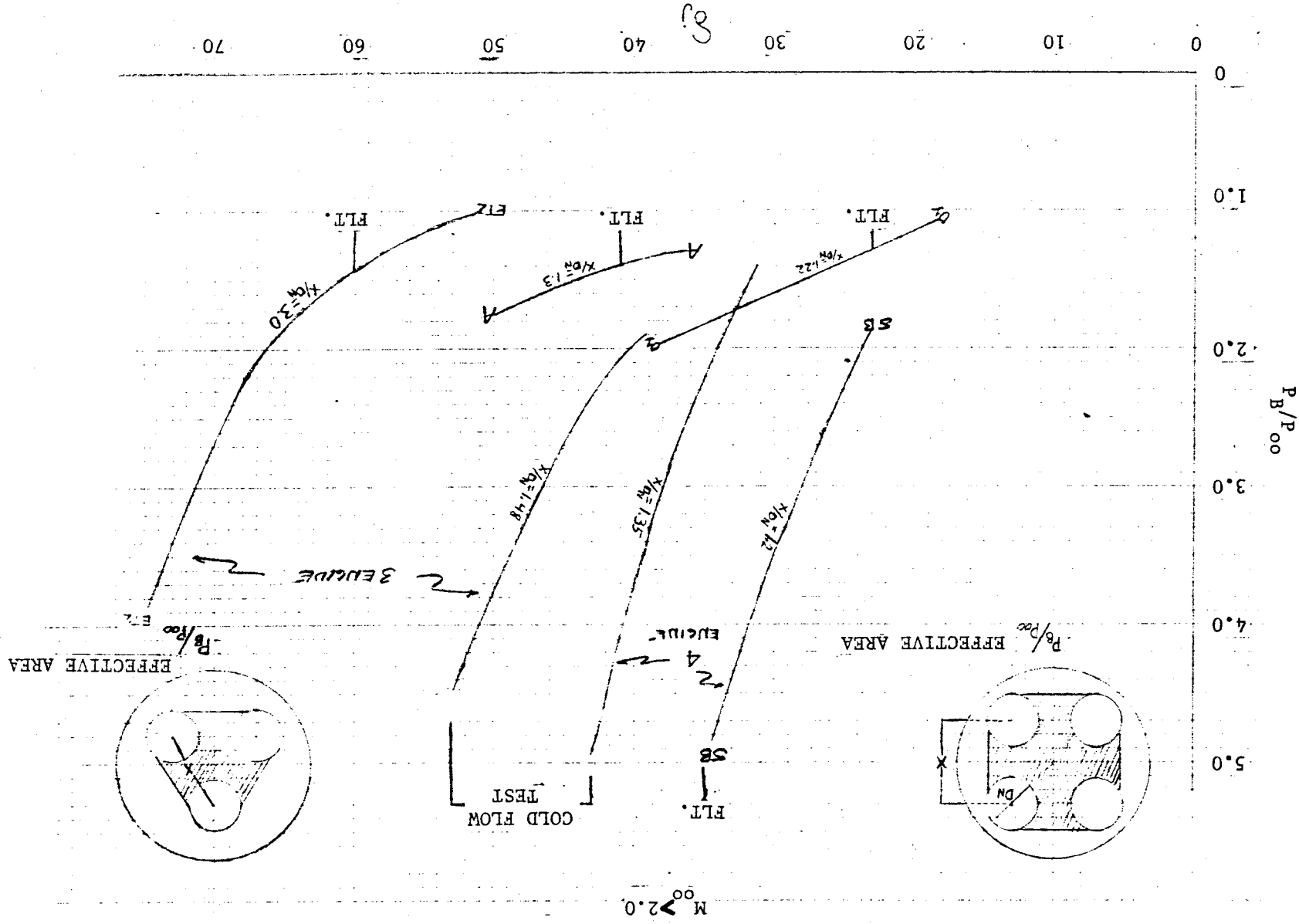
The integral is generally simplified to the summation form when evaluating the base drag if the base pressure or base pressure coefficient varies over the base area. Thus the form used is:

$$C_D = \frac{-1}{S_{REF}} \sum_{i=1}^{M} C_{P_i} A_i \qquad (2.9)$$

If the base is not flat and has a complex contour the above equation converts to:

$$C_D = \frac{-1}{S_{REF}} \sum_{i=1}^{M} C_{P_i} A_i \cos\psi_i; \qquad (2.10)$$

where ψ is the local slope of the base surface with respect to the vehicle centerline.

If a rear view of the base is drawn on a sheet of paper the layout represents the axial projection (i.e., $A_i \cos\psi_i$). Thus, the area increments and the proper angles are converted into axial components.

The band of data presented in Fig. 2-16 represents the base pressure coefficient outside the nozzle control band and shows that the majority of the base pressure environment is not influenced by the number of nozzles. The nozzle configurations presented in the lower portion of Fig. 2-16 are sized such that the thrust of each configuration is the same. The nozzle exit area is sized by the number of nozzles using the following equations:

$$A_{EXIT \atop MULTIPLE \atop NOZZLES} = \frac{A_{SINGLE\ NOZZLE}}{\eta} \qquad (2.11)$$

where η = number of nozzles

The equivalent single nozzle exit diameter is thus:

$$D_{\substack{EXIT \\ SINGLE\ NOZZLE}} = \sqrt{\eta\, D^2_{EXIT}} \qquad\qquad (2.12)$$

Thus, the thrust coefficient correlation parameter should be applicable for correlation of the base pressure environment of the outer base area of multiple nozzle configurations. The additional correlation techniques, as discussed above, are required for the prediction of the base pressure environment inside the nozzle envelope of three and four nozzle configurations.

Fins

Fins located near the base of a vehicle will reduce the base pressure and increase the base drag. Power-off correlations of the effect are presented in Ref. 8. The math model developed in Ref. 5 is the following:

$$\Delta C_{D_B} = \frac{t}{c}\left(\frac{0.825}{M_\infty^2} - \frac{.05}{M_\infty}\right) n$$

where t/c = thickness to chord ratio of fin

n = number of fins.

The influence of an operating jet was evaluated in Ref. 6 using the above relationship and the power on influence of fins appeared to be approximately half the power-off values. The above equation was thus modified for the power-on influence and developed into a basic curve versus Mach number for the increment in base pressure ratio for four fins. Fin configurations with a thickness ratio (t/c) of 0.10 were used to develop the curve. The resultant curve is shown in Fig. 2-18. The dashed portion of

LOCKHEED-HUNTSVILLE RESEARCH & ENGINEERING CENTER

t/c=.1
4 FINS
POWER ON

$$\overline{\Delta}(P_B/P_{oo}) = \Delta(P_B/P_{oo})\left[(t/c)/.1\right]\left[n/4\right]$$

n= NUMBER OF FINS

t/c @ 1/3 span

FINS AT BASE PLANE

$\Delta P_B/P_{oo}$

MACH NUMBER
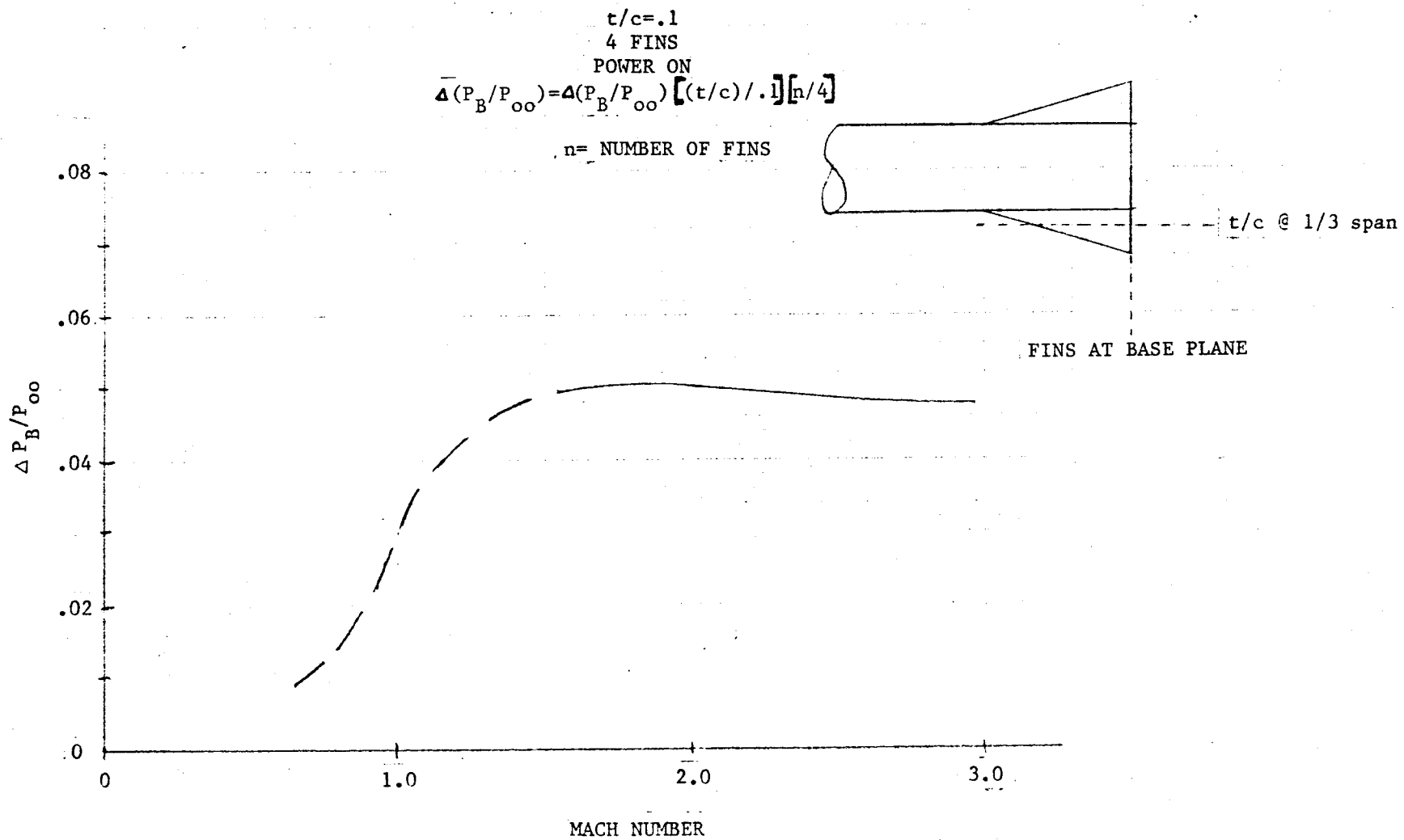
Fig. 2-18 - Correction Due To Fins

the curve has been estimated. The equation at the top of the figure is used
if the fin thickness and number of fins is different from the specified
values.

2.2 FLIGHT DATA CORRELATION M < 2.0

The basic subsonic and transonic flight data correlation uses the
thrust coefficient. Examples of the uncorrected (i.e., as measured on each
vehicle) data correlation with thrust coefficient is presented in Figs.
2-19, 2-20 and 2-21 corresponding to Mach numbers of 0.6, 1.25, and 1.75
respectively. These curves show a wide band of flight data. The major
flight data outside the main grouping is noted to be from the NACA vehicles,
the Space Shuttle ET, and the Titan IIIC core vehicle. (Data and references
presented in appendix).

The major corrections required to the NACA data was the plume angle
correction. This was a major correction because of the large difference
between the plume angles of the NACA vehicles compared to the other flight
vehicles (see Fig. 2-10). The correlation of the data for the Mach 2.0
flight regime thus considered the plume angle to be within the major band of
flight data in Fig. 2-10. The flight ascent trajectory band must also be in
the band of the majority of the flight vehicles as presented in Fig. 2-1.
The NACA vehicles do not fall within this flight envelope and thus the quan-
titative correlation of the NACA data was not pursued. The qualitative
trends have been used, however, to separate the geometric influence of a
boattail/flare from the influence of plume shape on the base pressure. The
major difference between the base pressure ratio for the NACA vehicles and
the other flight vehicle data presented in Fig. 2-19 is the plume angle   .
The major difference in the NACA flight data presented in Figs. 2-20 and
2-21 is due to the combination of plume angle and boattail configuration.
The specific values of the correlation parameters developed, need refinement
as shown by the difference in the bottail correction and the flare correc-
tion (normalized to an area ratio of 2.0 using the linear curve technique)

$$M_{oo} = 0.60$$
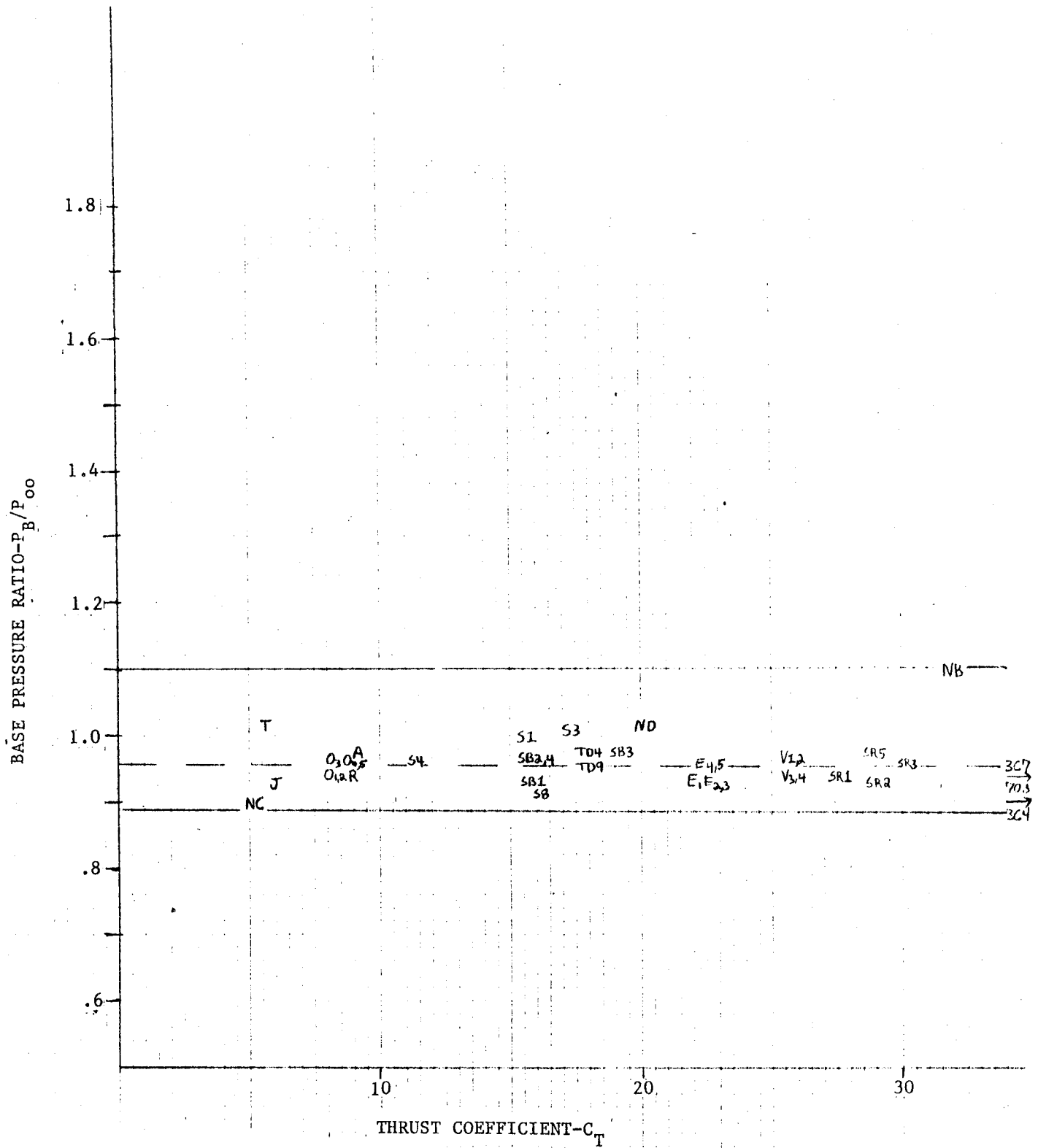
Fig. 2-19 – Base Pressure Correlation ($M_{\infty} = 0.60$)
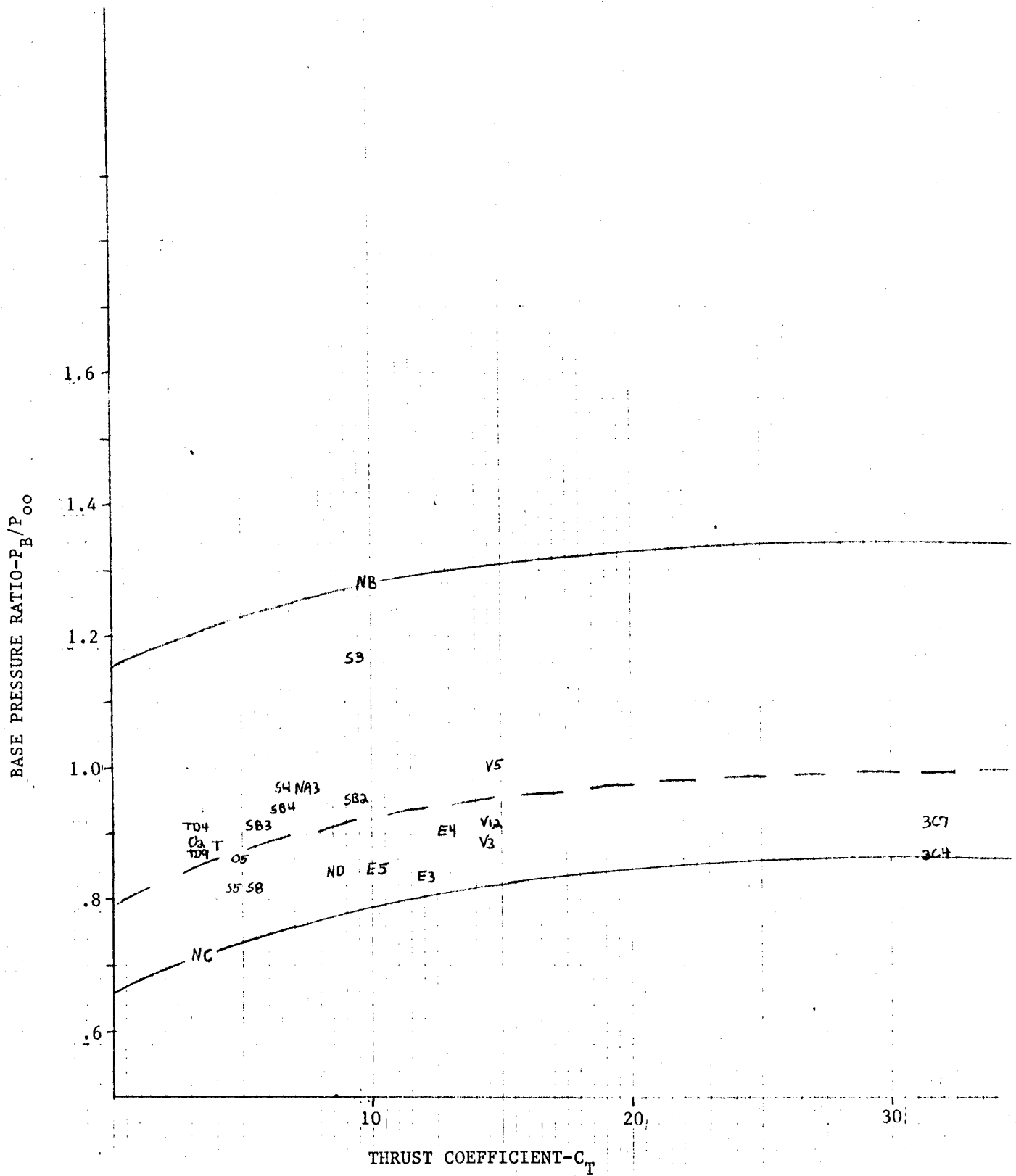
Fig. 2-20 – Base Pressure Correlation (M$_\infty$ = 1.25)
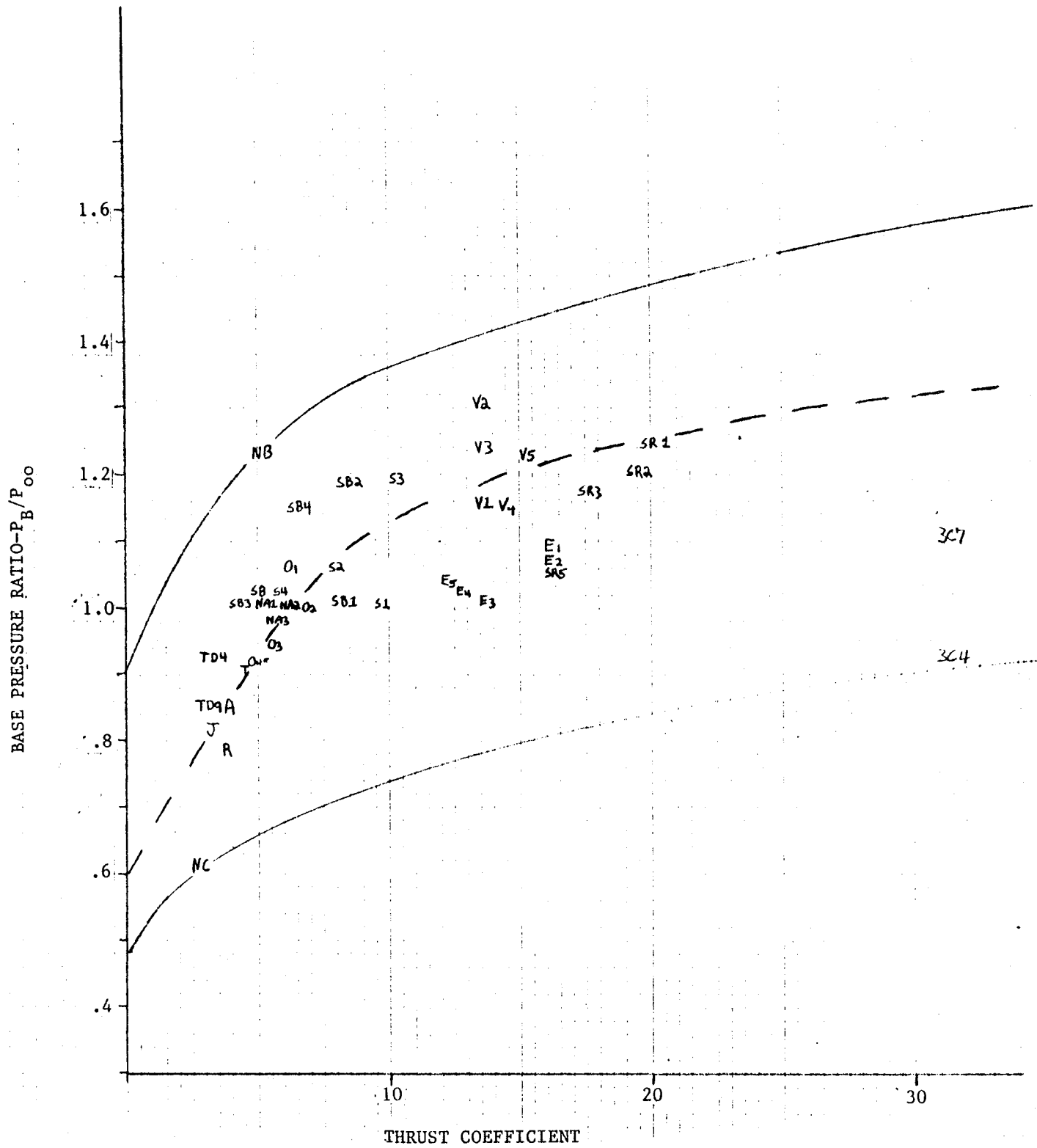
Fig. 2-21 - Base Pressure Correlation (M_{∞} = 1.75)

presented in Fig. 2-15. This result indicates that the linear curve presented in Fig. 2-14 does not hold for the transonic flight regime.

Major corrections are also required for the multibody vehicles that include the Space Shuttle ET and the Titan IIIC core stage. It is noted from the figures that the Space Shuttle orbiter and the Thor Delta core vehicle do not require major corrections. This difference in correlation has been attributed to the fact that the Space Shuttle ET and the Titan IIIC core (at the lower Mach numbers) are non-propulsive elements while the Space Shuttle Orbiter and the Thor Delta core are propulsive elements. Thus it can be concluded that the primary influence on the base pressure ratio for an element of a multi-element vehicle is its own propulsion system. This conclusion is based on comparing data trends in terms of thrust coefficient. It is noted that experimental data exists on multiple element vehicles that show the influence the engine thrust of one element on the base pressure of an adjacent element with its own propulsive device. An example of this is the Space Shuttle cold flow wind tunnel data that shows the influence of the SRB power level on the Orbiter base pressure. The influence of adjacent element propulsion systems can be shown in experimental data but could not be extracted from the flight data.

The major propulsive influence on the base pressure of vehicle elements without propulsion is thus the thrust characteristics of the vehicle elements that have operating propulsion systems. If the thrust coefficient for non-propulsive elements is defined to include the thrust from all elements and the total base area of all elements, the correlation of the base pressure falls closely into the central group of the data in Figs. 2-19 through 2-21.

Seven curves of flight data correlation were developed similar to the curves presented in Figs. 2-19 through 2-21 covering the Mach number range from 0.6 to 1.75. The basic flight data was found to correlate to a

slightly different curve for each Mach number. It is noted that below Mach 2.0 the data is presented in terms of base pressure ratio P_B/P_∞ for specific Mach numbers. These data could be correlated to base pressure coefficients since the Mach number is specified for each data curve. The data correlation curves were left in the form of base pressure ratio because the data correlation above Mach 2.0 uses base pressure ratio. Thus the base pressure ratio was also used for Mach numbers less than 2.0.

The example data correlation curves presented in Figs. 2-19, 2-20, and 2-21 were developed using no corrections to nozzle axial position, flare configuration, nozzle spacing, or fins. The general shape of the curve was thus developed. Corrections to the flight data to eliminate the configurational differences were then made to the curves to develop a consistent geometric model. The geometry model that was used to finalize the data has a cylindrical afterbody with no fins and a nozzle extension of 0.34 base diameters. These data correlation curves are presented in Section 3.0.

The effective base area for use in the thrust coefficient calculation for single and multiple nozzle vehicles is each element's total base area. The base area for nonpropulsive elements of multi-body configurations is the total base area of all elements. The thrust is the total thrust of all elements. The base area of multi-body elements with propulsion is the element base area and the thrust is only the thrust of the element of interest. Thus thrusting elements of a multi-body configuration are conceived to be isolated while non propulsive elements are evaluated considering the total vehicle. The concept is shown in Fig. 2-22.

2.3   FLIGHT DATA CORRELATION M ≥ 2.0

The correlation of the flight base pressure data for Mach numbers greater than 2.0 was expected to be simpler than the transonic correlation. Base pressure correlations from Ref. 6 are cylindrical afterbody configurations with no nozzle extensions appearing to prove this correlation.

ISOLATED   ISOLATED   TOTAL

SRB DATA   ORBITER DATA   ET DATA
BASE AREA   BASE AREA   BASE AREA
THRUST= SRB   THRUST= 3 SSME'S   THRUST= 3 SSME'S+2 SRB'S
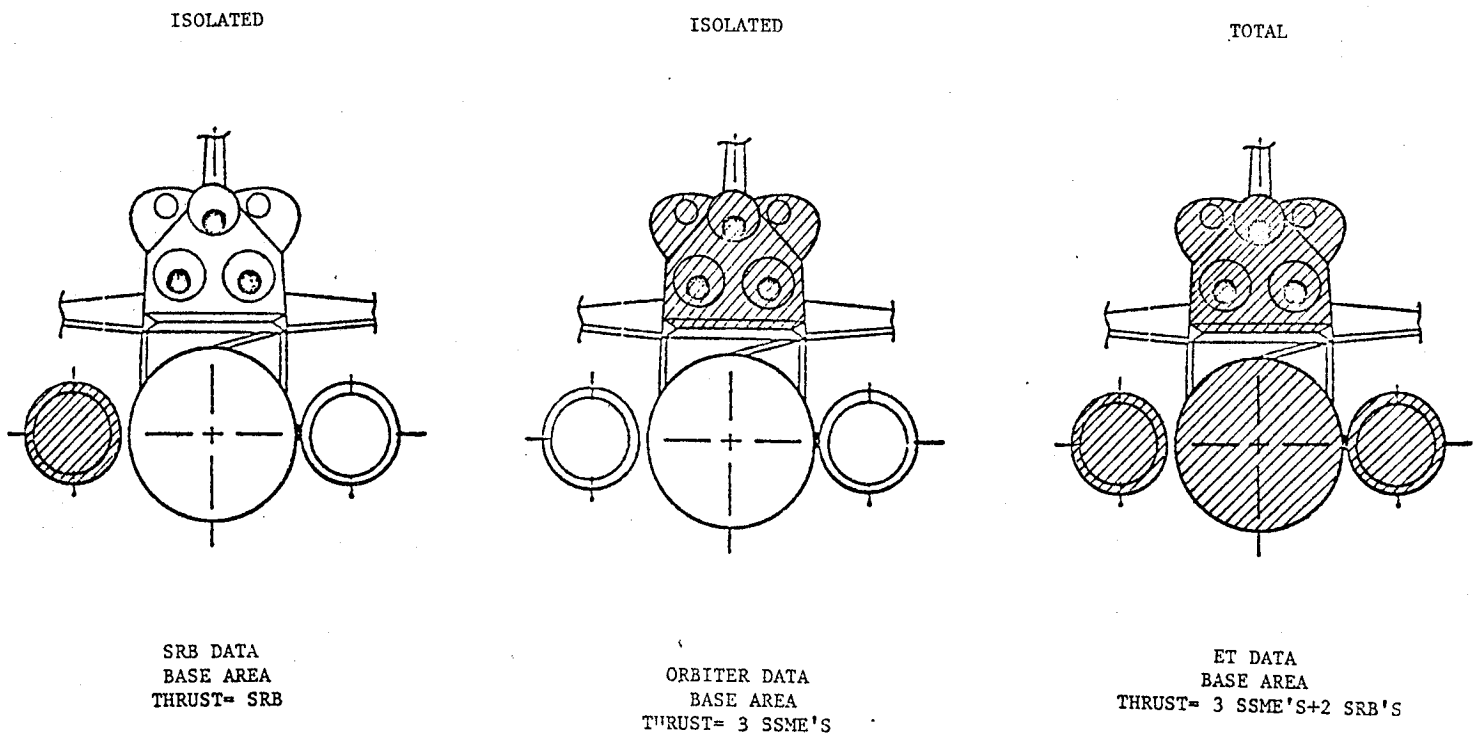
Fig. 2-22 - Effective Thrust Base Area, Multi Body Configurations

An example of the expected correlation is presented in Fig. 2-23. Figure 2-23 presents the base pressure coefficient for a single nozzle vehicle versus Mach number. The base pressure coefficient is presented versus Mach number for various jet pressure ratios. Overlayed on the figure are constant values of base pressure ratio corresponding to a power level (P_j/P) of 1.6 and 7.0. Note that the base pressure ratio for this power level is a constant for Mach numbers greater than 2.0.

The variation in base pressure coefficient is then only due to the Mach number variation in the term ($\gamma/2 \, M^2$) in Eq. (2.2). The base pressure ratio form of correlation simplifies the data handling in that the data have only two independent variables, power level and nozzle to base area, both incorporated in the thrust coefficient, C_T. Attempts to correlate the flight data with thrust coefficient failed in that the base pressure ratio band was unacceptable. The main difficulty with the thrust coefficient correlation was the dynamic pressure variation at the upper altitudes. At the higher Mach numbers and altitudes the decrease in dynamic pressure was so different for the various flight vehicles that the base pressure ratio could not be correlated with a correlation parameter that contained dynamic pressure. Including the influence of base flare, fins, plume angle, and nozzle area all failed to correlate the data within an acceptable data band. A re-evaluation of the results shown in Fig. 2-23 shows that altitude is an effective correlation parameter. This is evident from Fig. 2-23 by noting that the two constant levels of base pressure ratio correspond to separate power level ratios (P_j/P_∞). Thus the level of base pressure ratio is also a function of altitude for a constant power level P_j. The difficulty of including dynamic pressure in any correlation parameter was known and thus a thrust level and base area correlation parameter, thrust loading (T/A), was attempted along with flight altitude. Typical results of the altitude correlation are presented in Figs. 2-24 and 2-25. The results shown in the figures showed a good initial correlation for uncorrected data. Notice that the base thrust loading (T/A) is also required to correlate the data. The figures also show that major corrections to the Space Shuttle ET and SRB
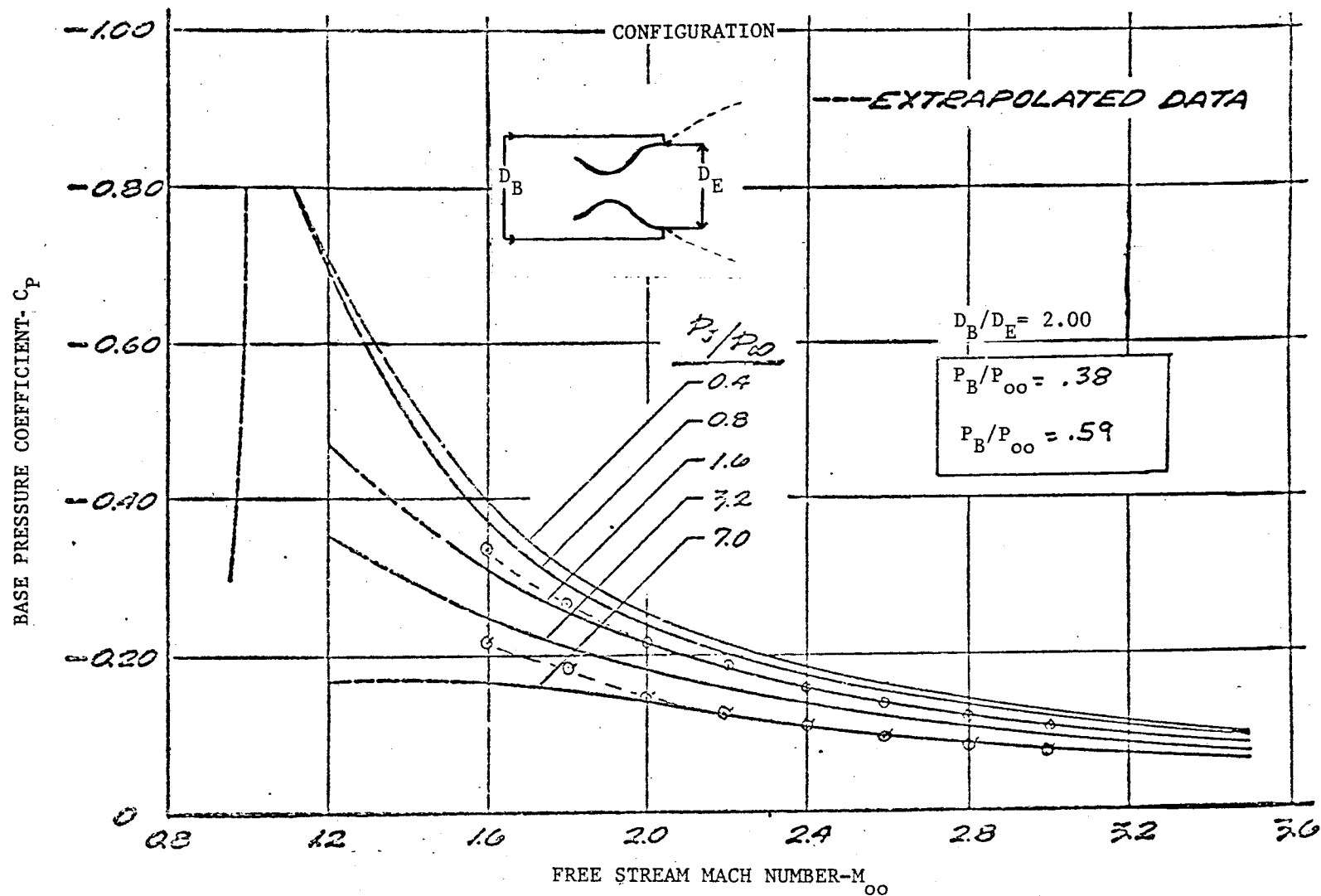
Fig. 2-23 – Base Pressure Coefficient versus Mach Number

ALT. > 60,000 ft.
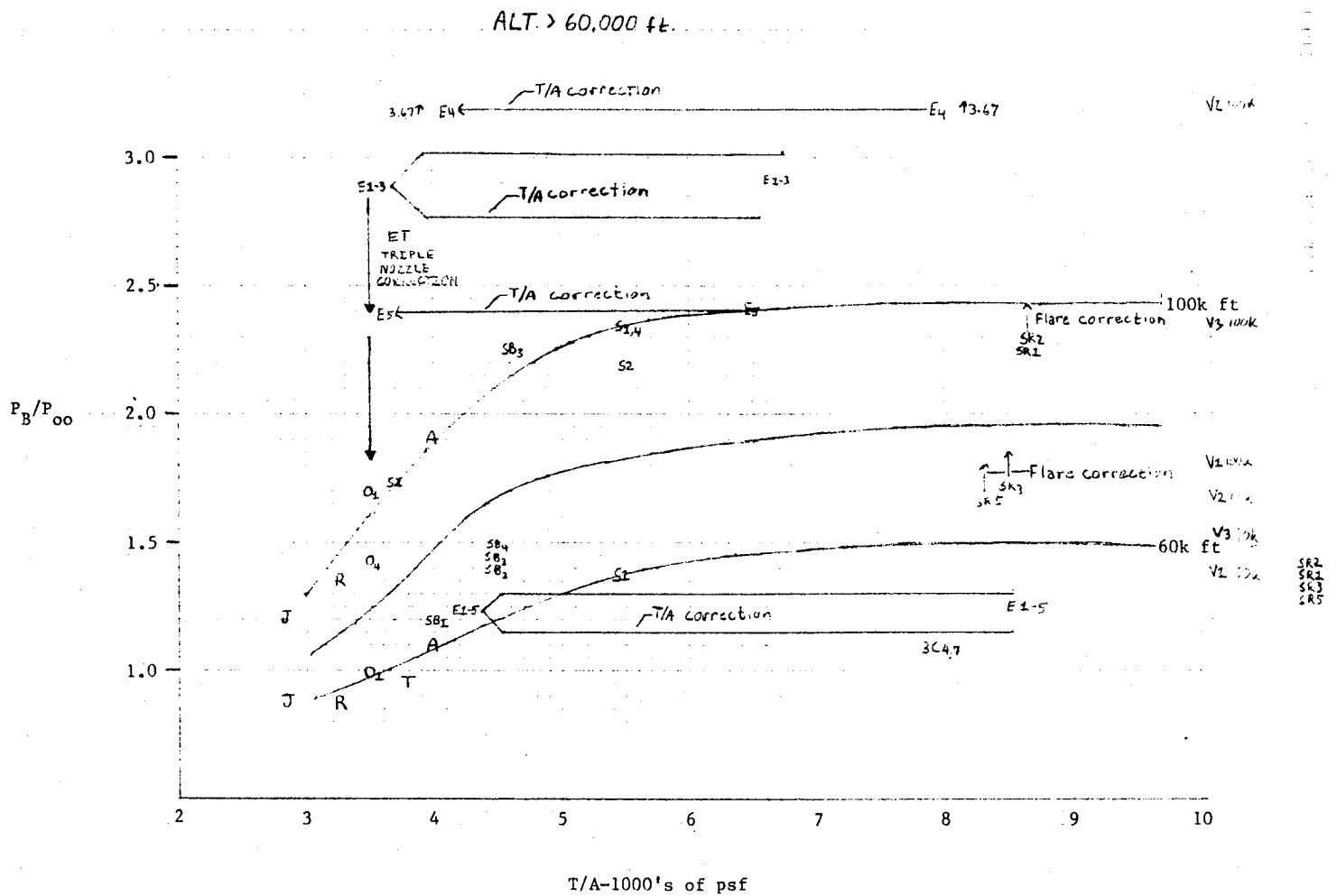
Fig. 2-24 – Base Pressure Ratio Altitude Correlation (h = 60 k, 100 k)

2-40
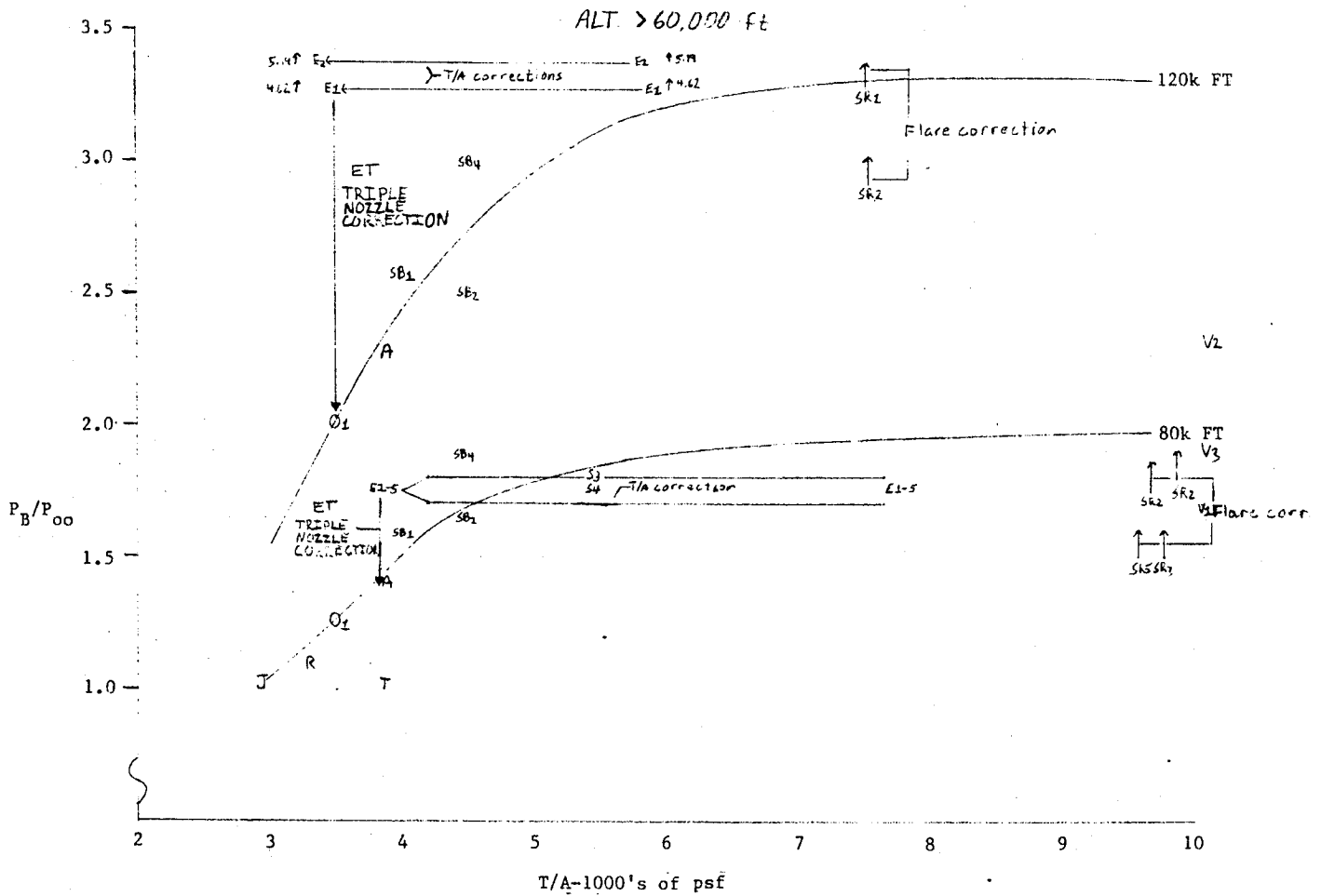
Fig. 2-25 – Base Pressure Ratio Altitude Correlation (h = 80 k, 120 k)

are required. The figure shows that major corrections to the ET are required that include the effective base area similar to the thrust coefficient correction. This is evident at 60,000 ft and 80,000 ft. altitude. Using the total Space Shuttle thrust and the total Space Shuttle base area corrects the lower altitude ET data to the major data band. At the higher altitude the ET data cannot be correlated with the correction to the thrust loading. The additional correction required to the ET data is the correction due to the effective triple engine configuration. The triple engine configuration is composed of the SSME combined engine and the two SRB engines. The three engine arrangement is of such a nature as to encompass an effective higher base pressure environment for the total ET base. The high ET base pressure ratio is due to the large SRB plume angles at high altitudes as shown in Fig. 2-17. The increment in base pressure due to the triple nozzle arrangement presented in Fig. 2-17 closely matches the delta base pressure ratio between the curves presented in Figs. 2-24 and 2-25 at the ET corrected data.

The SRB flare correction uses the correction factors as developed for the lower Mach number range. This is because the flare influence on base pressure ratio is a Mach number influence and is thus Mach number dependent. Likewise the corrections due to nozzle extension and fins are also Mach number dependent. The general curves presented in Figs. 2-24 and 2-25 were thus reformulated for the development of a math model as a function of altitude for various values of thrust loading. The curves were developed for the generic configuration with a cylindrical afterbody and a nozzle extension ratio of 0.34 as was used for the lower Mach numbers.

It is important to note that for the $M \geq 2.0$ flight regime the primary variables in determining the base pressure ratio are altitude and base thrust loading. Corrections to the base pressure ratio due to a flare or boattail, nozzle position, and fins that are a function of Mach number may

LOCKHEED-HUNTSVILLE RESEARCH & ENGINEERING CENTER

be required in this flight regime. Thus the higher Mach number flight regime model uses a base pressure prediction technique that is a function of both altitude and Mach number.

The data correlations presented above have been formulated into a math model with design charts for predicting the base pressure ratio, base drag coefficient and base drag. The math model is presented in Section 3. It is noted that the design charts presented do not cover all the flight data. The various correlations discussed above enabled the evaluation of flight data from several flights of the same vehicle. Some flight data for the same vehicle will not group into a constant data subset. These data were given less weight than vehicle flight data that formed a tight subset data correlation.

3. MATH MODEL

A math model based on the data correlations from Section 2 has been developed for use in predicting the base pressure and base drag. The math model is divided into the M $\leq$ 2.0 flight regime and the flight regime for M $\geq$ 2.0. Different techniques are used for the different flight regimes. The math model is developed for a basic vehicle configuration with a cylindrical afterbody and a single nozzle $(X_{exit}/D_B) = .34$. Special techniques are presented for thrusting and non-thrusting elements of multi-element vehicles. Base pressure curves are presented that are to be used to predict environments for the generic configuration.

Correction techniques are presented to modify the base pressure to account for flare or boattail configurations, the axial position of the nozzle with respect to the base, the spacing of multi-nozzle configurations and the influence of fins. Uncertainties in the base pressure prediction techniques are also presented. Methods are then presented to convert the base pressure predictions into base pressure coefficients, drag coefficients and the base drag forces.

3.1 INPUT DATA REQUIRED

Certain data will be required prior to using the charts to predict the flight base pressure and drag. The data required include a definition of the base configuration including the base area, nozzle exit area, and nozzle position with respect to the base. Additional data that are required are the trajectory data including at least altitude and Mach number. Flight dynamic pressure can be calculated from static pressure and Mach number. The engine thrust versus altitude is also required. From these data, tables of Mach number, altitude, dynamic pressure, thrust, thrust coefficient and thrust loading can be constructed similar to the tables presented in the

appendix. The thrust coefficient requires the base area as input. The base area is the total base area including nozzles. Multi-body configurations require separate treatment depending on the element.

Vehicle elements that contain engine units are treated as separate vehicles and the thrust coefficient is calculated assuming that the element is a separate vehicle. Elements that do not contain operating engine units are evaluated as a complete vehicle considering all elements. Thus the thrust coefficient of the Titan IIIC vehicle core stage would use the total base area of both SRBs and the core vehicle along with the thrust of both SRBs. The thrust coefficient of the Space Shuttle ET element uses the thrust from both SRBs and all three SSME engines and the base area of the total vehicle. Examples of the effective areas of multi-element vehicles are presented in Fig. 2-22.

3.2 BASE PRESSURE MATH MODEL

The base pressure math model consists of charts developed from the flight data that are used to preduct the base pressure ratio for a generic vehicle configuration. The math model has the following functional form:

$$\underline{M < 2.0} \qquad\qquad \underline{M \geq 2.0}$$

$$\frac{P_B}{P_\infty} \sim \left[\left(\frac{P_B}{P_\infty}\right)_{f \ (Mach, \ (C_T))} \right] \sim \left[\left(\frac{P_B}{P_\infty}\right)_{f \ (Altitude, \ Thrust \ Loading)} \right] \tag{3.1}$$

Generic
Vehicle

The generic vehicle has the same total base area, thrust, equivalent nozzle exit diameter and flight conditions as the new vehicle.

Corrections to the base pressure ratio are now required for configurational differences that may exist between the generic vehicle and the vehicle of interest. Differences between the generic vehicle and the new

vehicle may include nozzle position, afterbody configuration, multiple nozzles and fins. These differences in configuration will require corrections to the base pressure ratio of the generic configuraion to develop the proper base pressure for the vehicle of interest. The corrections to the generic vehicle base pressure need to be performed in a certain order. The order of correction is (1) nozzle extension, (2) flare or boattail, (3) multiple nozzles, and (4) fins.

The following paragraphs discuss the charts for the development of the base pressure environment for the generic vehicle and the curves for correcting the base pressure environment of the generic vehicle to the particular vehicle of interest.

3.3 BASE PRESSURE MATH MODEL M $<$ 2.0

The math model for Mach numbers less than 2.0 consists of using the charts of the P_B/P_∞ versus C_T presented in Figs. 3-1 through 3-7 corresponding to Mach numbers of 0.6, 0.9, 1.0, 1.1, 1.25, 1.5 and 1.75, respectively. The charts presented are only applicable as long as the nozzle to base area ratio is in the range of .2 to .6 and the nozzle exit axial position to base diameter ratio is in the range of .34. The curves require no corrections for number of nozzles or nozzle spacing. There is also no limit on the number of nozzles. Corrections to the basic data, if required, due to the base configuration, nozzles extension, nozzle spacing and fins are discussed in later sections.

3.4 MATH MODEL M $\gtrless$ 2.0

The math model for predicting the base pressure ratio for Mach numbers equal to or greater than 2.0 is correlated with the altitude and the base thrust loading (T/A). The base area used in the thrust loading is the same area used in the thrust coefficient. The correlation curves are presented in Fig. 3-8 for configurations with a cylindrical forebody with nozzles 0.34
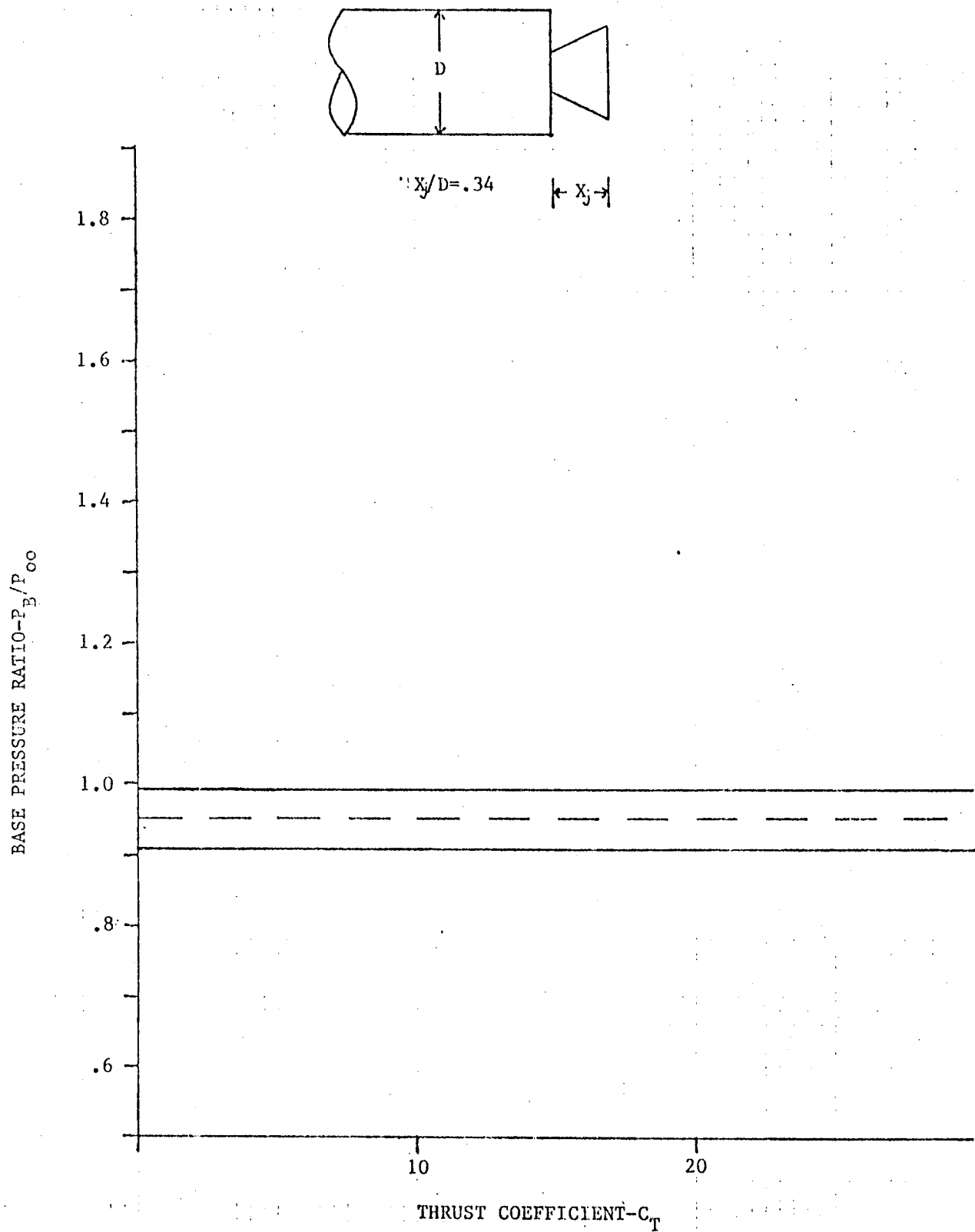
Fig. 3-1 - Base Pressure Ratio Math Model ($M_\infty = 0.60$)
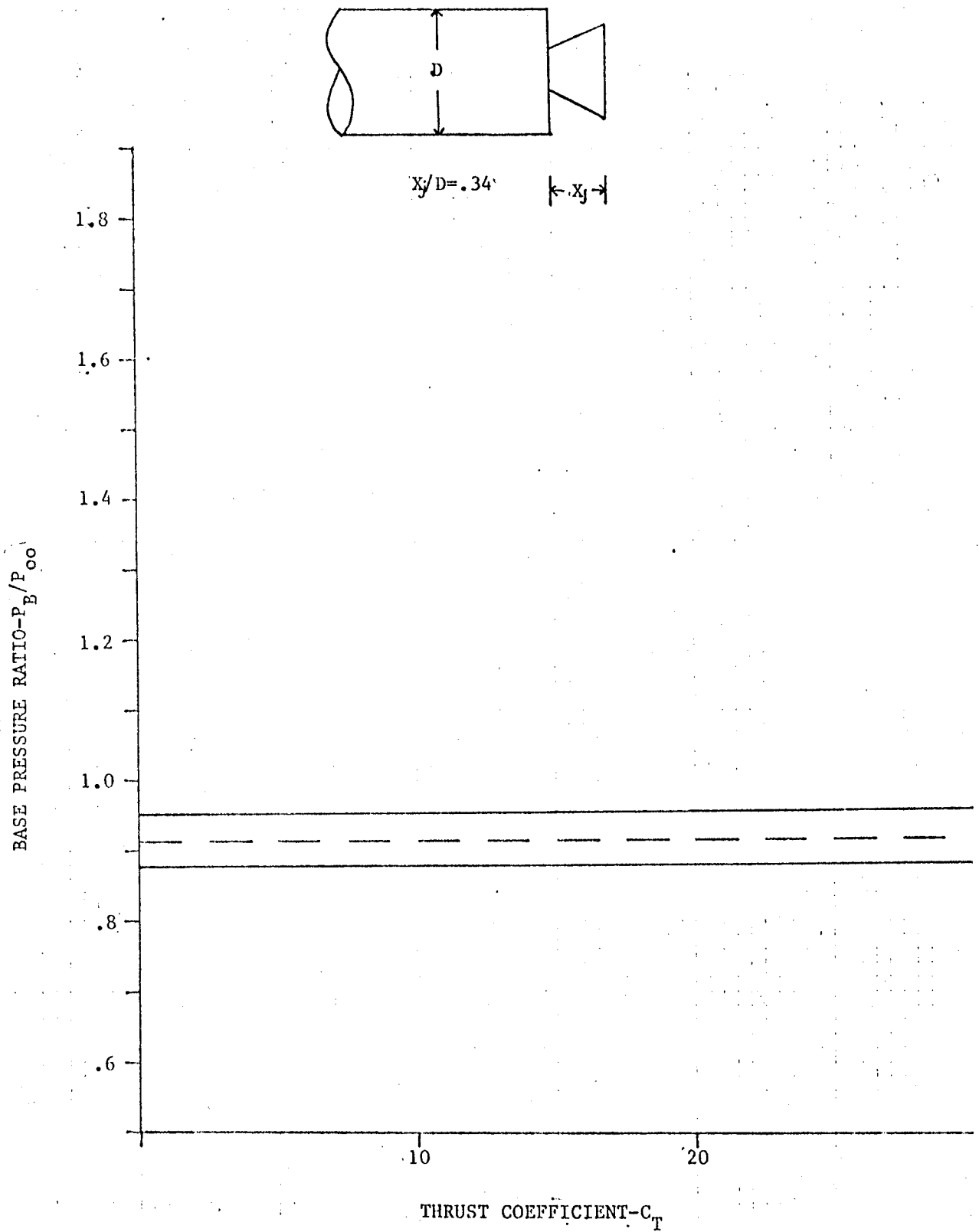
Fig. 3-2 - Base Pressure Ratio Math Model (M_∞ = 0.90)

LOCKHEED-HUNTSVILLE RESEARCH & ENGINEERING CENTER

$M_{oo} = 1.00$
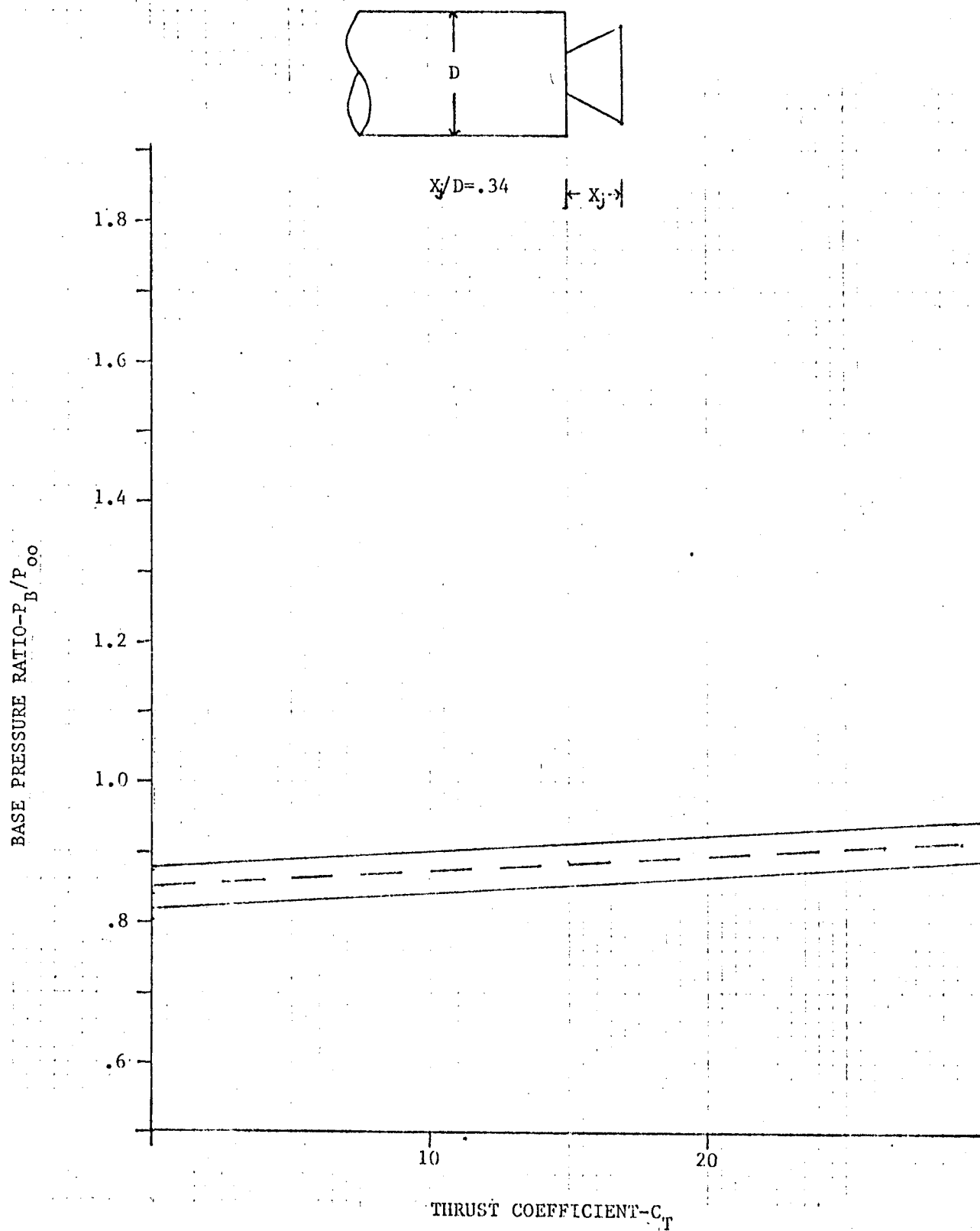
$X_j/D = .34$ $\leftarrow X_j \rightarrow$

Fig. 3-3 - Base Pressure Ratio Math Model ($M_{oo} = 1.00$)
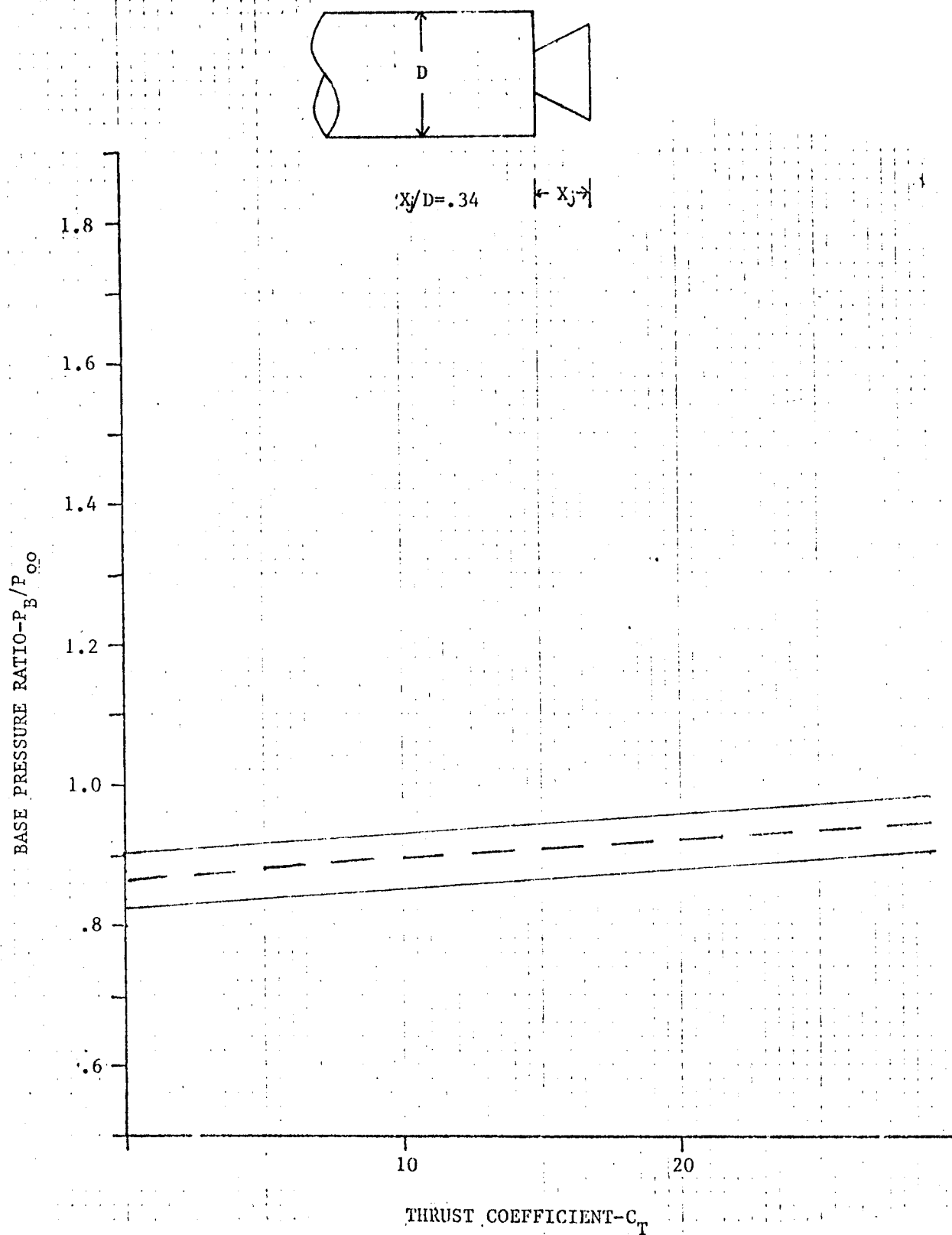
Fig. 3-4 - Base Pressure Ratio Math Model (M_∞ = 1.10)
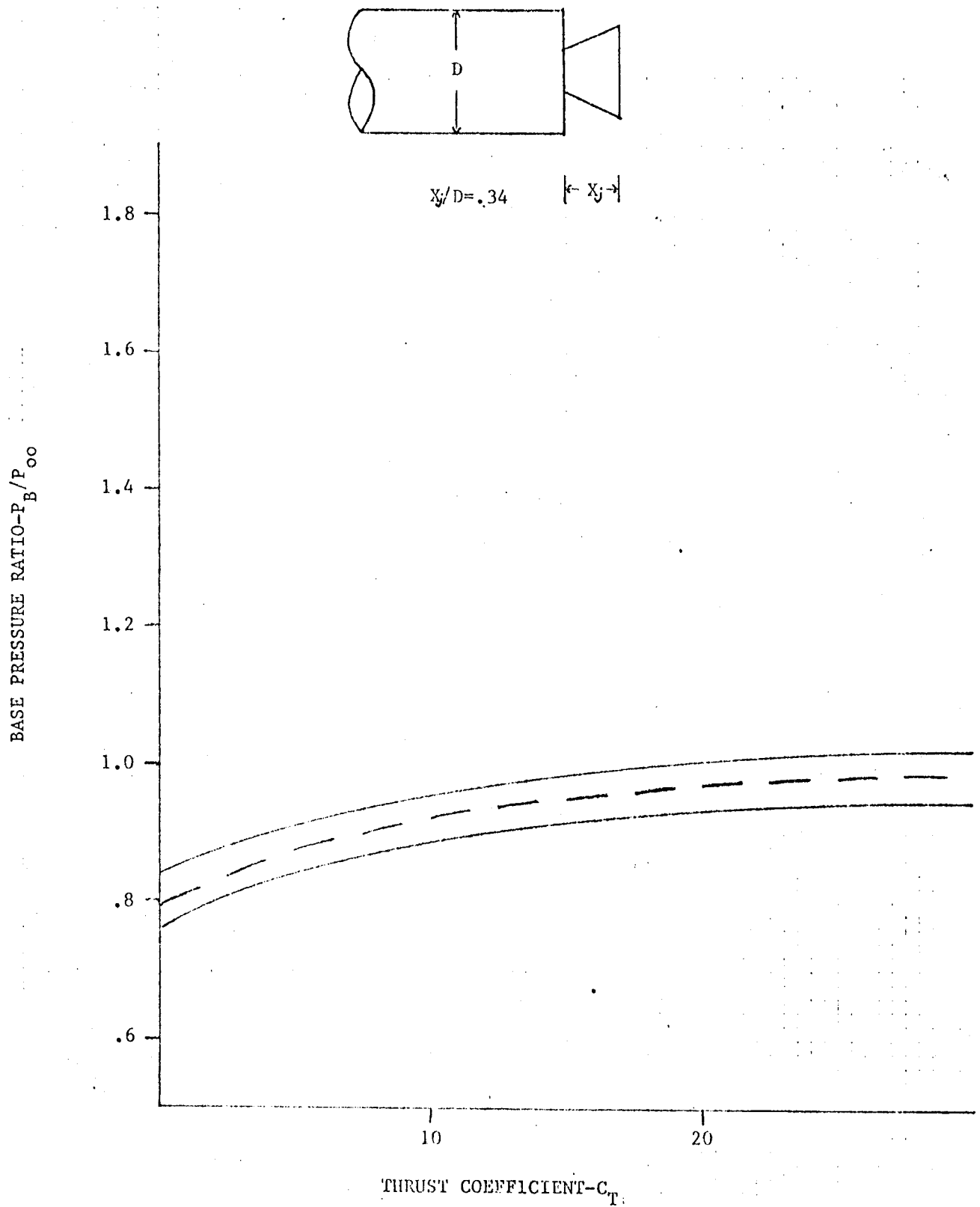
Fig. 3-5 - Base Pressure Ratio Math Model (M_∞ =1.25)

$M_{oo} = 1.50$

$X_j/D = .34$ $|\!\leftarrow X_j \rightarrow\!|$

BASE PRESSURE RATIO–P_B/P_{oo}

1.8

1.6

1.4

1.2

1.0

.8

.6

10   20

THRUST COEFFICIENT–C_T
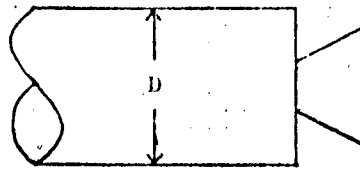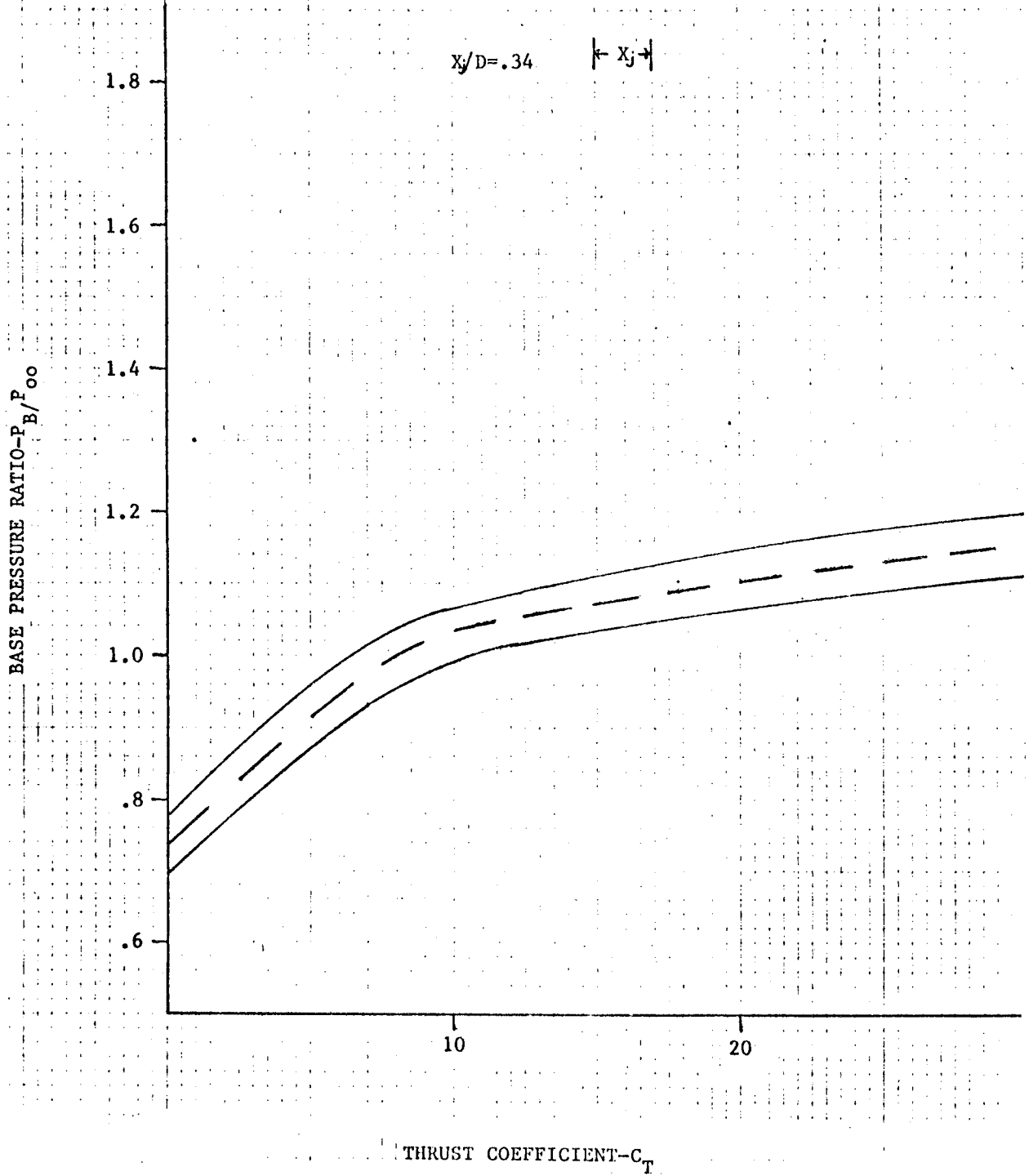
Fig. 3-6 – Base Pressure Ratio Math Model (M_{oo} =1.50)

3-9
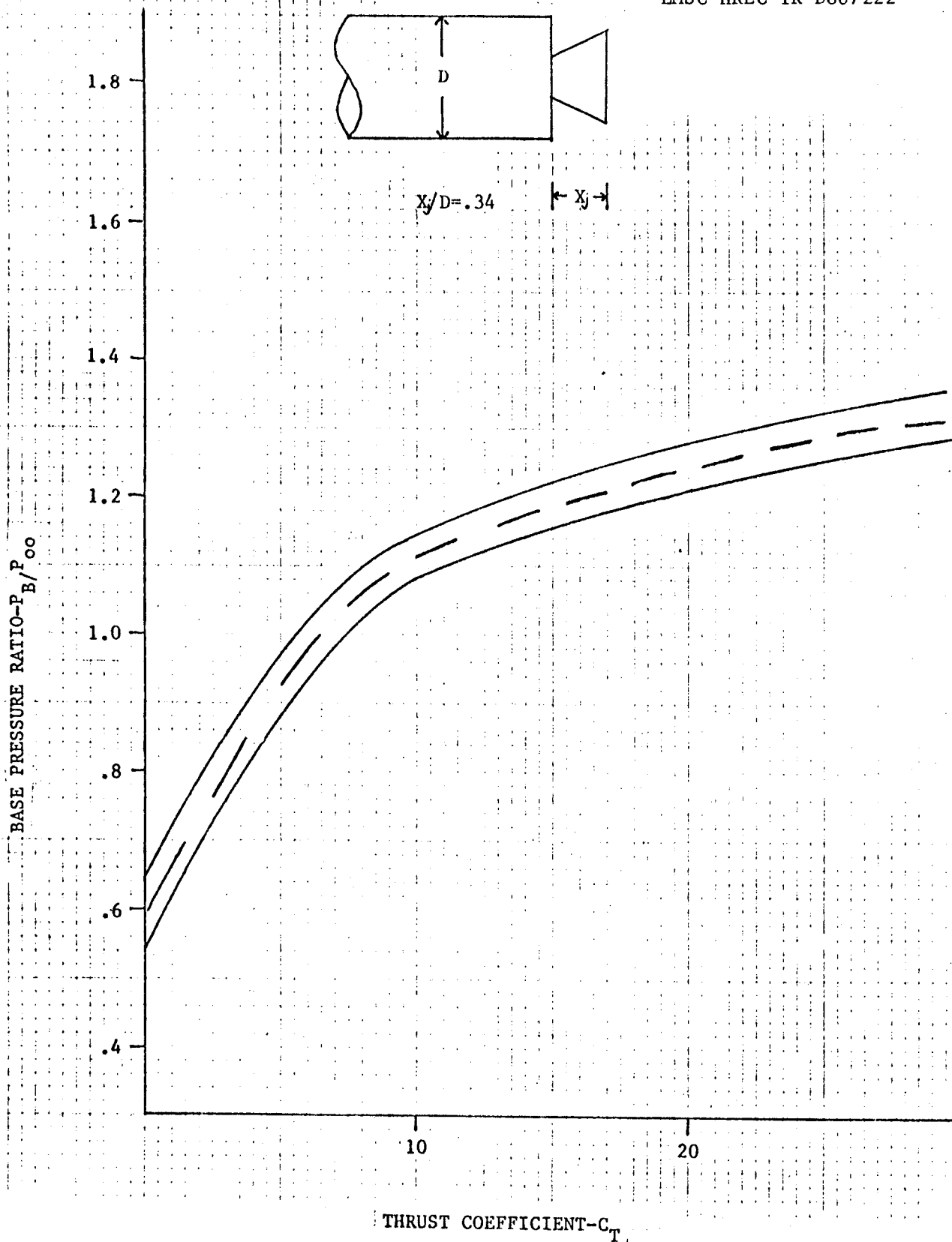
Fig. 3-7 – Base Pressure Ratio Math Model (M_∞ = 1.75)
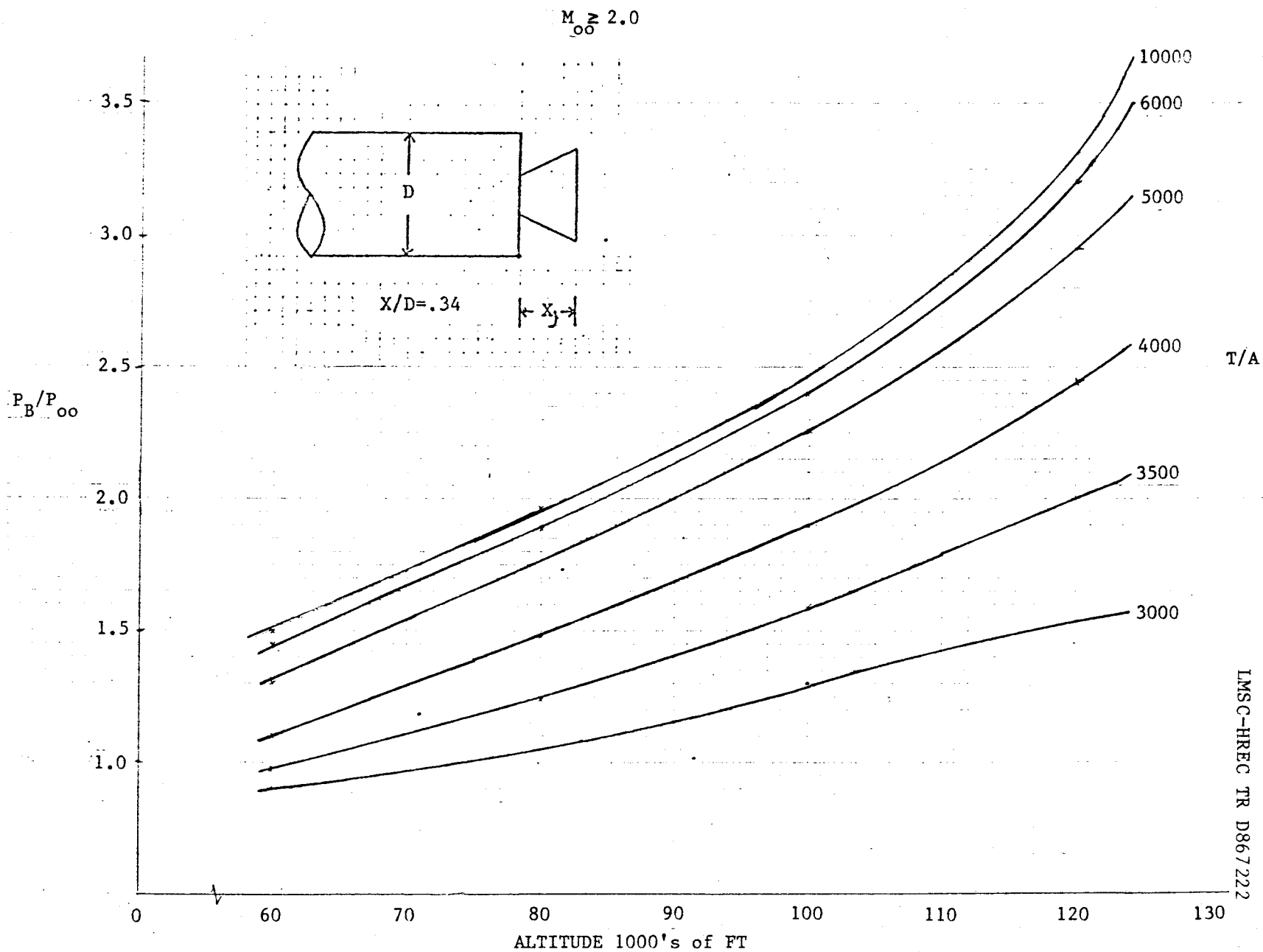
Fig. 3-8 – Base Pressure Math Model ($M \geq 2.0$)

diameters aft of the base. The curves presented in Fig. 3-8 are only for large nozzle spacing ($X/D_E = 2.0$) and plume angles less than 35 deg. For smaller nozzle spacings and larger plume angles, corrections are required as discussed in Section 3.7.

3.5 CORRECTIONS DUE TO NOZZLE EXTENSION

Corrections to the base pressure ratio are required at all Mach numbers if the nozzle position to base diameter is not equal to 0.34. Figure 3-9 should be used to develop the correction to the base pressure due to the nozzle extension ratio being different from 0.34. Configurations with nozzle extension ratios higher than .34 have positive $\Delta X_j/D_B$ and generate positive base pressure ratio increments. Configurations with no nozzle extension have negative values of $\Delta X_j/D_B$ and generate negative base pressure ratio increments.

3.6 CORRECTIONS DUE TO NONCYLINDRICAL BASE

Corrections to the base pressure ratio are required if the configuration has a boattail or a flare forebody configuration. The correction is presented in Fig. 3-10 as a function of the base area to cylindrical base area A_b/A_{cyl}. The noncylindrical base pressure ratio is determined as follows:

$$(P_B/P_\infty)_{cyl} = \text{from Figs. 3-1 through 3-8}$$

$$(P_B/P_\infty)_{non\ cyl} = (P_B/P_\infty{}_{cyl}) \times \left[\frac{1}{P_{B_{cyl}}/P_{B_{non\ cyl}}} \right] \text{(Fig. 3-10)} \quad (3.2)$$

$\Delta X/D_B = X/D_B - .34$

NOTE: $(+)\Delta X/D_B$ GIVES $(+)\Delta P_B/P_{OO}$

$(-)\Delta X/D_B$ GIVES $(-)\Delta P_B/P_{OO}$
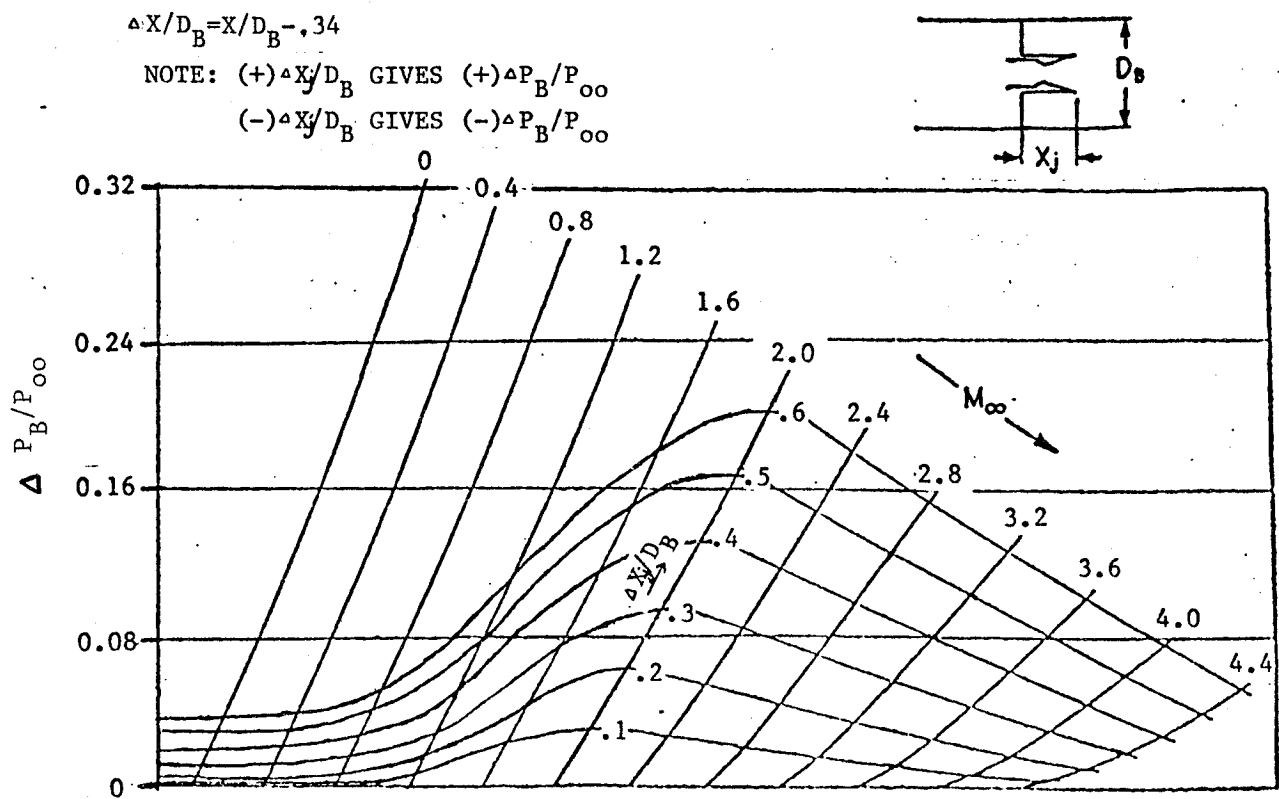
Fig. 3-9 – Correction Due to Nozzle Position

3-13
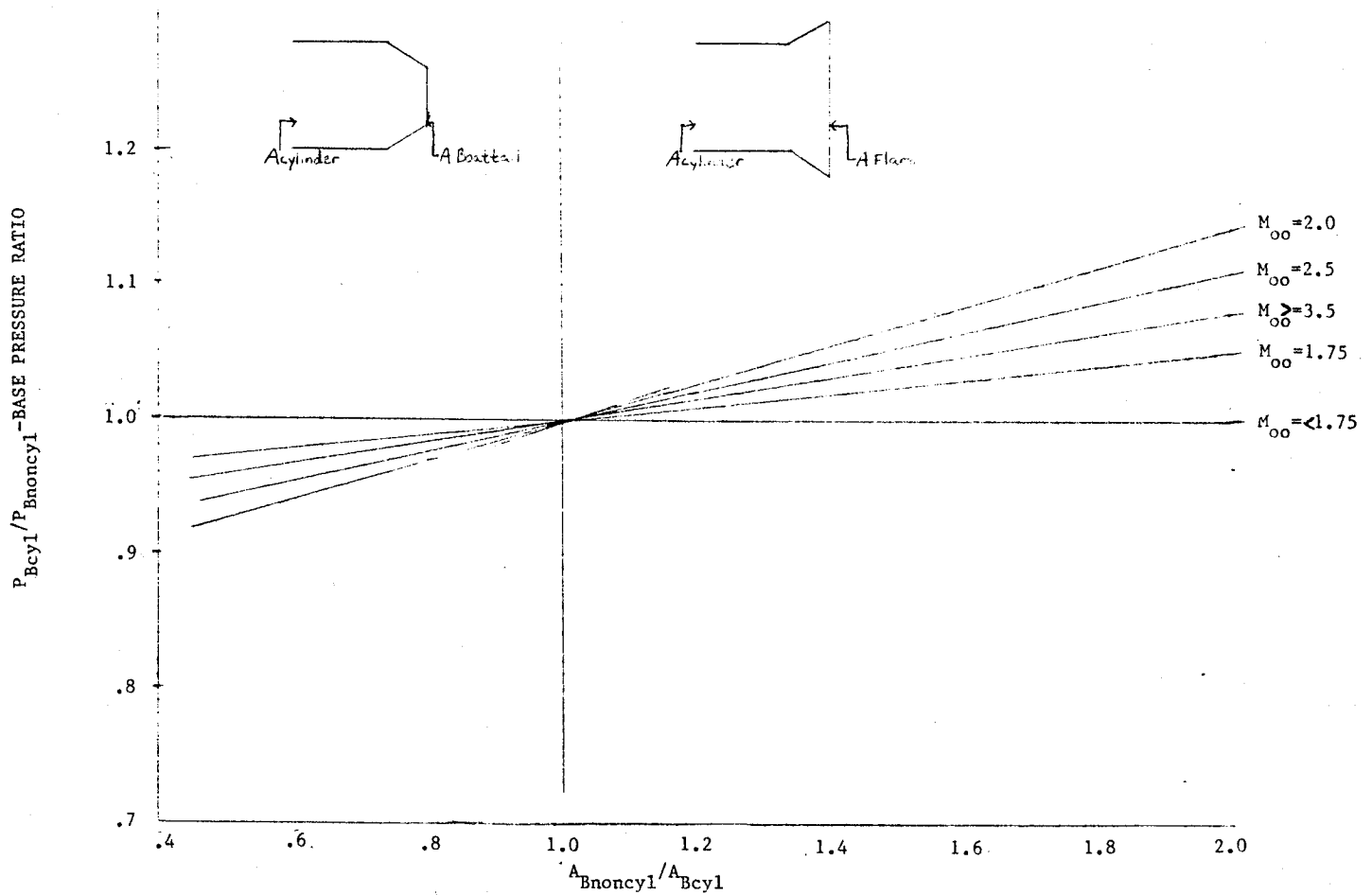
Fig. 3-10 - Base Pressure Ratio versus Base Area Ratio

It is noted that the noncylindrical base pressure correction presented in Fig. 3-10 is a function of Mach number only. This correction is also used for the flight regime for Mach numbers greater than 2.0 since the noncylindrical correction is a Mach number dependent correction to an altitude derived base pressure ratio.

3.7 CORRECTIONS DUE TO NOZZLE SPACING

Configurations with mutli-nozzles that are closely spaced will require corrections to the base pressure ratio due to the interaction of the plumes. The correction to the base pressure ratio is presented in Fig. 3-11 as a function of the plume expansion angle. The base pressure correction is only required for configurations with 3 or 4 nozzles. The base pressure correction is only applicable for the area inside the nozzle boundary shown in Fig. 3-11. When several areas of the base have different levels of base pressure ratio or base pressure coefficients, equation 2.9 is used to determine the area weighted resultant. The corrections to 4 nozzle configurations are large for plume angles of 25 deg and higher. The corrections to 3 nozzle configurations are large for plume angles of 40 degrees and higher.

The plume angle δ_j has no simple formula for determining exact values. Approximations can be made by using the values of δ_j presented in the appendix. The plume angle is a function of the motor chamber pressure, the ambient pressure, and the nozzle area ratio. At a given altitude the plume angle can be approximated by the following equation:

$$\delta_j = K (P_c)^{.8} (\epsilon)^{-.5} \tag{3.3}$$

This equation can be used to approximate the plume angle at a given altitude by solving for K using the motor operating characteristics and plume angle for a similar engine configuration presented in the appendix. Equation 3.3 is then used to determine the value of plume angle for the new engine configuration at the same altitude.

3-15

Careful attention should be given to multi-body configurations that have three or more strap-on propulsion elements and a non-propulsive core stage. The strap on element nozzle spacing is also a consideration at high altitude operation where the plume angles can be large.

3.8 CORRECTIONS DUE TO FINS

The presence of fins near the base of a launch vehicle or rocket affects the vehicle base pressure because the base pressure of the fins is lower than the base pressure of the vehicle. Thus there is a tendancy of the fins to lower the base pressure of the vehicle if the fin trailing edge is near the base. The reduction in base pressure due to fins with a trailing edge near the base of the vehicle can be estimated from the curve presented in Fig. 3-12. The curve is applicable to all Mach numbers. The equation at the top of the figure is used if the fin thickness and number are different from the specified values.

For delta fins the trailing edge thickness (t) and the chord length (c) should be taken at 1/3 semispan from the body. The P_B/P_∞ calculated from the equation shown in Fig. 3-12 should be subtracted from the base pressure ratio.

3.9 PREDICTION UNCERTAINTIES

Estimates of the uncertainty in the prediction of the base pressure ratio are presented in Fig. 3-13. The base pressure ratio uncertainty curve is presented versus Mach number up to Mach 2.0 and then versus altitude to correspond to the math model. The level of uncertaintly covers the variation in the flight data that is considered consistent and the uncertainty in the math model.
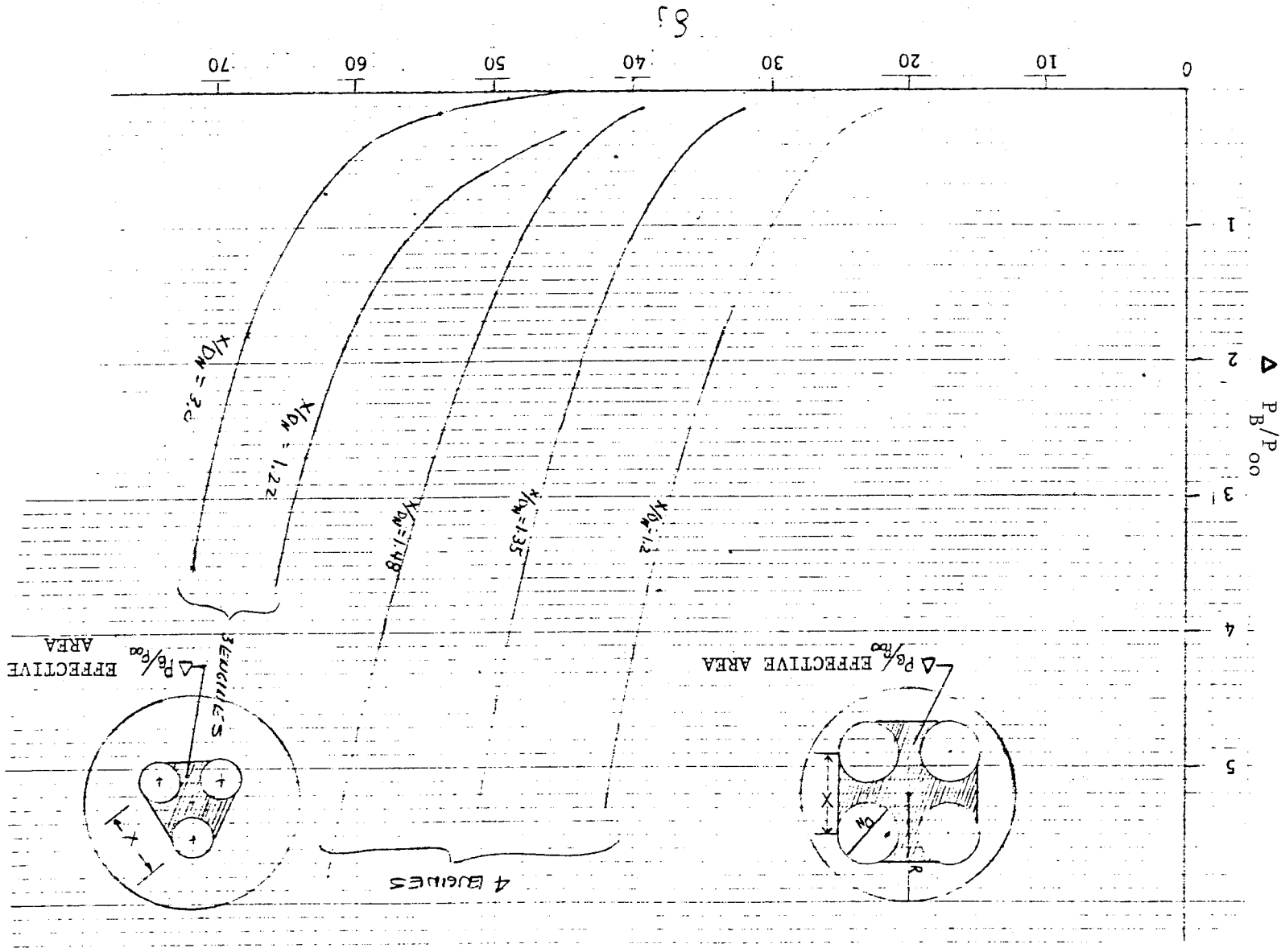
Fig. 3-11 — Correction Due To Nozzle Spacing

t/c=.1
4 FINS
POWER ON

$$\Delta(P_B/P_{OO}) = \Delta(P_B/P_{OO}) \left[(t/c)/.1\right]\left[n/4\right]$$

n= NUMBER OF FINS

t/c @ 1/3 span

FINS AT BASE PLANE
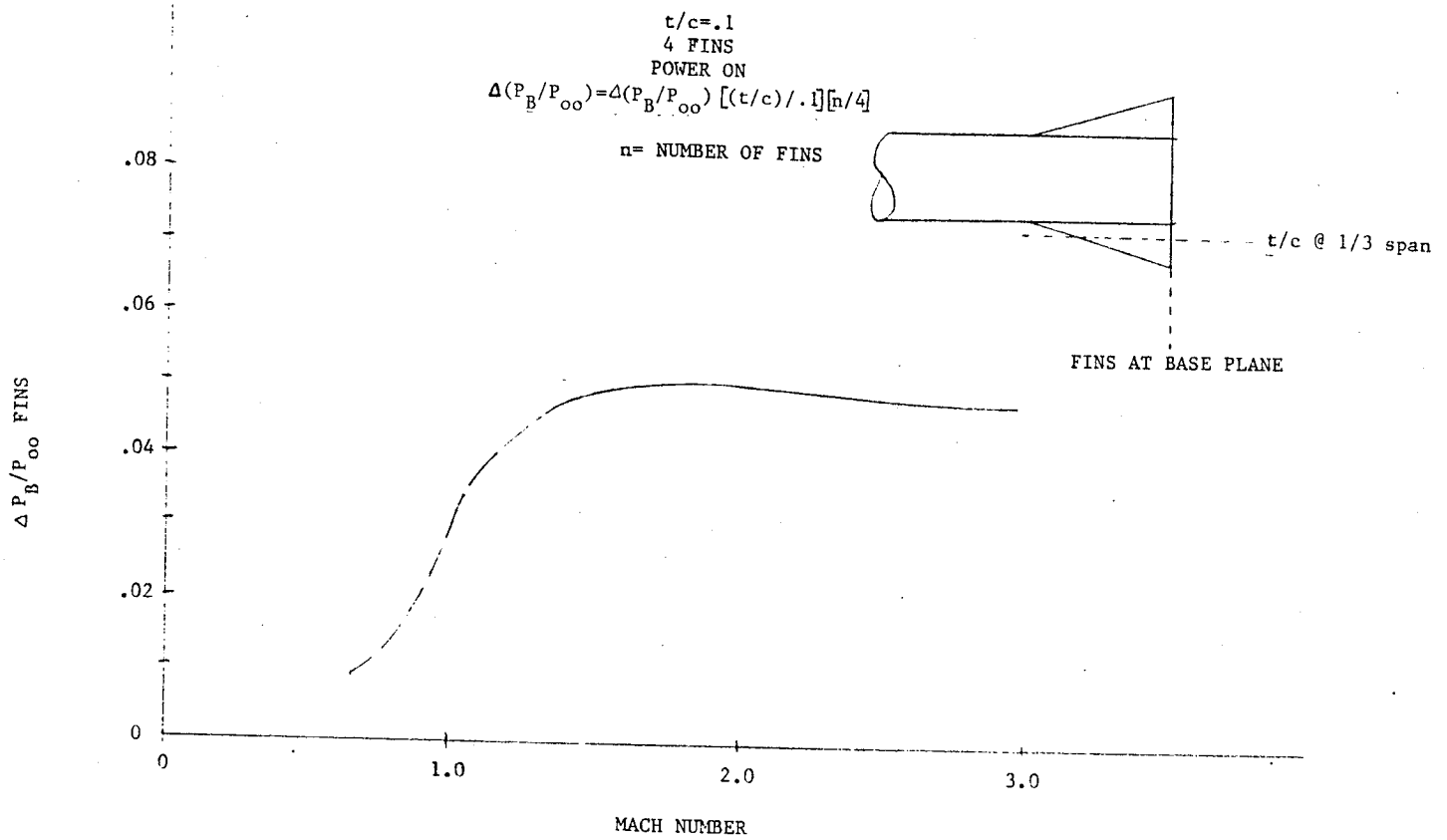
MACH NUMBER

Fig. 3-12 - Correction Due to Fins

3-18

Fig. 3-13 — Base Pressure Prediction Uncertainty

P_B/P_{oo} vs Mach

P_B/P_{oo} vs Mach
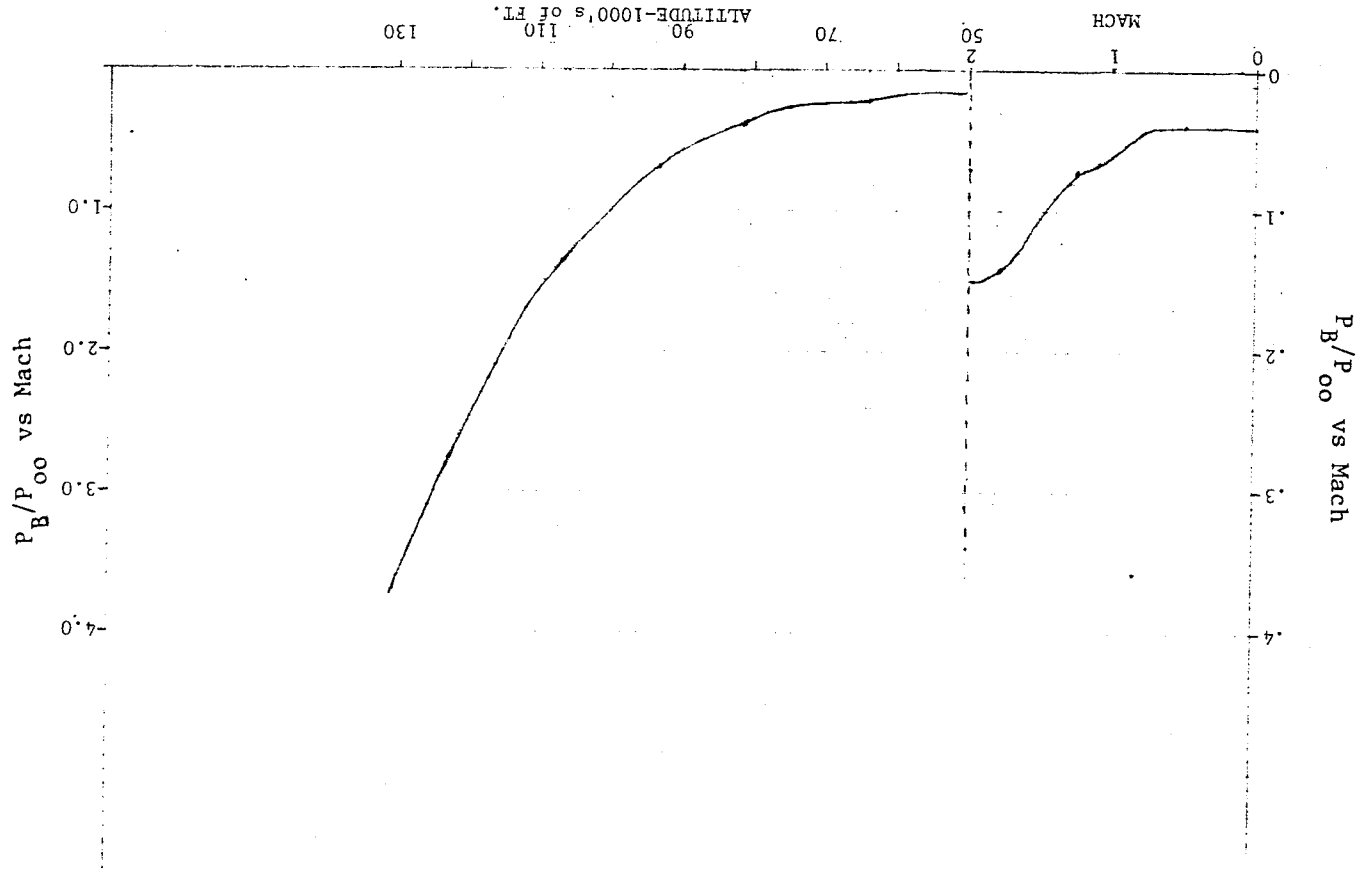
3.10 BASE DRAG MODEL

The base pressure prediction math model will have developed a set of base pressure ratios versus Mach number for the ascent trajectory conditions along with a set of uncertainty base pressure ratios. These data can be converted into base pressure coefficients using Eq. (2.2) and base drag coefficients using Eq. (2.1) or (2.3). Under certain conditions Eq. (2.1) will be required. This will occur if corrections to the base pressure are required due to closely spaced nozzles and large plume angles discussed in Section 3.7. The larger base pressure is confined to an area contained within the nozzle spacing and thus this high pressure area is only active over that portion of the base. The area outside the nozzle ring will not be appreciably influenced. The base drag is calculated by using the following equation:

$$\text{Drag} = C_{D_{BASE}} \, q_\infty \, A_{ref} \tag{3.4}$$

The nominal base drag will be calculated from the nominal base drag coefficient. The uncertainties are calculated from the delta uncertainties and added or subtracted from the nominal.

4. EXAMPLE PROBLEMS

Two example problems are presented to demonstrate the techniques developed for predicting of the base pressure and drag characteristics. The two problems include the Space Shuttle SRB and External Tank (ET). Both of these vehicle elements of the Space Shuttle represented the most difficult to correlate vehicle configurations and use almost all of the data and corrections. The examples are presented below.

4.1 SPACE SHUTTLE SRB EXAMPLE PROBLEM

The SRB example trajectory data are presented in Table 4-1 and represent the trajectory data from STS-2. The Space Shuttle SRB and ET geometry is presented in the Appendix. The thrust coefficient presented in Table 4-1 is calculated using the base area of 236.3 ft^2 up to Mach 2.0. For Mach number greater than 2.0 the base thrust loading T/A is used. The cylindrical to SRB base pressure ratio is obtained from Fig. 3-9. The cylindrical base pressure ratio is converted to a flare base pressure ratio and is noted in the third column of Table 4-2. Corrections due to the nozzle extension being different from 0.34 are neglected since the ΔX/D is only .06. Since this is a single nozzle configuration, no correction for nozzle spacing is required. The nominal value of base pressure ratio is then converted to base pressure coefficients and base drag coefficients using the Space Shuttle reference area of 2690 ft^2.

The uncertainty in the base pressure ratio is obtained from Fig. 3-13. The evaluation of the base pressure ratio including the uncertainties and the development of the base drag coefficient and base drag including uncertainties is presented in Table 4-3.

Table 4-1

STS-2 LEFT SRB ELEMENT TRAJECTORY DATA

Mach	Alt.(ft)	P_{oo}(psf)	q_{oo}(psf)	Left SRB Thrust (lbs.)	C_T (Lft. SRB)	$AB = 236.3\,ft^2$ T/A (lbs/ft^2)
.60	8,975	1523.52	383.93	2597000	28.63	
.80	14,925	1215.36	544.48	2402000	18.67	
.90	18,306	1064.16	603.38	2342000	16.43	
.95	20,118	989.28	624.98	2321000	15.72	
1.05	24,520	825.12	636.79	2281000	15.16	
1.10	26,847	747.36	633.01	2254000	15.07	
1.15	28,647	691.20	639.88	2270000	15.01	
1.25	33,043	568.80	622.13	2340000	15.92	
1.40	38,810	434.88	596.66	2425000	17.20	
1.55	43,995	339.84	571.53	2484000	18.39	
1.80	51,400	236.16	535.61	2523000	19.93	
1.94	55,397	191.00	503.19	2542000	21.38	
2.20	64,169	125.28	424.45	2543000	25.35	10,761
2.50	74,260	77.76	340.20	2372000	29.51	10,038
2.69	81,603	53.00	268.46	2234000	35.22	9,454
3.00	93,710	31.00	195.30	2126000	46.07	8,997
3.29	106,615	17.00	128.81	1942200	63.80	8,218
3.50	122,428	8.64	74.09	1714000	97.90	7,253

LOCKHEED-HUNTSVILLE RESEARCH & ENGINEERING CENTER

Table 4-2

STS-2 – LEFT SRB ELEMENT BASE PRESSURE PREDICTION

Mach	(P_B/P_{oo}) GENE IC	$(P_B/P_{oo})_{SRB}$	C_{P_B}	$C_D^{(1)\ (2)}$ (2 SRB)	Drag (lb.)	Flt. (3) Drag-(lbs)
.60	.95		-.198	.01715	14,944	16,400
.80						
.90	.915		-.150	.0130	21,100	18,980
.95						
1.05	.88		-.155	.0134	22,953	22,997
1.10	.90		-.118	.0102	17,368	19,911
1.25	.95		-.046	.004	6,694	8,697
1.40						
1.55	1.09		+.054	-.0047	-7,225	-6,658
1.80	1.26	1.20	+.088	-.0076	-10,950	-11,231
1.94						
2.20	1.59	1.40	.118	-.0102	-11,646	-12,856
2.50	1.83	1.65	.149	-.0129	-11,800	-11,500
2.69	2.02	1.84	.165	-.0143	-10,327	-9,507
3.00	2.28	2.09	.173	-.0150	-7,870	-7,735
3.29	2.65	2.46	.192	-.0166	-7,984	-8,124
3.50	3.50	3.27	.264	-.0228	-4,538	-3,935

(1) Base Drag Area = $A_{B_{TOTAL}}$ – A_{NOZZLE} = 116.7 ft^2 – One SRB

(2) Reference Aero Space Shuttle = 2,690 ft^2

(3) Using Base Pressure Ratio in Appendix

LOCKHEED-HUNTSVILLE RESEARCH & ENGINEERING CENTER

Table 4-3

STS-2 LEFT SRB ELEMENT BASE PRESSURE PREDICTION TOLERANCE

Col. 1	2	3	4	5	6	7	8	9	10
Alt. (1000 ft) Mach	$(P_B/P_{oo})_{SRB}$	Col. 2 +Flt. Tol.	Col. 2 -Flt. Tol.	+Tol. C_{P_B}	-Tol. C_{P_B}	+Tol. (2 SRB) C_D	-Tol. (2 SRB) C_D	+Tol. Drag lbs.	-Tol. Drag lbs.
.60	.950	.980	.920	-.079	-.317	.006	.028	5228	24398
.90	.915	.967	.863	-.058	-.242	.005	.021	8116	34085
1.05	.880	.943	.817	-.074	-.237	.006	.021	10278	35972
1.10	.900	.967	.833	-.039	-.197	.003	.017	5108	28948
1.25	.950	1.023	.877	.021	-.112	-.002	.010	-3347	16735
1.80	1.200	1.342	1.058	.151	.026	-.013	-.002	-18730	-2882
64.1 2.20	1.400	1.610	1.190	.180	.056	-.016	-.005	-18268	-5709
74.7 2.50	1.650	1.930	1.370	.213	.085	-.018	-.007	-16472	-6406
81.6 2.69	1.840	2.230	1.450	.243	.089	-.021	-.008	-15165	-5777
93.7 3.00	2.090	2.800	1.380	.286	.06	-.025	-.005	-13134	-2627
106.6 3.29	2.460	3.840	1.080	.375	.011	-.033	-.001	-11435	-346
122.4 3.50	3.270	6.040	.500	.588	-.058	-.051	.005	-10164	997

LOCKHEED-HUNTSVILLE RESEARCH & ENGINEERING CENTER
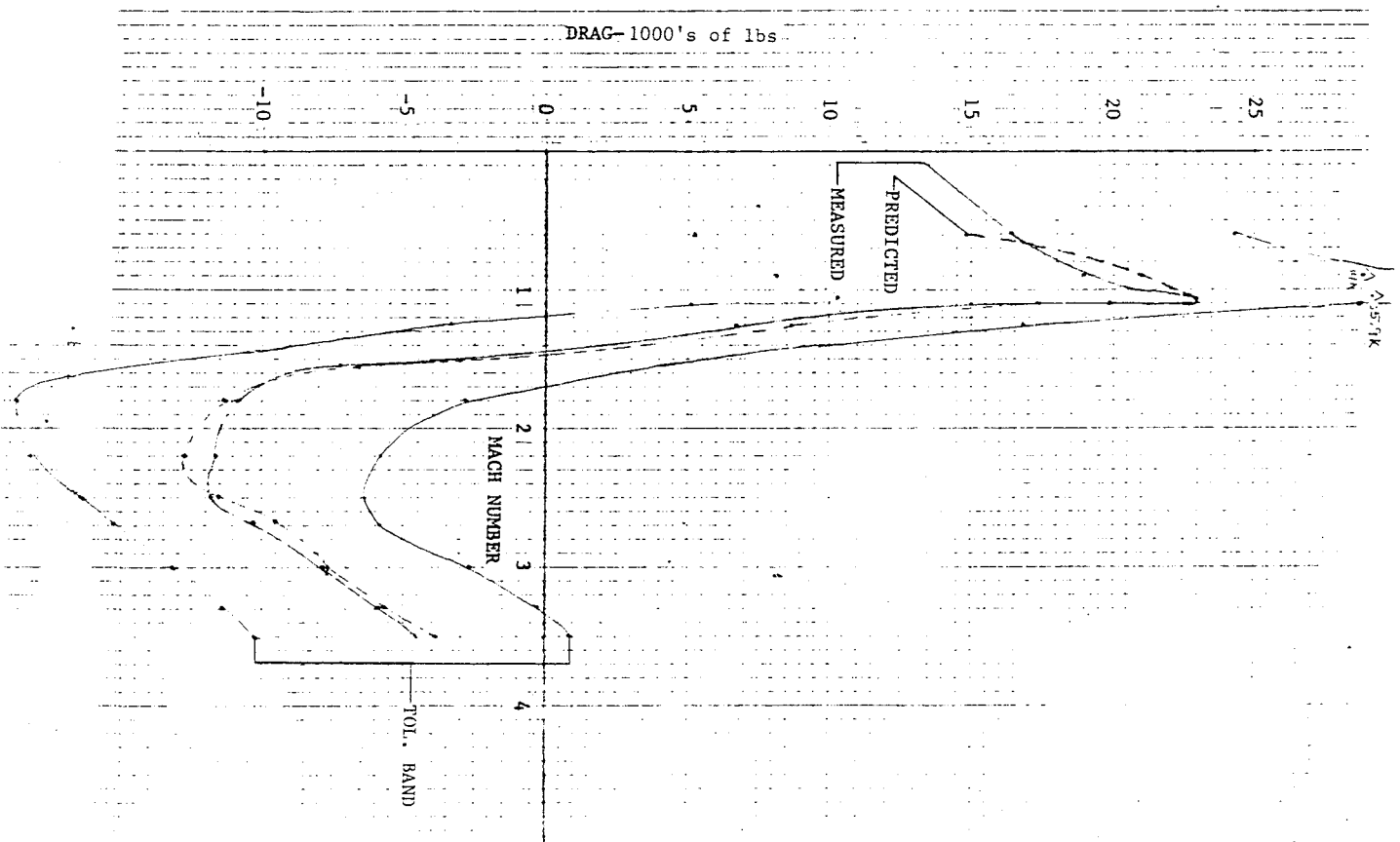
Fig. 4-1 – Comparison of Predicted and Measured Space Shuttle SRB
Drag Force with Tolerance Band

The base drag and base drag uncertainty is calculated using Eq. (3.6) and the Table 1 dynamic pressure. A comparison of the STS-2 SRB base drag based on actual flight measured pressure data with the calculated base drag is presented in Fig. 4-1. The uncertainties in the base drag are also presented in the figure.

4.2 SPACE SHUTTLE EXTERNAL TANK EXAMPLE PROBLEM

The Space Shuttle ET trajectory data are the same as the SRB. Thus the ascent trajectory data are the same and are presented in Table 4-4. The thrust coefficient is determined using the total thrust of both SRBs and all three SSMEs as shown in the table. The base area includes all elements. The basic ET base pressure ratio is taken from Figs. 3-1 to 3-7 for Mach numbers less than 2.0. For Mach numbers of 2.0 and greater the basic base pressure ratio is taken from Fig. 3-8. The value of T/A is noted in Table 4-4. The data require correction due to the position of the SRB nozzles being farther aft than the basic X/D of 0.34. The X/D position of the SRBs is $300/524.5_{eq.}$ = 0.57 (see appendix). The SSMEs have a X/D of .3 thus the average X/D = 0.48. The correction to the base pressure ratio due to the SRB nozzle extension is taken from Fig. 3-10 for a ΔX/D of 0.14 to be less than .04 and thus it is neglected. An additional correction to the ET data is required at high altitudes due to the effective triple nozzle spacing and the high plume angles. The correction due to plume angle is taken from Fig. 3-11 using the values of δ_j for the SRB from the Appendix. These corrections modify the total ET base pressure since the ET is within the nozzle ring. The corrected ET base pressure ratios are presented in the fifth column of Table 4-5. The base drag coefficient is calculated from the base pressure coefficient and the base area of 600 ft^2 and a reference area of 2690 ft^2. The base drag is calculated using the STS-2 flight dynamic pressure from Table 4-4. The uncertainty in the base pressure ratio is obtained from Fig. 3-13. The evaluation of the base pressure ratio, including uncertainties, and the development of the uncertainty in base drag is presented in Table 4-6. A comparison of the ET

4-6

flight base drag and the calculated ET base drag is presented in Fig. 4-2 along with the uncertainty in the calculated ET base drag.

The predicted base drag is noted to be close to the flight value and the tolerance on the prediction covers the flight drag curve.

Table 4-4 STS-2 EXTERNAL TANK TRAJECTORY DATA

Mach	Alt.(ft)	P_{oo}(psf)	q_{oo}(psf)	Thrust (lb.) Total	A_B=1500 ft^2* C_T	T/A (LB/ft^2)
.60	8,975	1523.52	383.93	6417000	11.14	
.80	14,925	1215.36	544.48	6064000	7.43	
.90	18,306	1064.16	603.38	5961000	6.59	
.95	20,118	989.28	624.98	5762000	6.15	
1.05	24,520	825.12	636.79	5407000	5.66	
1.10	26,847	747.36	633.01	5359000	5.64	
1.15	28,647	691.20	639.88	5401000	5.63	
1.25	33,043	568.80	622.13	5556000	5.95	
1.40	38,810	434.88	596.66	5820000	6.50	
1.55	43,995	339.84	571.53	6335000	7.39	
1.80	51,400	236.16	535.61	6429000	8.00	
1.94	55,397	191.00	503.19	6474000		4,316
2.20	64,169	125.28	424.45	6487000		4,325
2.50	74,260	77.76	340.20	6151000		4,101
2.69	81,603	53.00	268.46	5873000		3,915
3.00	93,710	31.00	195.30	5662000		3,775
3.29	106,615	17.00	128.81	5294200		3,529
3.50	122,428	8.64	74.09	4840000		3,227

$$* \; A_{BASE} = A_{B_{ORB}} + A_{B_{ET}} + A_{B_{(2\,SRB's)}}$$

Table 4-5 STS-2 EXTERNAL TANK BASE PRESSURE PREDICTION

Mach	(P_B/P_{oo}) GENERIC	δ_j – SRB App. A (Deg)	$\Delta(P_B/P_{oo})$	$(P_B/P_{oo})_{ET}$	C_{P_B}	C_D	Drag(lbs)	Drag-Flt. (lbs)
.60	.95			.95	−.198	.0441	45,545	48,835
.80								
.90	.915			.915	−.150	.033	53,562	60,458
.95								
1.05	.86			.86	−.181	.040	68,520	70,683
1.10	.88			.88	−.142	.032	54,489	68,365
1.15								
1.25	.88			.88	−.110	.025	41,838	51,512
1.40								
1.55	.98			.98	−.012	.0026	3,997	5,829
1.80	1.07			1.07	+.031	−.007	−10,085	−9,962
1.94								
2.20	1.25	49.2	.05	1.30	.088	−.0196	−22,378	−25,721
2.50	1.40	54.0	.15	1.55	.126	−.028	−25,623	−27,352
2.69	1.47	59	.35	1.82	.162	−.036	−25,997	−27,866
3.00	1.65	63.5	.8	2.45	.230	−.052	−27,318	−27,421
3.29	1.72	68	1.80	3.52	.332	−.074	−25,641	−25,813
3.50	1.75	72	3.5	5.25	.495	−.110	−21,923	−23,338

LOCKHEED-HUNTSVILLE RESEARCH & ENGINEERING CENTER

Table 4-6

STS-2 EXTERNAL TANK BASE PRESSURE PREDICTION TOLERANCE

Col. 1	2	3	4	5	6	7	8	9	10
			Col. 2 +Flt. Tol.	Col. 2 -Flt. Tol.	+Tol. C_{P_B}	-Tol. C_{P_B}	+Tol. C_D	-Tol. C_D	+Tol. Drag-lbs.	-Tol. Drag-lbs.
Alt. (1000 ft)	Mach	$(P_B/P_{oo})_{ET}$								
	.60	.950	.980	.920	-.079	-.317	.018	.071	18590	73327
	.90	.915	.967	.863	-.058	-.242	.013	.054	21100	95762
	1.05	.860	.923	.797	-.100	-.263	.022	.059	37685	101065
	1.10	.880	.947	.813	-.063	-.221	.014	.049	23839	83437
	1.25	.880	.953	.807	-.043	-.176	.010	.039	16735	65268
	1.80	1.070	1.212	.928	.093	-.032	-.021	.007	-30257	10086
64.1	2.20	1.300	1.510	1.090	.151	.027	-.034	-.006	-38820	-6851
74.7	2.50	1.550	1.830	1.270	.190	.062	-.042	-.014	-38436	-12812
81.6	2.69	1.820	2.210	1.430	.239	.085	-.053	-.019	-38274	-13721
93.7	3.00	2.450	3.160	1.740	.343	.117	-.077	-.026	-40453	-13659
106.6	3.29	3.520	4.900	2.140	.515	.150	-.115	-.033	-39847	-11435
122.4	3.50	5.250	8.020	2.480	.819	.173	-.183	-.039	-36472	-7773

LOCKHEED-HUNTSVILLE RESEARCH & ENGINEERING CENTER
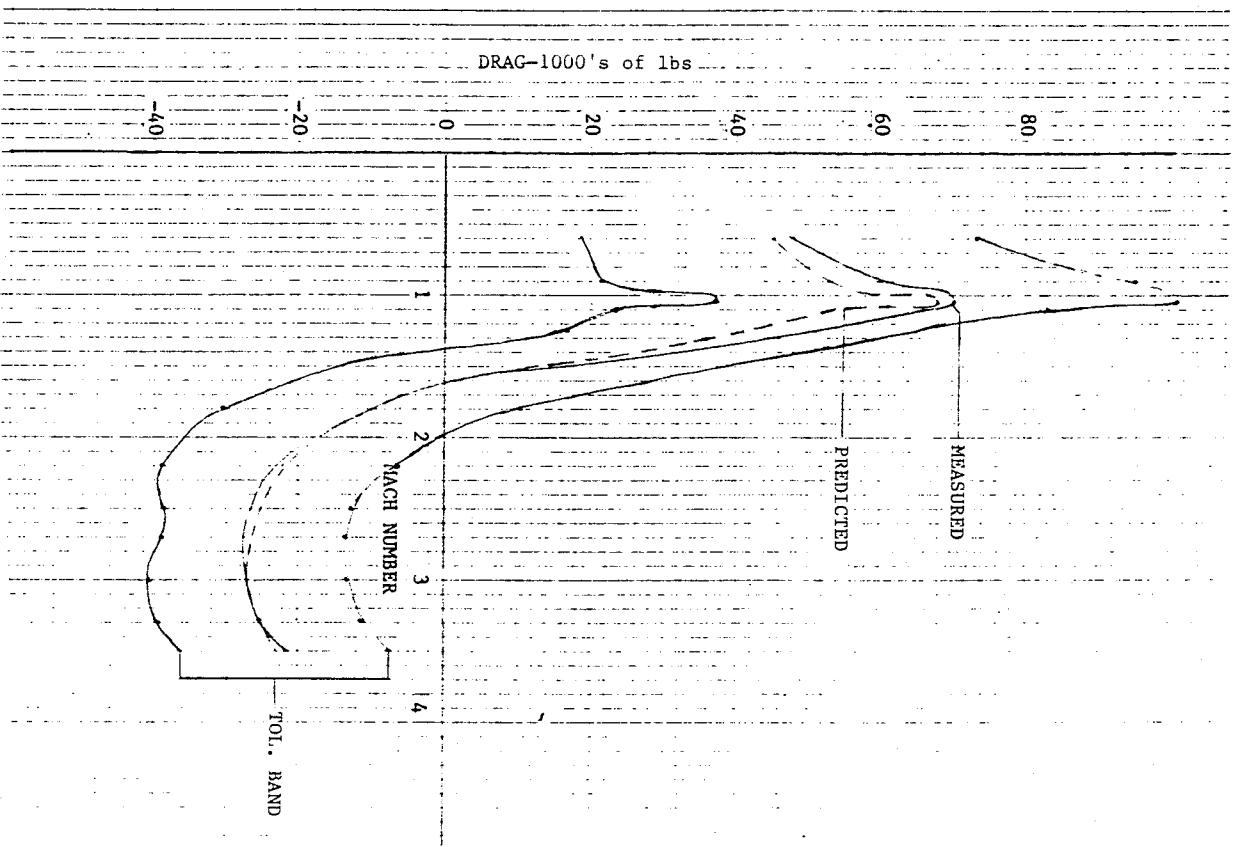
Fig. 4-2 – Comparison of Predicted and Measured Space Shuttle
ET Drag Force with Tolerance Band

5. CONCLUSIONS

A compendium of flight measured base pressure on a variety of launch vehicles and rockets has been assembled and formulated into a math model for prediction of flight base pressure environments and drag characteristics during power on ascent flight. The math model is applicable for single-nozzle, multi-nozzle, and multi-body configurations. Methods are presented to evaluate the base pressure environment, base drag coefficient, and drag forces at near zero angle of attack. Uncertainties are presented that allow for variation in the flight measured data and the math model.

The example problems utilizing elements of the Space Shuttle vehicle have shown the model is accurate and will be useful in the prediction of flight base pressure on new vehicle concepts.

The math model uses the thrust coefficient formulation at low altitudes and altitude correlation with thrust loading at high altitudes. These variables allow the rapid prediction of the base pressure environment, base drag coefficient, and base drag within reasonable uncertainty levels.

LOCKHEED-HUNTSVILLE RESEARCH & ENGINEERING CENTER

6. RECOMMENDATIONS

The analysis of the flight base pressure math model identified several areas where additional work would improve the model. These additional areas are base bleed influence from engine turbopump exhaust and nozzle exhauster-ators, the influence of plume angle, δ_j, and the influence of base air scoops that were on the Saturn V 501 and certain Saturn 1 stages.

It is also recommended that additional data be added to the data base. Additonal data is available on the Minuteman, Polaris, and Atlas vehicles.

LOCKHEED-HUNTSVILLE RESEARCH & ENGINEERING CENTER

7. REFERENCES

1. Brazzell, C. E., and J. H. Henderson, "An Empirical Technique for Estimating Power-On Base Drag of Bodies-of-Revolution with a Single Jet Exhaust," Proceedings of a Specialists' Meeting Sponsored by the AGARD Fluid Dynamics Panel Held in Mulhouse, France, 5-8 September 1966.

2. Brazzel, C. E., "Estimated Power-On Base Drag for a Rocket-Assisted Projectile," RD-TM-70-7, U.S. Army Missile Command, Redstone Arsenal, Ala., July 1970.

3. Hastings, R. C., and J. Reid, "The Effect of a Central Set on the Base Pressure of a Cylindrical Afterbody in a Supersonic Stream," RAE Report Aero 2621, Royal Aircraft Establishment, Farnborough, England, December 1959.

4. Penny, M. M., and P. R. Sulyma, "Development of Base Pressure Similarity Parameter for Application to Space Shuttle Launch Vehicle Power On Aerodynamic Testing," NASA Contract NAS8-32658, Marshall Space Flight Center, Huntsville, Alabama, September 1978.

5. Charczenko, N., and C. Hayes, "Jet Effects at Supersonic Speeds on Base and Afterbody Pressures of a Missile Model Having Single and Multiple Jets," NASA TND-2046, November 1963.

6. Blackwell, K. L. and L. M. Hair, "Space Shuttle Afterbody Aerodynamics/ Plume Simulation Data Summary," NASA Technical Paper 1384, Marshall Space Flight Center, Huntsville, Alabama, December 1978.

7. "S-IB Stage Environmental Summary Flight Evaluation," Report TN-AP-68-333, Chrysler Corporation, Space Division, Huntsville, Ala., July 1968.

8. Honeywell, E. E., "Completion of Power-Off Base Drag Data and Empirical Methods for Predicting Power-Off Base Drag," Report No. TM 334-337, Convair, Pomona, Calif., 1959.

9. Boren, T. C., and W. Hatalsky, "Jet Effects Upon Base Drag," Report P-63-6-534-399, General Dynamics, Pomona, Calif., 1964.

Appendix

VEHICLE CONFIGURATIONS ENGINE CHARACTERISTICS AND
SOURCE FLIGHT BASE PRESSURE DATA

Appendix

The Appendix contains the source flight test base pressure data used in the analysis. The source data is presented in the published form for reference along with tabulations in the form of base pressure coefficients and base pressure ratios correlated to trajectory data. Also included is the base and engine area, trajectory, and base pressure data for each vehicle. The Appendix is divided into single engine, multi-engine, and multi-body headings. Reference sources are listed under each vehicle heading.

REDSTONE

REDSTONE

The Redstone missile was an Army field artillery tactical missile designated as a medium range (less than 500 miles) ballistic (projectile) type rocket. It was guided from lift-off to impact by an inertial guidance and control system. Its primary function was for tactical field operations by U.S. Army personnel (field artillery missile battalions) in order to provide general support for a field Army, to fulfill requirements for a medium range missile, to supplement or extend range of firepower of existing artillery weapons, to provide increasd heavy power fire support for deployed ground forces, and to compensate for expanding dimensions of battle areas.

The Redstone's overall length is approximately 69 ft and its approximate weight is 16,500 lb when empty and 61,300 lb when fully loaded with fuel and payload. The missile is divided into two main sections - the body unit and the thrust unit. The body unit is divided into two sections - the aft section which houses the guidance and control instruments and is constructed of an alloy steel skin and aluminum ring frames, and the warhead section which houses the payload and is constructed of an alloy steel skin and ring frames. The thrust unit is also divided into two sections, the center section and the tail section. The center section carries the fuel and the liquid oxygen used to power the rocket motor and is constructed of an aluminum skin and ring frames. The tail section houses the rocket engine and supports the control surfaces and is constructed of an aluminum skin and ring frames.

The engines used in the flights RS-2, RS-7, and RS-11 were bipropellant type developing a nominal 78,000 lb thrust at sea level without the carbon jet vanes. The propellants used were LOX and 75% ethyl alcohol at a nominal mixture ratio of 1.354 at sea level conditions. An electrically fired pyrotechnic ignitor is used to initiate combustion. The chamber pressure was initially 300 psia at sea level and peaked after about 30 to 40 sec after which it slowly decayed until cutoff.

A-2

Powered flight thrust vector control is provided by vanes that entered into the airstream and nozzle exhaust. The thrust values do not account for the jet vane losses.

The Redstone configuration and engine operating characteristics are presented in Figs. A-1 and A-2. Redstone trajectory data are presented in Figs. A-3 and A-4. The trajectory data for the Redstone missile flights RS-2, RS-7 and RS-11 were estimated from trajectories of other Redstone missiles. The Redstone engine thrust versus altitude and plume expansion angle are presented in Figs. A-5 and A-6. The thrust versus altitude was estimated. The most probable engine thrust versus altitude is noted in the figure as A-3 corresponding to the A-3 engine characteristic from Reference 1. The error included by not using the curve labeled A-3 in the analysis has been estimated to be very small and thus the Redstone thrust values were not changed.

The plume expansion angle presented in Figure A-6 was estimated from the nozzle operating characteristics presented in Figs. A-1 and one-dimensional isentropic gas tables. The source base pressure data for the Redstone is presented in Fig. A-7. These data were obtained from Reference 1. The Redstone trajectory data, thrust, and base pressure characteristics are presented in Tables A-1 and A-2. The nominal base pressure coefficient presented in Table A-2 is an average through the flight measured data. The nominal base pressure ratio was derived from the nominal base pressure coefficient. The maximum and minimum base pressure coefficient was estimated from the most probable variation of the flight test data presented in Fig. A-7. The maximum and minimum base pressure ratio correspond to maximum and minimum base pressure coefficient. This method of developing flight measured base pressure variation is used when data from multiple flights is available.

REDSTONE REFERENCES

1. Ordnance Missile Laboratories, 1 September - 30 November 1955, Report No. 18, Field Artillery Guided Missile System (Redstone), Project TU-1-2030.

2. "Overall Study and Flight Evaluation of the Redstone Missile and Associated Systems," Report No. RP-TR-61-11, U. S. Army Ballistic Missile Agency, Redstone Arsenal, Ala., 7 April 1961.

3. "Aeroballistic Evaluation of Redstone Test Flight CC-45," Report No. DA-M-15-58, U.S. ARmy Ballistic Missile Agency, Redstone Arsenal, Ala., 25 April 1958.

LOCKHEED-HUNTSVILLE RESEARCH & ENGINEERING CENTER
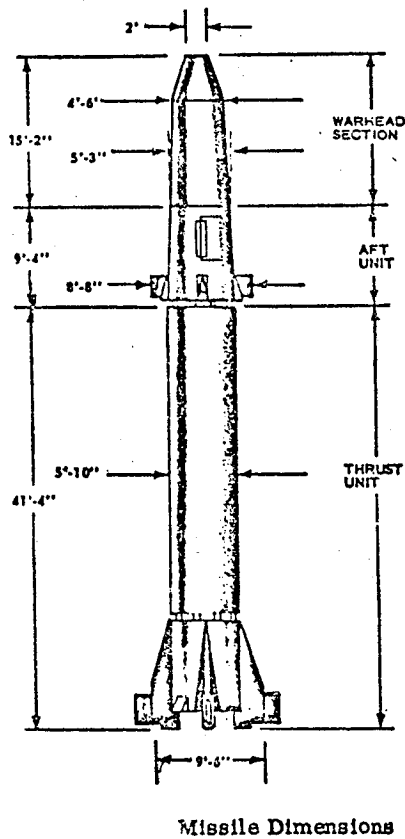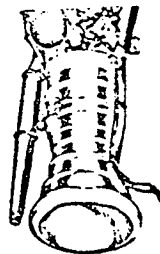
REDSTONE

Rocket Engine LR43-NA-1

Missile Dimensions

ENGINE: ROCKETDYNE LR43-NA-1

THRUST: 78000 lb S.L. LOX ALCOHOL

87700 lb VAC

P_c : 317.5 psi

P_E ; 13.5 psi

γ_E : 1.20

M_E : 2.65

Dia. : 29.05 in

θ_L = 5°

ϵ : 3.61

AIR RUDDERS (4)

TAIL UNIT

CARBON JET VANES (4)
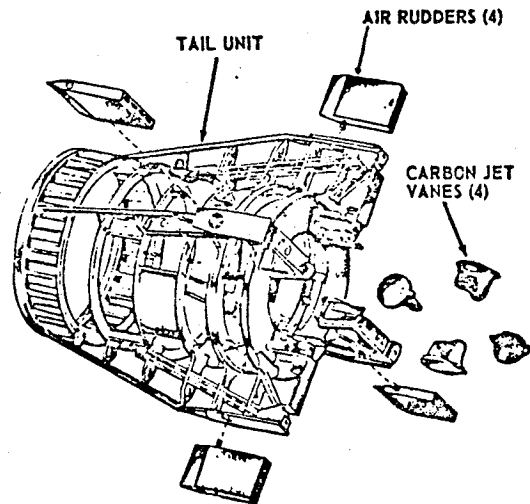
Fig. A-1 – Redstone Missile Configuration and Engine Characteristics
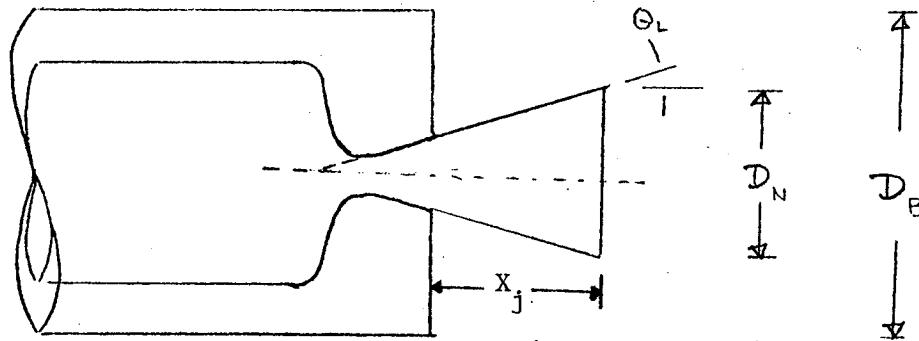
D_B= 70.00 in A_B= 26.70 ft^2

D_N= 29.05 in. A_N/A_B= .172

X_j= 0 X_j/D_B= 0

θ_L= 5°

Fig. A-2 - Base Geometry - Redstone
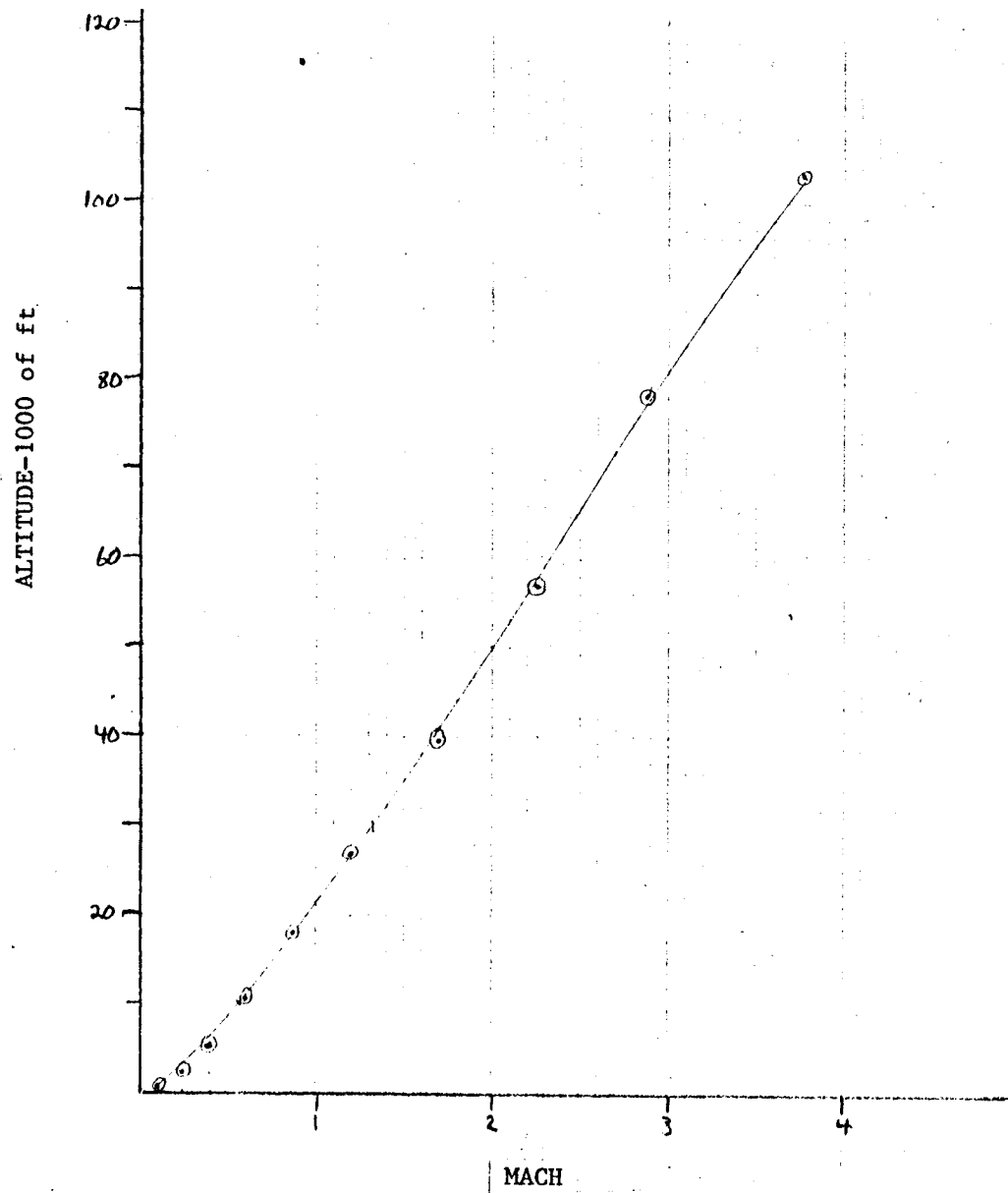
LOCKHEED-HUNTSVILLE RESEARCH & ENGINEERING CENTER

Fig. A-3 - Flight Altitude versus Mach Number - Redstone

LOCKHEED-HUNTSVILLE RESEARCH & ENGINEERING CENTER

DYNAMIC PRESSURE-q_{oo}-psf

MACH

Fig. A-4 — Flight Dynamic Pressure versus Mach Number — Redstone

LOCKHEED-HUNTSVILLE RESEARCH & ENGINEERING CENTER

A-8

LMSC-HREC TR D867 222
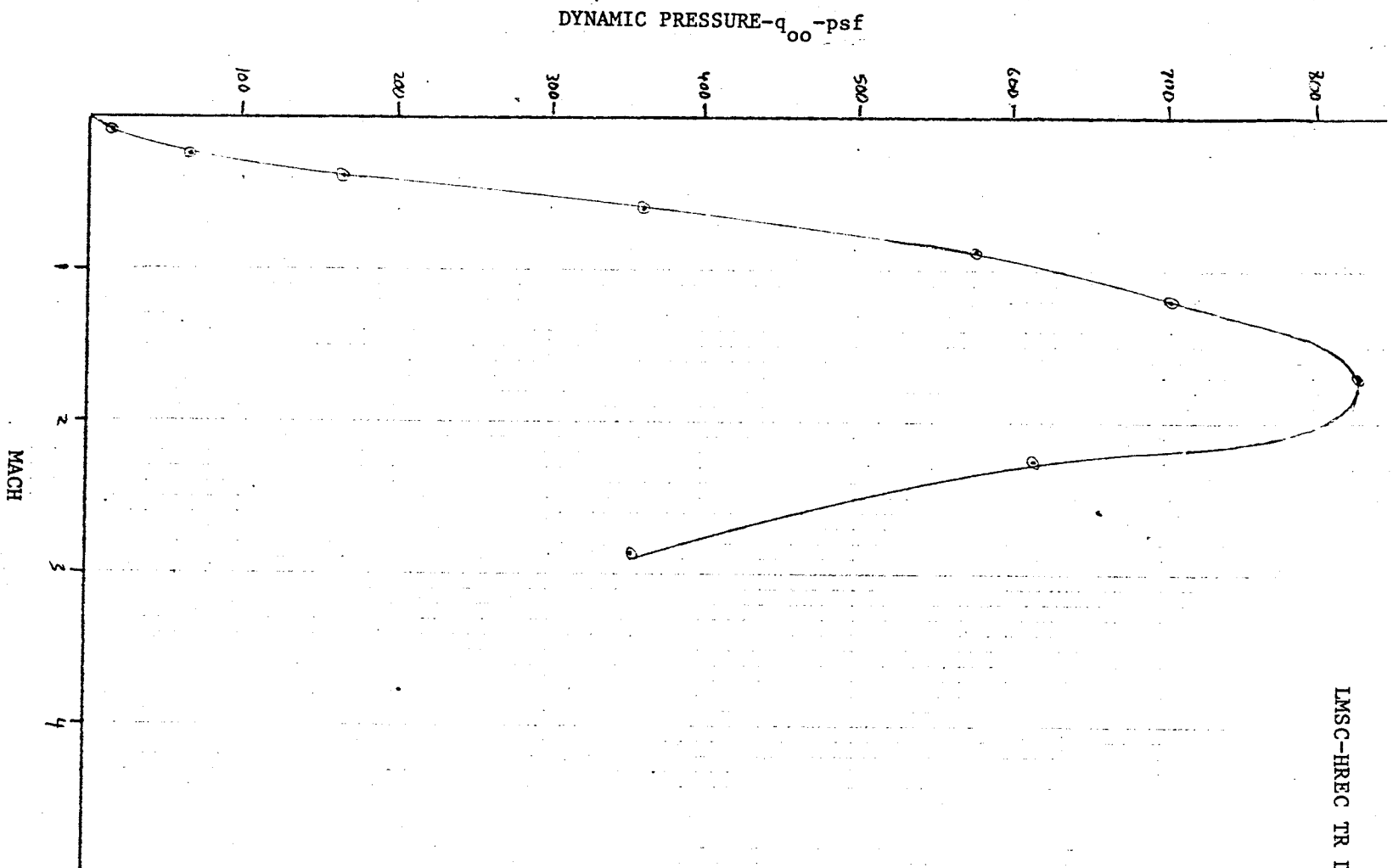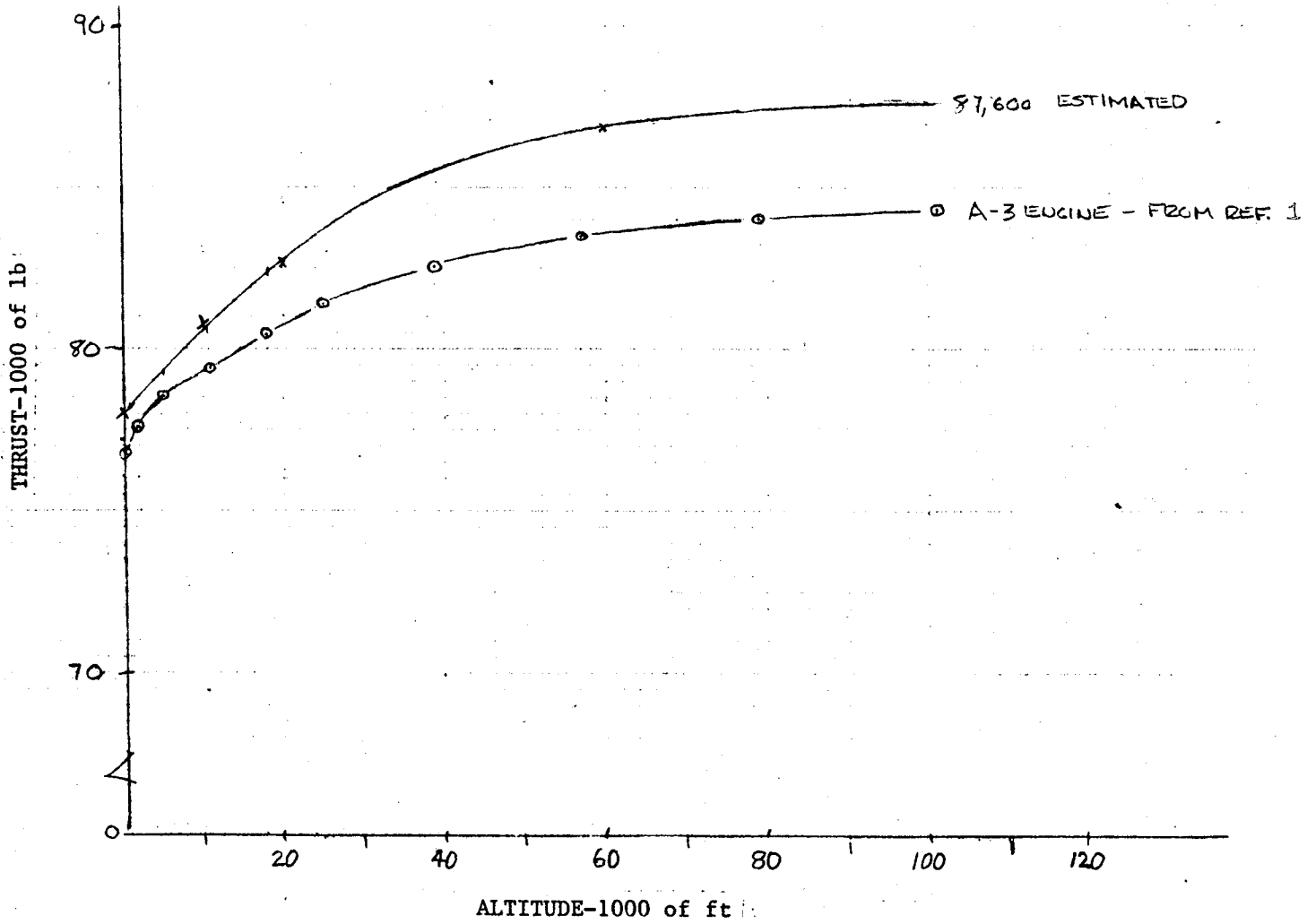
Fig. A-5 - Thrust versus Altitude - Redstone
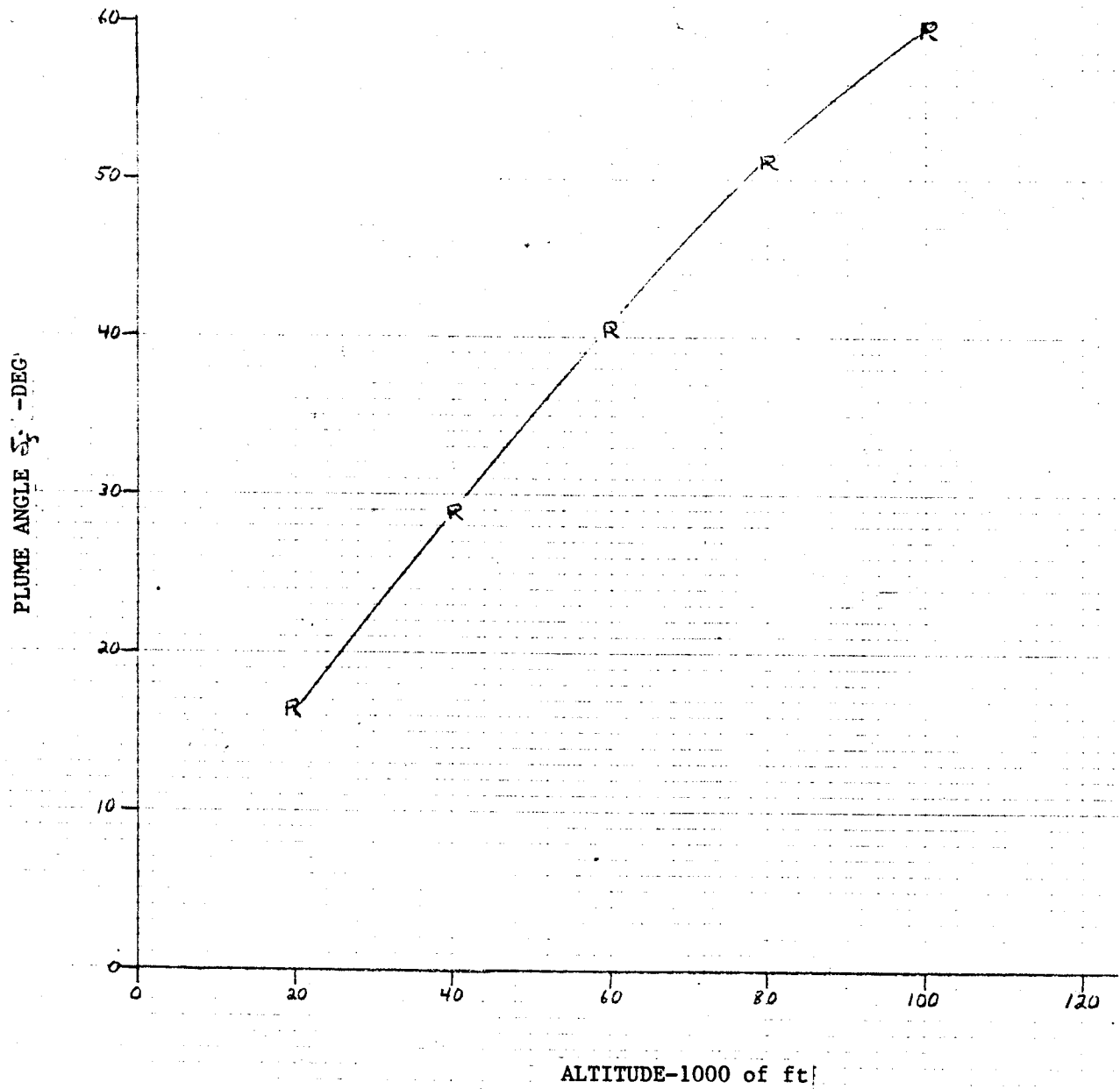
Fig. A-6 – Plume Angle versus Altitude – Redstone
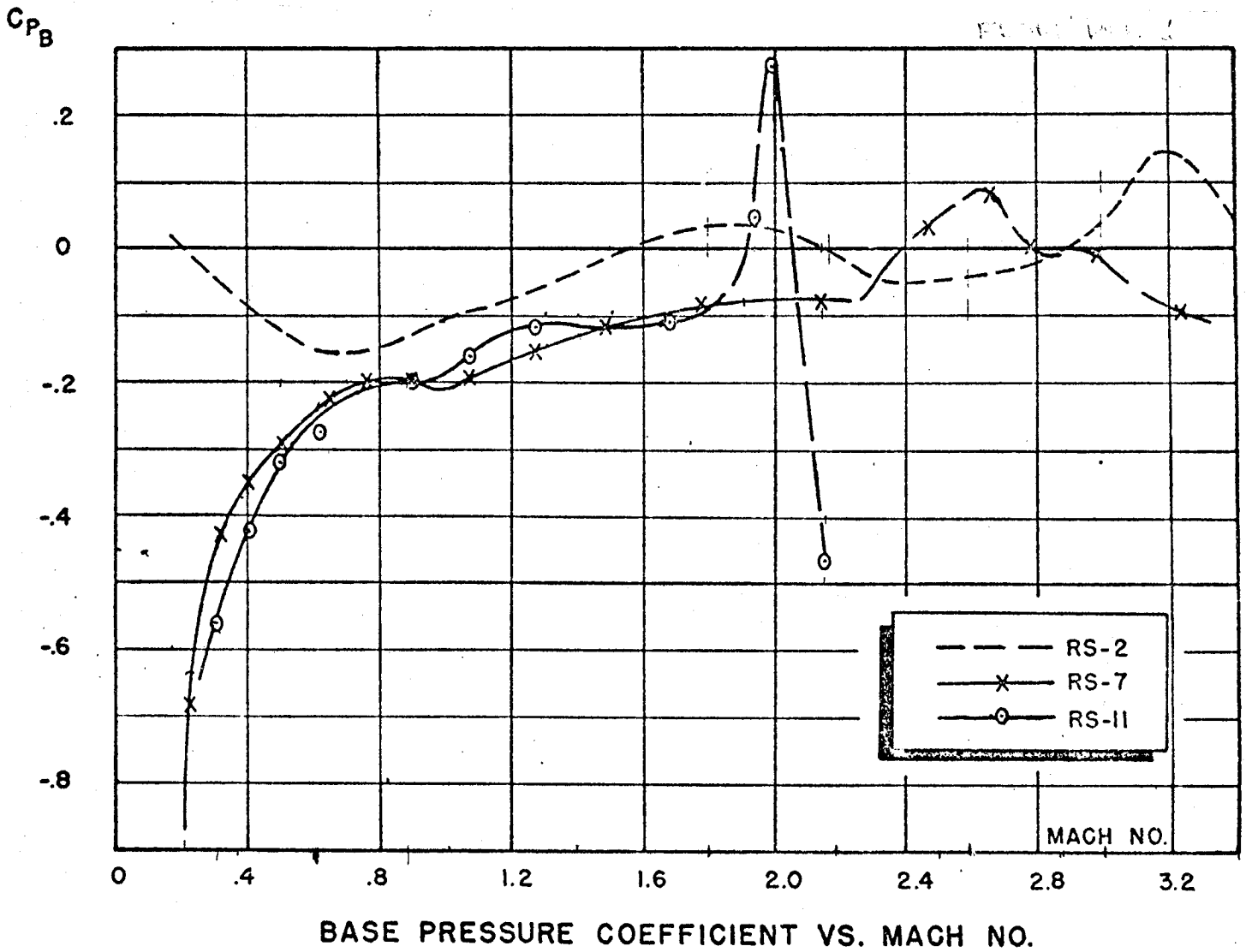
Fig. A-7 - Redstone Base Pressure Source Data

LOCKHEED-HUNTSVILLE RESEARCH & ENGINEERING CENTER

Table A-1 REDSTONE

MACH	ALT ft	P_∞ psf	q_∞ psf	THRUST lb	C_T AB=26.7 ft²
.10	500	2087.79	14.61	78000	199.96
.22	2000	1969.82	66.74	78500	44.05
.37	5000	1744.11	167.14	79500	17.81
.60	10500	1436.31	361.95	80700	8.35
.88	18000	1066.98	578.39	82800	5.36
1.20	25500	697.64	703.22	83700	4.46
1.70	39000	410.38	830.20	85500	3.86
2.25	57000	174.42	618.08	86800	5.26
2.87	79000	61.57	355.00	87500	9.23
3.78	103000	20.51	205.14	87600	15.99

Table A-2   REDSTONE

MACH	C_{PB}	C_{PB} max	C_{PB} min	PB/P_{00}	PB/P_{00} max	PB/P_{00} min
.10	−1.710	−1.850	−1.430	.988	.987	.989
.22	− .760	− .900	− .480	.974	.970	.984
.37	− .428	− .540	− .320	.959	.948	.969
.60	− .250	− .330	− .200	.937	.917	.949
.88	− .212	− .250	− .140	.885	.864	.924
1.20	− .150	− .200	− .070	.849	.798	.929
1.70	− .100	− .130	.020	.797	.737	1.040
2.25	− .037	− .045	.060	.869	.841	1.212
2.87	.014	− .035	.090	1.081	.798	1.519
3.78	.040	− .035	.100	1.400	.649	2.000

LOCKHEED-HUNTSVILLE RESEARCH & ENGINEERING CENTER

JUPITER

JUPITER

The Jupiter, produced by the Army Ballistic Missile Agency (ABMA), was an intermediate range, inertially guided ballistic missile. On 8 November 1955 the Secretary of Defense directed the secretaries of the Army and Navy to establish a joint program for the design and development of the IRBM system proposed by the Army through Dr. Wernher von Braun. The specifications were for a ballistic missile capable of carrying a 3,000 lb warhead 1,000 miles with a circular probable error (CPE) not to exceed 1,500 yards and the capability to be launched from shipboard or a land base.

The development of the Jupiter missile was divided into two programs: The Jupiter "A" program which used the Redstone missile to test Jupiter components and, the Jupiter "C" program which used a highly modified Redstone to support the development of the Jupiter nose cone. The Jupiter firing plan was then revised to allow for only land based deployment which allowed a relaxation of overall length limitations.

The final design of the Jupiter missile called for an overall length of about 766 in. and an outside diameter of approximately 105 in. The gross weight of the missile was about 10,640 lb with the warhead weighing approximately 2,720 lb. It used a Rocketdyne LR3-NA-18 bipropellant engine which delivered 150,000 lb of thrust at sea level and which burned for approximately 162 sec. The maximum range of the Jupiter was slated at 1500 miles and had a flight time of approximately 1,010 sec.

Pitch and yaw control during powered ascent flight was provided by gimbaling the main engine nozzle. Roll control was provided by swiveling the turbine exhaust nozzle. The Jupiter configuration is the only missile with no base turbine exhaust.

The Jupiter configuration and engine operating characteristics are presented in Figs. A-8 and A-9. Estimated ascent trajectory characteristics

are presented in Figs. A-10 and A-11. The engine thrust versus altitude and nozzle plume expansion angle are presented in Figs. A-12 and A-13.

The Jupiter flight base pressure source data is presented in Fig. A-14. The base pressure source data was obtained from Reference 6.

The Jupiter trajectory data, thrust and base pressure characteristics are presented in Tables A-3 and A-4.

LOCKHEED-HUNTSVILLE RESEARCH & ENGINEERING CENTER

JUPITER BIBLIOGRAPHY

1. Sims, J., "Calculated Jupiter Base Pressure Coefficients for Power-On Flight," Report No. DA-TN-5-58, U.S. Army Ballistic Missile Agency, Redstone Arsenal, Ala., 19 March 1958.

2. "Overall Study and Flight Evaluation of the Jupiter Missile Propulsion and Associated Systems," Report No. RJ-TR-61-1, U.S. Army Ballistic Missile Agency, Redstone Arsenal, Ala., 13 june 1961.

3. Rivett, J.E., "Aeroballistic Flight Test Evaluation of Jupiter CM-31," Report No. TM AA-M35J, 12 april 1960.

4. "Summary of Aerodynamic Characteristics for the Jupiter IOC Missile," Report No. DA-TN-35-58, U.S. Army Ballistic Missile Agency, Redstone Arsenal, Ala., 2 July 1958.

5. Uherka, Myrow, "Missile Description of Jupiter Intermediate Range Ballistic Missile Model AM-25," Report No. DSL-TM-41-59, U.S. Army Ballistic Missile Agency, Redstone Arsenal, Ala., 24 August 1959.

6. Weisler, A. C. and C. C. Hagood, "Jupiter Summary Report, Vol. VI, Aerodynamics," ABMA Report RF-TR-61-10, June 1961.

JUPITER

ENGINE : ROCKETDYNE LR3-NA-18
THRUST : 150000 lb S.L. LOX RP-1
         174500 lb VAC
P_c : 550 psi
P_E : 13 psi
γ_E : 1.23
M_E : 2.93
Dia_E : 44.75 in
θ_L : 4.7°
ϵ : 8.00

Nose Geometry
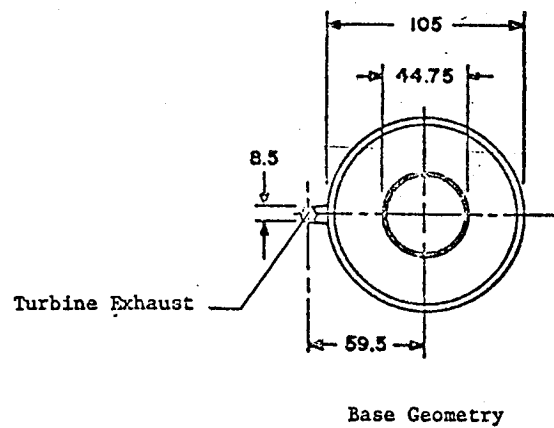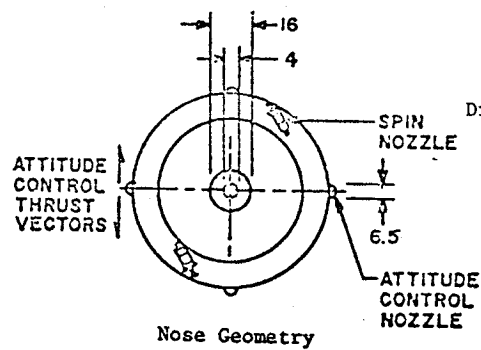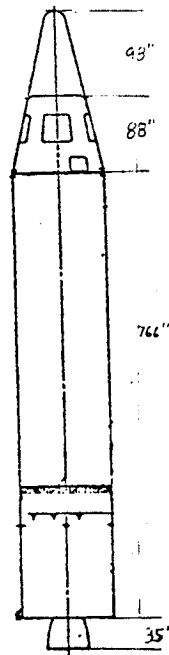
Base Geometry

Fig. A-8 – Jupiter Missile Configuration and Engine Characteristics

LOCKHEED-HUNTSVILLE RESEARCH & ENGINEERING CENTER
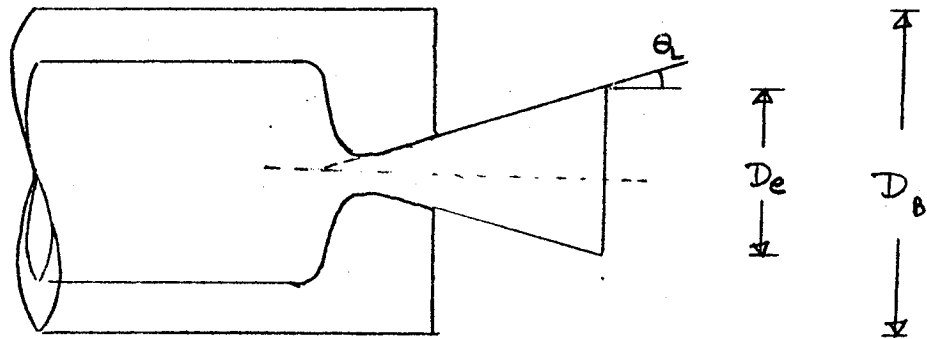
$D_B = 105.0''$

$D_e = 45.7''$

$X_j = 34.94''$

$\theta_e = 4.7°$

$\dfrac{A_N}{A_B} = .189$

$\dfrac{X_j}{D_B} = .333$

Fig. A-9 - Base Geometry - Jupiter

LOCKHEED-HUNTSVILLE RESEARCH & ENGINEERING CENTER
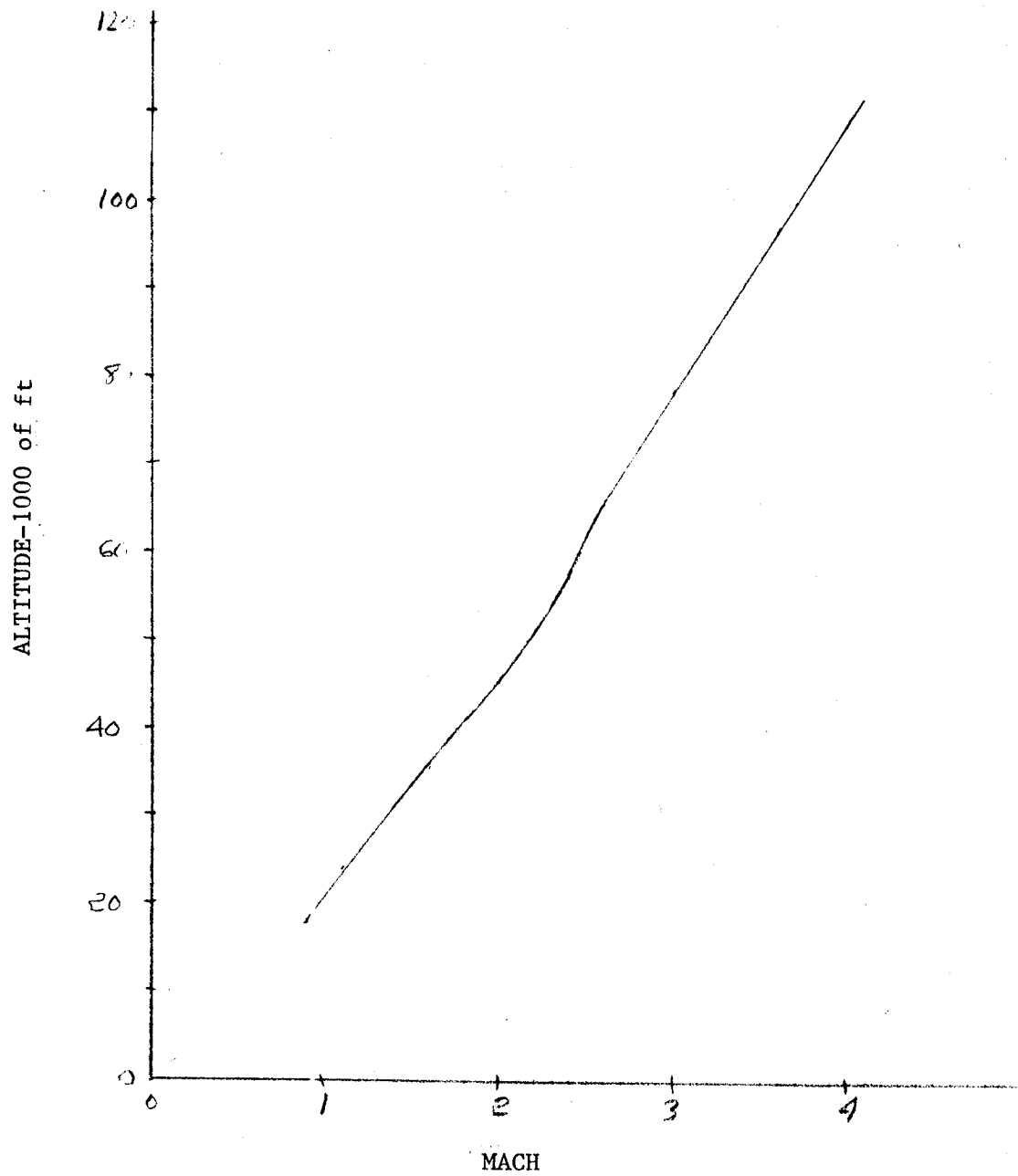
Fig. A-10 Flight Altitude versus Mach Number - Jupiter
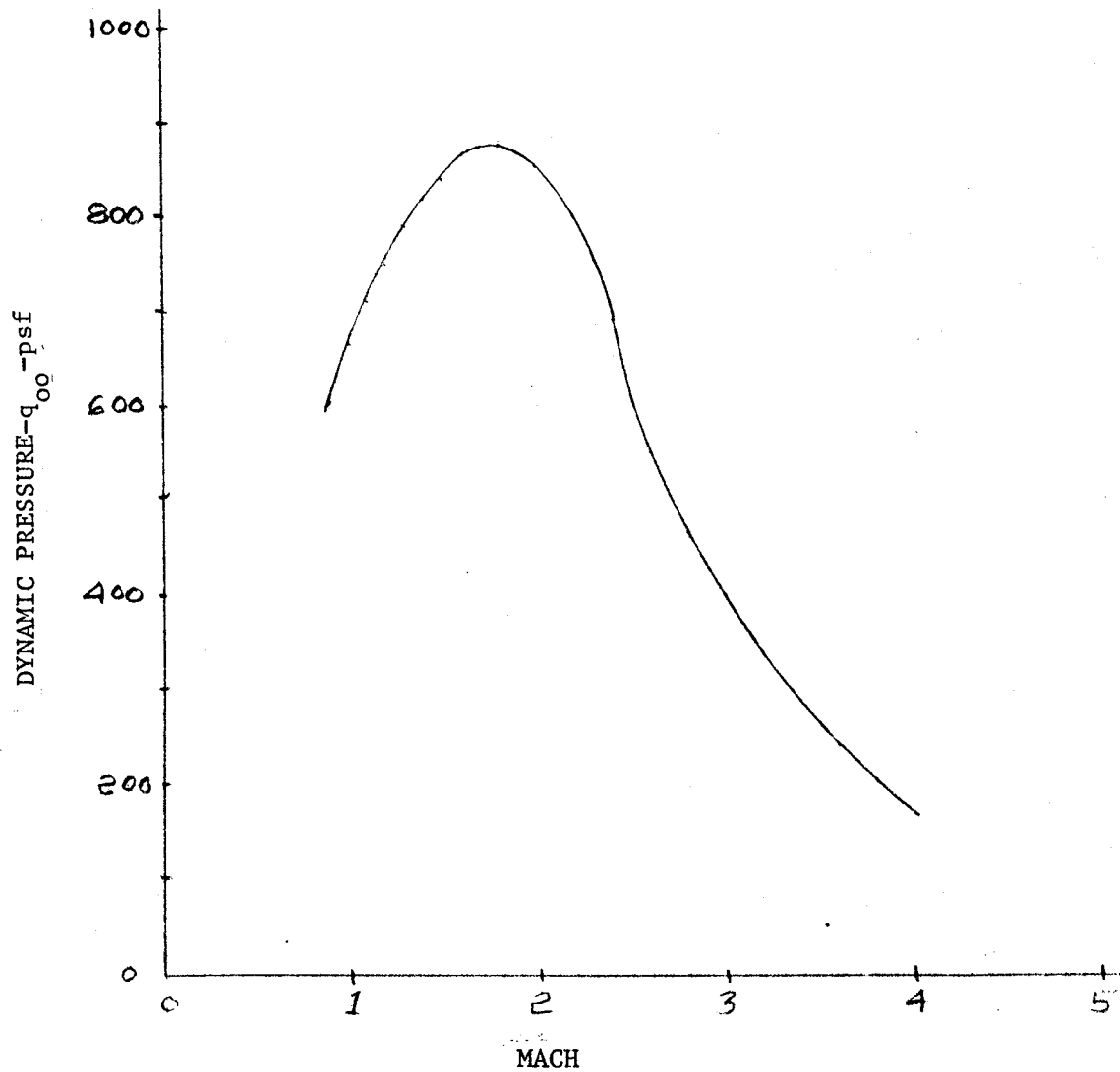
Fig. A-11 - Flight Dynamic Pressure versus Mach Number - Jupiter

LOCKHEED-HUNTSVILLE RESEARCH & ENGINEERING CENTER
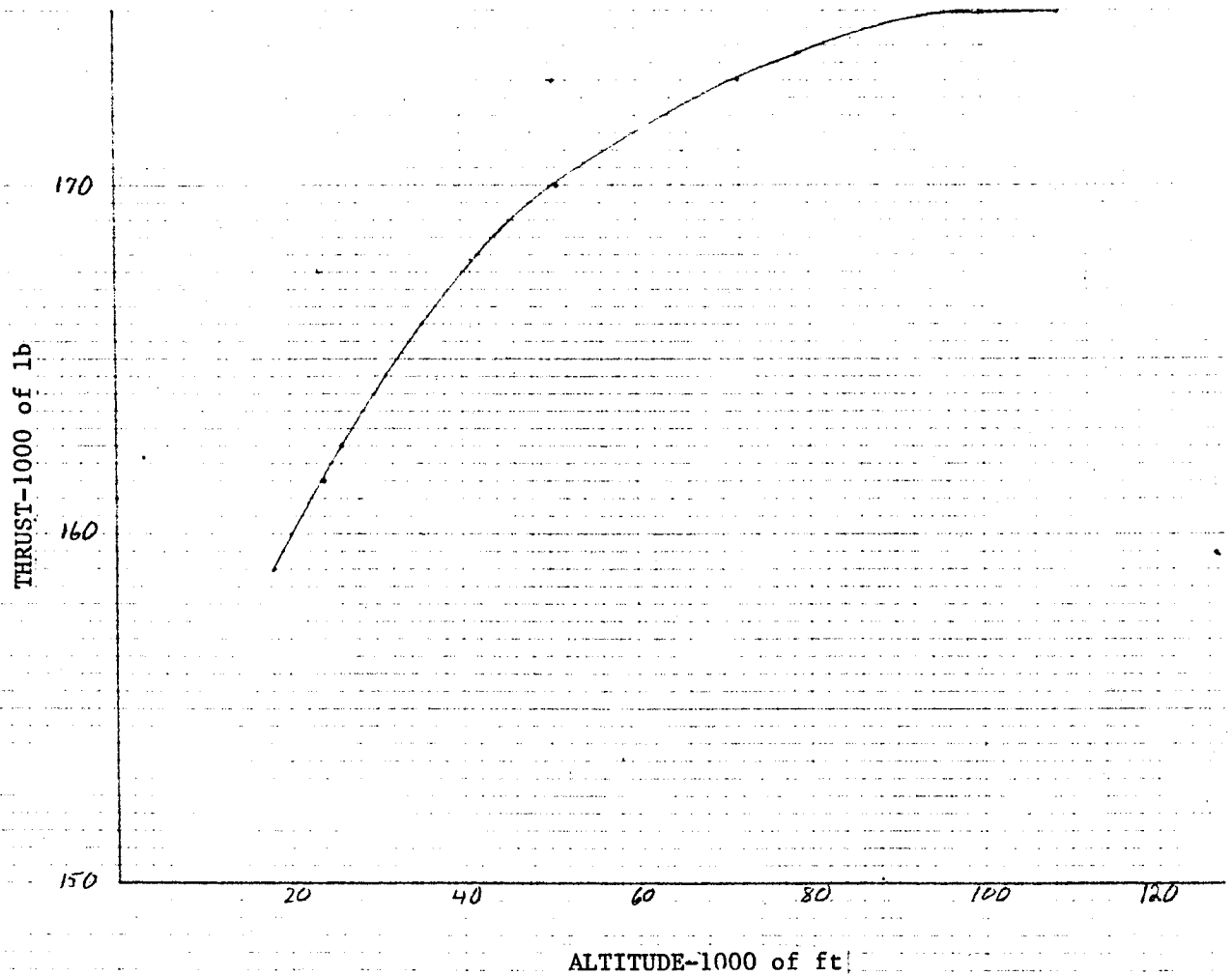
Fig. A-12 - Thrust versus Altitude - Jupiter

LOCKHEED-HUNTSVILLE RESEARCH & ENGINEERING CENTER
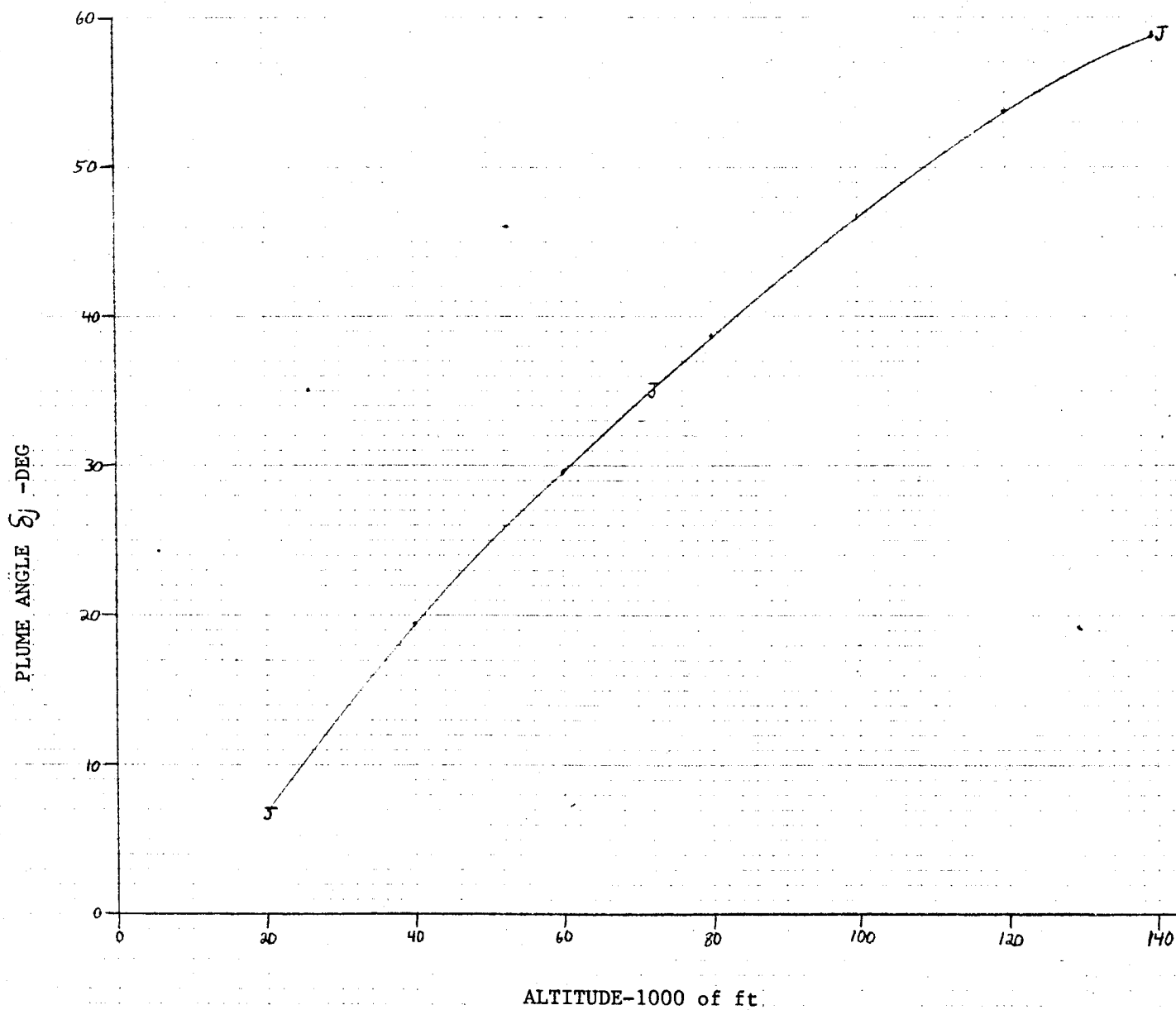
Fig. A-13 – Plume Angle versus Altitude – Jupiter

FROM REF. 6

ENGINE SEA LEVEL THRUST = 150,000 LBS.
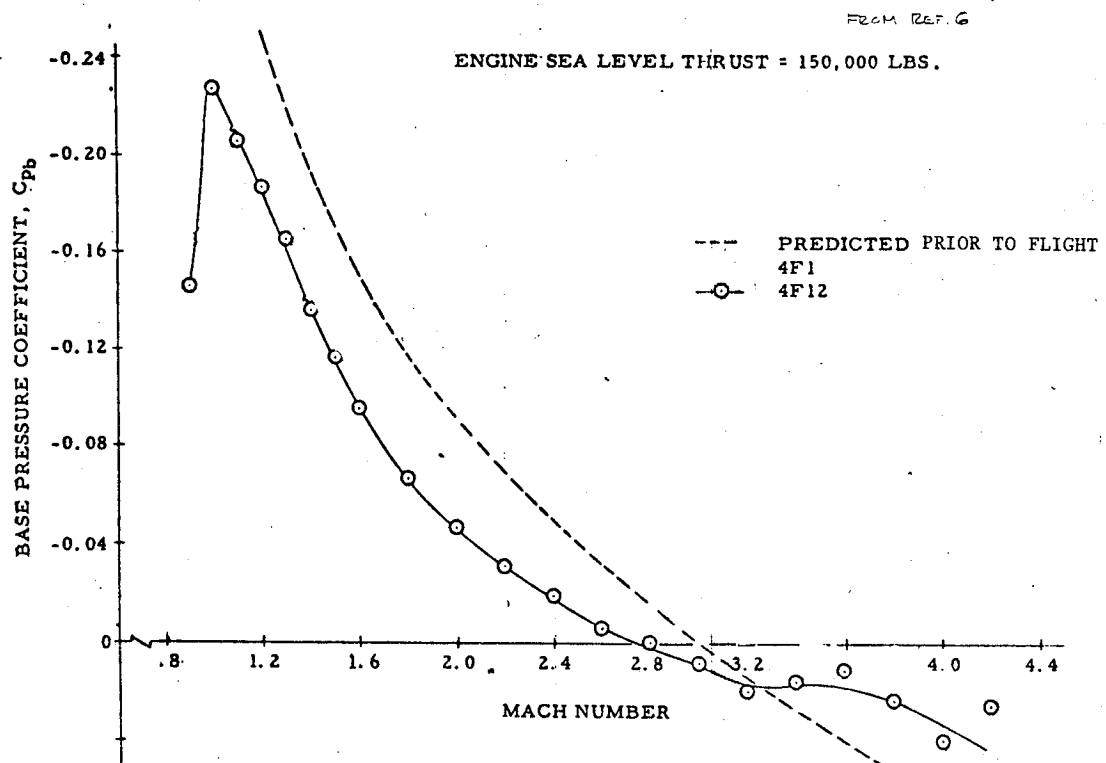
Fig. A-14 – Jupiter Base Pressure Source Data

LOCKHEED–HUNTSVILLE RESEARCH & ENGINEERING CENTER

Table A-3 Jupiter

MACH	ALT ft	P$_{oo}$psf	q$_{oo}$psf	THRUST lb	C$_m$ AB-60.13 ft^2
.90	18000	1067.00	605.00	159000	4.37
1.00	20500	950.00	665.00	160500	4.02
1.10	24000	838.30	710.00	161500	3.79
1.20	26000	744.00	750.00	162500	3.61
1.30	29000	667.80	790.00	163500	3.44
1.40	31000	597.70	820.00	164500	3.34
1.50	33500	533.30	840.00	165200	3.27
1.60	35500	482.70	865.00	166000	3.19
1.80	41000	385.80	875.00	167700	3.19
2.00	45500	305.40	855.00	169000	3.29
2.20	51000	236.10	800.00	170000	3.54
2.40	57500	174.90	705.00	171300	4.04
2.60	65500	116.20	550.00	172000	5.20
2.80	72000	84.73	465.00	173000	6.19
3.00	78500	63.49	400.00	173800	7.23
3.20	85000	47.73	340.00	174200	8.40
3.40	91000	35.21	285.00	174900	10.04
3.60	97000	26.46	240.00	175000	11.89
3.80	103000	20.28	205.00	175000	14.56
4.00	109000	15.18	170.00	175000	17.65

LOCKHEED-HUNTSVILLE RESEARCH & ENGINEERING CENTER

Table A-4 JUPITER

MACH	c_{PB}	c_{PB} max	c_{PB} min	PB/P_{oo}	PB/P_{oo} max	PB/P_{oo} min
.90	-.155	-.165	-.146	.912	.906	.917
1.00	-.204	-.180	-.228	.857	.874	.840
1.10	-.209	-.213	-.206	.823	.819	.825
1.20	-.191	-.195	-.188	.807	.803	.810
1.30	-.176	-.188	-.166	.792	.778	.804
1.40	-.139	-.142	-.137	.809	.805	.812
1.50	-.117	-.177	-.117	.816	.721	.815
1.60	-.101	-.108	-.096	.819	.806	.828
1.80	-.077	-.095	-.067	.825	.785	.848
2.00	-.058	-.068	-.048	.838	.809	.866
2.20	-.037	-.043	-.032	.875	.854	.892
2.40	-.028	-.038	-.020	.887	.847	.919
2.60	-.013	-.202	-.007	.938	.905	.967
2.80	-.005	-.011	0.000	.973	.939	1.000
3.00	.005	-.010	.008	1.032	.937	1.050
3.20	.013	-.003	.018	1.093	.978	1.130
3.40	.015	-.005	.025	1.121	.959	1.202
3.60	.015	.013	.010	1.136	1.118	1.090
3.80	.022	.004	.022	1.222	1.040	1.222
4.00	.040	.030	.040	1.448	1.336	1.448

LOCKHEED-HUNTSVILLE RESEARCH & ENGINEERING CENTER

THOR

THOR

The Thor was designed as an intermediate range ballistic missile to carry a General Electric reentry vehicle (warhead).

The design specifications for the Thor called for it to stand approximately 80 ft in height with an outside diameter of approximately 8 ft. The Thor IRBM is inertially guided and has a range of approximatly 1,500 miles. The propulsion system consists of a Rocketdyne LR79-NA-11 with 150,000 lb of thrust at sea level. The Thor also contained verniers in the base structure of the vehicle which influenced base pressure data. The Thor first stage vehicle (burn time approximately 146 sec) was also augmented by strap-on solid boosters and designated the Thor Delta.

The Thor ABLE was a two stage ICBM version with a range of 500 n.mi. and had orbit capability. The Thor AGENA used the improved DM-21 booster with a 170,000 lb thrust engine. Earlier boosters used a 150,000 lb thrust engine. The Thor Delta is the system developed for NASA to deliver precise space trajectories and Orbiters (Ref. 1). The early Delta vehicles used a modified DM-18A booster redesignated the DM-19 booster. The main engine developed 150,000 lb of thrust. The NASA Delta vehicles were a three stage vehicle that used two liquid propellant stages and a third solid propellant stage. The Improved Thor Delta used the DM-21 booster with the 170,000 lb thrust main engine. The Improved Thor Delta was designated DSV-3A. The DSV-3 vehicles do not use fins.

The configuration descriptions of the Thor vehicle and main engine operating characteristics are presented in Figures A-15 and A-16. Ascent trajectory characteristics are presented in Figs. A-17 and A-18. The engine thrust versus altitude and nozzle plume expansion angle are presented in Figs. A-19 and A-20 versus altitude. The Thor flight base pressure source data from Reference 1 is presented in Fig. A-21. Thor trajectory data, thrust and base pressure characteristics are presented in Table A-5.

THOR REFERENCES

1. Ripley, J. J., "The Thor History," REport SM-41860, Douglas Aircraft Co., Space Systems Division, May 1962.

2. Jackson, R. H., "Base Region REsults Obtained from Three Thor Boosters," Report No. SM-46507, Douglas Missile & Space Division, June 1965.

3. Hill, L. L., "Solid Motor, Main Engine, and Vernier Engine Exhaust Plume Contours for the Six-Solid Retrofit Booster," Douglas Aircraft Memo A2-260-AAA5-D9442, dated 9 September 1969.

4. Hong, Y. S., "Base Flow Environment Analysis of a Single Engine Booster," AIAA/SAE 7th Propulsion Joint Specialist Conference, Paper 71-643, June 15, 1971.

LOCKHEED-HUNTSVILLE RESEARCH & ENGINEERING CENTER

THOR Booster

ENGINE : ROCKETDYNE LR79-NA-11

THRUST : 170000 lb S.L. LOX RP

195000 lb VAC

P_c : 595 psi

P_E : 13.2 psi

γ_E : 1.25

M_E : 3.02

Dia : 45.6 in

θ_L = 4.72°

1061"

56"

96"

TURBINE
EXHAUST
DUCT

VERNIER
ENGINE

Vernier Engine Heat Shield

THOR BOOSTER

46,000 Ft Plume Boundaries

Main Engine Plume Boundaries
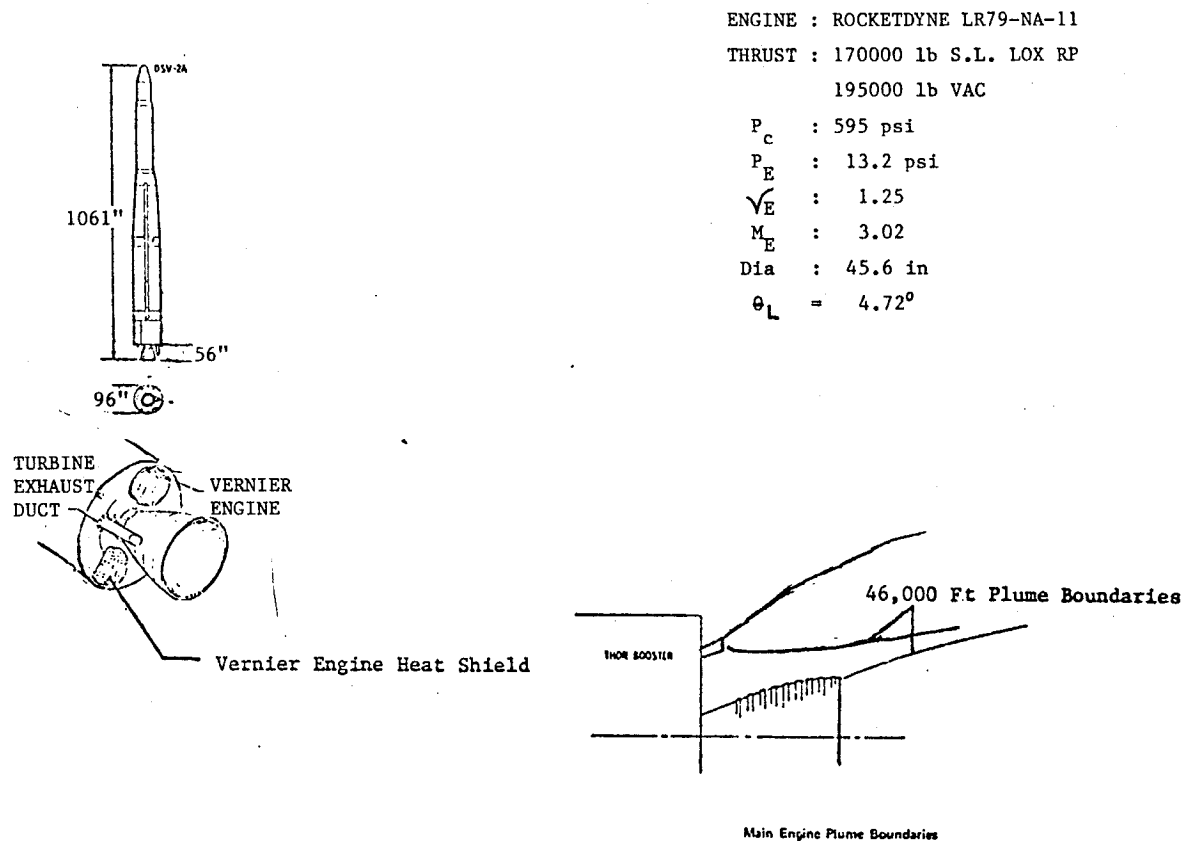
Fig. A-15 - THOR Missile Configuration and Engine Characteristics

A-27
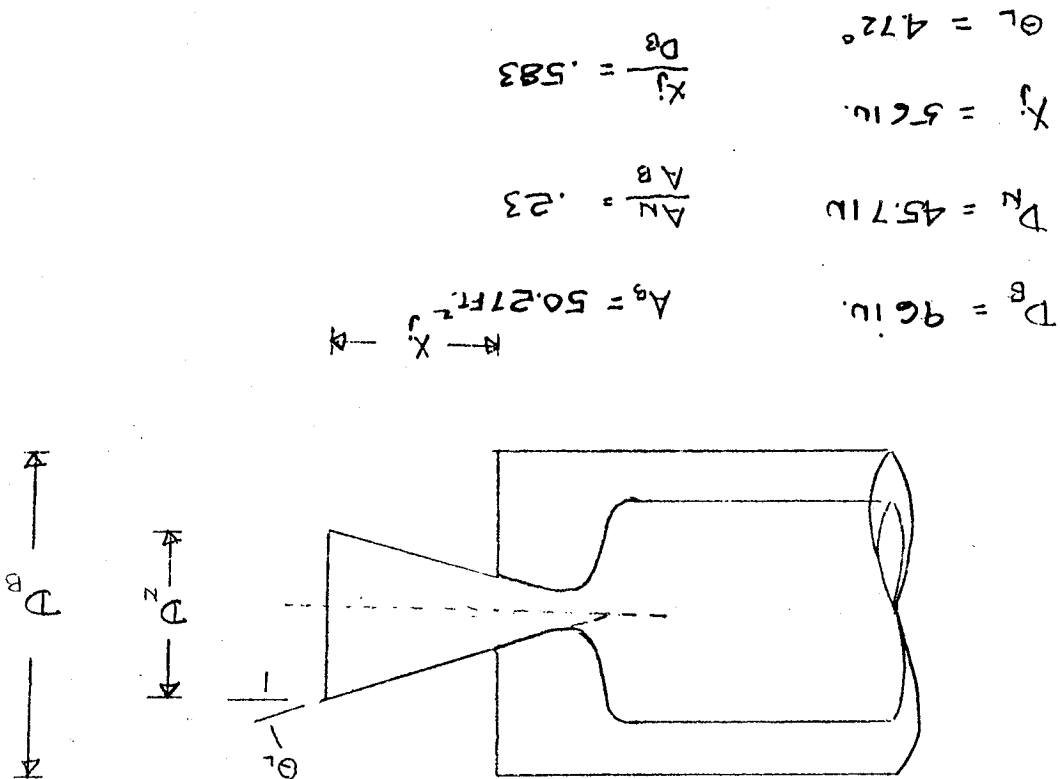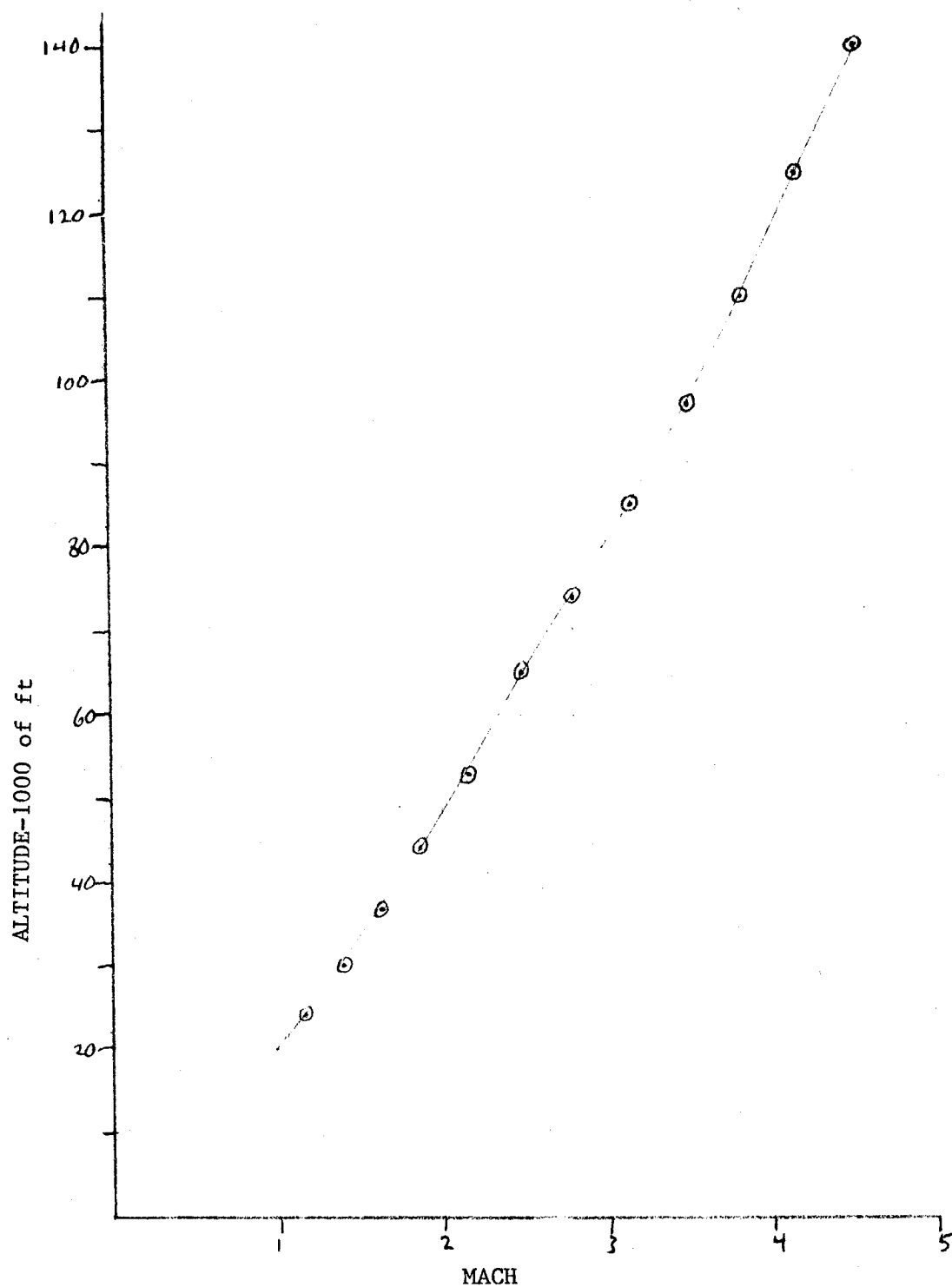
Fig. A-17 - Flight Altitude versus Mach Number - THOR
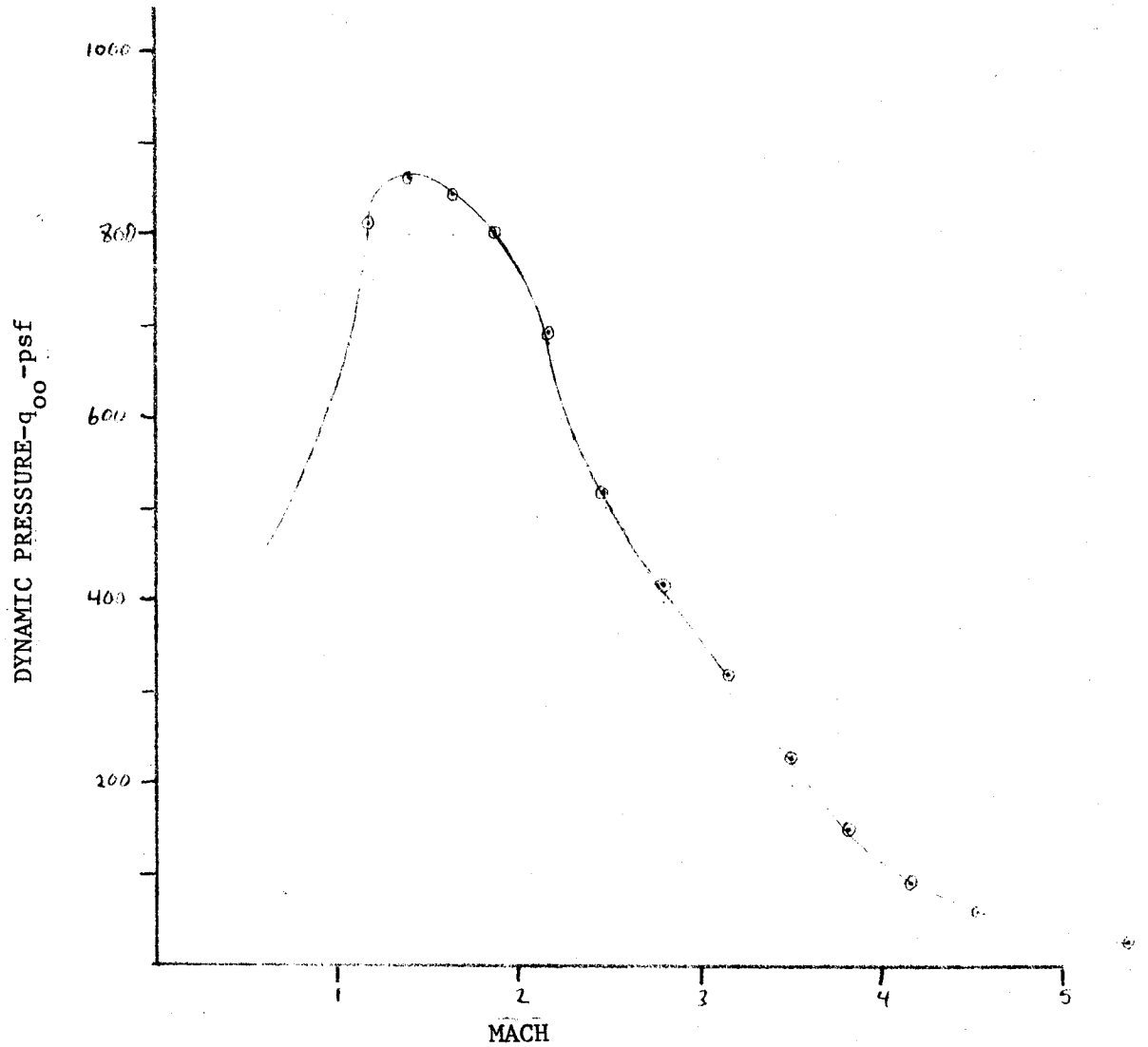
Fig. A-18 - Flight Dynamic Pressure versus Mach Number - THOR
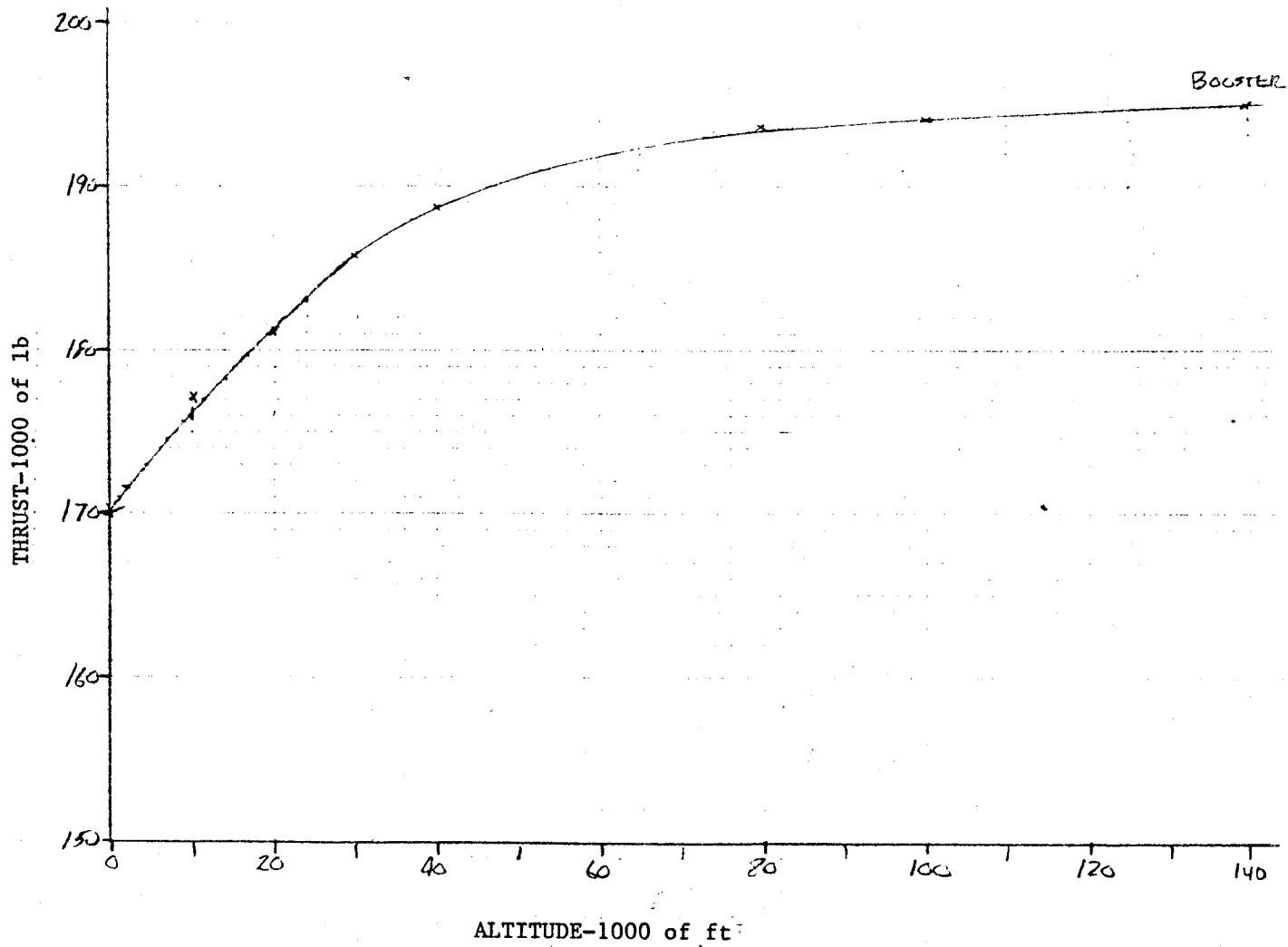
Fig. A-19 – Thrust versus Altitude – THOR

Fig. A-20 - Plume Angle versus Altitude - THOR

LOCKHEED-HUNTSVILLE RESEARCH & ENGINEERING CENTER

BASE PRESSURE COEFFICIENT HISTORIES
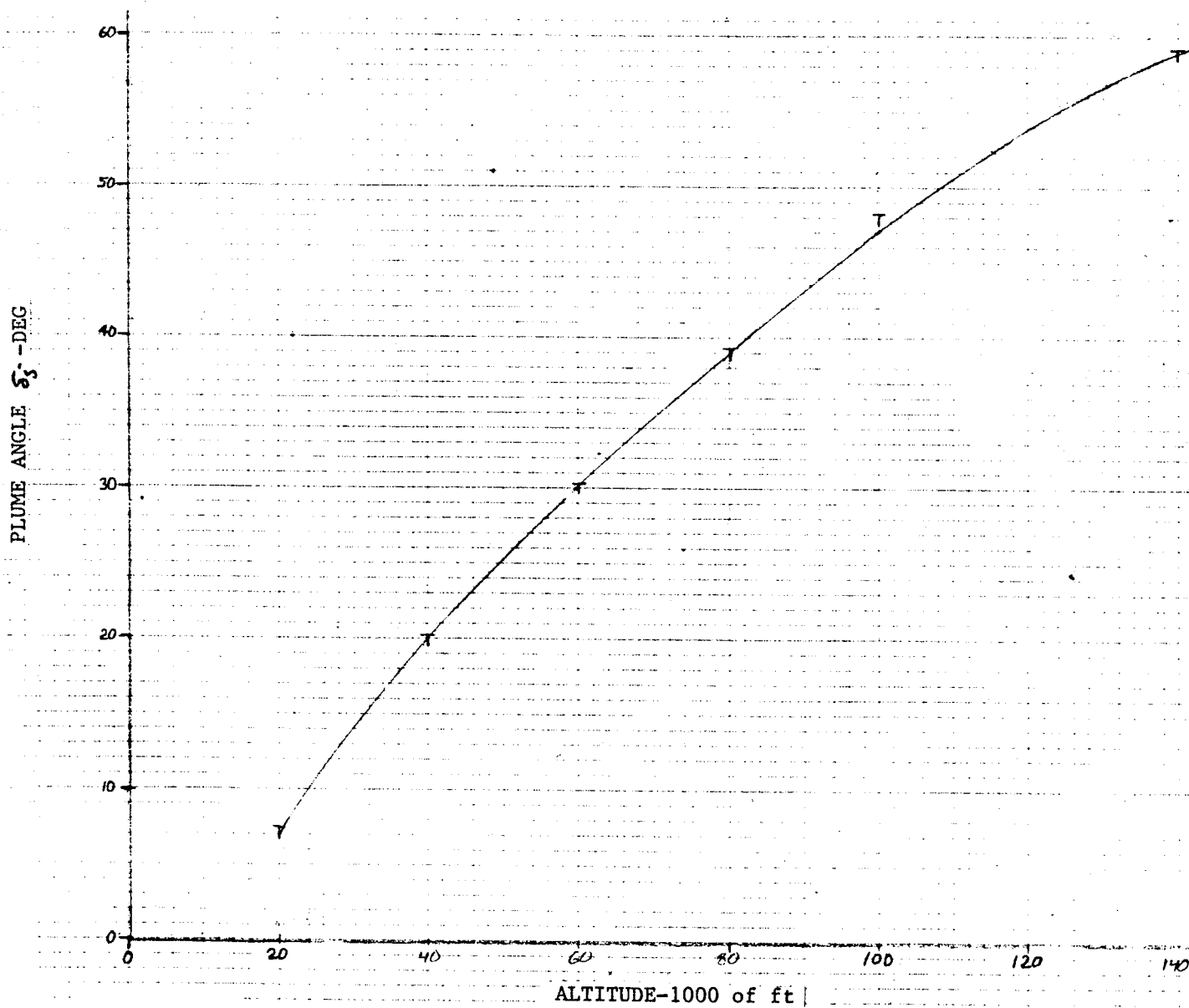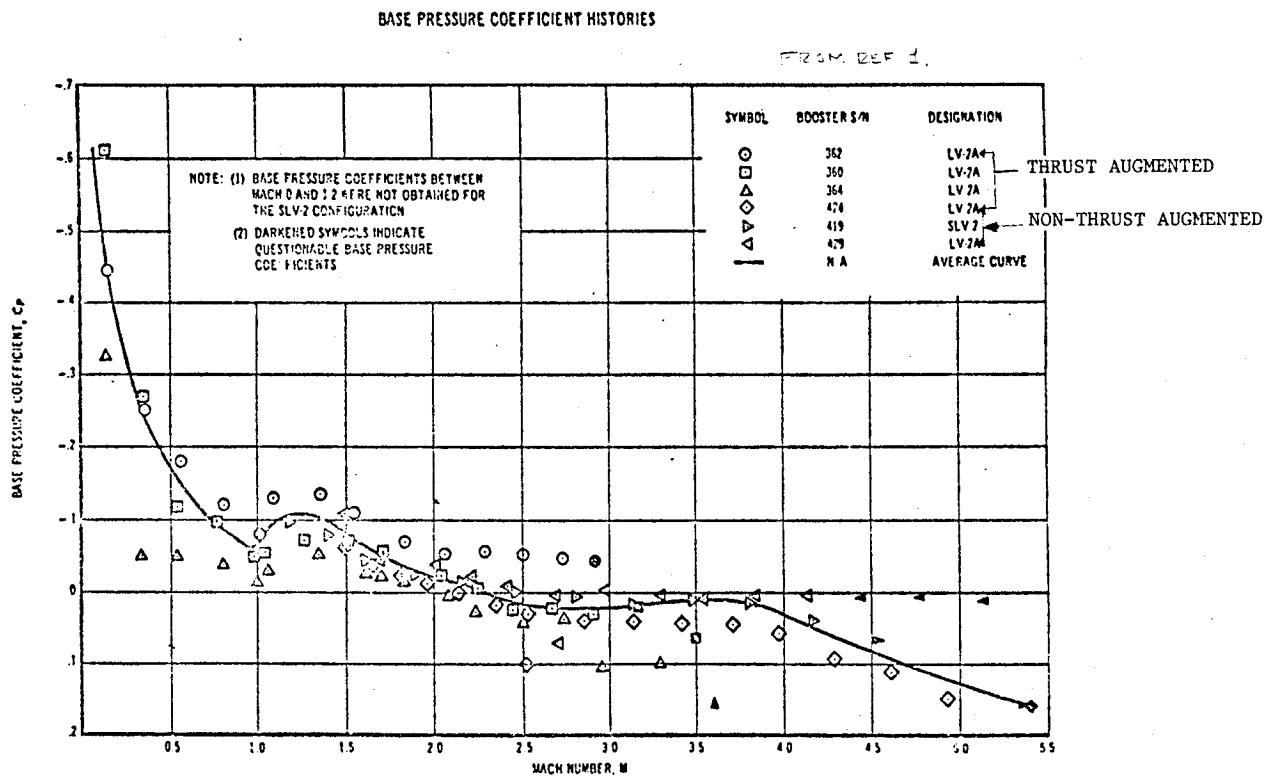
Fig. A-21 - THOR Flight Base Pressure Source Data

LOCKHEED-HUNTSVILLE RESEARCH & ENGINEERING CENTER

Table A-5   THOR

M	Alt ft	P_{oo} psf	q_{oo} psf	Thrust (lb)	C_T AB=50.27 ft^2	C_{PB}	PB/P_{oo}
1.19	24000	821.17	814.00	183000	4.47	-.100	.900
1.40	30000	629.66	863.89	185900	4.28	-.100	.863
1.63	37000	453.86	844.10	188000	4.43	-.050	.907
1.88	44000	324.62	803.14	189400	4.69	-.030	.926
2.17	53000	211.05	695.67	191000	5.46	-.020	.934
2.47	65000	118.93	507.91	192300	7.53	-0-	1.000
2.80	74000	77.56	425.65	193000	9.02	.005	1.027
3.15	85000	46.35	321.94	193600	11.96	.010	1.069
3.50	97000	26.68	228.78	194000	16.87	.005	1.043
3.81	110000	14.84	150.79	194200	25.62	.010	1.100
4.16	125000	7.77	94.13	194800	41.17	.040	1.485
4.53	140000	4.21	60.48	195000	64.14	.070	2.010
5.37	165000	1.61	32.50				

NACA

NACA VEHICLES

The NACA rocket-motor powered flight research test vehicles developed
flight base pressure data incidental to other research objectives. The NACA
has assembled the base pressure data and conducted an analysis that
indicated that the jet effects on drag are of sufficient importance to
deserve consideration in the design of jet-motor nozzles. The models used
by the NACA were for stabilized bodies of revolution. The external
configuration of the models is shown in Figs. A-22 and A-23. The sustainer
motor characteristics are presented in Fig. A-24. The base and nozzle
characteristics for each configuration is presented in Figs. A-25 and A-26.
Trajectory characteristics are presented in Figs. A-27 through A-30.
Estimates of the nozzle plume angle is presented in Fig. A-31. The base
pressure source data (from Ref. 1) for each configuration is presented in
Figs. A-32 through A-35. The trajectory data thrust data and base pressure
characteristics are presented in Tables A-6 and A-7.

LOCKHEED-HUNTSVILLE RESEARCH & ENGINEERING CENTER

NACA REFERENCE

1. Purser, Paul E., Jospeh G. Thebodaux, and H. Herbert Jackson, "Notes on Some Observed Effects of Rocket Motor Operation on the Base Pressures of Bodies in Free Flight," NACA Research Memorandum RM L50I18, 16 November 1950.

LOCKHEED-HUNTSVILLE RESEARCH & ENGINEERING CENTER

Circular-arc profile, t/c = 0.10

9.07 (A)
18.14 (B)

64.5 (A)
129.0 (B)

60°

17.94 (A)
35.88 (B)

73.25 (A)
146.5 (B)

Models A and B.

Circular-arc profile, t/c = 0.10

7.00

58.65

60°

17.87

64.8

Model C

7.24

12.06

c/4

45°

40.00

Free-stream airfoil NACA 65A009

8.37
1.38

56.93

Flat plate, t=0.091

NACA

40°

19.90

66.67

57.89
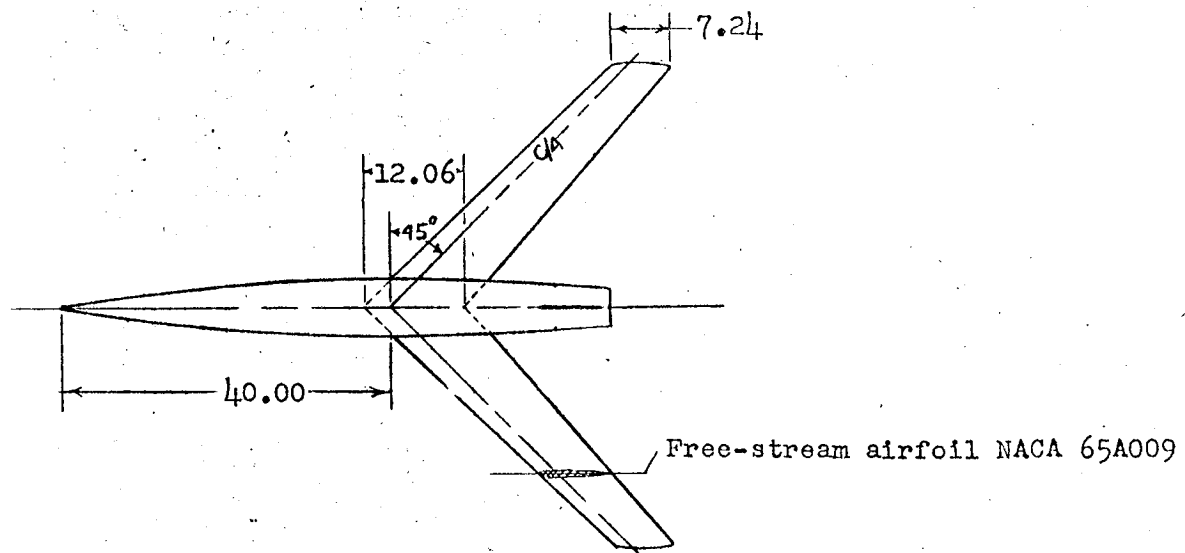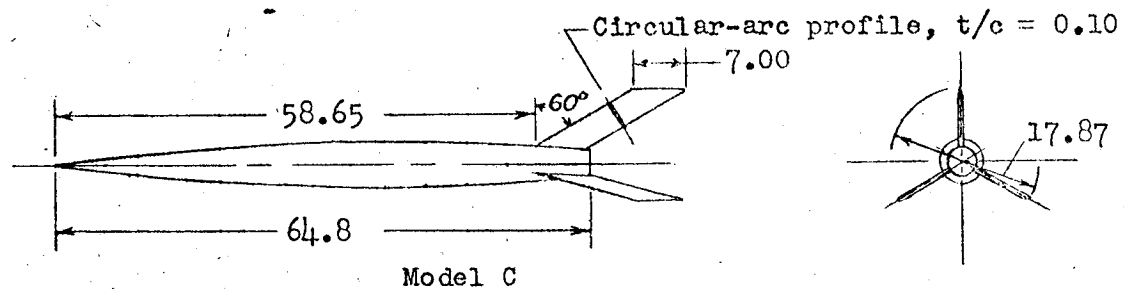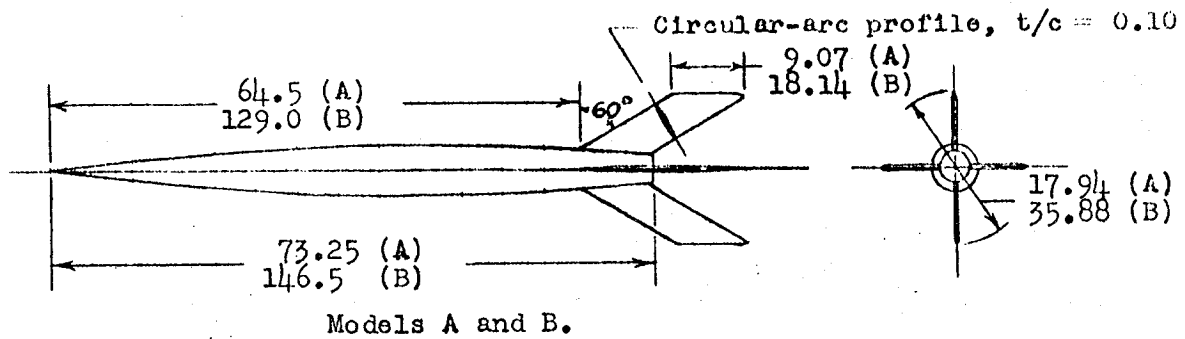
Model D

Fig. A-22 – External Configurations of Models

FUSELAGE COORDINATES
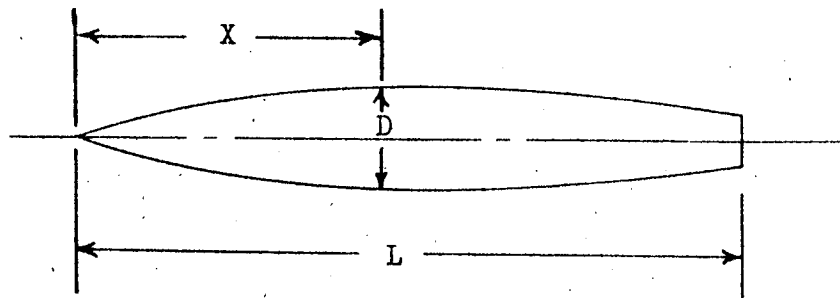
Station	Diameter D/L		
X/L	Models A, B	Model C	Model D
0	0	0	0
.1	.0246	.0245	.0417
.2	.0447	.0448	.0667
.3	.0605	.0608	.0832
.4	.0719	.0723	.0927
.5	.0793	.0800	.0981
.6	.0819	.0832	.1000
.7	.0803	.0821	.0975
.8	.0744	.0767	.0888
.9	.0642	.0669	.0795
1.0	.0497	.0533	.0700

Fig. A-23 - Fuselage Dimensions

A-38

Model	Sustainer Motor				Booster motor
	Type	Nozzle half angle (deg)	Specific heat ratio of exhaust gas (γ)	Average thrust loading ratio $\left(\dfrac{F}{A_e}\right)_{average}$, lbs/sq in.	
A-1, A-2	Modified 3.25 Mk. 7	9	1.219	260	6.25-inch ABL Deacon
A-3	Modified 3.25 Mk. 7	30	1.219	245	6.25-inch ABL Deacon
B	6.25-inch ABL Deacon	30	1.26	195	None
C	Modified 2.25 Mk. 11	10	1.219	140	5-inch HVAR lightweight
D	Standard 3.25 Mk. 7	9	1.219	260	5-inch HVAR lightweight

Fig. A-24 – Motor Nozzle Characteristics

LOCKHEED–HUNTSVILLE RESEARCH & ENGINEERING CENTER
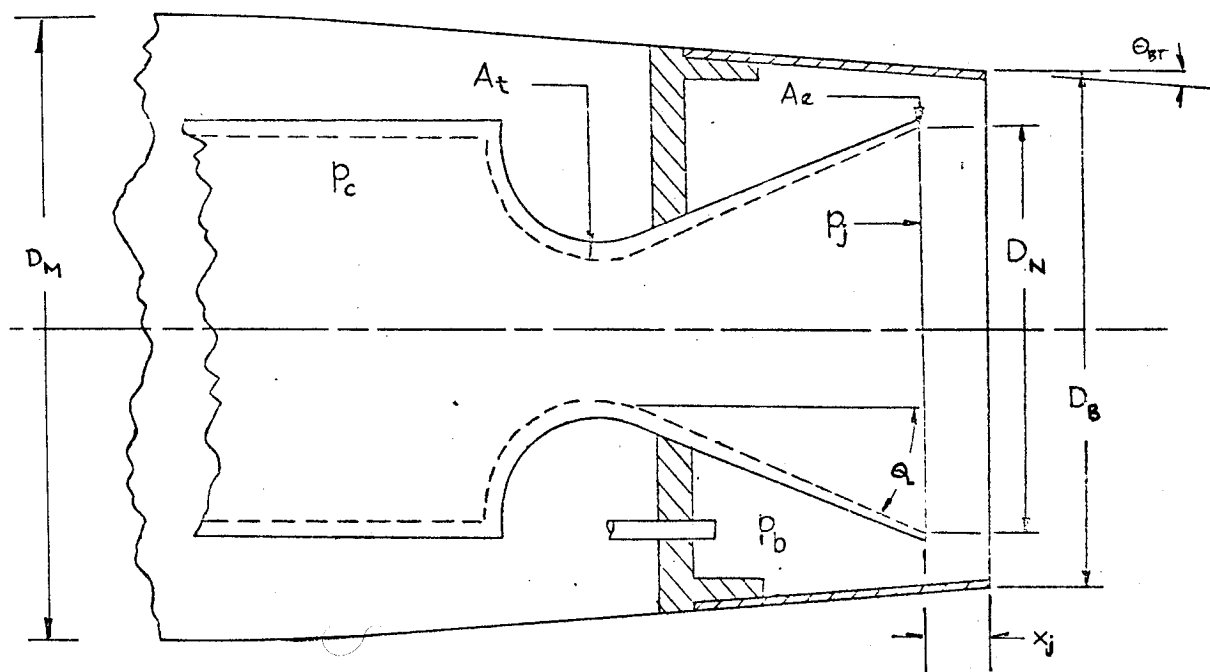
Fig. A-25 – General Arrangement of Rocket Nozzle and Model Base Nomenclature

NACA VEHICLES

MODEL	D_B/D_M	A_B/A_M	Θ_{BT}	D_N/D_B	A_N/A_B	Θ_L	X_N/D_B	ϵ
A1	.6	.36	4.15°	.791	.625	9°	-.06	3.67
A2	"	"	"	"	"	"	4	"
A3	"	"	"	"	"	30°	"	"
B	"	"	"	.86	.74	"	-.034	8.99
C	.64	.41	3.9°	.55	.30	10°	.06	4.49
D	.70	.49	2.7°	.66	.44	9°	.06	3.97

Fig. A-26 - Model Base Geometry

LOCKHEED-HUNTSVILLE RESEARCH & ENGINEERING CENTER
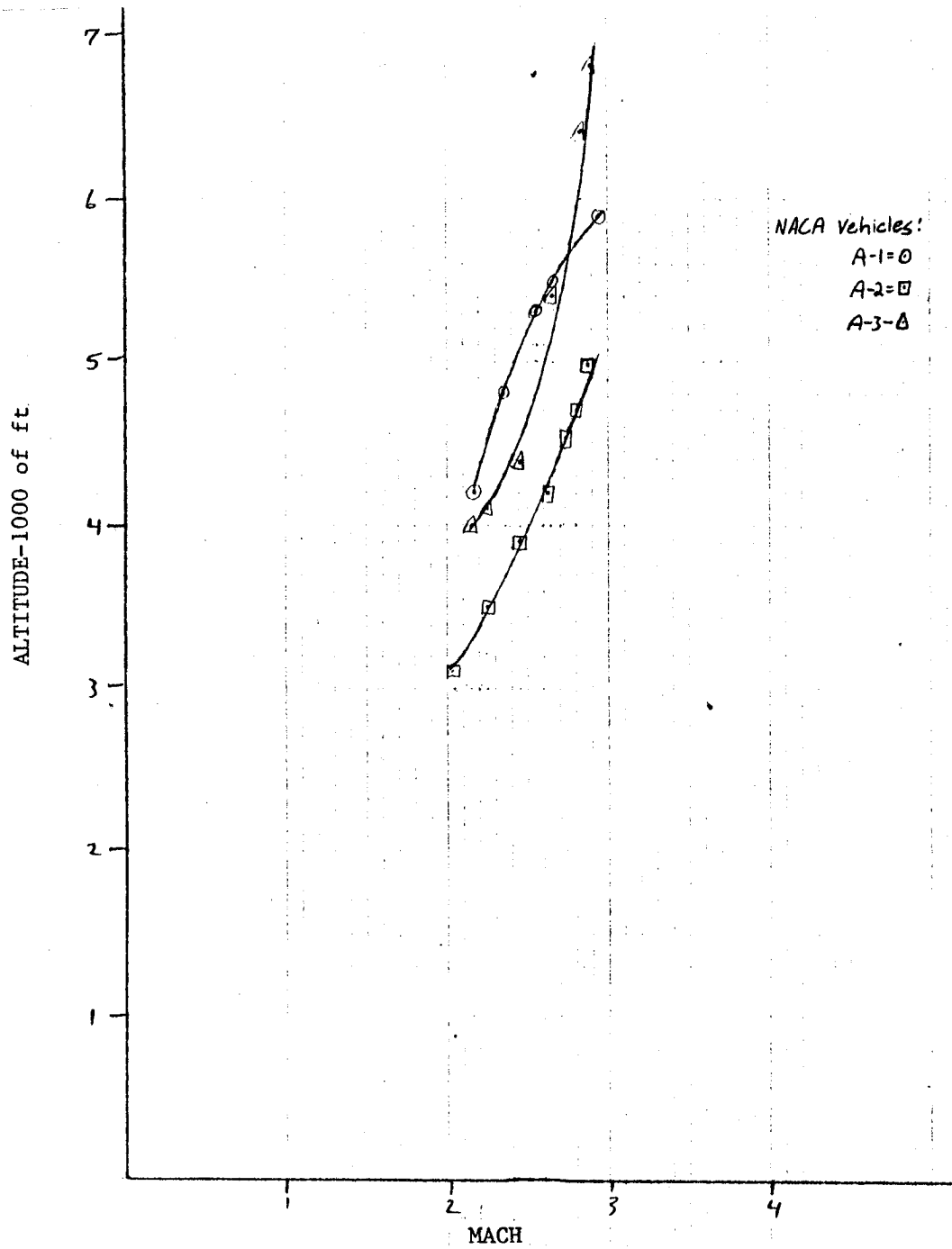
Fig. A-27 - Flight Altitude versus Mach Number - NACA
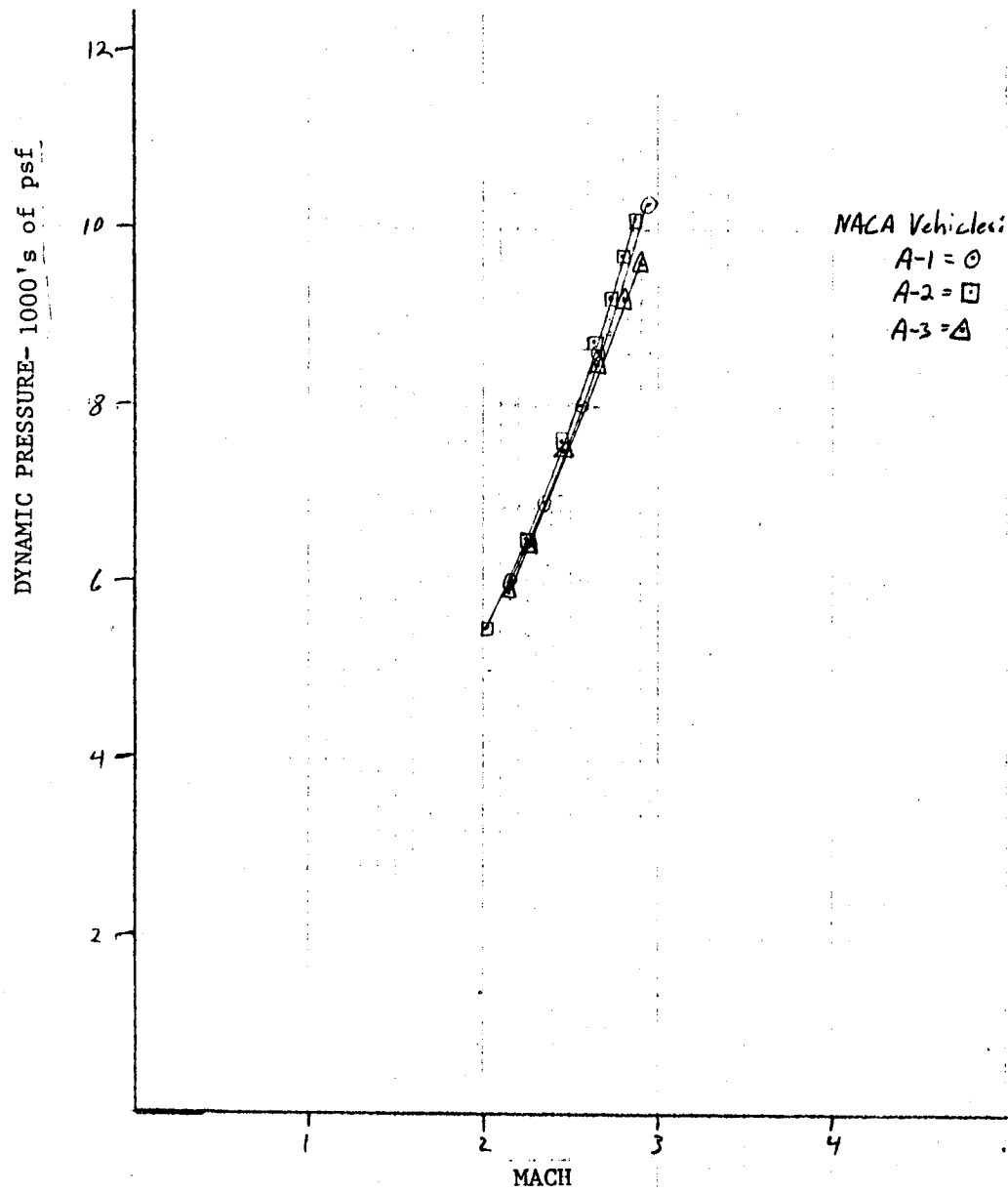
Fig. A-28 - Flight Dynamic Pressure versus Mach Number - NACA
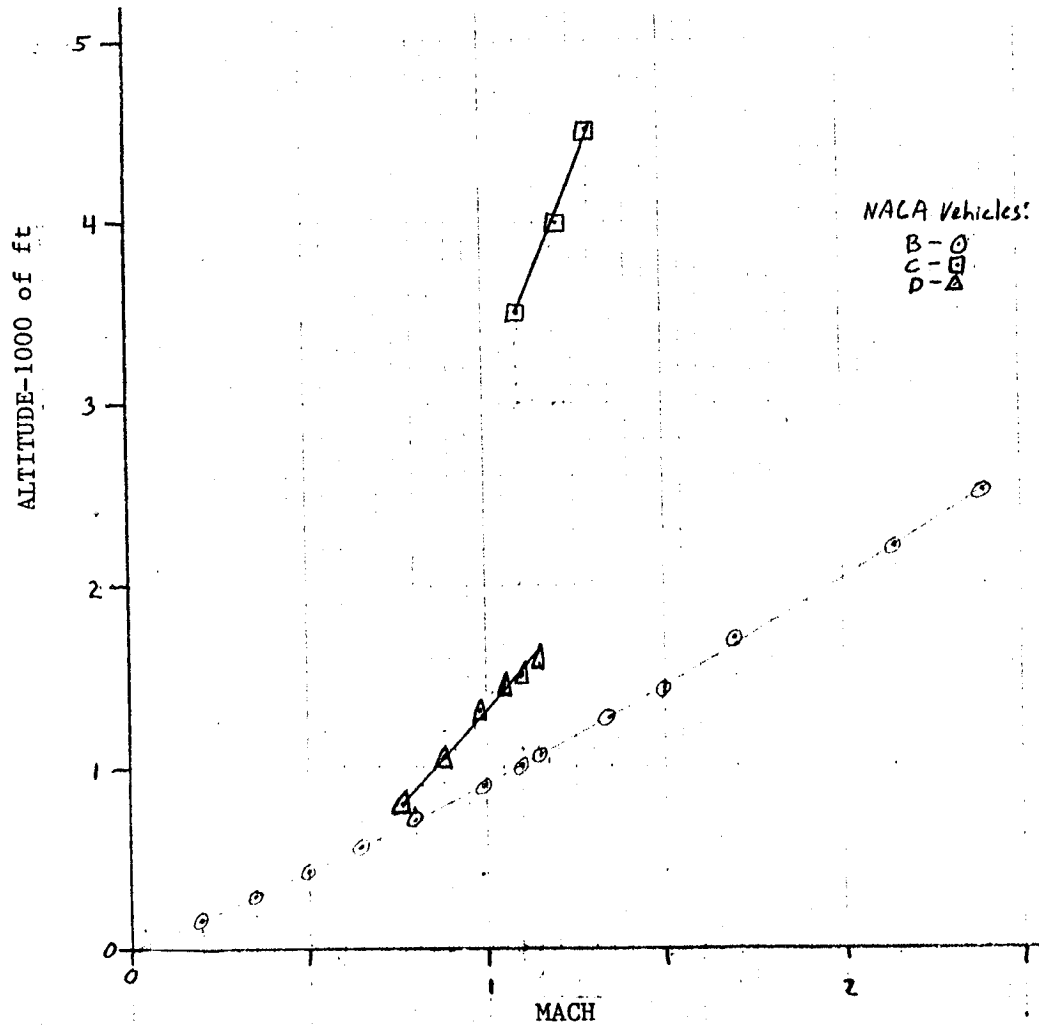
Fig. A-29 - Flight Altitude versus Mach Number - NACA

LOCKHEED-HUNTSVILLE RESEARCH & ENGINEERING CENTER

Fig. A-30 - Flight Dynamic Pressure versus Mach Number - NACA

LOCKHEED-HUNTSVILLE RESEARCH & ENGINEERING CENTER
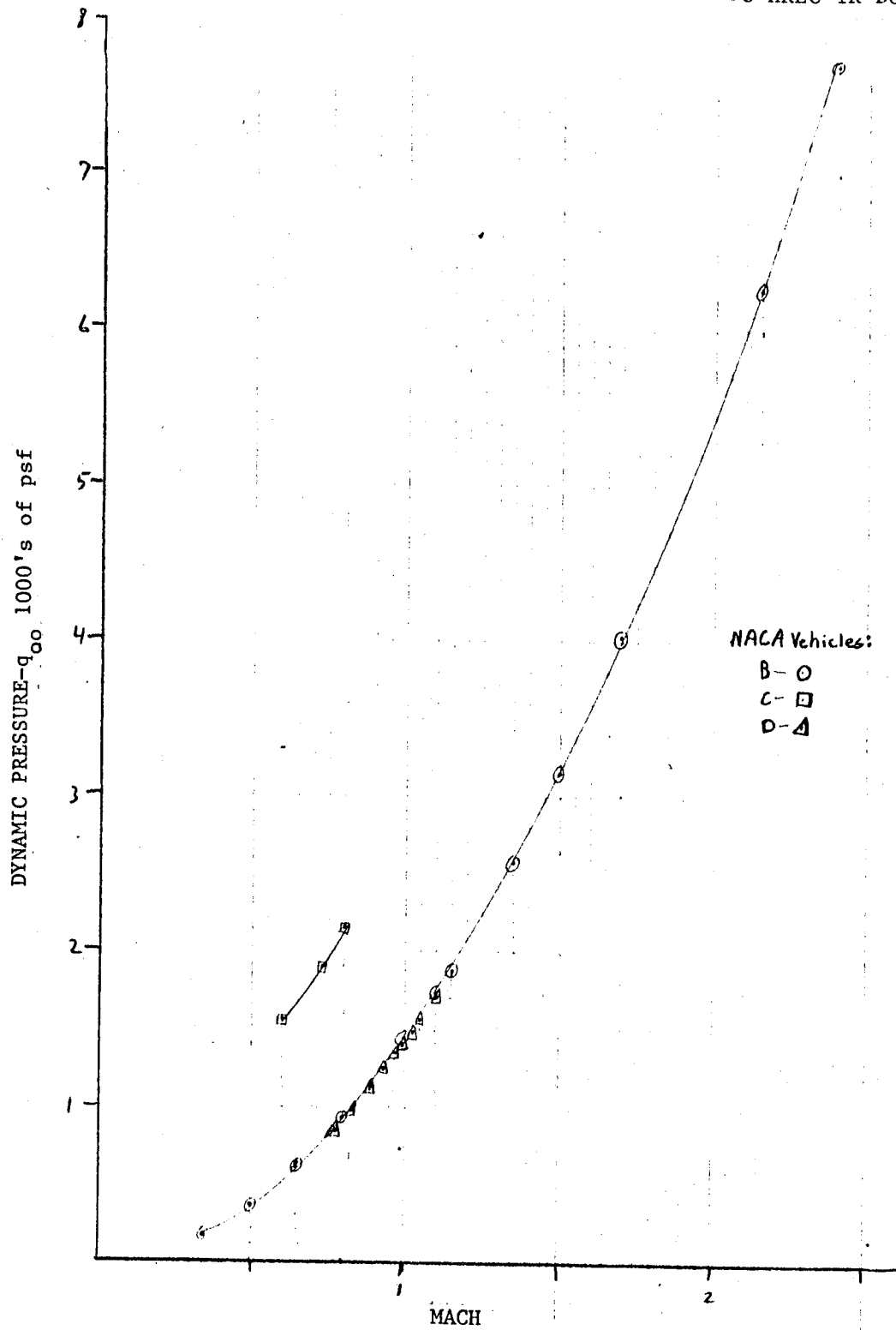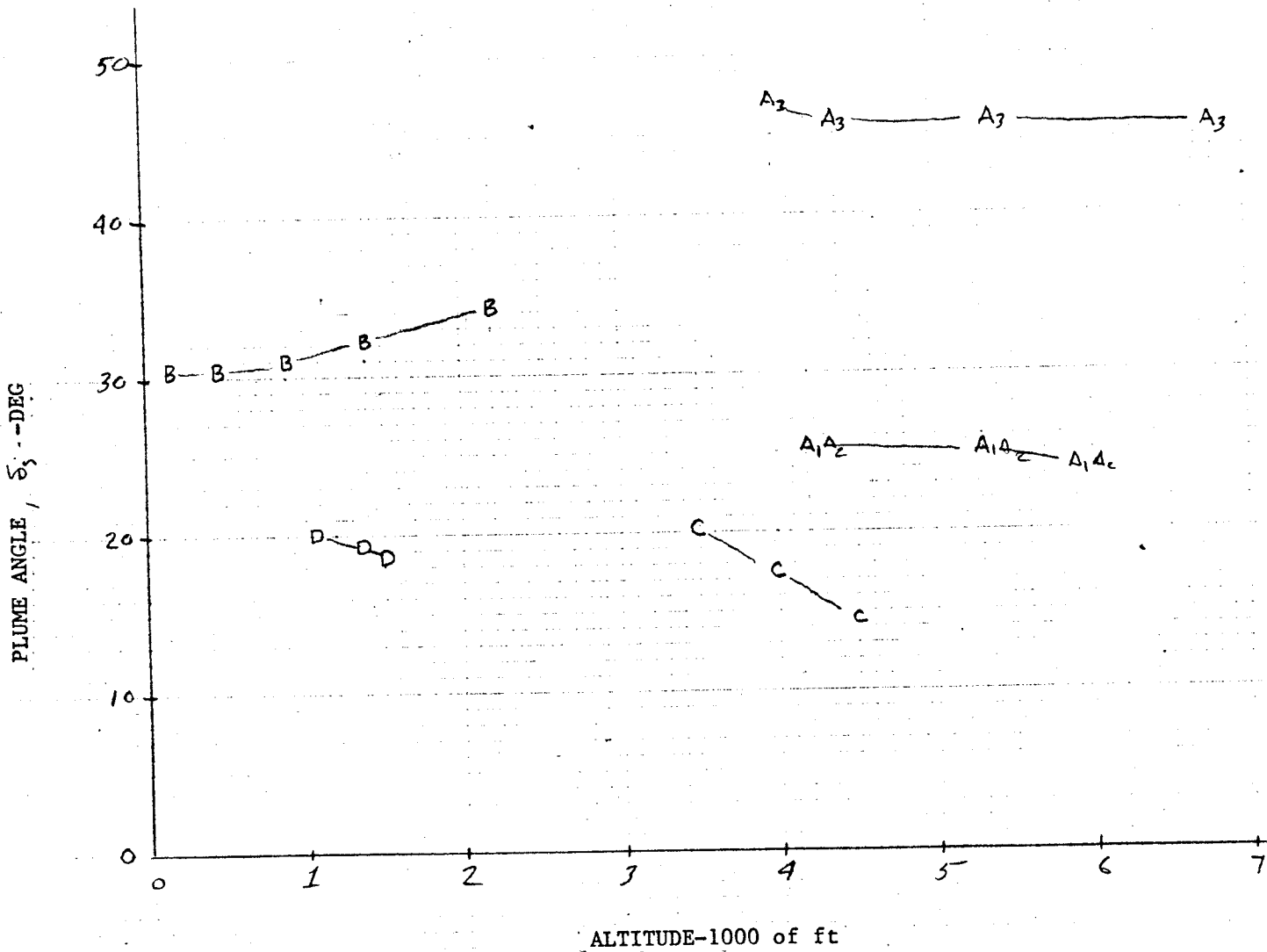
Fig. A-31 - Plume Angle versus Altitude - NACA

LOCKHEED-HUNTSVILLE RESEARCH & ENGINEERING CENTER
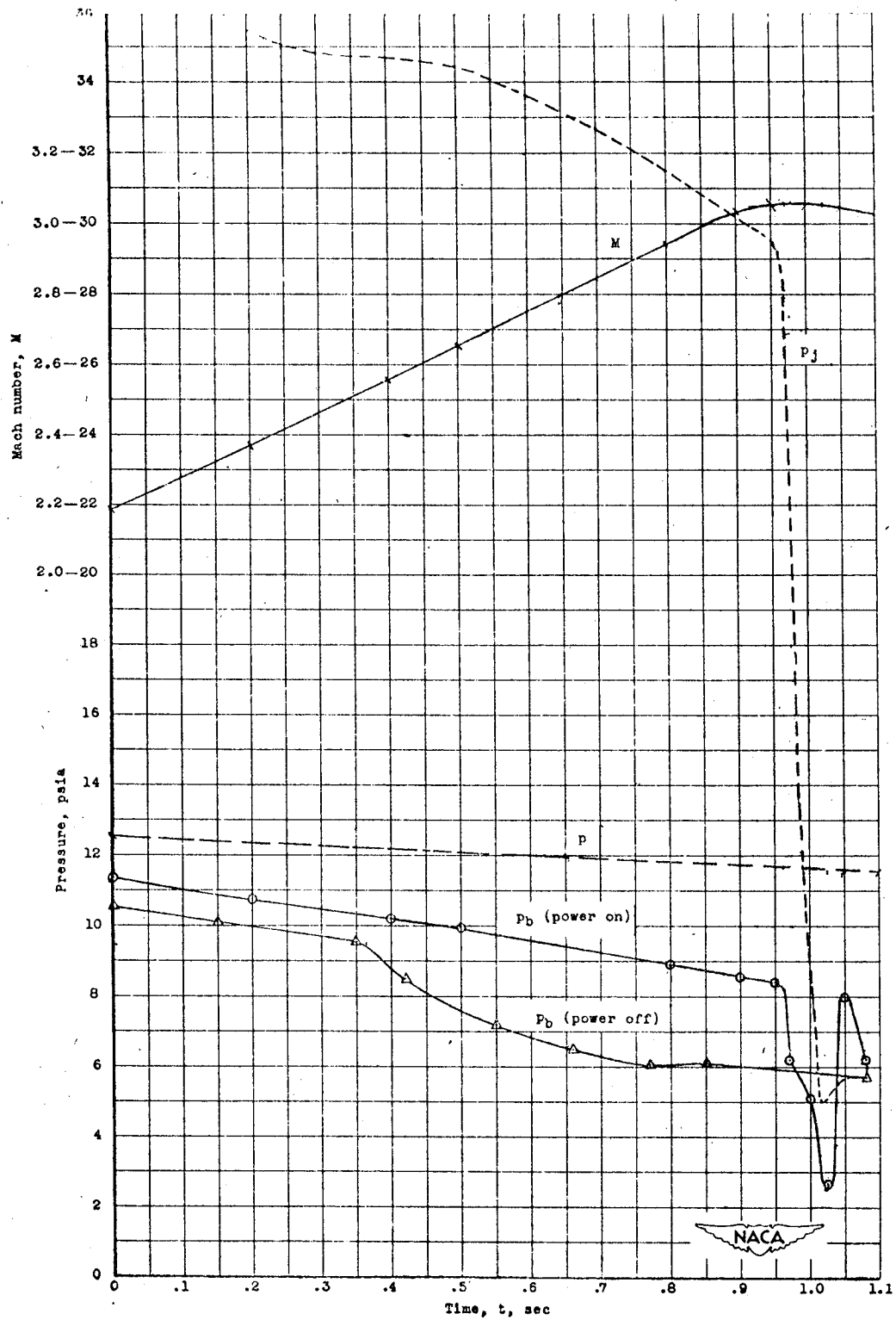
(a) Model A-1, 9° nozzle.

Fig. A-32 - Base Pressure Data for Model A - Source Data

A-47
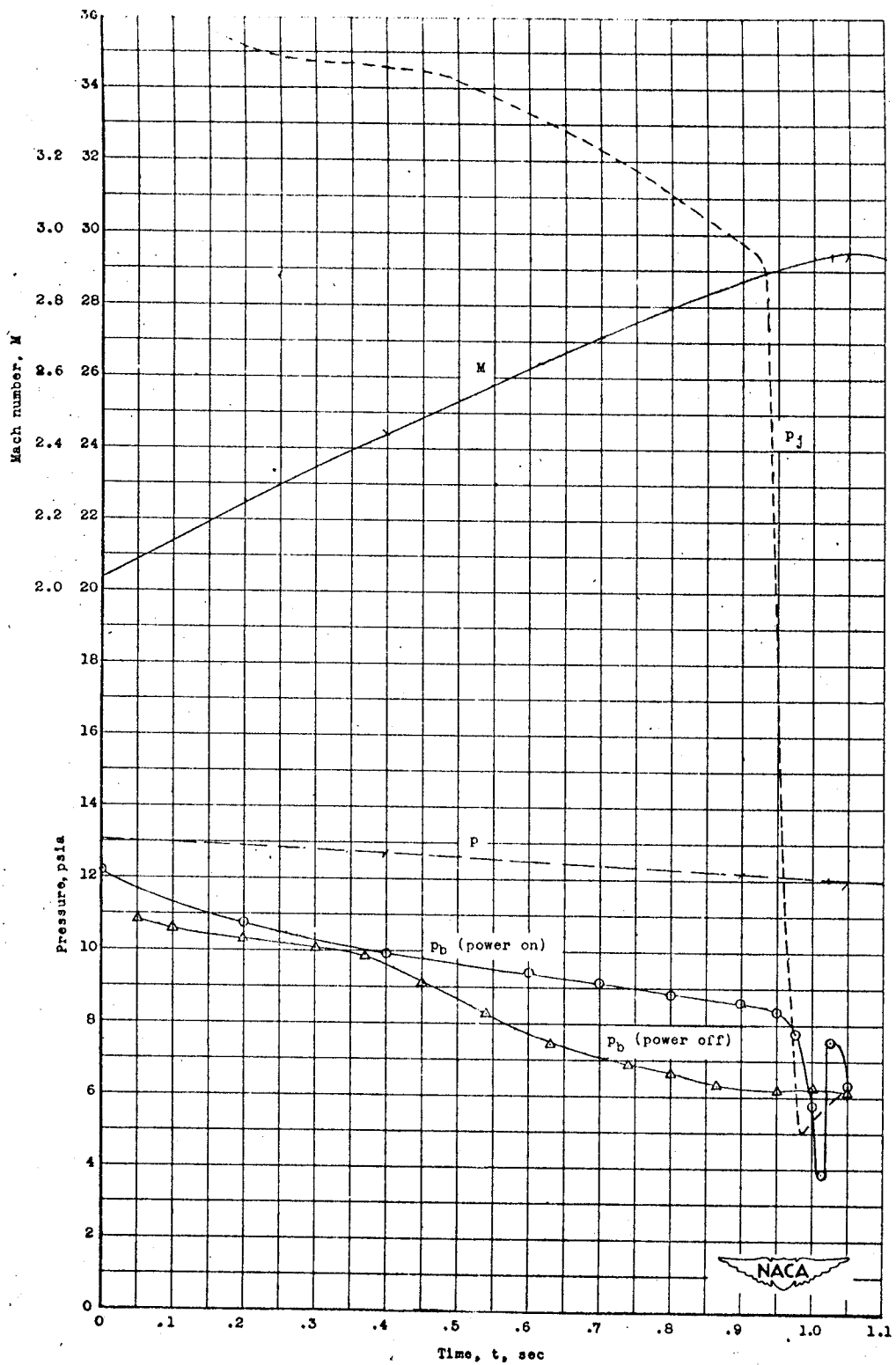
(b) Model A-2, 9° nozzle.

Fig. A-32 - Base Pressure Data for Model A - Source Data (Cont'd)

LOCKHEED-HUNTSVILLE RESEARCH & ENGINEERING CENTER
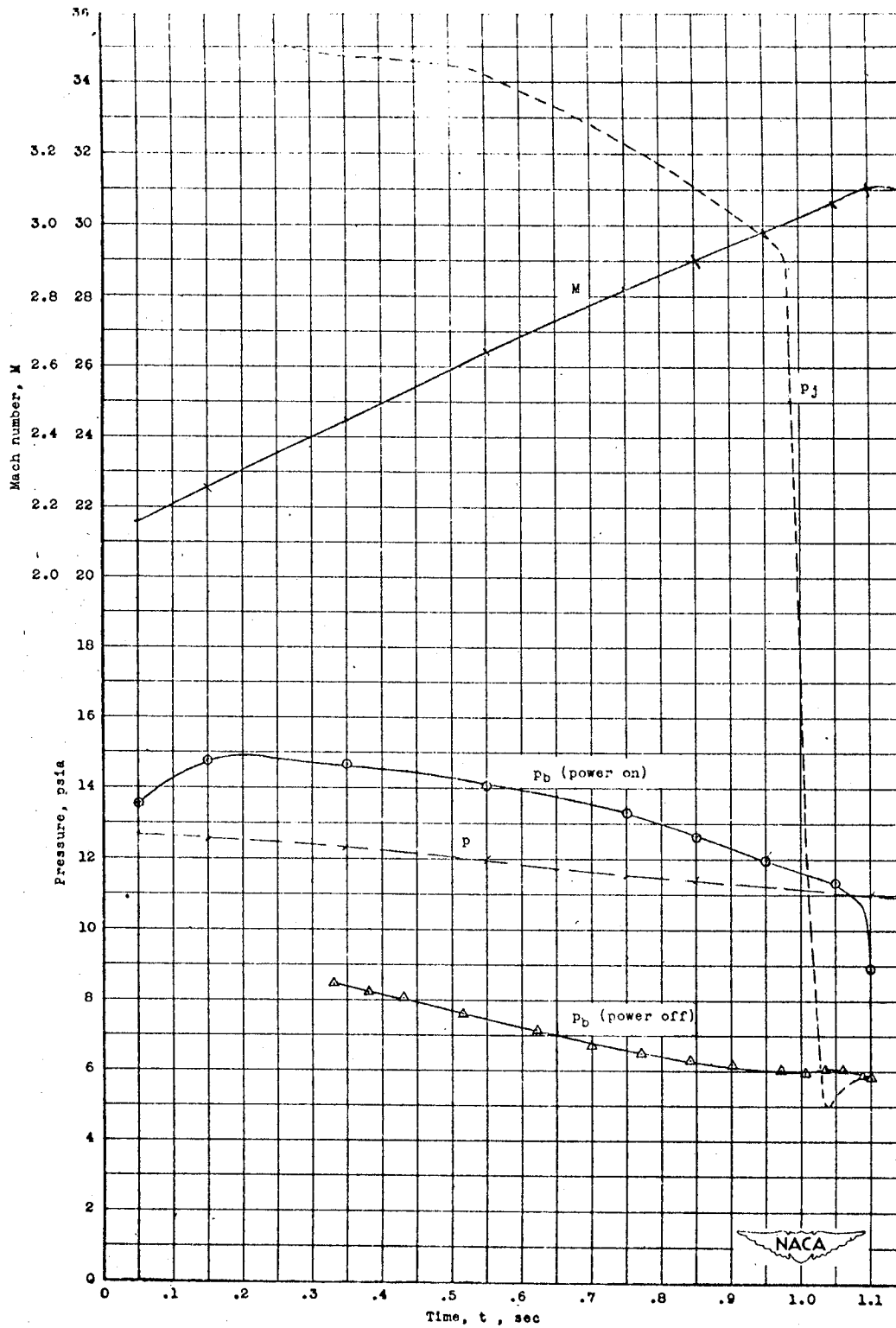
(c) Model A-3, 30° nozzle.

Fig. A-32 - Base Pressure Data for Model A - Source Data (Concl'd)

A-49

LOCKHEED-HUNTSVILLE RESEARCH & ENGINEERING CENTER
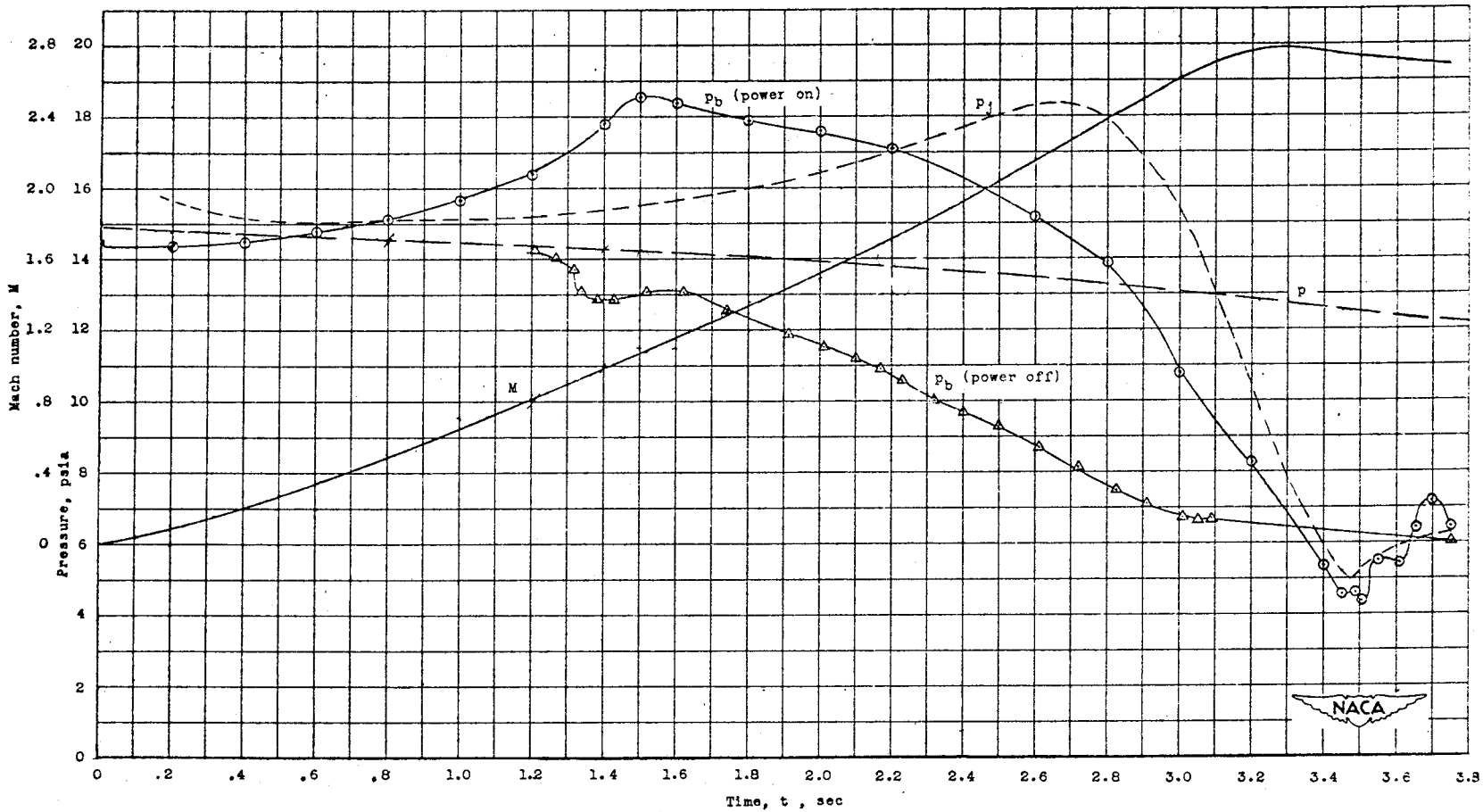
FIGURE A-33 BASE PRESSURE DATA FOR MODEL B-SOURCE DATA
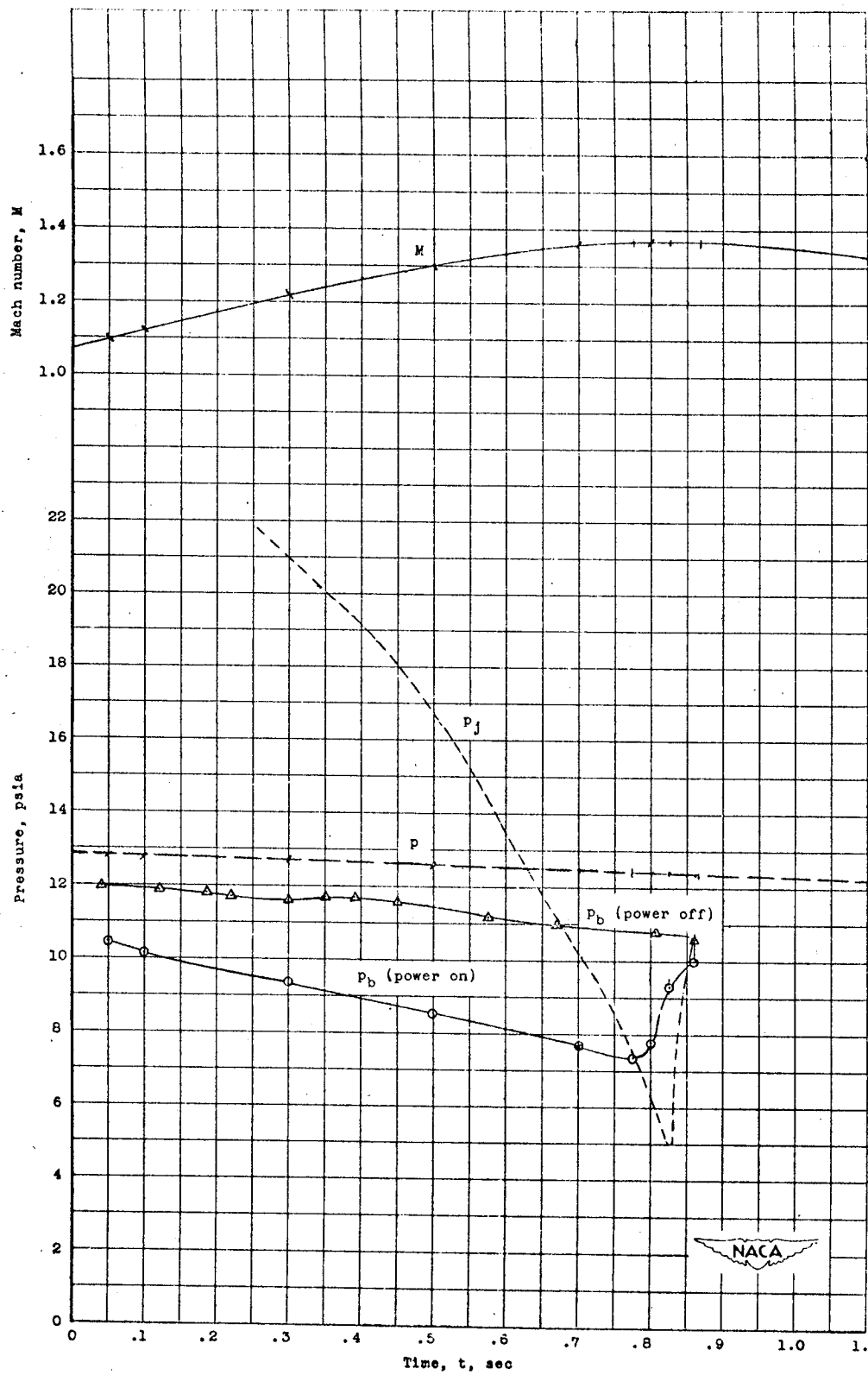
Fig. A-34 - Base Pressure Data for Model C - Source Data

LOCKHEED-HUNTSVILLE RESEARCH & ENGINEERING CENTER
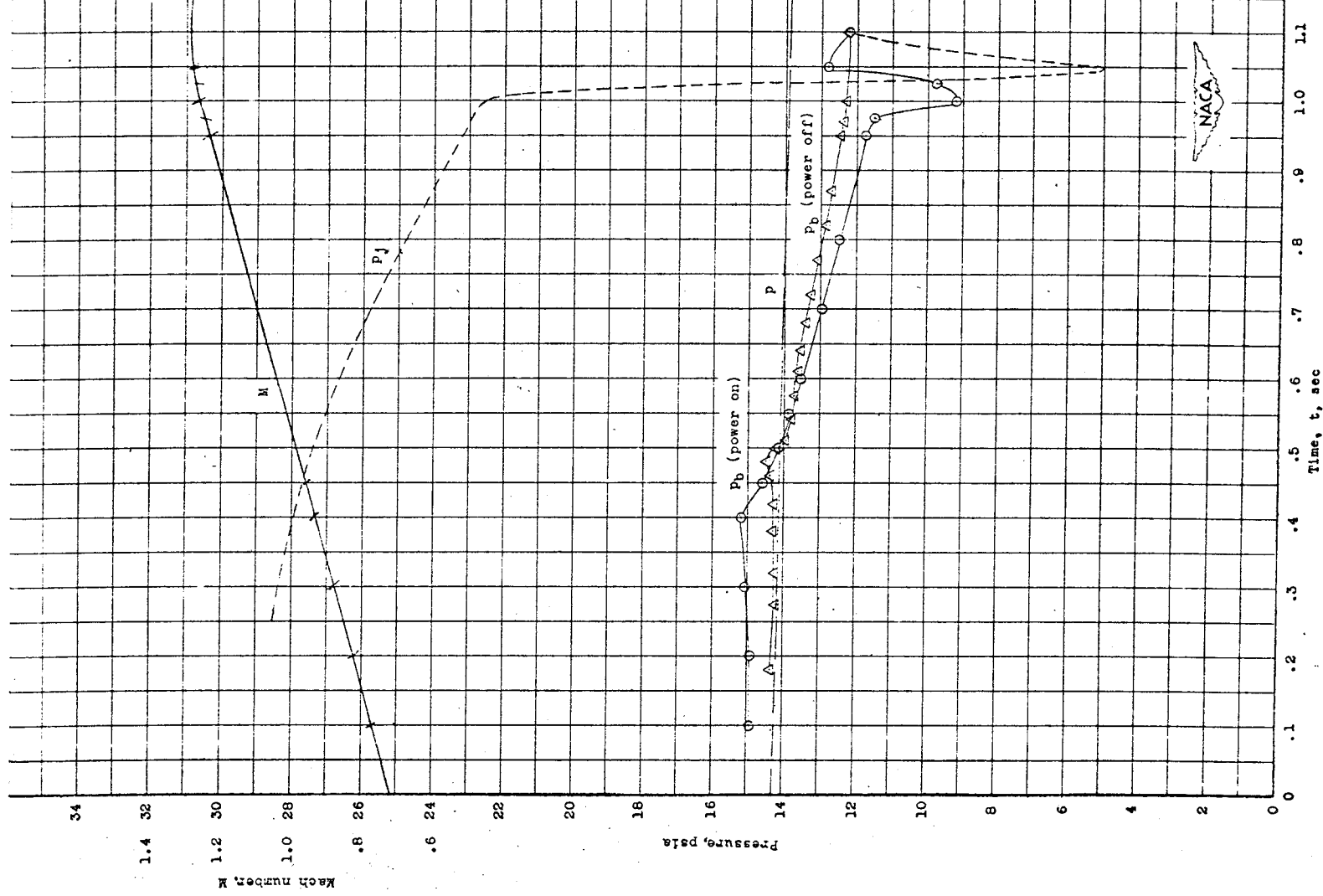
Fig. A-35 - Base Pressure Data for Model D - Source Data

LOCKHEED-HUNTSVILLE RESEARCH & ENGINEERING CENTER

Table A6 NACA

NACA VEHICLE A-1

M	Alt. (ft)	P (psf)	q (psf)	Thrust (lb)	CT AB=.072	C_{PB}	PB/p
2.19	4200	1800	6043	1690	3.88	-.026	.912
2.35	4800	1785.6	6902.68	1690	3.34	-.033	.871
2.56	5300	1756.8	8059.36	1690	2.91	-.036	.836
2.66	5500	1742.4	8629.97	1690	2.72	-.037	.818
2.95	5900	1699.2	10351.10	1690	2.27	-.040	.754

NACA VEHICLE A-2

M	Alt. (ft)	P (psf)	q (psf)	Thrust (lb)	CT	C_{PB}	PB/p
2.04	3100	1886.4	5495.30	1690	4.27	-.024	.931
2.25	3500	1857.6	6582.87	1690	3.57	-.046	.837
2.44	3900	1828.8	7621.56	1690	3.08	-.055	.772
2.63	4200	1800.0	8715.29	1690	2.69	-.049	.76
2.72	4500	1785.6	9247.41	1690	2.54	-.051	.738
2.80	4700	1771.2	9720.35	1690	2.41	-.052	.715
2.87	5000	1756.8	10129.41	1690	2.29	-.051	.705

NACA VEHICLE A-3

M	Alt. (ft)	P (psf)	q (psf)	Thrust (lb)	CT	C_{PB}	PB/p
2.16	4000	1828.8	5972.7	1690	3.93	.019	1.063
2.75	41000	1814.4	6429.8	1690	3.65	.049	1.175
2.45	4400	1800	7563.2	1690	3.10	.042	1.176
2.65	5400	1720.8	8459.0	1690	2.77	.037	1.18
2.82	6400	1663.2	9258.5	1690	2.54	.027	1.152
2.90	6800	1641.6	9774.1	1690	2.43	.019	1.114

Table A-7 NACA

NACA VEHICLE B

Mach	Alt. (ft)	P (psf)	q (psf)	Thrust	CT AB=.288 ft^2	C$_{PB}$	PB/p$_{oo}$
.10	0	2131.2	14.9	5967	1388.70	−3.860	.973
.20	150	2116.8	59.3	5967	349.60	− .500	.986
.35	300	2109.6	180.9	5967	114.50	.117	1.010
.50	450	2095.2	366.7	5967	56.50	.255	1.044
.65	550	2088.0	617.5	5967	33.60	.281	1.083
.80	700	2073.6	928.9	5967	22.30	.310	1.139
1.00	900	2059.2	1441.4	5967	14.37	.349	1.244
1.10	1000	2052.0	1738.0	5967	11.92	.360	1.305
1.15	1075	2044.8	1892.9	5967	10.95	.319	1.295
1.35	1300	2030.4	2590.3	5967	7.99	.212	1.270
1.50	1400	2001.6	3152.5	5967	6.57	.169	1.266
1.70	1700	1987.2	4020.1	5967	5.15	.118	1.239
2.15	2200	1944.0	6290.3	5967	3.29	.039	1.126
2.40	2500	1915.2	7722.1	5967	2.68	.011	1.045

NACA VEHICLE C (AB=.065 ft^2)

Mach	Alt. (ft)	P (psf)	q (psf)	Thrust	CT	C$_{PB}$	PB/p$_{oo}$
1.10	3500	1850.4	1567.3	391	3.84	− .216	.817
1.22	4000	1828.8	1905.4	391	3.16	− .253	.736
1.30	4500	1814.4	2146.4	391	2.80	− .272	.678

NACA VEHICLE D (AB=.11 ft^2)

Mach	Alt. (ft)	P (psf)	q (psf)	Thrust	CT	C$_{PB}$	PB/p$_{oo}$
.77	800	2052.0	851.6	1823	19.46	.118	1.049
.83	900	2044.8	986.1	1823	16.81	.109	1.053
.88	1050	2037.6	1104.5	1823	15.00	.124	1.067
.93	1100	2030.4	1229.3	1823	13.48	.129	1.078
.96	1200	2030.4	1309.9	1823	12.65	.054	1.035
.99	1300	2030.4	1393.0	1823	11.89	.015	1.010
1.02	1350	2023.2	1473.5	1823	11.25	− .015	.989
1.05	1400	2020.3	1559.2	1823	10.63	− .040	.969
1.10	1500	2017.4	1708.7	1823	9.69	− .085	.923
1.15	1600	2016.0	1866.3	1823	8.88	− .116	.893

SPACE SHUTTLE – SRB

SPACE SHUTTLE - SRB

The Space Shuttle vehicle (Figure A-36) consists of an Orbiter with Space Shuttle Main Engines (SSME), an External Tank (ET), and two solid rocket boosters (SRB). The Orbiter with SSMEs and the SRBs are reusable elements while the ET is expended after each launch. The three SSMEs produce a total sea level thrust of 1.125 million lb. They are fueled with LOX and liquid hydrogen stored in the external tank. The engines are bearing mounted and capable of gimbaling for Orbiter steering control. The External Tank reacts the SRB thrust through its intertank structure and provides attach structure to the Orbiter to react the SSME thrust. At liftoff the ET contains approximately 1.5 million lb of fuel. At main engine cutoff, the ET is separated from the Orbiter before orbital velocity is achieved. The ET then proceeds on a ballistic reentry path and breaks up prior to impact in the ocean. Each SRB produces approximately 2.65 million lb of thrust at sea level, and after about 55 sec they reduce thrust about one-third to prevent overstressing the vehicle during the period of maximum dynamic pressure. Two lateral sway braces and a diagonal attachment at the aft frame provide the structural attachment between the SRB and ET. The SRB forward attachment to the ET is by a single thrust attachment at the forward end of the forward skirt. The same forward skirt is used for attaching the main parachute riser attachments. The SRBs are released from the ET by pyrotechnic separation devices at the forward thrust attachment and aft sway braces. Eight separation motors on each SRB, four aft and four forward, separate the SRB from the Orbiter and ET.

The Space Shuttle SRB base pressure environment is primarily determined by the SRB engine operation. There is an influence of the SSME operation on SRB base pressures, but it is small. Thus the SRB is classified as a single engine configuration. The SRB configuration description is presented in Figs. A-37 through A-40. Trajectory data are presented in Figs. A-41 and A-42. Thrust characteristics and plume angle data are presented in Figs. A-43 and A-44. Table of trajectory data, thrust data, and base pressure characteristics are presented in Tables A-8 through A-15.

LOCKHEED-HUNTSVILLE RESEARCH & ENGINEERING CENTER

SPACE SHUTTLE REFERENCES

1. "Space Shuttle System Summary," Report SSV80-1, Rockwell International Space Systems Group, May 1980.

2   "STS-5 Postflight Report on Ascent External Aerodynamic Loads," Report SAS/AERO/83-094, Rockwell International, 1 March 1983.

LOCKHEED-HUNTSVILLE RESEARCH & ENGINEERING CENTER
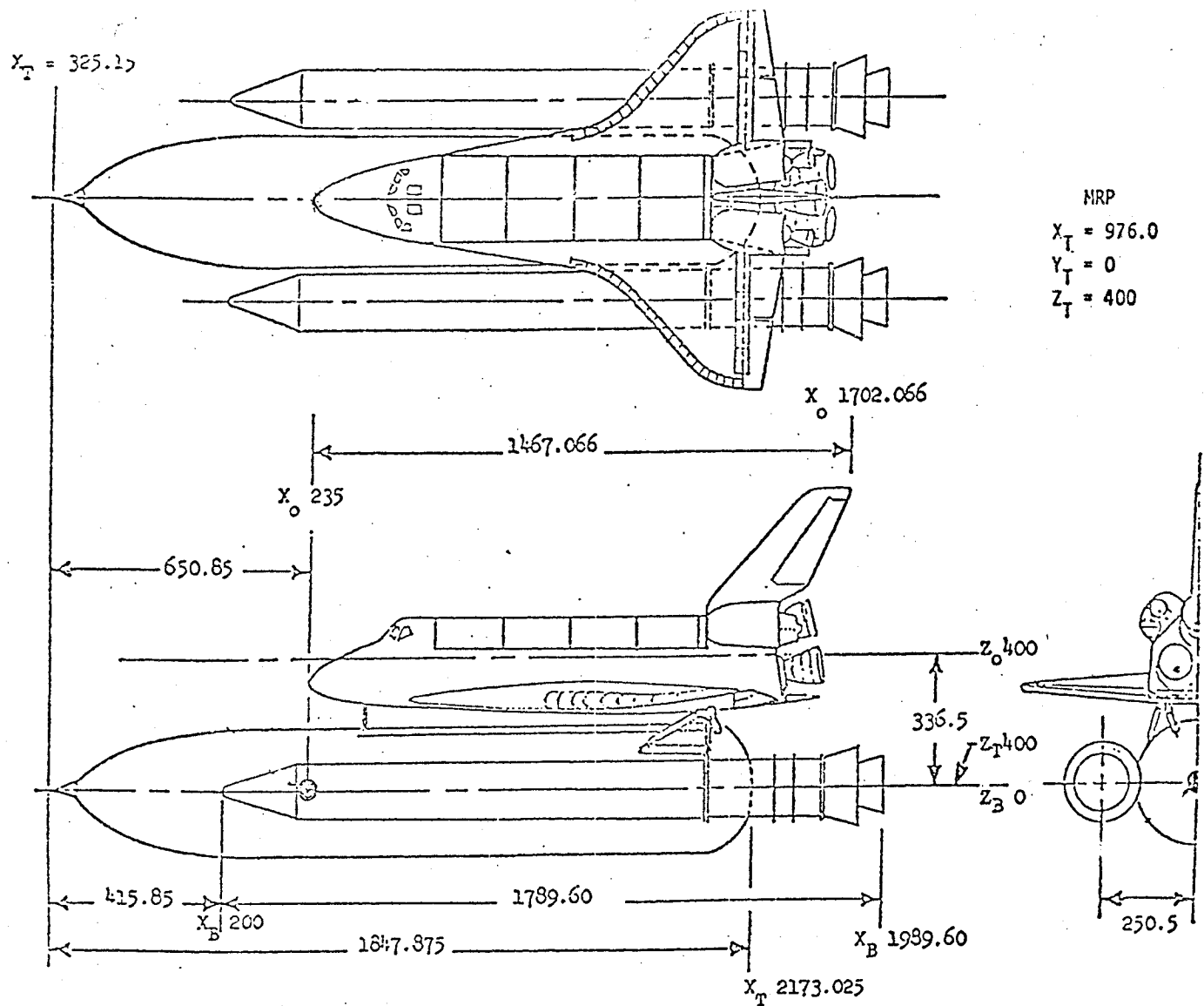
Fig. A-36 - Space Shuttle Launch Vehicle and Elements

NOZZLE & TVC
$\epsilon = 7.16{:}1$

4 SEPARATION MOTORS
20,000-LB THRUST EACH

4 SEPARATION MOTORS
20,000-LB THRUST EACH

MAIN PARACHUTE PACK

ET/SRB FORWARD
ATTACH

AFT SKIRT &
LAUNCH SUPPORT

SRB/ET ATTACH RING
& SWAY BRACES

DROGUE
CHUTE

SYSTEMS
TUNNEL

SEPARATION AVIONICS
OPERATIONAL FLIGHT
INSTRUMENTATION
RECOVERY AVIONICS

NOSE FAIRING

FORWARD
SKIRT

DIMENSIONS

LENGTH . . . 1790 IN.
DIAMETER . . 146 IN.

APPROXIMATE WEIGHTS & THRUST

| GROSS WEIGHT . . . 1,293,500 LB |
| INERT WT . . . . 184,600 LB |
| THRUST (SL) . . . . . 2.65M LB |

Fig. A-37 – Space Shuttle SRB Configuration
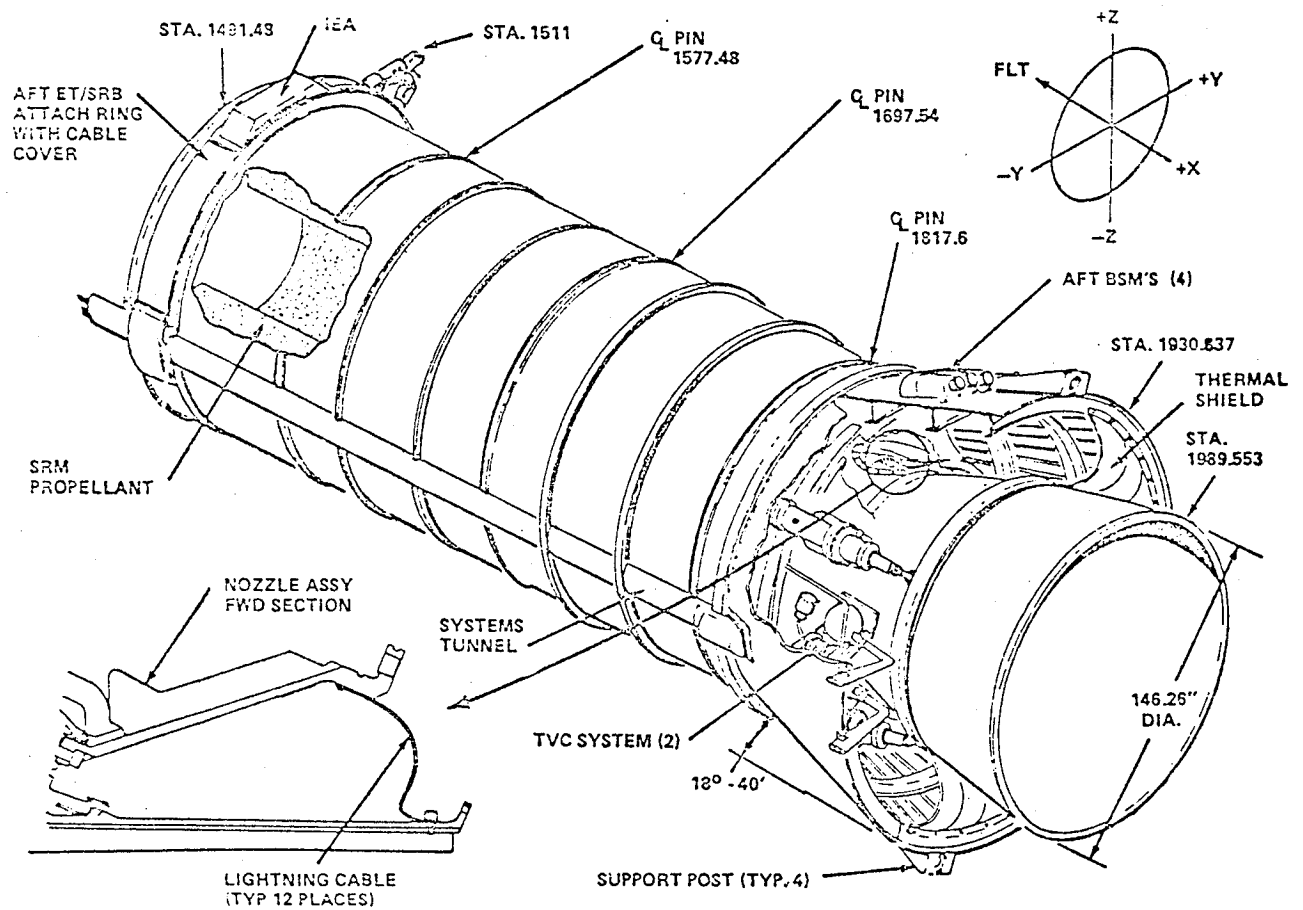
Fig. A-38 - Space Shuttle Aft Skirt Assembly
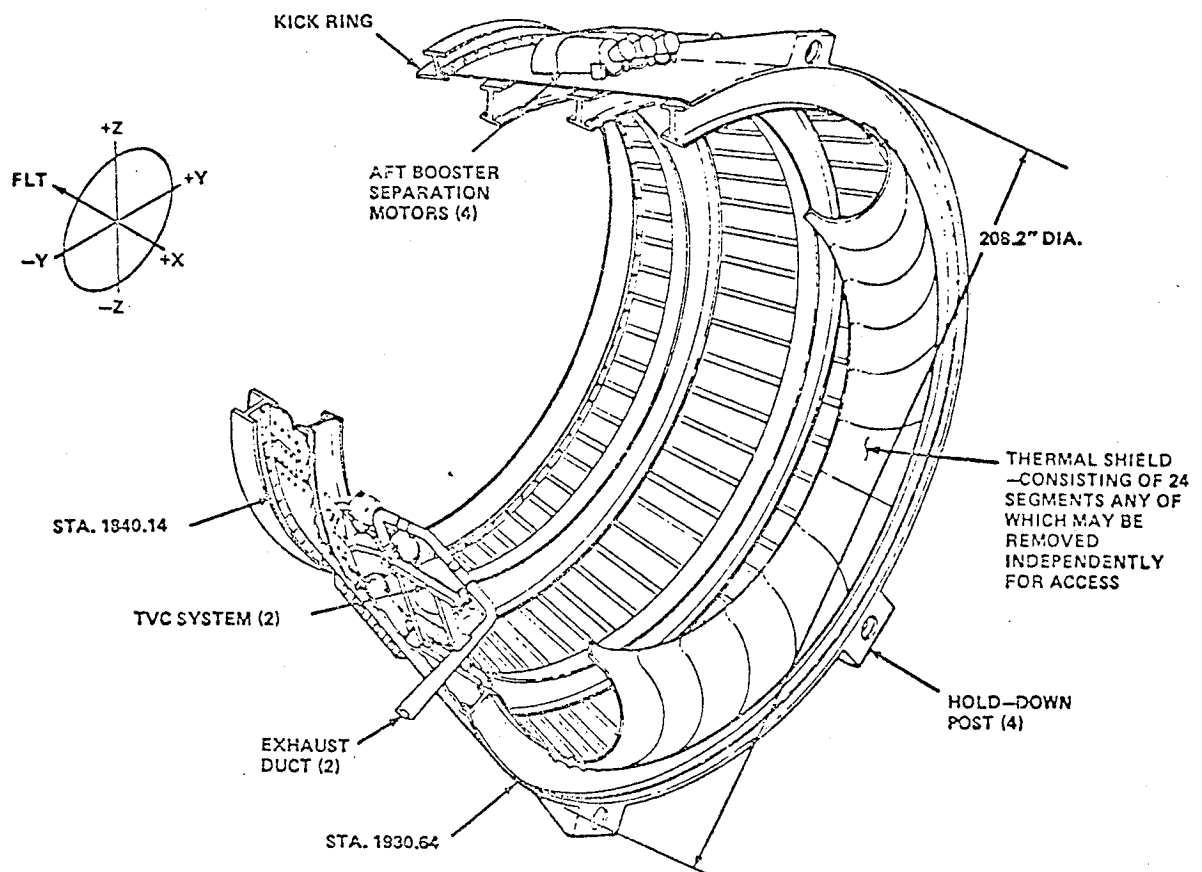
Fig. A-39 - Space Shuttle Aft Skirt Configuration

$D_c = 146$ IN.

$D_B = 208$ IN

$D_N = 146.3$ IN

$X_j = 58.9$ IN

$\Theta_L = 11°$

$L_s = 90.5$
$\Theta_s = 18.9°$

$A_B = 236.3$ FT.^{2}
$A_N = 116.7$ FT.^{2}

$\dfrac{A_N}{A_B} = .494$

$\dfrac{X_j}{D_B} = .28$

$\dfrac{L_s}{D_c} = .62$
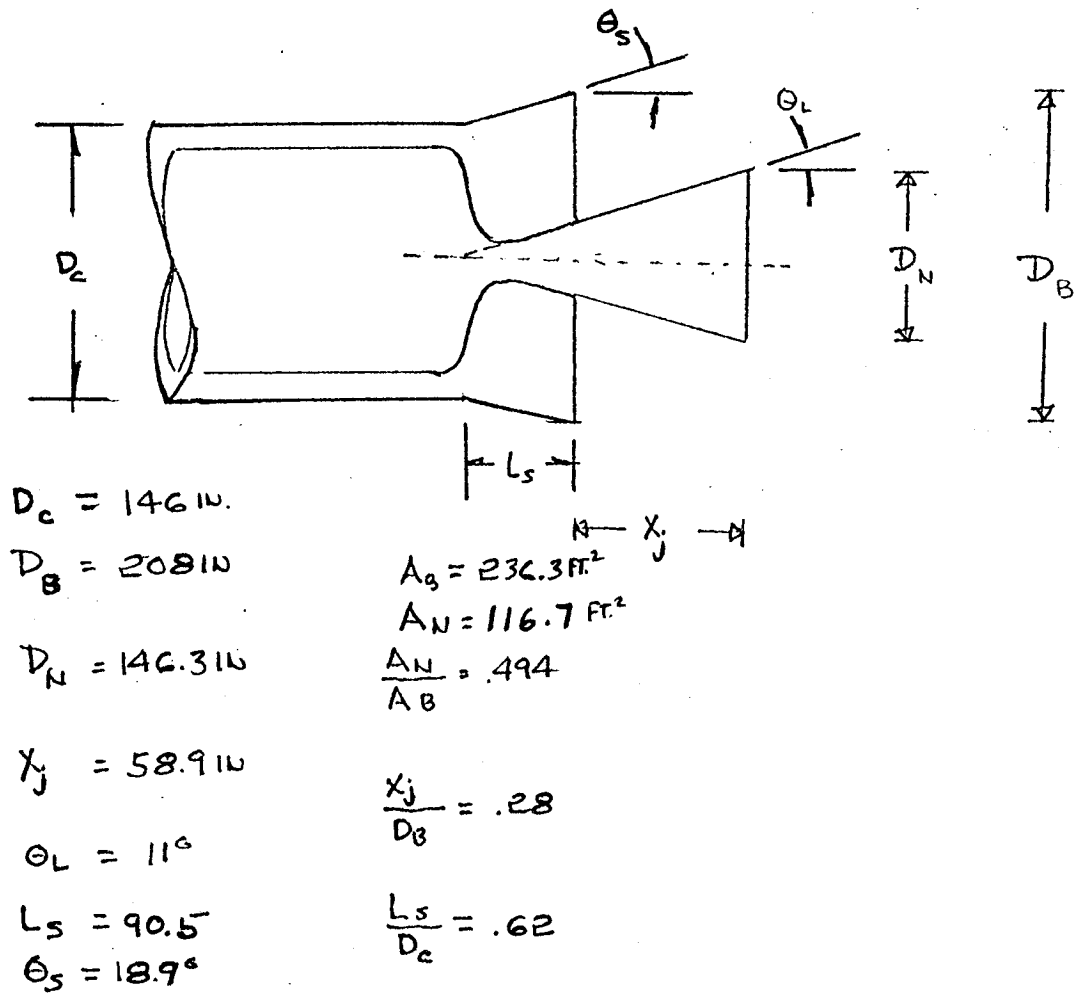
Fig. A-40 - Base Geometry - Space Shuttle SRB

A-61

LOCKHEED-HUNTSVILLE RESEARCH & ENGINEERING CENTER

140

120

100

ALTITUDE-1000 of ft

80

60

40

20

0

FLT DATA BAND FOR STS 1-5

0   1   2   3   4
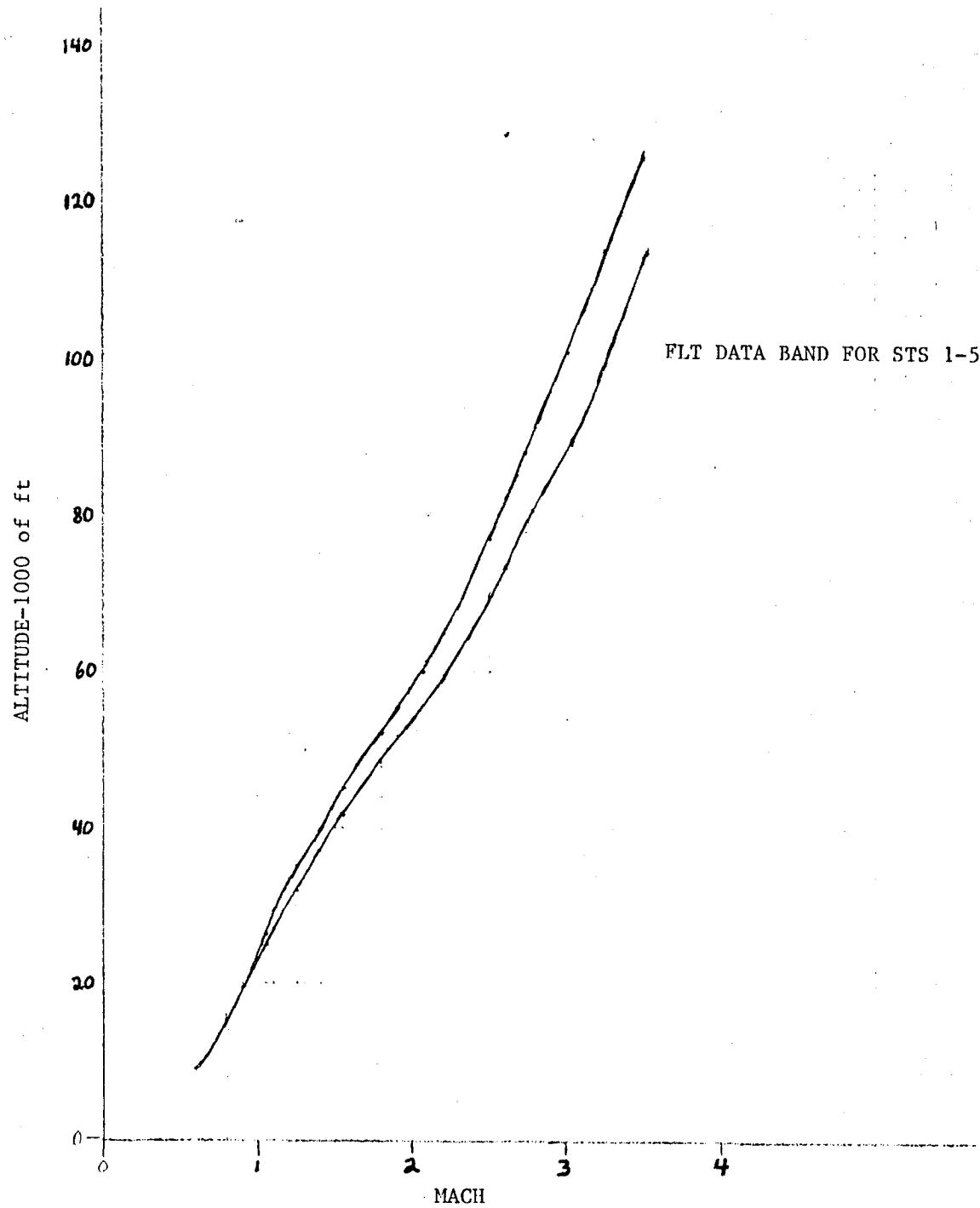
MACH

Fig. A-41 - Flight Altitude versus Mach Number - Space Shuttle

LOCKHEED-HUNTSVILLE RESEARCH & ENGINEERING CENTER

Fig. A-42 - Flight Dynamic Pressure versus Mach Number - Space Shuttle

LOCKHEED-HUNTSVILLE RESEARCH & ENGINEERING CENTER
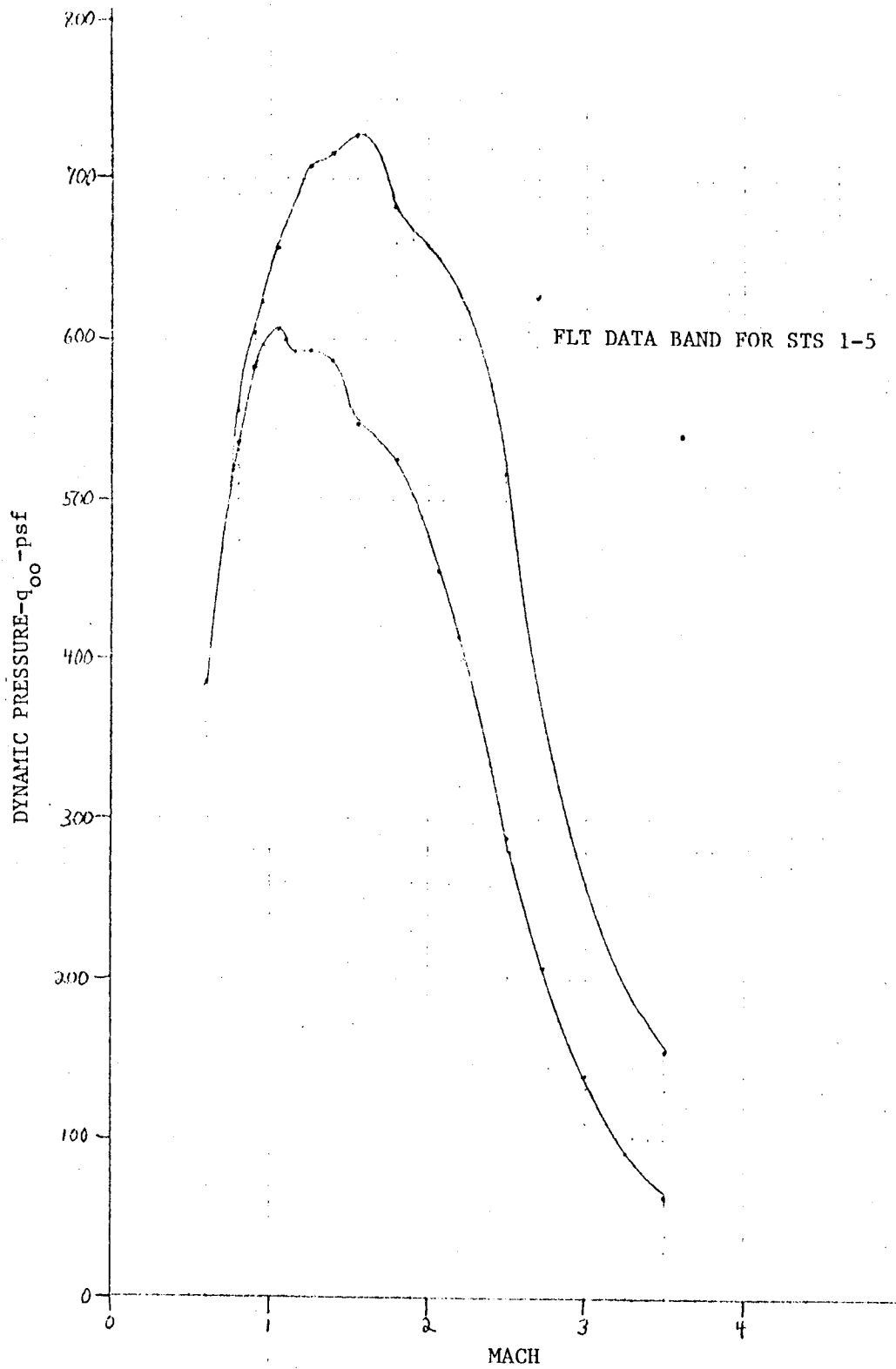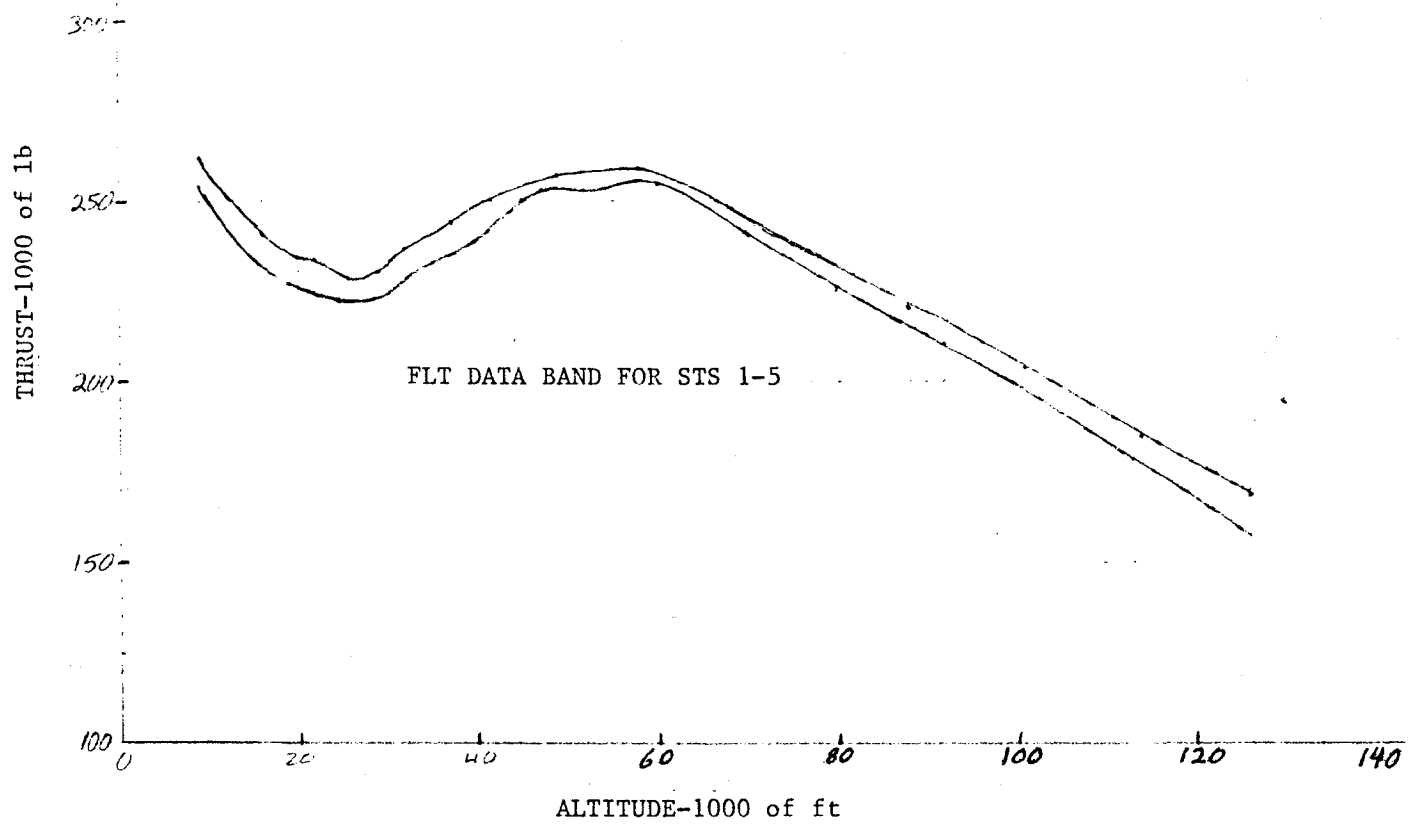
Fig. A-43 - Thrust versus Altitude - Space Shuttle SRB
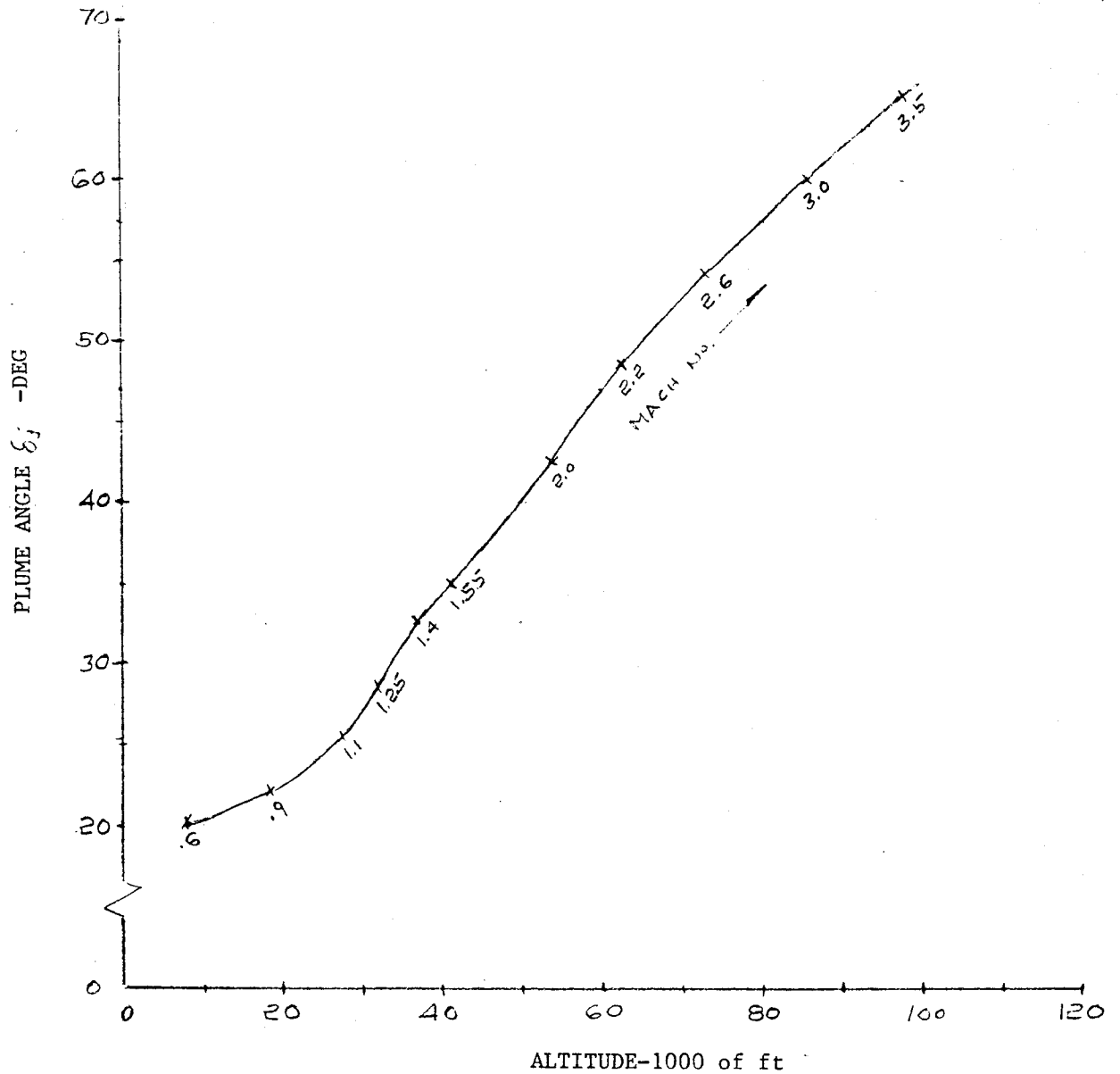
Fig. A-44 - Plume Angle versus Altitude - Space Shuttle SRB

LOCKHEED-HUNTSVILLE RESEARCH & ENGINEERING CENTER

Table A-8   STS-1 LEFT SRB ELEMENT

Mach	Alt ft	P_{oo} Psf	q_{oo} psf	Left SRB Thrust lb	AB=236.3 ft^2 C_T (1ft SRB)
.60	9387	1527.84	385.02	2542000	27.94
.80	15879	1198.10	536.75	2347000	18.50
.90	19861	1026.72	582.15	2275000	16.54
.95	21904	946.10	597.69	2269000	16.06
1.05	26410	786.24	606.78	2229000	15.55
1.10	28889	708.48	600.08	2230000	15.73
1.15	31247	639.36	591.89	2282000	16.32
1.25	35115	541.44	592.20	2333000	16.67
1.40	39953	429.12	588.75	2385000	17.14
1.60	45512	326.88	549.73	2503000	19.27
1.80	52390	231.84	525.81	2524000	20.31
2.08	60000	151.03	457.39	2544000	23.54
2.20	64909	122.40	414.69	2502000	25.53
2.50	77556	66.74	289.80	2361000	34.48
2.72	88080	40.33	208.86	2207000	44.72
3.00	101000	22.25	140.18	2040000	61.59
3.25	114800	12.44	91.98	1851000	85.16
3.50	126037	7.45	63.88	1691000	112.03

Table A-9 STS-1 LEFT SRB ELEMENT

Mach	C_{PB}	$C_{PB}Max$	$C_{PB}Min$	P_B/P_{oo}	$P_B/P_{oo}Max$	$P_B/P_{oo}Min$
.60	-.245	-.30	-.175	.938	.924	.956
.80	-.190	-.23	-.150	.915	.897	.933
.90	-.150	-.20	-.110	.915	.887	.937
.95	-.140	-.19	-.090	.912	.879	.943
1.05	-.130	-.18	-.075	.899	.861	.942
1.10	-.112	-.16	-.060	.905	.864	.949
1.15	-.075	-.11	-.035	.931	.898	.968
1.25	-.030	-.06	.010	.967	.934	1.010
1.40	.035	.02	.060	1.050	1.030	1.080
1.60	.075	.04	.110	1.140	1.070	1.200
1.80	.095	.06	.130	1.220	1.140	1.290
2.08	.115	.09	.145	1.350	1.270	1.440
2.20	.135	.10	.205	1.460	1.330	1.690
2.50	.160	.10	.250	1.700	1.440	2.090
2.72	.180	.10	.300	1.930	1.520	2.550
3.00	.200	.12	.320	2.260	1.760	3.020
3.25	.240	.14	.350	2.770	2.040	3.580
3.50	.320	.22	.420	3.740	2.890	4.600

Table A-10 STS-2 LEFT SRB ELEMENT

Mach	Alt ft	P_{oo} Psf	q_{oo} psf	Left SRB Thrust	AB=236.3 C_T (Lft SRB)
.60	8975	1523.52	323.93	2597000	28.63
.80	14925	1215.36	544.48	2402000	18.67
.90	18306	1064.16	603.38	2342000	16.43
.95	20118	989.28	624.98	2321000	15.72
1.05	24520	825.12	636.79	2281000	15.16
1.10	26847	747.36	633.01	2254000	15.07
1.15	28647	691.20	639.88	2270000	15.01
1.25	33043	568.80	622.13	2340000	15.92
1.40	38810	434.88	596.66	2425000	17.20
1.55	43995	339.84	571.53	2484000	18.39
1.80	51400	236.16	535.61	2523000	19.93
1.94	55397	191.00	503.19	2542000	21.38
2.20	64149	125.28	424.45	2543000	25.35
2.50	74760	77.76	340.20	2372000	29.51
2.69	81603	53.00	268.46	2234000	35.22
3.00	93710	31.00	195.30	2126000	46.07
3.29	106615	17.00	178.81	1942000	63.80
3.50	122428	8.64	74.09	1714000	97.90

Table A-11   STS-2 LEFT SRB ELEMENT

Mach	C_{PB}	C_{PB}Max	C_{PB}Min	P_B/P_{oo}	P_B/P_{oo}Max	P_B/P_{oo}Min
.60	−.220	−.260	−.175	.945	.934	.956
.80	−.162	−.185	−.145	.927	.917	.935
.90	−.135	−.160	−.115	.923	.909	.935
.95	−.130	−.155	−.105	.918	.902	.934
1.05	−.155	−.170	−.135	.880	.869	.896
1.10	−.135	−.160	−.110	.886	.864	.907
1.15	−.115	−.125	−.110	.894	.884	.898
1.25	−.060	−.070	−.040	.934	.923	.956
1.40	.012	−.005	.025	1.020	.993	1.030
1.55	.050	.035	.060	1.080	1.060	1.100
1.80	.090	.085	.100	1.200	1.190	1.230
1.94	.103	.090	.120	1.270	1.240	1.320
2.20	.130	.115	.150	1.440	1.390	1.510
2.50	.145	.128	.165	1.630	1.560	1.720
2.69	.152	.135	.172	1.770	1.680	1.870
3.00	.170	.155	.190	2.070	1.980	2.190
3.29	.195	.180	.220	2.480	2.360	2.670
3.50	.228	.205	.248	2.960	2.760	3.130

LOCKHEED-HUNTSVILLE RESEARCH & ENGINEERING CENTER

Table A-12   STS-3 LEFT SRB ELEMENT

Mach	Alt ft	P_{oo} Psf	q_{oo} psf	Left SRB Thrust	AB=236.3 C_T (1ft SRB)
.60	9051	1522.08	383.56	2618000	28.89
.80	16155	1166.40	522.55	2413000	19.54
.90	20043	1000.80	567.45	2348000	17.51
.95	21771	934.56	590.41	2346000	16.82
1.05	25781	792.00	611.23	2294000	15.88
1.10	27697	730.08	618.38	2288000	15.66
1.15	29376	676.80	626.55	2306000	15.58
1.25	32473	591.84	647.33	2362000	15.44
1.40	37832	463.68	636.17	2449000	16.29
1.55	41969	380.16	639.33	2502000	.16.56
1.80	48617	275.04	623.79	2563000	17.39
2.06	55020	191.70	569.45	2588000	19.23
2.20	59118	174.24	590.33	2588000	18.55
2.50	69861	98.72	410.03	2406000	24.83
2.79	80821	55.80	304.05	2259000	31.44
3.10	92684	33.00	221.99	2108000	40.19
3.50	113210	12.96	111.13	1781000	67.82

Table A-13 STS-3 LEFT SRB ELEMENT

Mach	C_{PB}	C_{PB} Max	C_{PB} Min	P_B/P_{oo}	P_B/P_{oo} Max	P_B/P_{oo} Min
.60	-.215	-.290	-.135	.946	.927	.966
.80	-.160	-.205	-.115	.928	.908	.948
.90	-.140	-.185	-.085	.921	.895	.952
.95	-.125	-.182	-.075	.921	.885	.953
1.05	-.130	-.170	-.085	.899	.869	.934
1.10	-.115	-.150	-.070	.903	.873	.941
1.15	-.075	-.100	-.055	.931	.907	.949
1.25	-.035	-.050	-.010	.962	.945	.989
1.40	-.020	-.040	.040	.973	.945	1.050
1.55	.040	-0-	.070	1.070	1.000	1.120
1.80	.075	.040	.100	1.170	1.090	1.230
2.06	.080	.055	.110	1.240	1.160	1.327
2.20	.079	.060	.110	1.270	1.200	1.370
2.50	.083	.060	.110	1.360	1.260	1.480
2.79	.085	.060	.110	1.460	1.330	1.590
3.10	.077	.055	.100	1.520	1.370	1.670
3.50	.115	.070	.140	1.990	1.600	2.200

Table A-14   STS-5 SRB ELEMENT

Mach	Alt ft	P_{oo} Psf	q_{oo} psf	Lft SRB Thrust	AB=236.3 C_T (1ft SRB)
.60	9169	1523.01	383.80	2606000	28.73
.80	14911	1239.51	555.30	2436000	18.56
.90	18999	1063.79	603.17	2358000	16.54
.95	20500	986.92	623.49	2344000	15.91
1.05	24388	852.91	658.23	2284000	14.68
1.10	26079	798.63	676.44	2265000	14.17
1.15	27753	739.81	684.88	2284000	14.11
1.25	31181	648.47	709.26	2336000	13.94
1.40	35703	523.02	717.58	2425000	14.30
1.55	39883	433.86	729.64	2474000	14.35
1.80	47021	301.28	683.30	2541000	15.74
2.20	56554	188.79	639.62	2577000	17.05
2.50	65726	118.36	517.83	2475000	20.23
3.50	108012	18.06	154.86	1821000	49.76

Table A-15   STS-5 LEFT SRB ELEMENT

Mach	C_{PB}	C_{PB}Max	C_{PB}Min	P_B/P_{oo}	P_B/P_{oo} Max	P_B/P_{oo} Min
.60	-.240	-.300	-.190	.939	.924	.952
.80	-.195	-.230	-.160	.913	.897	.928
.90	-.175	-.215	-.140	.901	.878	.921
.95	-.160	-.215	-.130	.899	.864	.918
1.05	-.165	-.216	-.130	.873	.833	.899
1.10	-.162	-.190	-.135	.863	.839	.886
1.15	-.140	-.160	-.110	.870	.852	.898
1.25	-.130	-.140	-.075	.858	.847	.918
1.40	-.060	-.080	-.035	.918	.890	.952
1.55	-.010	-.055	.005	.983	.908	1.010
1.80	.025	-.020	.048	1.050	.955	1.110
2.20	.060	.025	.085	1.200	1.080	1.290
2.50	.080	.048	.105	1.350	1.210	1.460
3.50	.083	.050	.110	1.710	1.430	1.940

ATLAS D SERIES

ATLAS D-SERIES

The Atlas D-Series was the initial operational version of the Atlas series using the radio inertial guidance system. The Atlas stood about 75 ft in length and had a diameter of about 10 ft. The total gross weight of the Atlas was about 260,000 lb. The Atlas was designed to be an intercontinental ballistic missile with a range of about 9,000 miles and a maximum altitude of 600-900 miles. The Atlas propulsion system consists of two Rocketdyne YLR-87-NA-7 engines as boosters with a total combined thrust of about 309,000 lb at sea level, and a Rocketdyne YLR-105-NA-7 as a sustainer with a thrust of about 56,700 lb at sea level. The Atlas was also equipped with turbine exhaust ducts in the base of the vehicle which influenced performance and base pressure data.

The Atlas configuration and engine characteristics are presented in Figs. A-45 through A-48. Ascent trajectory data are presented in Figs. A-49 and A-50. Engine thrust versus altitude and the nozzle plume angles are presented in Figs. A-51 and A-52. The base pressure source data from Reference 1 is presented in Fig. A-53. Trajectory data, thrust characteristics and base pressure characteristics are presented in Tables A-16 and A-17.

LOCKHEED-HUNTSVILLE RESEARCH & ENGINEERING CENTER

ATLAS REFERENCES

1. "Power-On Base Pressure Investigation for Space Shuttle Launch Configuration," General Dynamics Report No. GDC PIN 70-493, 20 July 1970.

2. Anon. "Mercury Booster flight Test Summary Report," GDA63-0890, General Dynamics, Astronautics, July 1963.

3. Frayer, R. G., "Atlas Base Drag Study," Report No. GD1C-BTD65-089, General Dynamics, Convair Division, June 1965.

LOCKHEED-HUNTSVILLE RESEARCH & ENGINEERING CENTER

GIMBAL ASSEMBLY — FUEL PUMP HEAT EXCHANGER THRUST CHAMBER
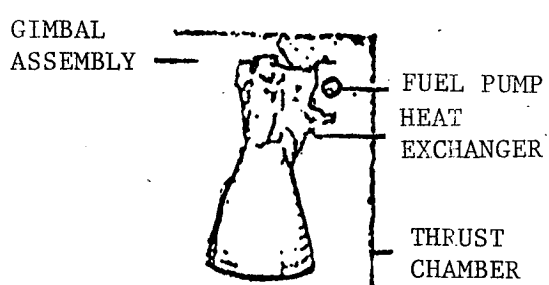
BOOSTER ENGINE
YLR 87-NA-7

GIMBAL ASSEMBLY — FUEL PUMP HEAT EXCHANGER THRUST CHAMBER
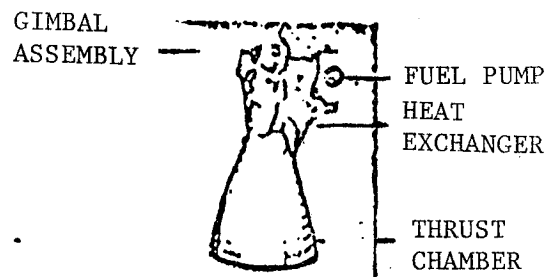
SUSTAINER ENGINE
YLR-105-NA-7

R= 60"

R= 37.5"

DIA= 46"

TURBINE EXHAUST DUCT
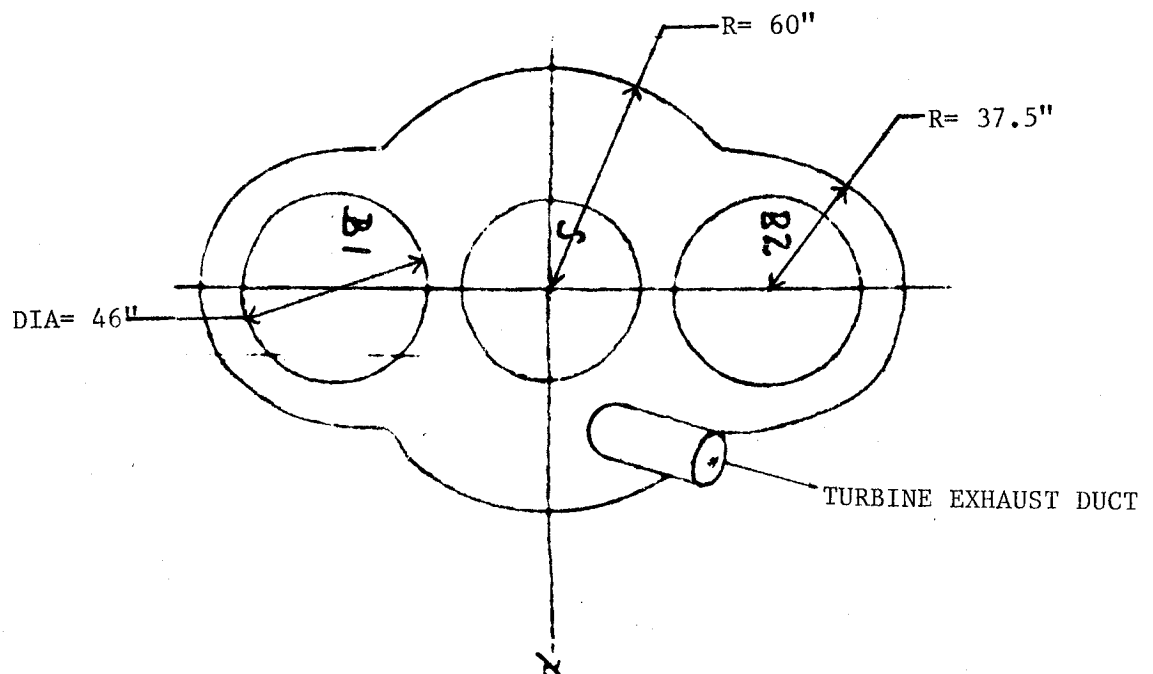
Fig. A-45 - Atlas Missile Configuration

ATLAS VEHICLE

BASE CONFIGURATION

—SUSTAINER ENGINE
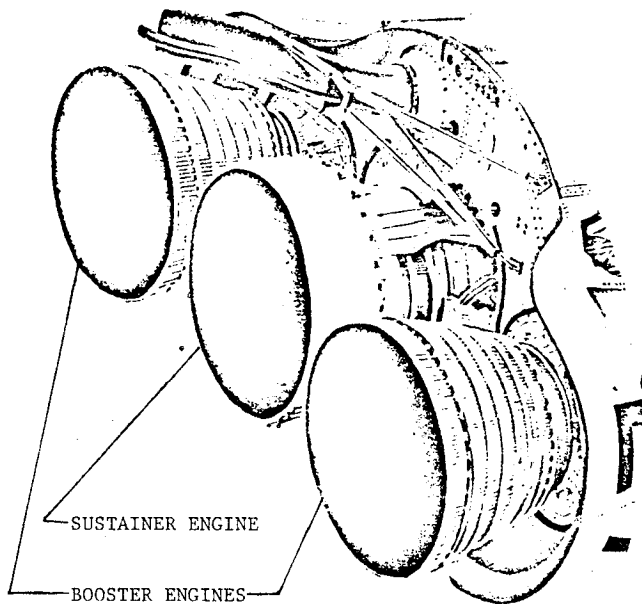
—BOOSTER ENGINES—

ENGINE CHARACTERISTICS

ATLAS D SERIES

BOOSTER: ROCKETDYNE YLR 87-NA-7

THRUST= 2X154,500= 309,000 lb. S.L.-LOX-RP1

$\approx$ 355,000 lb. VAC

SUSTAINER: ROCKETDYNE YLR-105-NA-7

THRUST= 56,700 lb. S.L.-LOX-RP1

$\approx$ 80,000 lb. VAC

VERNIER: ROCKETDYNE LR 101-NA-7

THRUST= 1000 lb.

BASE AREA= 109 ft^2

NOZZLE AREA= 34.6 ft^2

Fig. A-46 – Atlas Engine Configuration

A-77

D SERIES

BOOSTER
(2 ENGINES)

SUSTAINER

ENGINE: ROCKETDYNE YLR 87-NA-7

ENGINE: ROCKETDYNE YLR-105-NA-7

THRUST: 2 X 154500=309000 lb SL.
              355000 lb VAC

P_C= 548 psi

P_E= 13 psi

γ_E= 1.23

M_E= 2.93

DIA_E= 45.7

θ_L= 4.7°

ϵ = 8.0

THRUST: 56700 lb SL.
            80000 lb VAC

P_C= 681 psi

P_E= 2.2 psi

γ_E= 1.25

M_E= 3.80

DIA_E= 47.2

θ_L= 3.0°

ϵ = 25

Fig. A-47 - Atlas Engine Characteristics

A-78
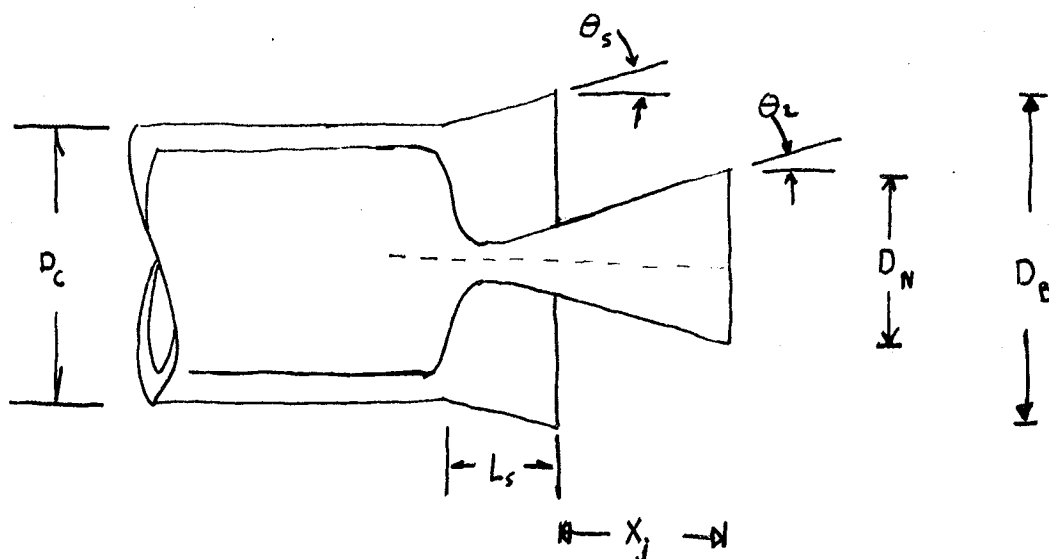
$D_c = 120$ in

$D_{B_{EQ}}^* = 141$ in

$D_N = 45.7$ in

$X_j = 47$ in

$\theta_L = 4.7°$

$L_s = 200$

$\theta_s = 3°$

$A_B = 109$ FT²

$A_N = 34.6$ FT²

$A_N/A_B = .317$

$X_j/D_B = .390$

$L_s/D_c = 1.700$

* NOTE
$$D_{B_{EQ}} = \sqrt{\frac{A_{BASE}}{\pi/4}}$$

Fig. A-48 - Base Configuration - Atlas
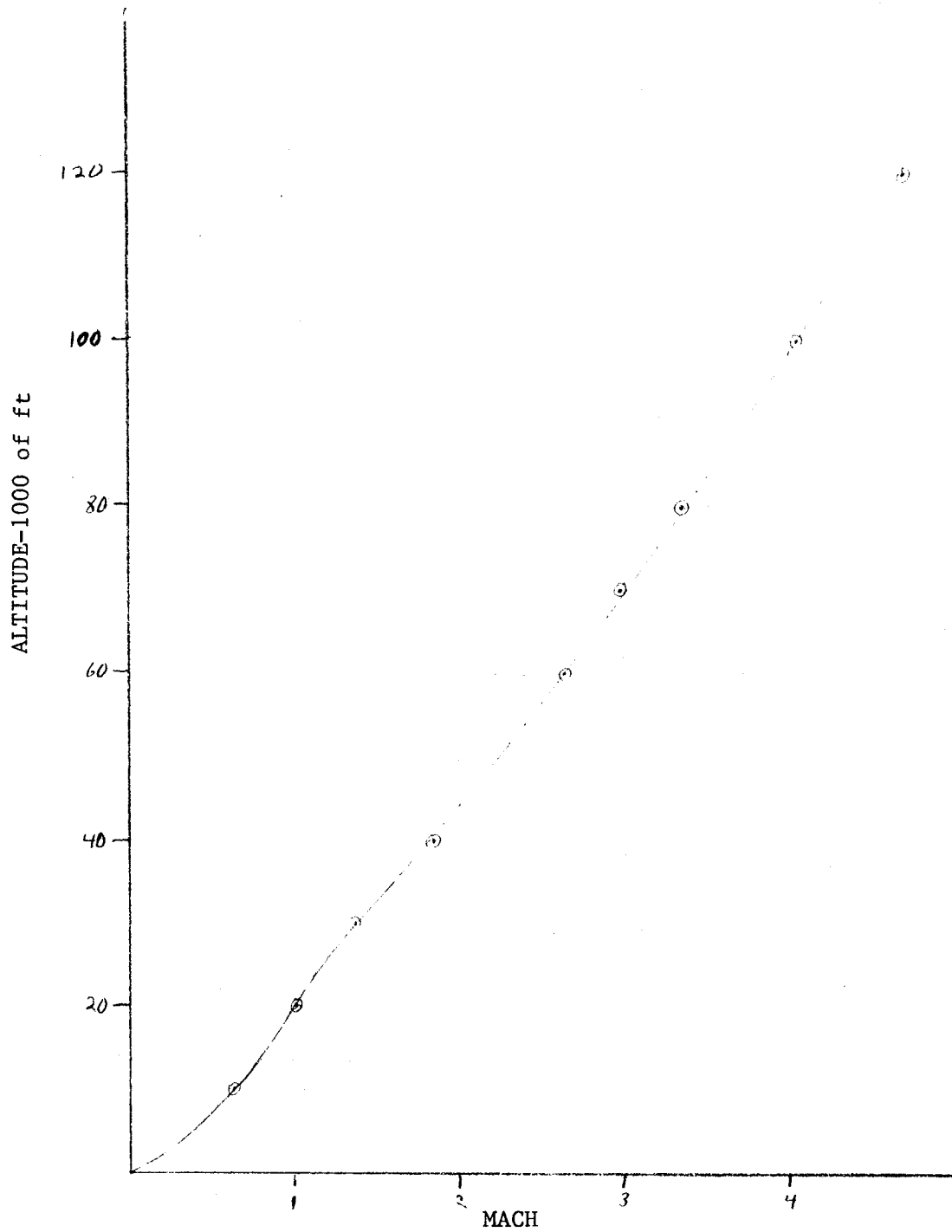
Fig. A-49 - Flight Altitude versus Mach Number - Atlas

Fig. A-50 – Flight Dynamic Pressure versus Mach Number – Atlas

LOCKHEED-HUNTSVILLE RESEARCH & ENGINEERING CENTER
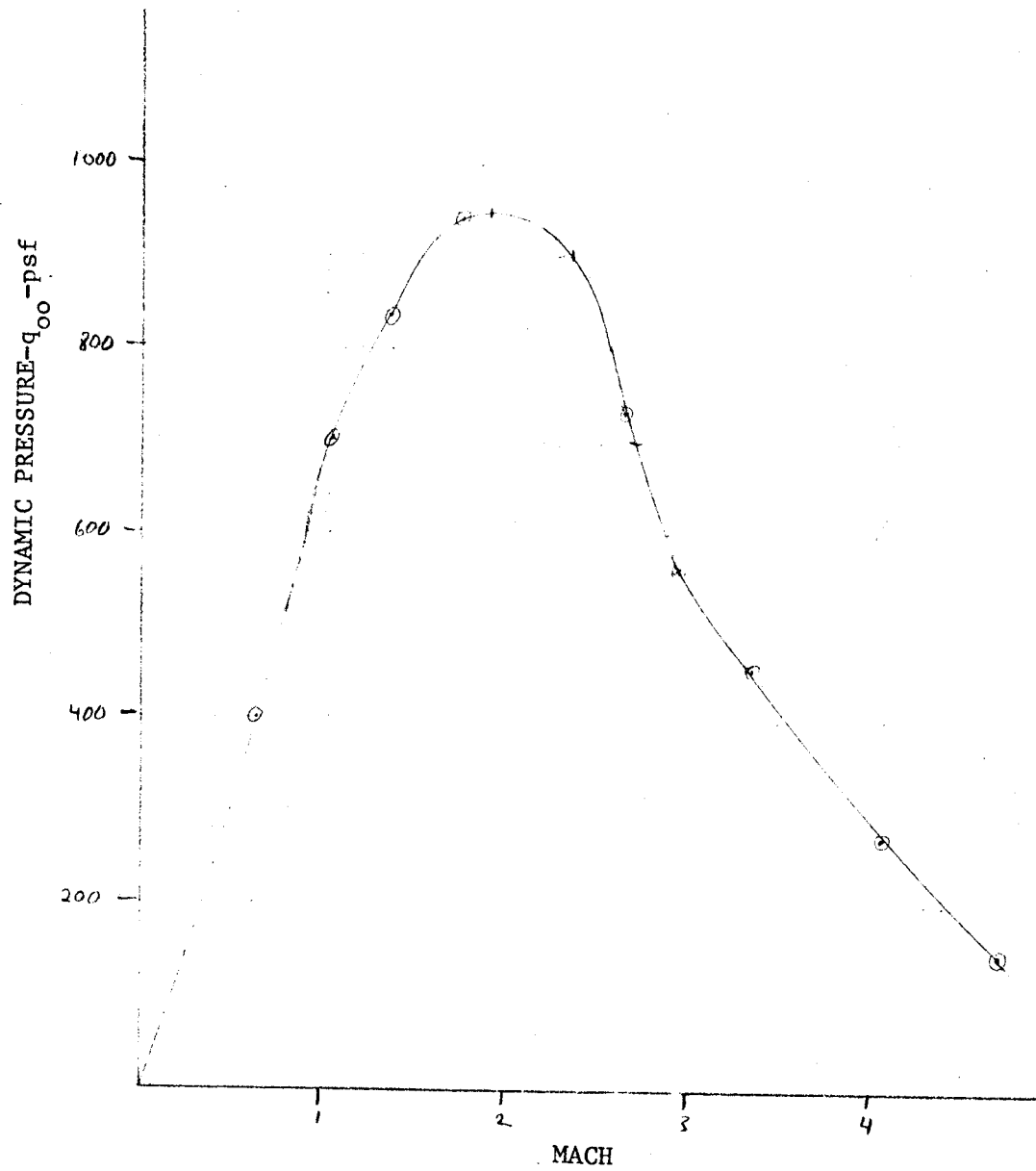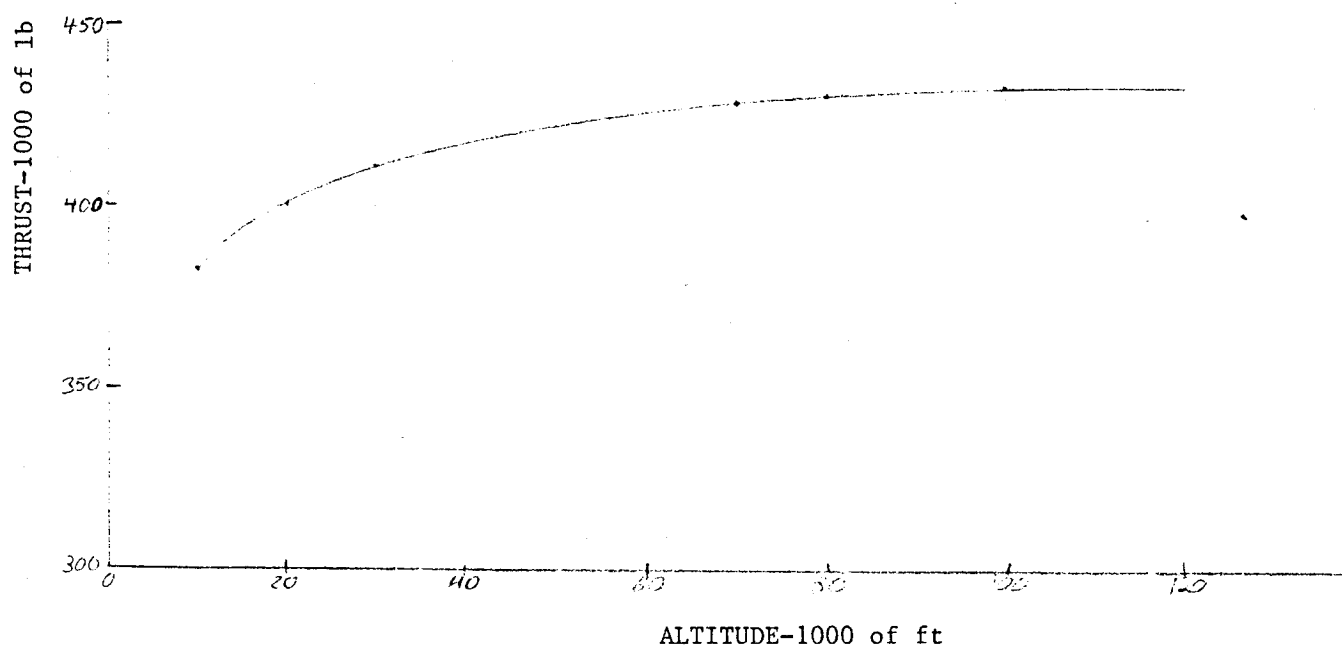
Fig. A-51 - Thrust versus Altitude - Atlas
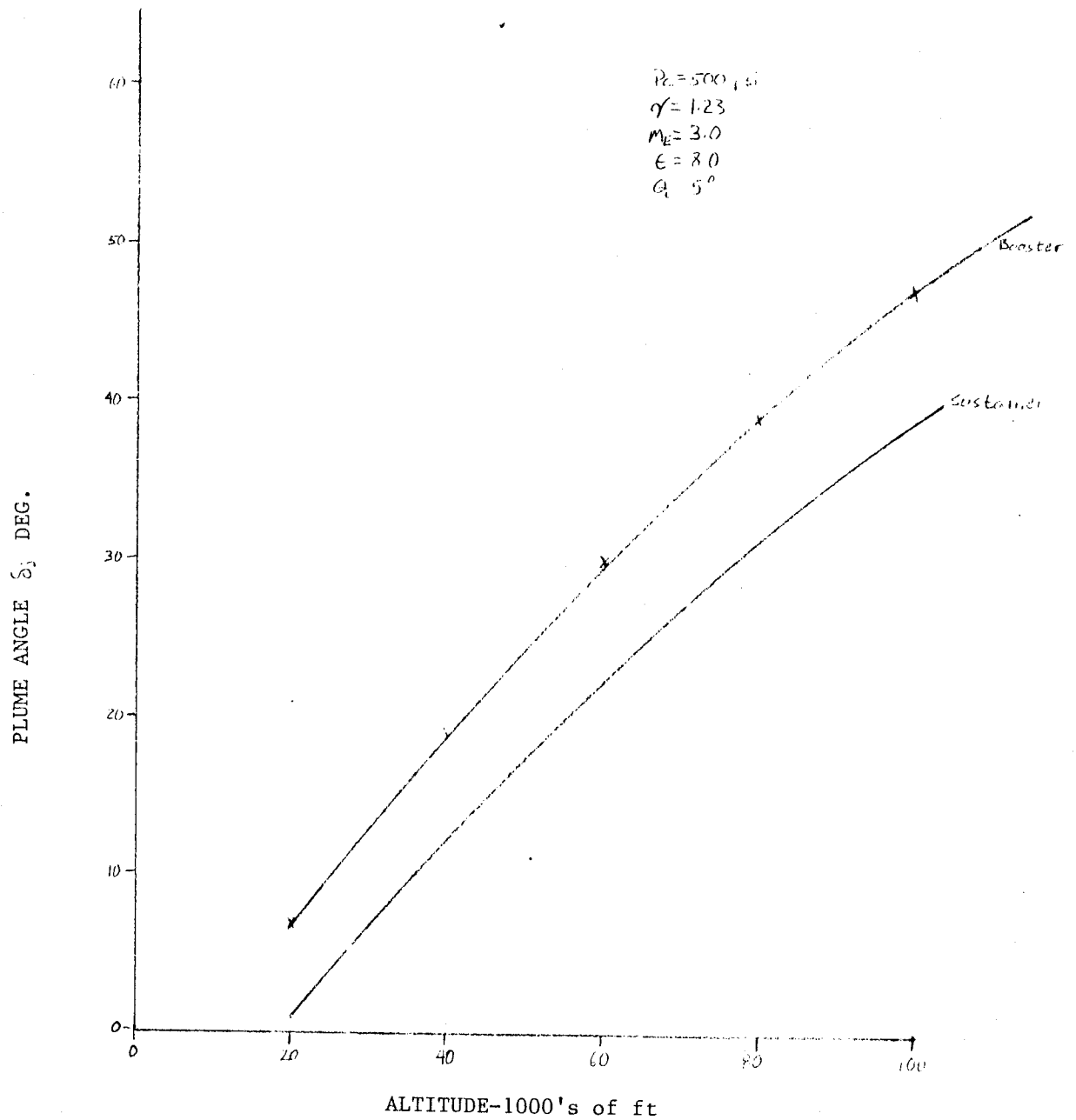
Fig. A-52 - Plume Angle versus Altitude - Atlas
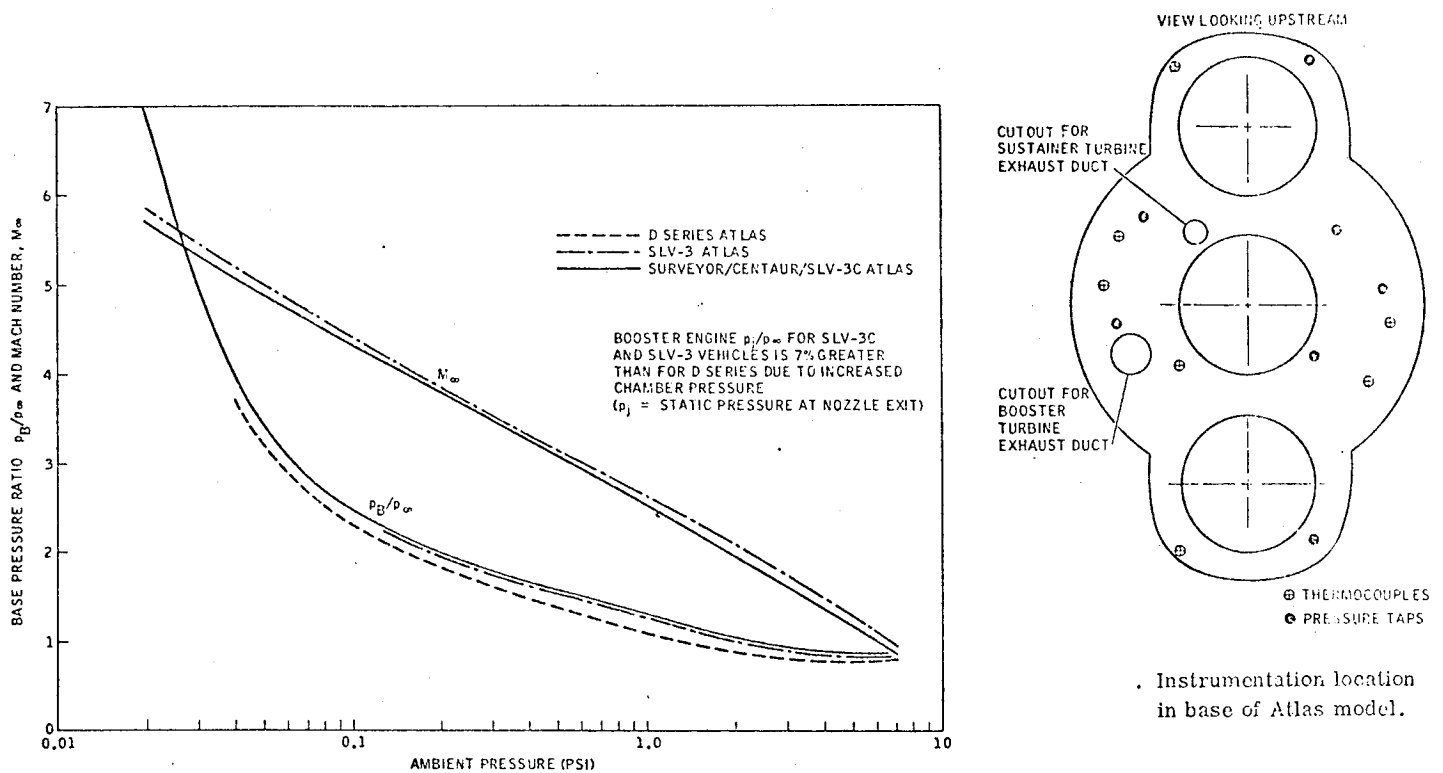
Fig. A-53 – Atlas Base Pressure Characteristics – Source Data

Table A-16   ATLAS D SERIES

$AB = 109 \text{ ft}^2$

Mach	Alt. ft.	P_∞ psf	q_∞ psf	Thrust	C_T
.63	10,000	1455.6	404.4	383,000	8.69
1.02	20,000	973.3	708.83	400,000	4.65
1.38	30,000	629.6	839.3	411,000	4.49
1.85	40,000	393.1	941.8	419,000	4.08
2.64	60,000	151.0	736.7	425,000	5.29
2.93	70,000	93.7	563.1	429,000	6.99
3.35	80,000	58.5	459.6	431,000	8.60
4.05	100,000	23.2	266.4	434,000	14.95

Table A-17   ATLAS D SERIES

Mach	C_{P_B}	C_{P_B} max	C_{P_B} min	PB/p_∞	PB/p_∞ max	PB/p_∞ min
.63	-.08	.11	-.05	.977	.969	.986
1.02	-.21	-.24	-.18	.847	.825	.869
1.38	-.14	-.17	-.11	.813	.773	.853
1.85	-.06	-.09	-.03	.856	.784	.928
2.64	+.02	-.01	+.05	1.098	.951	1.244
2.93	+.04	+.01	+.07	1.24	1.060	1.421
3.35	+.05	+.02	+.08	1.393	1.157	1.628
4.05	+.08	+.05	+.11	1.919	1.574	2.263

SATURN 1 BLOCK 1

SATURN 1 BLOCK I

The primary mission of the Saturn 1 Block I as an R&D vehicle was to flight test the 1st stage (S1 stage) of the Saturn 1 launch vehicle. Because of its mission the SIV and the SV stages were filled with water to simulate the mass characteristics of the line stage. The payload of the Block I vehicles was a Jupiter nose cone and aft section. The S1 stage of the Block I vehicles consists of a cluster of eight 70 in. diameter propellant con- tainers, alternately LOX and fuel, surrounding a 105 in. diameter center LOX container. These are held together at the forward end by an I-beam frame or "spider-beam," and at the aft end by a thrust frame and tail section assembly. The tail section and engines are enclosed by a shroud and heat shield arrangement. Eight Rocketdyne H-2 engines, four fixed inboard and four gimbaled outboard, each with 165,000 lb of thrust at sea level, provide a total standard sea level thrust of 1,320,000 lb burning LOX and RP1 propellants. There were four flights of the Block I vehicles after which the new configuration was designated Block II.

The Saturn 1 Block I configuration and engine operating characteristics are presented in Figs. A-54 through A-57. Trajectory data are presented in Figs. A-58 and A-59. Engine thrust versus altitude and plume angles are presented in Figures A-60 and A-61. The Saturn 1 Block I base pressure source data is presented in Fig. A-62. These data are from Reference 1. The trajectory data, thrust data, and base pressure characteristics are presented in Tables A-19 through A-26.

LOCKHEED-HUNTSVILLE RESEARCH & ENGINEERING CENTER

SATURN 1 BLOCK I REFERENCES

1. Jones, Ira P., "Summary of Base Thermal Environment Measurements on the Saturn 1 Block I Vehicles," NASA TM X-53326, 3 September 1965.

2. Mullen, C. R. et al., "Saturn Base Heating Handbook," NASA CR-61390, The Boeing Company, Huntsville, Ala., May 1972.

LOCKHEED-HUNTSVILLE RESEARCH & ENGINEERING CENTER
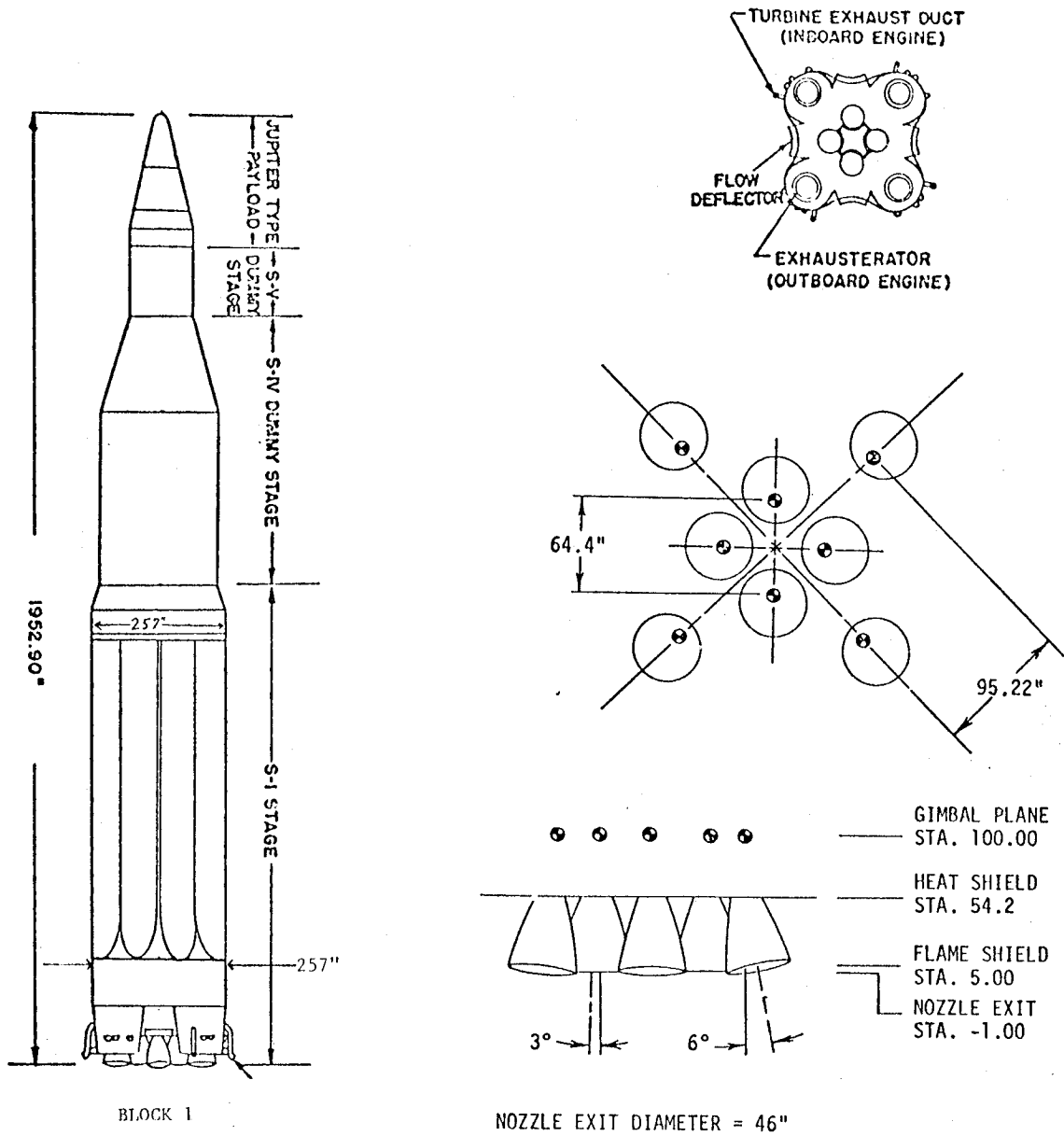
Fig. A-54 - Configuration Saturn 1 - Block 1

FLOW DEFLECTOR

TAIL BARREL

TURBINE EXHAUST DUCT (INBOARD ENGINE)

AIR SCOOPS

EXHAUSTERATOR

HEAT SHIELD

ENGINE SHROUD

FLAME SHIELD
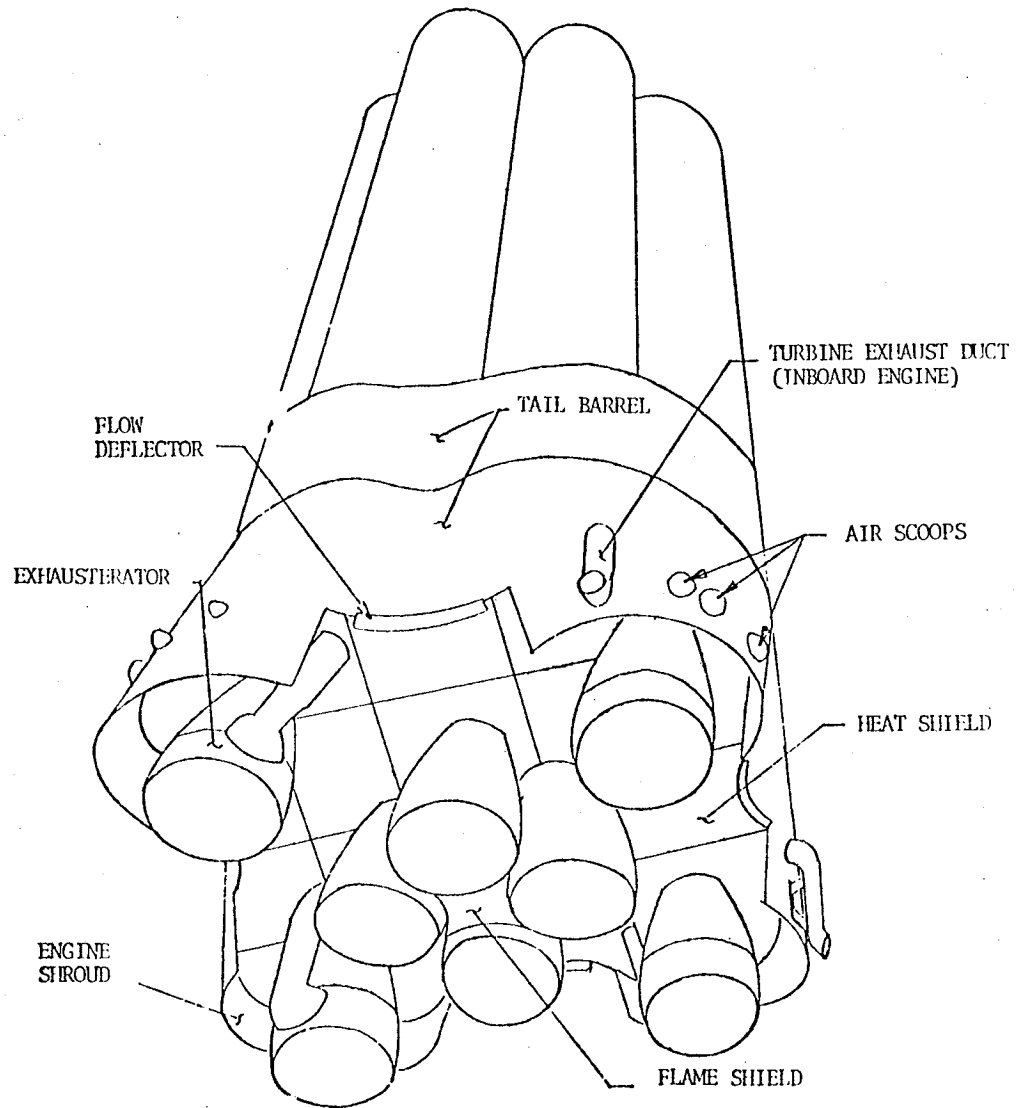
Fig. A-55 — Base View of Saturn 1 Block 1, S-1 Stage

$D_c = 257 \text{ in.}$

$D_B = 225.6$

$A_B = 277.5 \text{ in}^2$

$D_N = 102.2 \text{ EQ.}$

$\dfrac{A_N}{A_B} = .205$

$X_j = 58 \text{ in}$

$\dfrac{X_j}{D_B} = .257$

$\Theta_L = 5°$
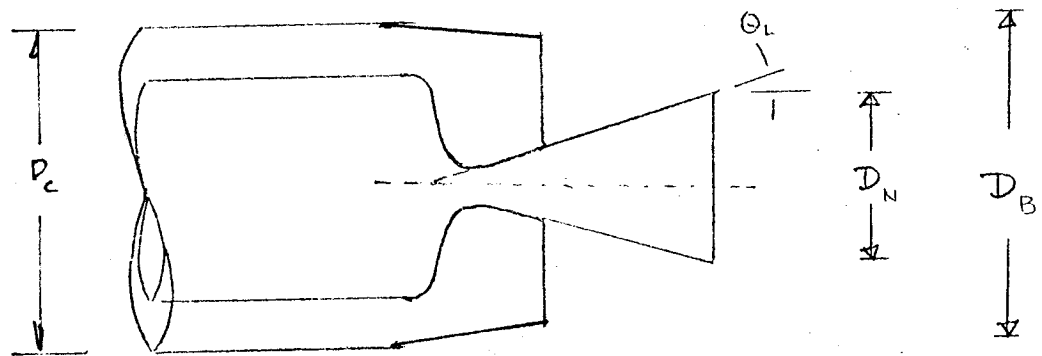
Fig. A-56 - Base Configuration - Saturn 1 Block 1

LOCKHEED-HUNTSVILLE RESEARCH & ENGINEERING CENTER
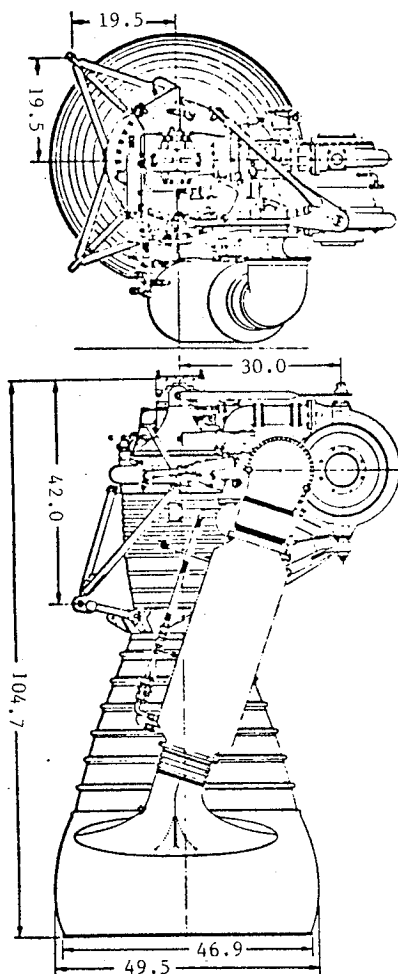
SPECIFICATIONS·

Thrust (sea level):	165,000 lb.
Type:	Liquid bipropellant, pump-fed
Propellants:	
Fuel	RP-1 (kerosene)
Oxidizer	Liquid Oxygen
Mixture Ratio (o/f)	2.23:1

COMPONENTS

Thrust Chamber:	Nozzle Area Ratio 8:1 Regeneratively· cooled, tubular wall nozzle.

ENGINE OPERATING CHARACTERISTICS

P_C = 578 psi

P_E = 8.4 psi

γ_E = 1.3

M_E = 3.0

DIA_E = 45.7 in

θ_L = 5°

ϵ = 8

Fig. A-57 - Engine Characteristics - Saturn 1 Block 1
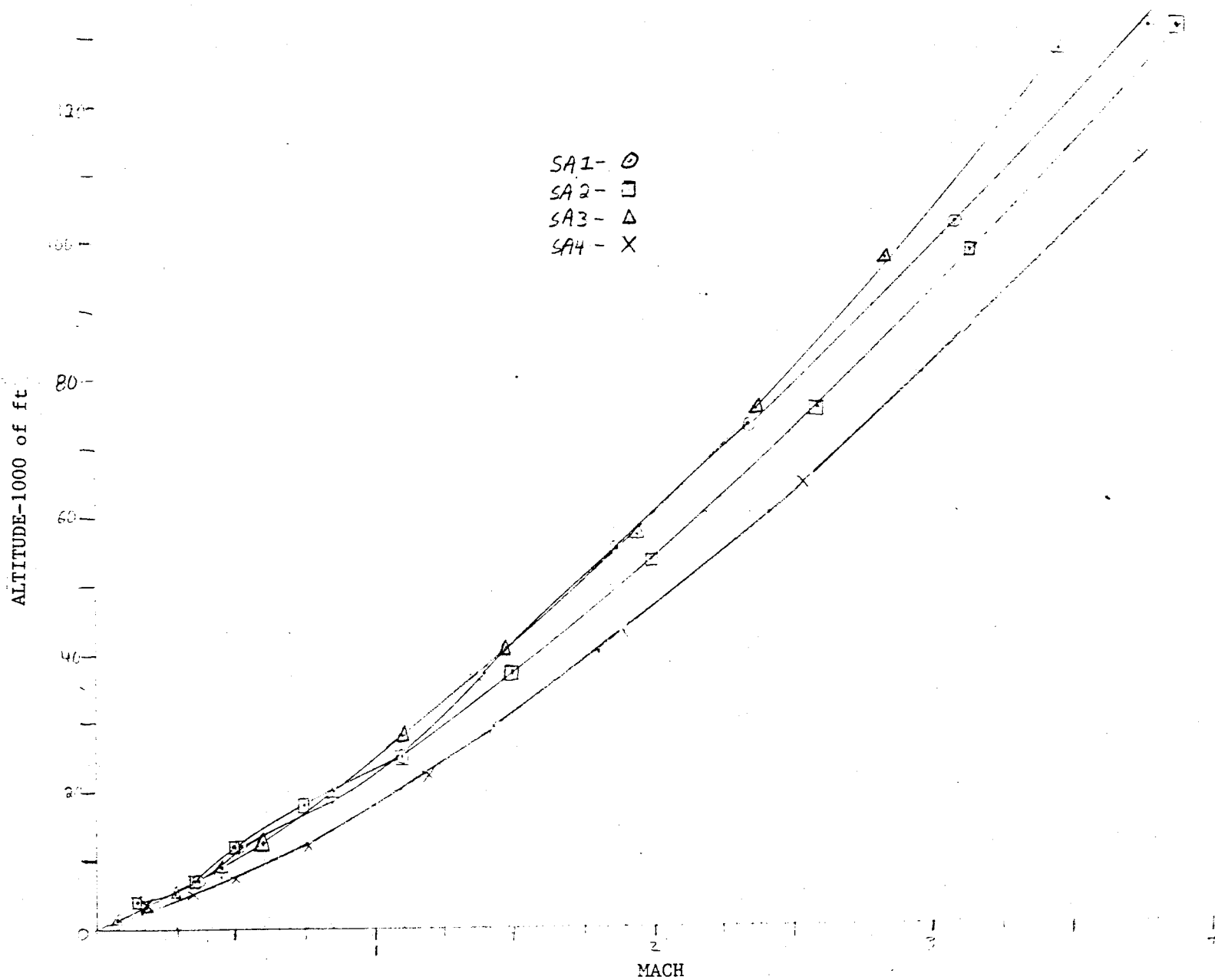
FIGURE A-58 FLIGHT ALTITUDE VERSUS MACH NUMBER-SATURN 1 BLOCK 1
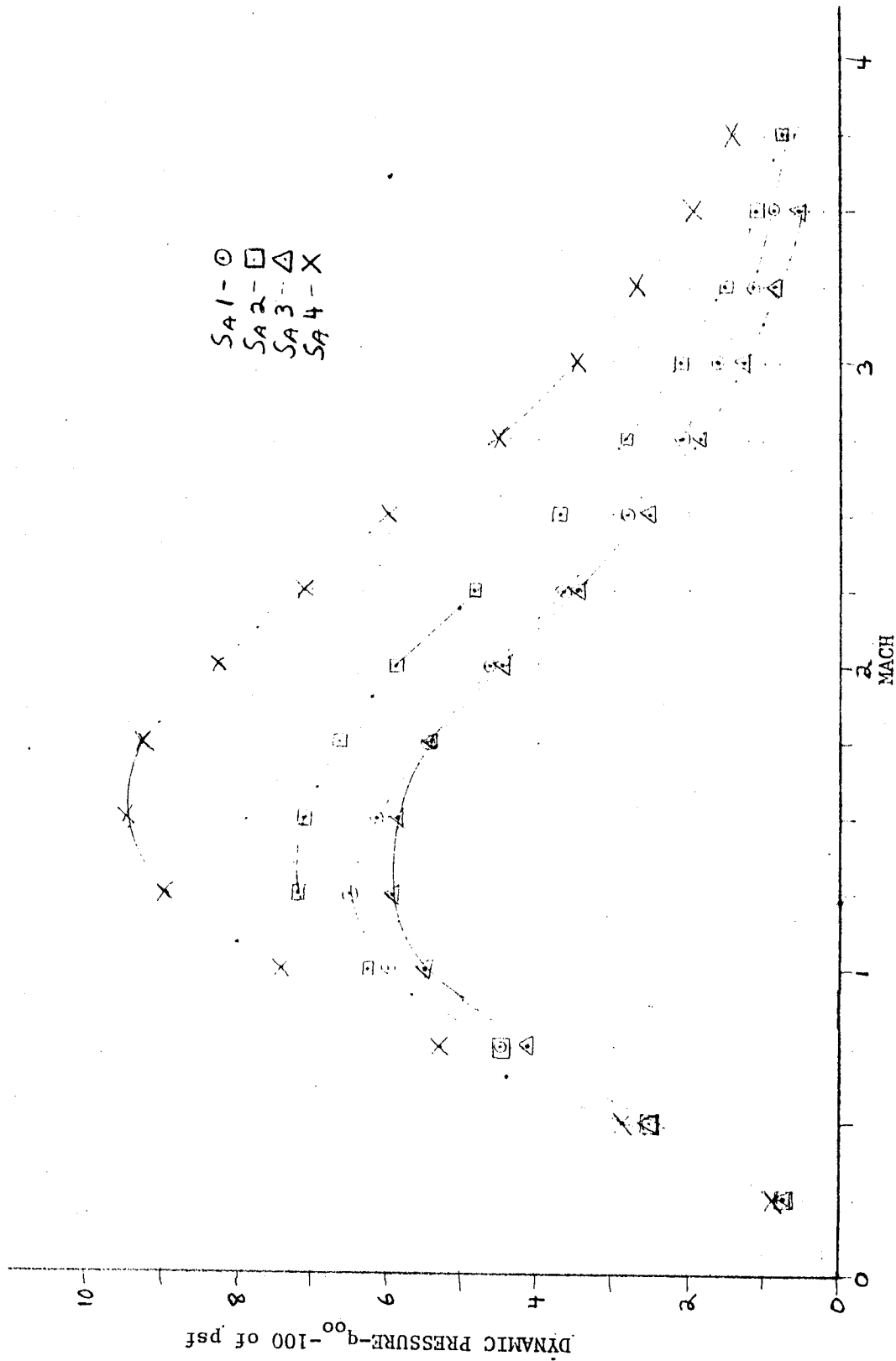
FIGURE A–59 FLIGHT DYNAMIC PRESSURE VERSUS MACH NUMBER–SAT 1 BLOCK 1
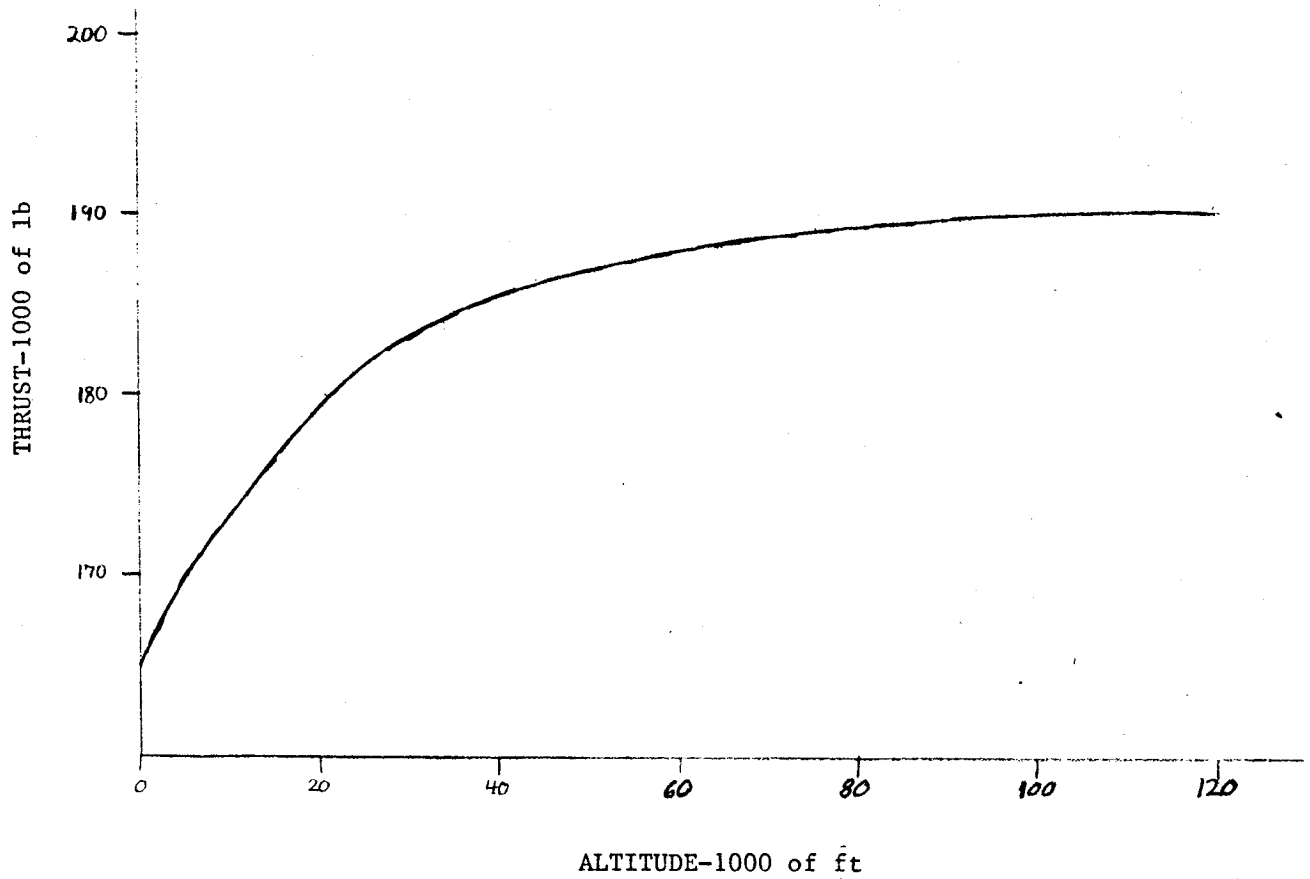
Fig. A-60 – Thrust versus Altitude – H-2 Engine
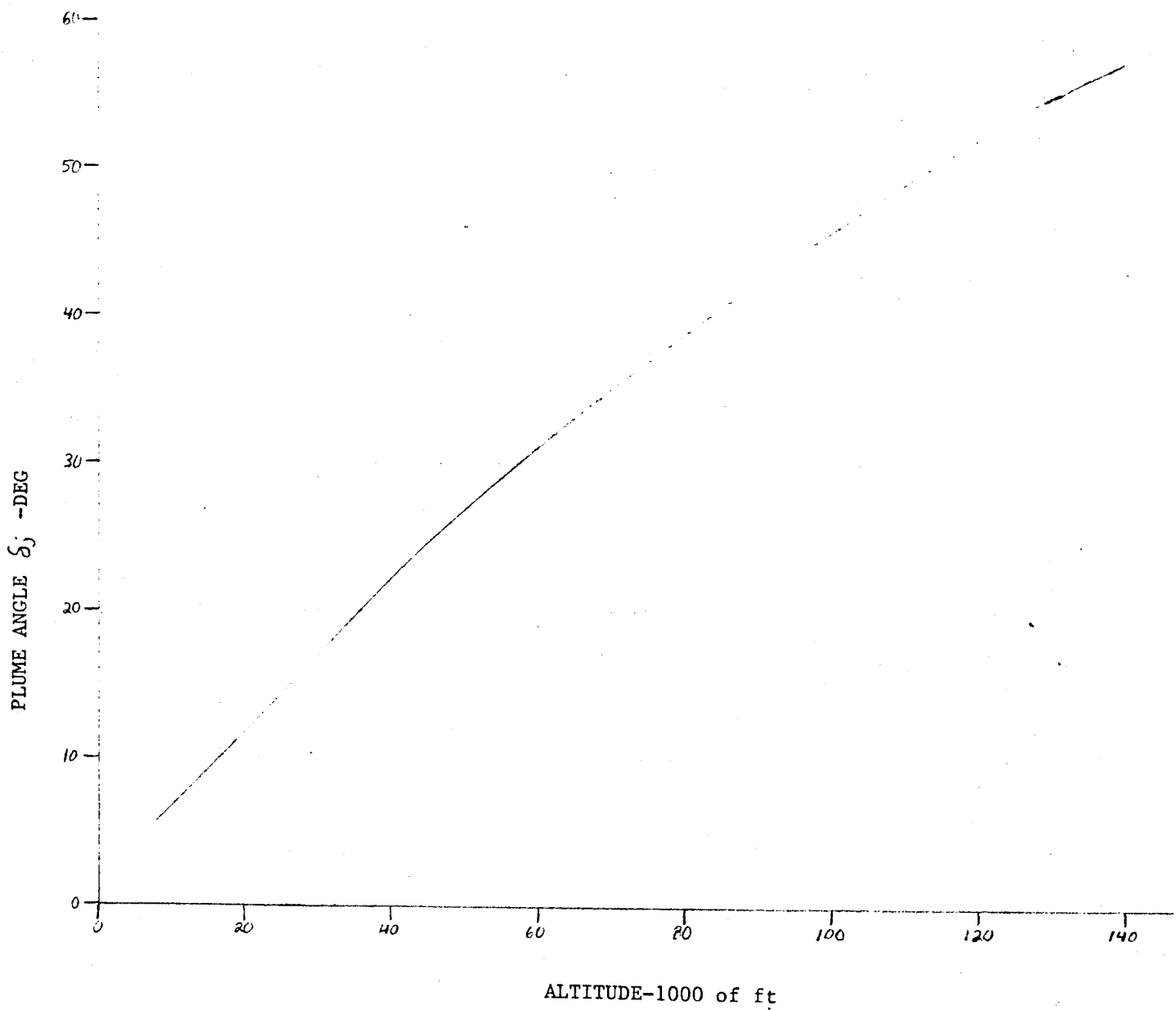
Fig. A-61 - Plume Angle versus Altitude - H-2 Engine
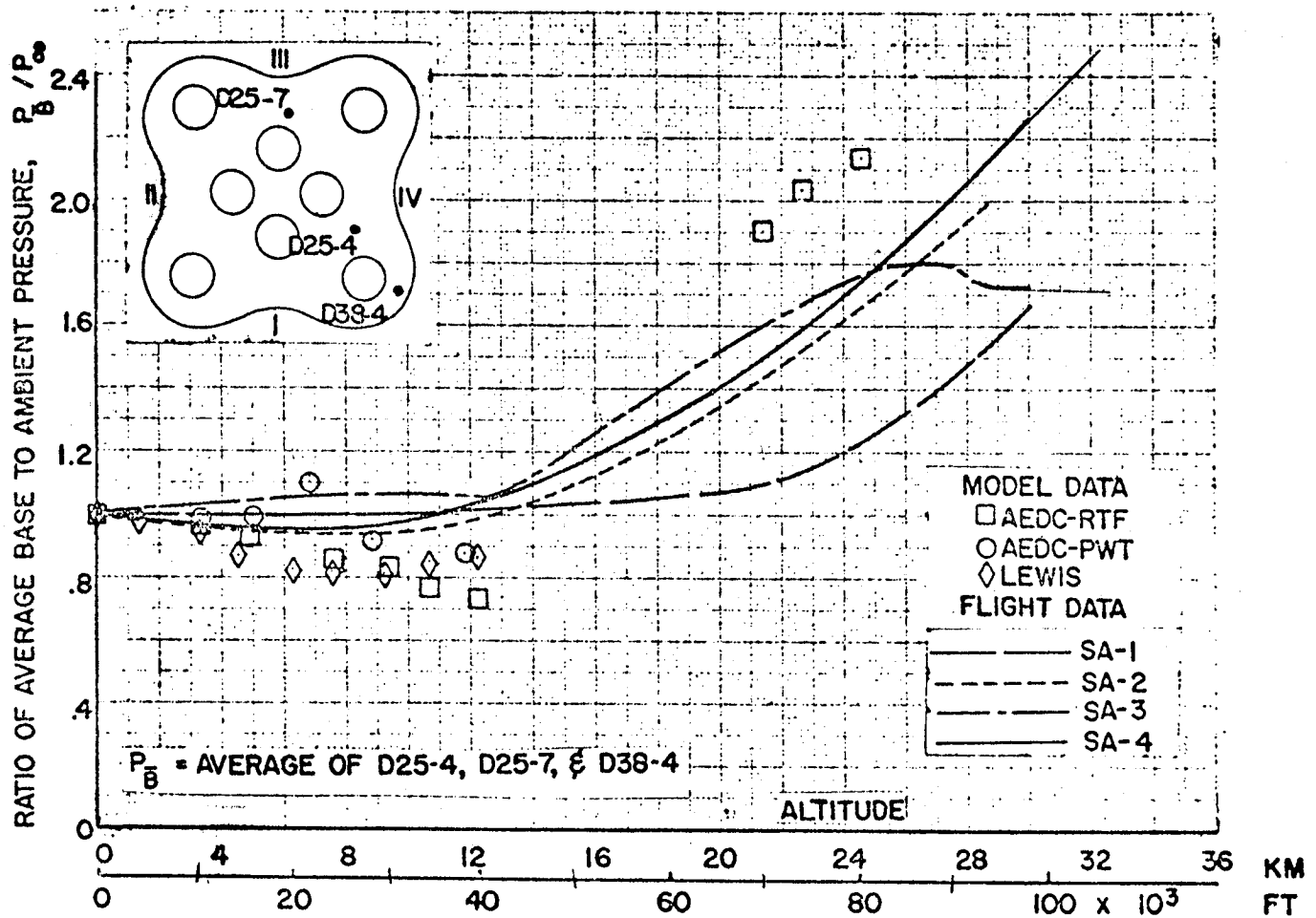
Fig. A-62 – Saturn 1 Block 1 Base Pressure Source Data

Table A-18   SATURN 1 VEHICLE, BLOCK 1 SA-1

Mach	Alt-ft	P_{oo}psf	q_{oo}psf	Thrust-lb	AB=277.5 ft^2 C_T
.47	10,000	1455.60	225.08	1396000	22.35
.84	20,000	973.26	480.71	1440000	10.79
1.12	30,000	629.66	552.89	1464000	9.54
1.48	40,000	393.12	602.76	1480000	8.85
1.78	50,000	243.61	540.30	1496000	9.98
2.05	60,000	151.03	444.29	1504000	12.20
2.30	70,000	93.73	347.08	1510400	15.68
2.56	80,000	58.51	268.42	1513600	20.32
2.81	90,000	36.78	203.29	1518400	26.92
3.07	100,000	25.20	166.26	1520000	32.96
3.30	110,000	14.84	113.13	1521000	48.45
3.53	120,000	9.60	83.74	1522000	65.50

Table A-19   SATURN I VEHICLE BLOCK 1 SA-1

Mach	C_{PB}	$C_{PB}max$	$C_{PB}min$	P_B/P_{oo}	$P_B/P_{oo}max$	$P_B/P_{oo}min$
.47	-0-	.050	-.050	1.000	1.010	.992
.84	-0-	.050	-.050	1.000	1.020	.975
1.12	-0-	.050	-.050	1.000	1.040	.956
1.48	.002	.052	-.048	1.003	1.080	.926
1.78	.010	.060	-.040	1.020	1.130	.911
2.05	.019	.069	-.031	1.060	1.200	.908
2.30	.030	.080	-.020	1.110	1.290	.926
2.56	.050	.100	-0-	1.230	1.460	1.000
2.81	.080	.130	.030	1.440	1.720	1.170
3.07	.125	.175	.075	1.820	2.150	1.490

LOCKHEED-HUNTSVILLE RESEARCH & ENGINEERING CENTER

Table A-20 SATURN I VEHICLE BLOCK 1 SA-1

$A_B = 277.5$

Mach	Alt ft	P_{oo}psf	q_{oo}psf	Thrust lb	C_T
.50	10000	1455.60	254.73	1396000	19.75
.92	20000	973.26	576.64	1440000	9.00
1.28	30000	629.66	722.14	1464000	7.31
1.60	40000	393.12	704.47	1480000	7.57
1.90	50000	243.61	615.60	1496000	8.76
2.19	60000	151.03	507.05	1504000	10.69
2.48	70000	93.73	403.53	1510400	13.49
2.72	80000	58.51	303.02	1513600	18.00
2.97	90000	36.78	227.10	1518400	24.09
3.21	100000	25.20	181.76	1520000	30.14
3.44	110000	14.84	122.93	1521000	44.59
3.67	120000	9.60	90.51	1522000	60.60

Table A-21   SATURN I VEHICLE BLOCK 1 SA-2

Mach	C_{PB}	$C_{PB}max$	$C_{PB}min$	P_B/P_{oo}	$P_B/P_{oo}max$	$P_B/P_{oo}min$
.50	-.225	-.275	-.175	.961	.952	.969
.92	-.115	-.165	-.065	.932	.902	.961
1.28	-.048	-.095	.002	.945	.891	1.002
1.60	-.005	-.055	.045	.991	.901	1.080
1.90	.035	-.015	.085	1.090	.962	1.210
2.19	.072	-.022	.122	1.240	1.074	1.410
2.48	.100	-.050	.150	1.430	1.215	1.650
2.72	.130	-.080	.180	1.670	1.414	1.930
2.97	.148	-.098	.198	1.910	1.605	2.220
3.21	.166	.116	.216	2.200	1.837	2.558

Table A-22   SATURN I VEHICLE BLOCK 1 SA-3

Mach	Alt ft	P_{oo}psf	q_{oo}psf	Thrust lb	A_B= 277.5 ft^2 C_T
.48	10000	1455.60	234.76	1396000	21.43
.90	20000	973.26	613.15	1440000	8.46
1.16	30000	629.66	593.09	1464000	8.90
1.47	40000	393.12	594.65	1480000	8.97
1.76	50000	243.61	528.22	1496000	10.21
2.03	60000	151.03	435.67	1504000	12.44
2.27	70000	93.73	338.09	1510400	16.10
2.50	80000	58.51	255.98	1513600	21.31
2.72	90000	36.78	190.48	1518400	28.73
2.94	100000	25.20	152.47	1520000	35.92
3.13	110000	14.84	101.77	1521000	53.86
3.34	120000	9.60	74.97	1522000	73.16

LOCKHEED-HUNTSVILLE RESEARCH & ENGINEERING CENTER

Table A-23   SATURN I VEHICLE   BLOCK   I SA-3

Mach	C_{PB}	$C_{PB}max$	$C_{PB}min$	P_B/P_{oo}	$P_B/P_{oo}max$	$P_b/P_{oo}min$
.48	.180	.130	.230	1.030	1.020	1.040
.90	.125	.075	.175	1.070	1.040	1.100
1.16	.080	.030	.130	1.080	1.050	1.190
1.47	.040	-.010	.090	1.060	.985	1.140
1.76	.090	.040	.140	1.190	1.090	1.300
2.03	.150	.010	.200	1.430	1.080	1.580
2.27	.170	.120	.220	1.610	1.430	1.790
2.50	.175	.125	.225	1.770	1.550	1.980
2.72	.154	.104	.204	1.790	1.540	2.060
2.94	.123	.073	.173	1.740	1.440	2.050

LOCKHEED-HUNTSVILLE RESEARCH & ENGINEERING CENTER

Table A-24 SATURN I VEHICLE BLOCK 1 SA-4

Mach	Alt ft	P_{oo}psf	q_{oo}psf	Thrust lb	A_B= 277.5 ft^2 C_T
.65	10000	1455.60	430.49	1396000	11.69
1.09	20000	973.26	809.43	1440000	6.41
1.47	30000	629.66	952.44	1464000	5.54
1.81	40000	393.12	901.53	1480000	5.92
2.13	50000	243.61	773.66	1496000	6.97
2.43	60000	151.03	624.27	1504000	8.68
2.72	70000	93.73	485.42	1510400	11.21
2.98	80000	58.51	363.71	1513600	15.00
3.25	90000	36.78	271.94	1518400	20.12
3.50	100000	25.20	216.09	1520000	25.35
3.75	110000	14.84	146.08	1521000	37.52

LOCKHEED-HUNTSVILLE RESEARCH & ENGINEERING CENTER

Table A-25 SATURN I VEHICLE BLOCK I SA-4

Mach	C_{PB}	$C_{PB}max$	$C_{PB}min$	P_B/P_{oo}	$P_B/P_{oo}max$	$P_B/P_{oo}min$
.65	-.123	-.173	-.073	.964	.949	.978
1.09	-.090	-.140	-.040	.925	.884	.966
1.47	-.020	-.070	.030	.969	.894	1.050
1.81	.015	-.035	.065	1.030	.919	1.150
2.13	.055	.005	.105	1.170	1.020	1.330
2.43	.077	.027	.127	1.320	1.110	1.520
2.72	.096	.046	.146	1.490	1.240	1.760
2.98	.120	.070	.170	1.750	1.440	2.060
3.25	.139	.089	.189	2.030	1.660	2.400
3.50	.155	.105	.205	2.330	1.900	2.760

LOCKHEED-HUNTSVILLE RESEARCH & ENGINEERING CENTER

SATURN 1 BLOCK II

SATURN 1 BLOCK II

The Saturn 1 Block II R&D vehicles were used to flight test the boiler-plate Apollo command and service module. Unlike the Block I vehicles which carried an S-V stage, to reflect an escape mission, the Block II vehicles no longer had this as a mission requirement and therefore did not carry an escape stage (S-V). The Block II vehicles also had a live S-IV stage as opposed to the dummy carried by the Block I vehicles. The Block II vehicles also had four large fins and four stub fins mounted around the base of the S-1 stage for increased stability during aerodynamic ascent. The fuel and LOX container lengths, on the S-1 stage, were also increased from 677 in. to 749 in. to handle the increased propellant load necessitated by the higher performance H-1 engines used on the Block II vehicles. The sea level thrust capabilities were increased from 165,000 lb per engine on the Block I's to 188,000 per engine on the Block II's. These changes, along with a decreased hold-down time at liftoff (from 3.6 to 3.4 sec), combined to increase the payload capability and overall performance of the Saturn 1 vehicles with no major design changes.

The Saturn 1 Block II configuration and engine operating characteristics are presented in Figs. A-63 through A-66. The H-1 engine thrust is uprated to 188,000 lb thrust for the Saturn 1 Block II. The difference in the base is noted in Figs. A-63 and A-64. Saturn 1 Block II configuration has a circular base with engine shrouds added to protect the outboard engines. The trajectory characteristics are presented in Figs. A-67 and A-68. Engine thrust versus altitude and engine plume angles are presented in Figs. A-69 and A-70. The base pressure source data from Reference 1 are presented in Fig. A-71. Saturn 1 Block II trajectory data, thrust data and base pressure characteristics are presented in Tables A-26 through A-29.

SATURN 1 BLOCK II REFERENCES

1. Foley, J.E., S.R. Newman, and G.G. Lamotha, "Summary of Aerodynamic Data Obtained from the Saturn 1 Block II Flight Test Program," Chrysler Tech Note, TN-AE-66-140.

2. Mullen, C. R. et al., "Saturn Base Heating Handbook," NASA CR-61390, The Boeing Company, Huntsville, Alabama, May L972.

LOCKHEED-HUNTSVILLE RESEARCH & ENGINEERING CENTER

TURBINE EXHAUST DUCT
(INBOARD ENGINE)

ENGINE
SHROUD
SCOOPS

HYDROGEN
VENT LINES

$A_B = 439.5$ ft^2.

APOLLO PAYLOAD

INSTRUMENT UNIT

S-IV STAGE

2284.47"

257"

S-I STAGE
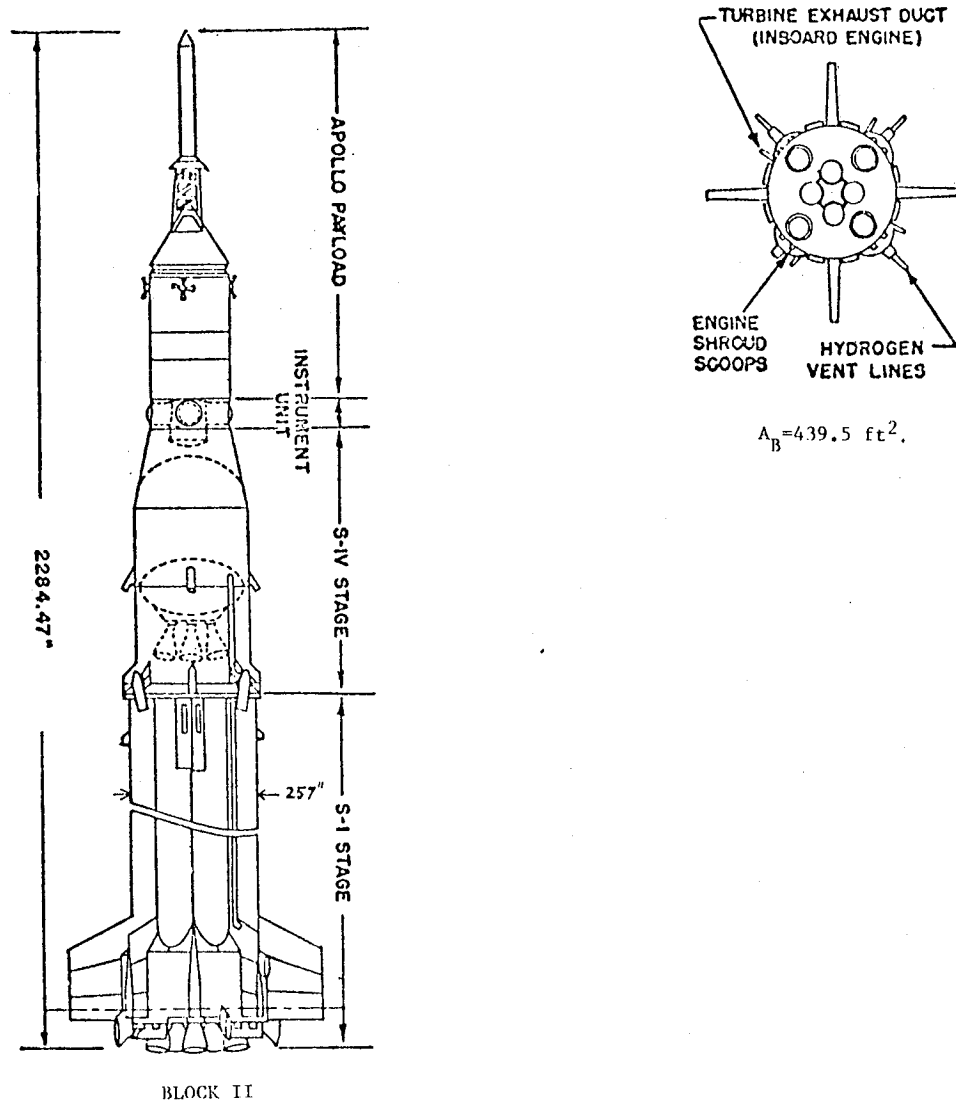
BLOCK II

Fig. A-63 - Configuration: Saturn I Block II
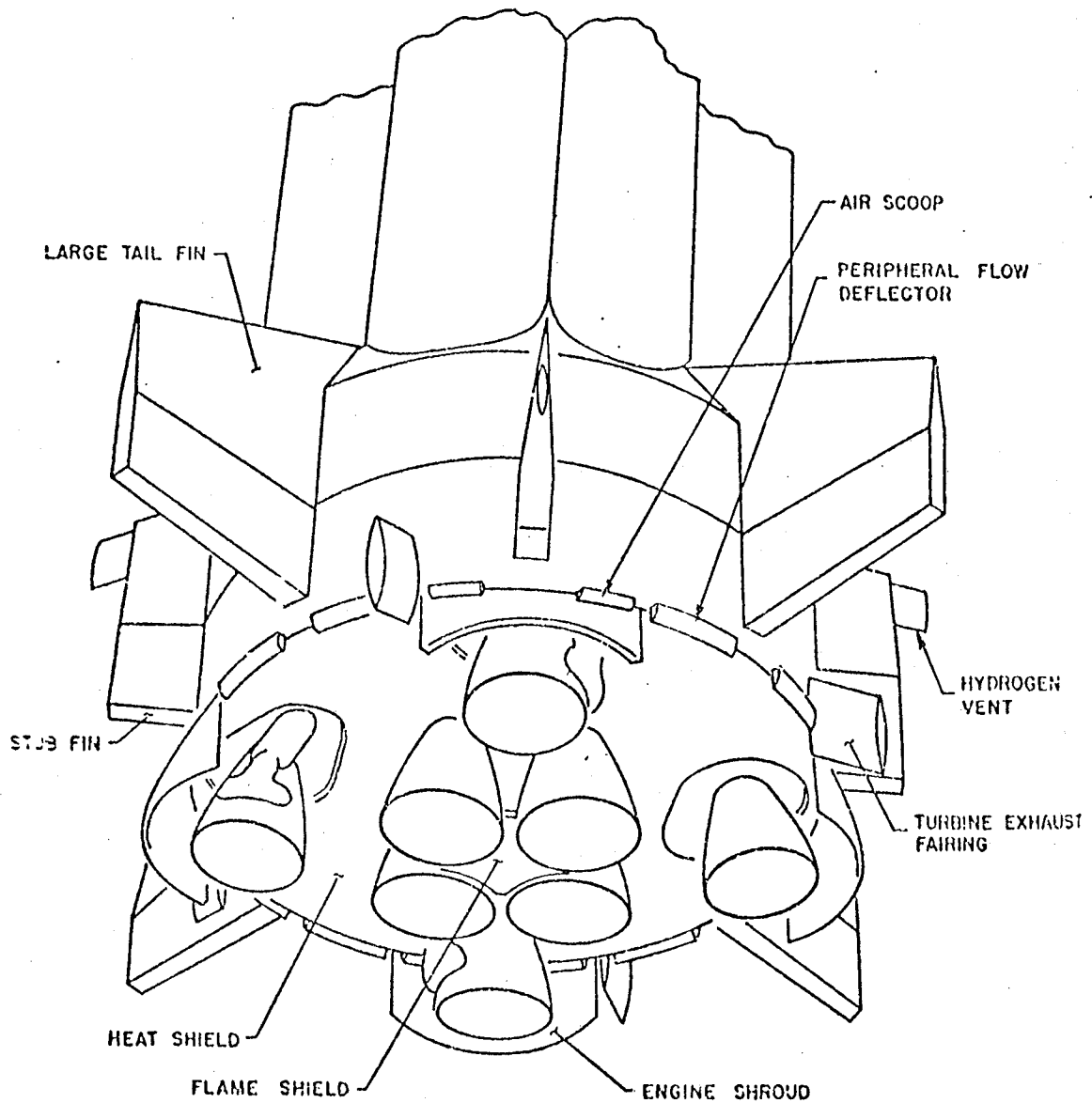
Fig. A-64 - Base View of Saturn I Block II

$D_c = 257_{REF}$

$D_B = 284 \text{ in}$

$D_N = 45.7$

$X_j = 58 \text{ in}$

$\Theta_L = 5^o$

$L_s = 174 \text{ in.}$

$A_B = 439.5 \text{ ft}^2$

$A_N = 57.0 \text{ ft}^2 \text{ eq.}$

$\dfrac{A_N}{A_B} = .13$

$\dfrac{X_j}{D_B} = .2$

$\dfrac{L_s}{D_c} = .67$
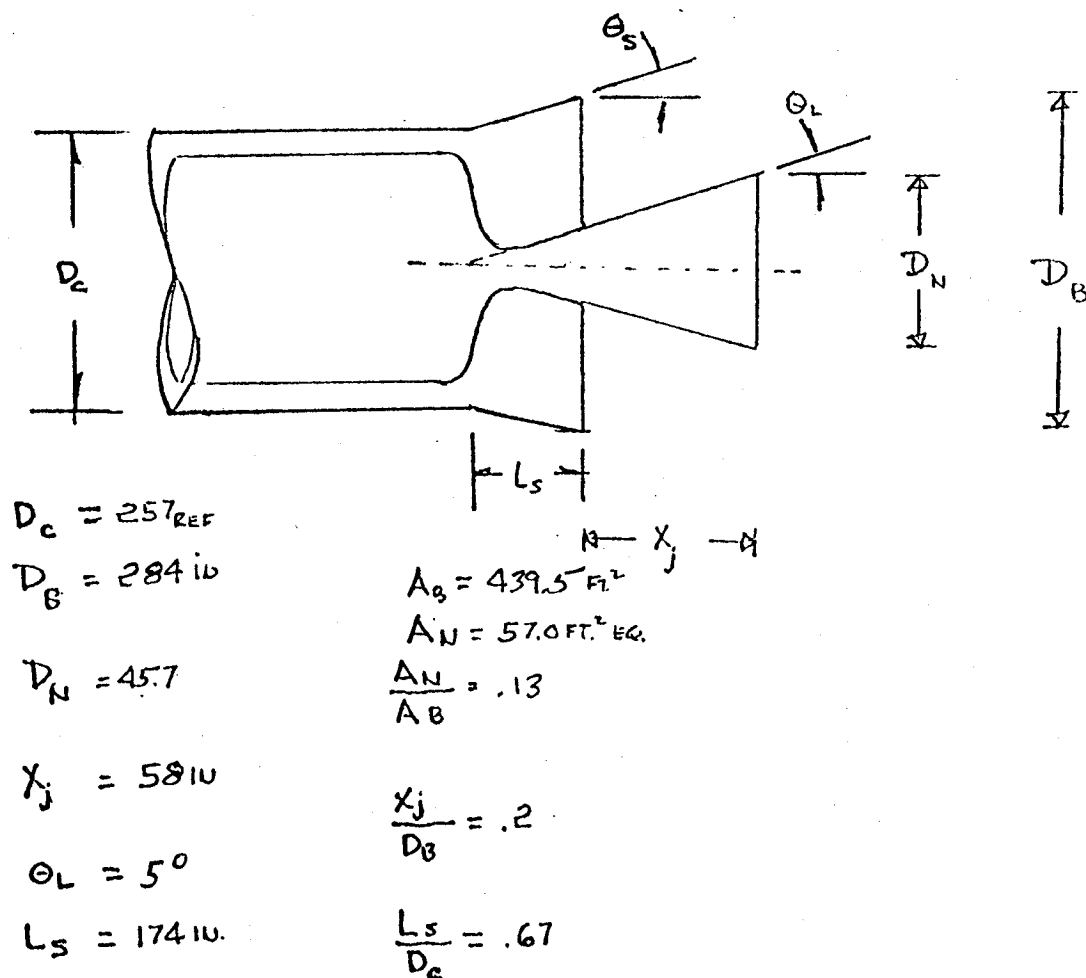
Fig. A-65 – Base Configuration: Saturn I Block II

A-110

ENGINE OPERATING CHARACTERISTICS
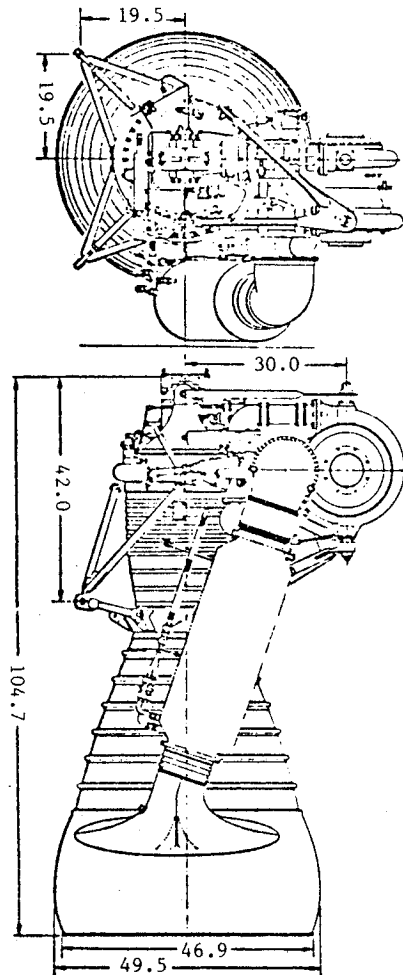
SPECIFICATIONS

Thrust (sea level):	188,000 lb.	
Type:	Liquid bipropellant, pump-fed	

Propellants:

Fuel	RP-1 (kerosene)
Oxidizer	Liquid Oxygen
Mixture Ratio (o/f)	2.23:1

COMPONENTS

Thrust Chamber: Nozzle Area Ratio 8:1
Regeneratively cooled,
tubular wall nozzle.

$$P_C = 650 \text{ psi}$$
$$P_E = 10.96 \text{ psi}$$
$$E = 1.3$$
$$M_E = 3.14$$
$$DIA_E = 45.7 \text{ in}$$
$$\theta_L = 5^\circ$$
$$\epsilon = 8$$

Fig. A-66 - Engine Characteristics: Saturn I Block II

A-111
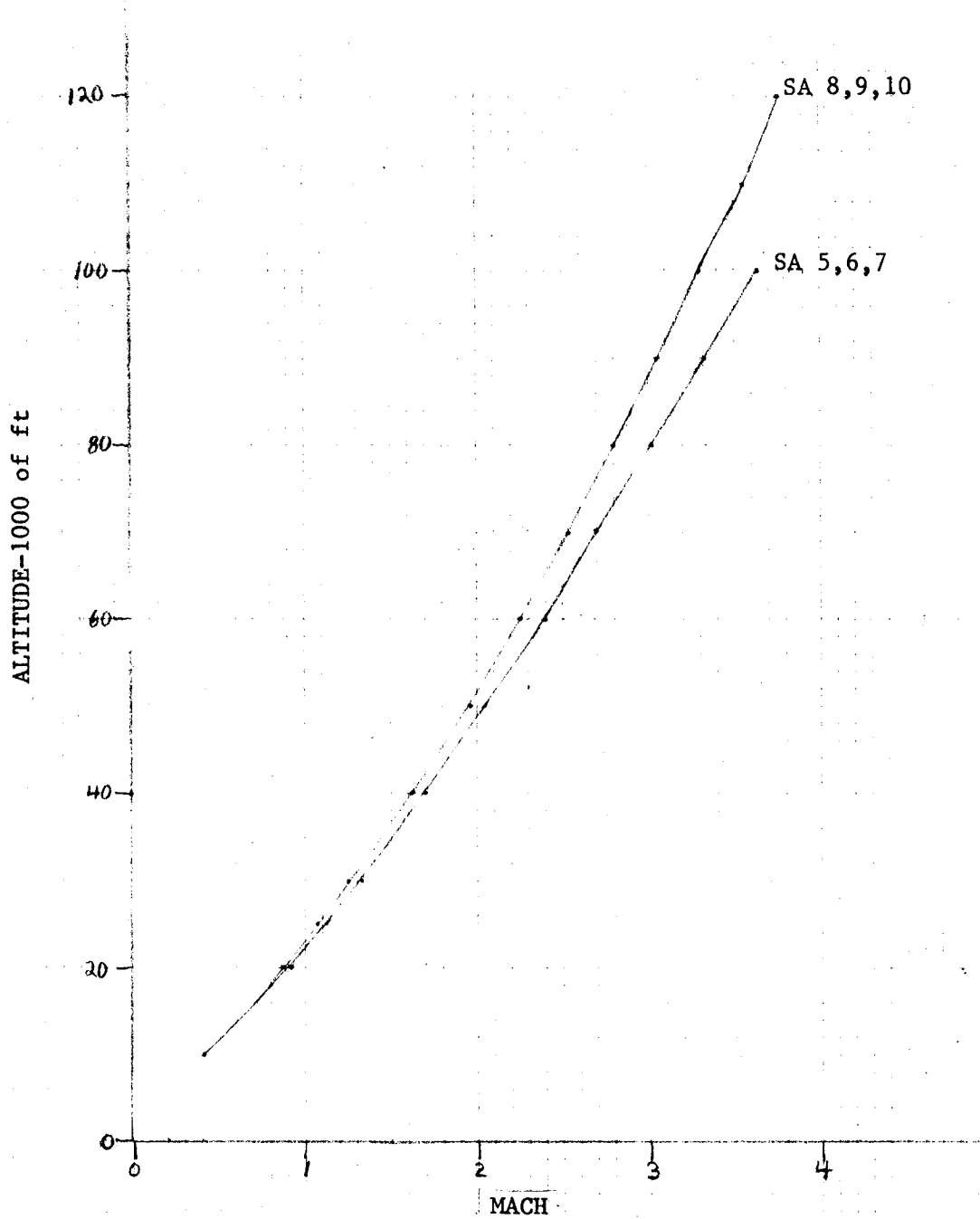
Fig. A-67 - Flight Altitude versus Mach Number: Saturn I Block II
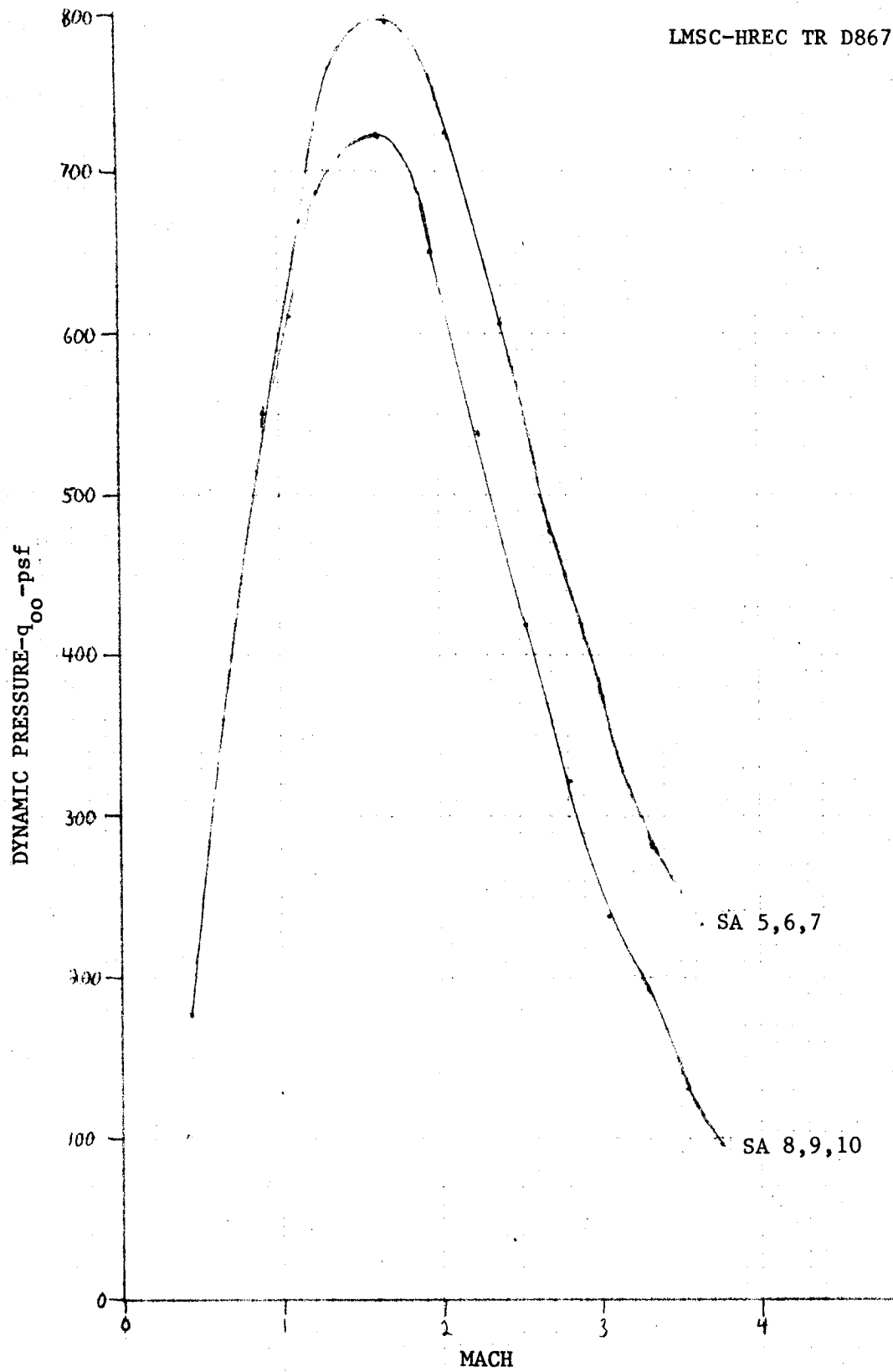
Fig. A-68 – Flight Dynamic Pressure versus Mach Number: Saturn I Block II

LOCKHEED-HUNTSVILLE RESEARCH & ENGINEERING CENTER
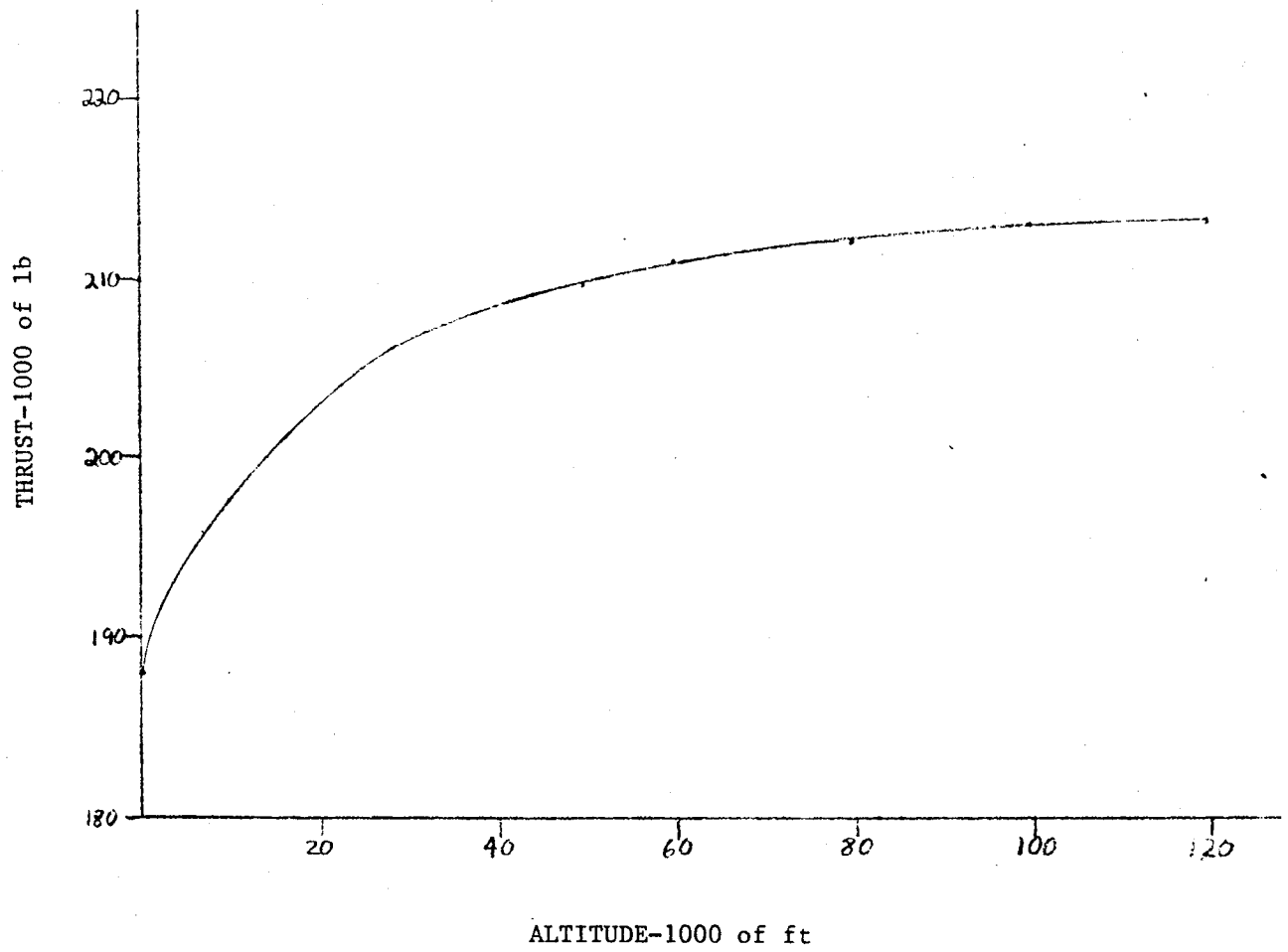
Fig. A-69 - Thrust versus Altitude: H1 Engine
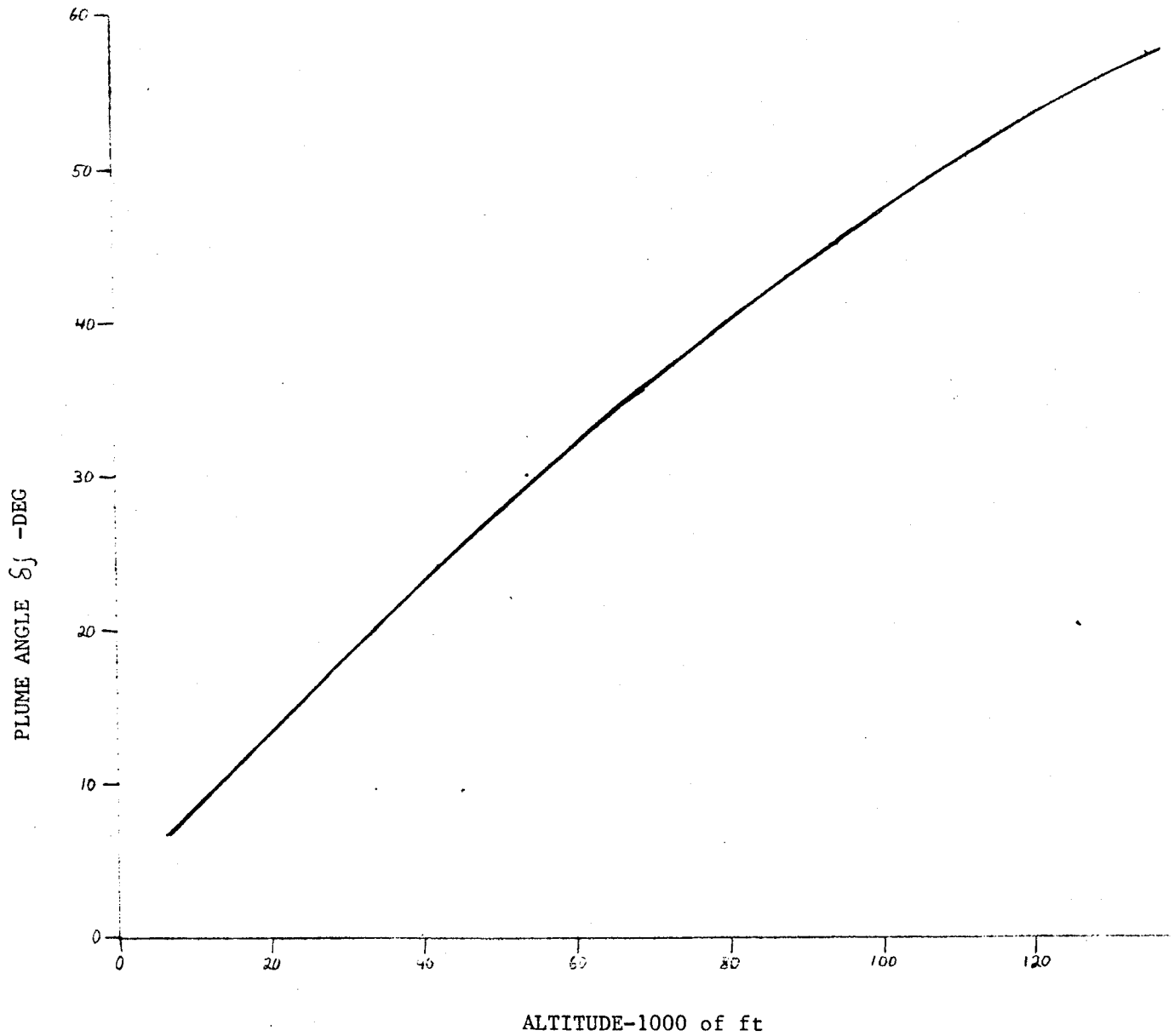
Fig. A-70 - Plume Angle versus Altitude: Saturn I Block II
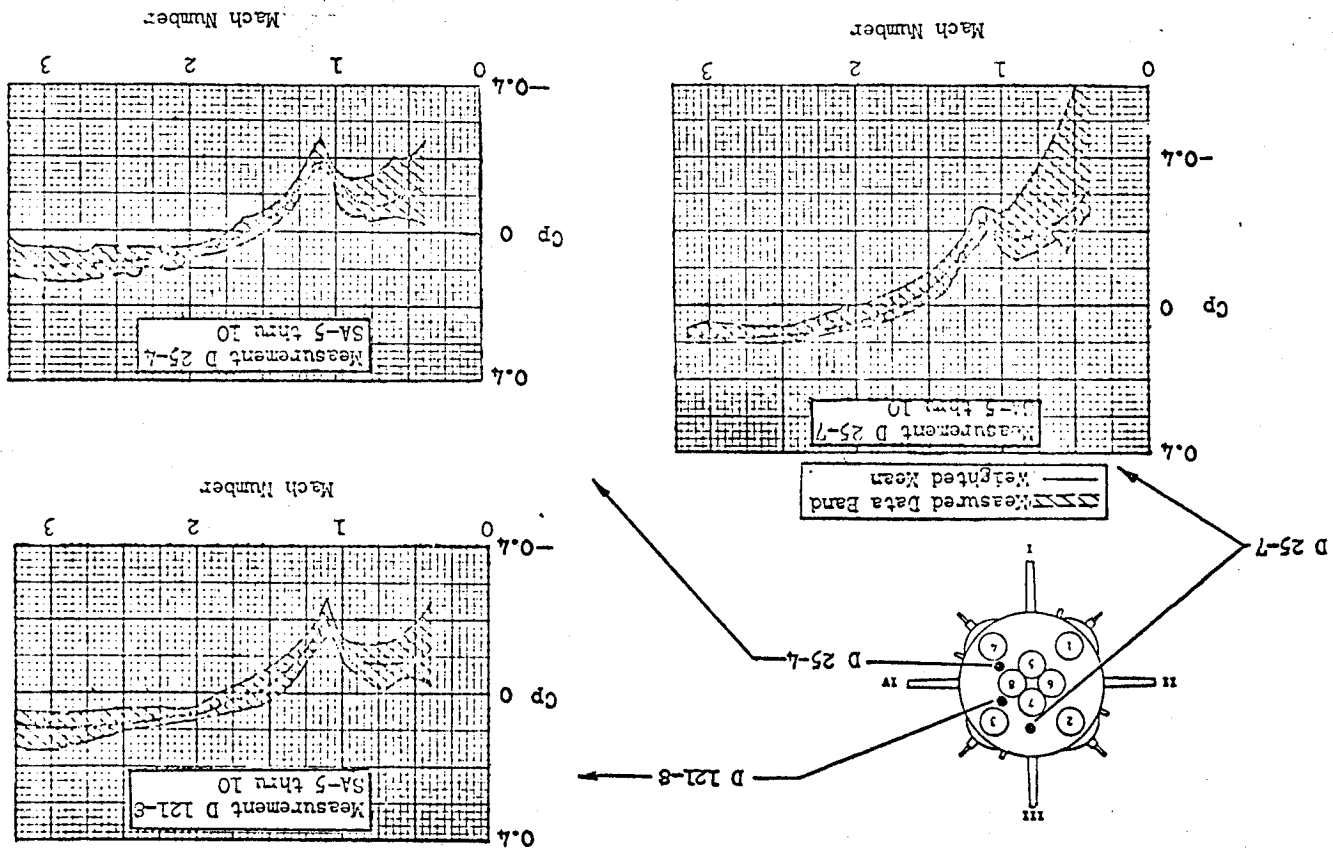
LOCKHEED-HUNTSVILLE RESEARCH & ENGINEERING CENTER
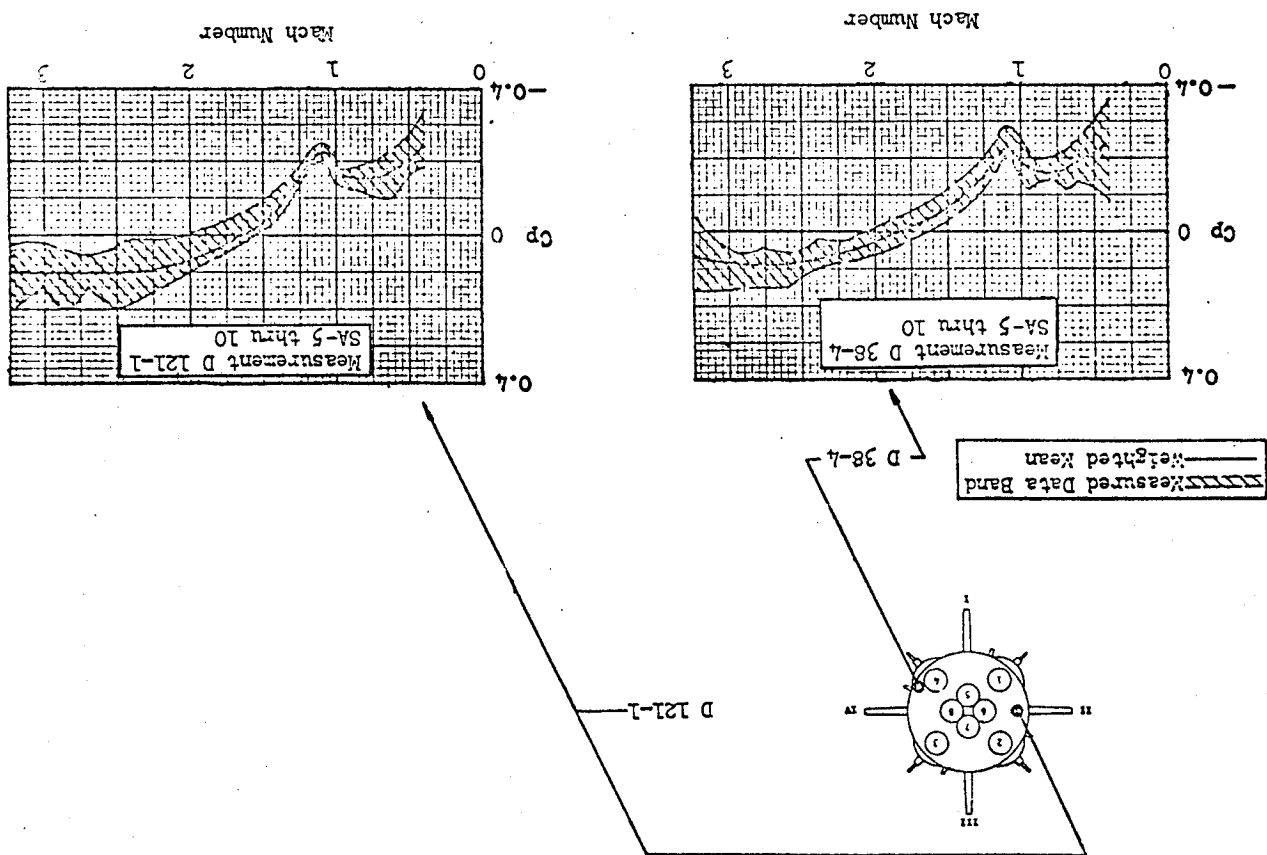
Table A-26   SATURN 1 BLOCK II SA 5, 6, 7

Mach	Alt. (ft)	P_∞ (psf)	q_∞ (psf)	Thrust (lb)	A_B= 439.5 ft^2 CT
.42	10,000	1455.60	179.74	1580000	20.00
.90	20,000	973.26	551.84	1624000	6.70
1.13	25,000	750.00	670.37	1636000	5.55
1.32	30,000	629.66	767.98	1648000	4.88
1.70	40,000	393.12	795.28	1664000	4.76
2.06	50,000	243.61	723.65	1678400	5.28
2.40	60,000	151.03	608.95	1688000	6.31
2.70	70,000	93.73	478.30	1695200	8.06
3.02	80,000	58.51	373.54	1697600	10.34
3.32	90,000	36.78	283.78	1702400	13.65
3.63	100,000	25.20	232.44	1704000	16.68

Table A-27   SATURN 1 BLOCK II SA 8, 9, 10

Mach	Alt. (ft)	P_∞ (psf)	q_∞ (psf)	Thrust (lb)	A_B= 439.5 ft^2 CT
.42	10,000	1455.6	179.74	1580000	20.00
.87	10,000	973.6	515.84	1624000	7.16
1.07	25,000	750.0	601.07	1636000	6.19
1.25	30,000	629.66	688.69	1648000	5.44
1.62	40,000	393.12	722.19	1664000	5.24
1.96	50,000	243.61	655.09	1678400	5.83
2.26	60,000	151.03	539.98	1688000	7.11
2.53	70,000	93.73	419.97	1695200	9.18
2.80	80,000	58.51	321.10	1697600	12.03
3.05	90,000	36.78	239.50	1702400	16.17
3.30	100,000	25.20	192.10	1704000	20.18
3.54	110,000	14.84	130.18	1705000	29.80
3.75	120,000	9.60	94.50	1706000	41.08

LOCKHEED-HUNTSVILLE RESEARCH & ENGINEERING CENTER

Table A-28   SATURN 1 BLOCK II OUTSIDE TAPS SA5-10

Mach	Cp_B	$Cp_{B\ max}$	$Cp_{B\ min}$	PB/P_∞	$PB/P_{\infty\ max}$	$PB/P_{\infty\ min}$
.42	−.250	−.600	−.240	.969	.926	.970
.80	−.180	−.280	−.120	.898	.841	.932
1.13	−.215	−.260	−.180	.808	.768	.839
1.32	−.120	−.160	−.080	.854	.805	.902
1.70	0	−.040	.030	1.000	.919	1.060
2.06	.060	.010	.060	1.180	1.030	1.180
2.40	.080	.050	.100	1.320	1.200	1.400
2.70	.080	.050	.100	1.410	1.260	1.510
3.02	.080	.050	.100	1.510	1.320	1.640
3.32	.080	.050	.100	1.620	1.390	1.770
3.63	.080	.050	.100	1.740	1.460	1.920

LOCKHEED–HUNTSVILLE RESEARCH & ENGINEERING CENTER

Table A-29   SATURN 1 BLOCK II WEIGHTED MEAN SA 5-10

Mach	Cp_B	$Cp_{B\ max}$	$Cp_{B\ min}$	PB/P_∞	$PB/P_{\infty\ max}$	$PB/P_{\infty\ min}$
.42	-.240	-.280	-.182	.971	.965	.977
.90	-.150	-.170	-.113	.915	.904	.936
1.13	-.210	-.225	-.185	.812	.799	.835
1.32	-.110	-.143	-.105	.866	.826	.872
1.70	0	-.028	.017	1.000	.943	1.030
2.06	.050	.030	.070	1.150	1.090	1.210
2.40	.080	.065	.100	1.320	1.260	1.400
2.70	.100	.086	.116	1.510	1.440	1.590
3.02	.100	.080	.122	1.640	1.510	1.780
3.32	.082	.050	.125	1.630	1.390	1.960

LOCKHEED-HUNTSVILLE RESEARCH & ENGINEERING CENTER

SATURN 1B

SATURN 1B

Design modifications and new materials for the Saturn 1B produced more power at less weight, which raised the payload capacity over Saturn I by 6 - 11,000 lb. The difference in propulsion came from a further uprating of the H-1 engines from 188,000 lb to 200,000 lb each at sea level. This modification required stainless steel in place of nickel for thrust chamber tubes, different injector design, and modified designs for the turbopump, LOX valve, fuel valve, and LOX feed duct to withstand higher operating loads. The Saturn 1B also contained scoops in the base of the 1st stage which influenced the performance and base pressure environment of the vehicle. There was, however, a considerable difference on the second stages between the S1 and the S1-B. The S-IV had six RL-10-A-3 engines at 15,000 lb thrust each while the S-IVB had one S-2 engine at 200,000 lb thrust and larger hydrogen and LOX tanks for much increased performance. Another major modification was on the handling of turbine exhaust gases. Prior to vehicle SA-203 these gases were routed through the vehicle skin and dumped overboard. Starting with flight SA-203 the turbine exhaust gases were dumped into the thrust chamber exhaust plumes of the inboard engines on the S-IB stage. The fur- ther modifications were mainly in materials substitution which when combined with the uprated engines produced a vehicle with greatly increased perfor- mance capabilities.

The S-IB configuration and engine operating characteristics are presented in Figs. A-72 through A-76. It is noted that SA-201 has engine shrouds similar to the Saturn I Block II vehicle. The shrouds were removed for subsequent flights. The ascent trajectory data are presented in Figs. A-77 and A-78. Engine plume angles are presented in Fig. A-798. The S-1B stage base pressure source data from Reference 1 is presented in Fig. A-80. Ascent trajectory data, thrust data and base pressure characteristics are presented in Tbles A-30 through A-37.

A-122

SATURN 1B REFERENCES

1. "S-1B Stage Environmental Summary Flight Evaluation Report S-1B-1
   Through S-1B-4," Chrysler Corporation Technical Note, TN-AP-68-333, 23
   July 1968.

2. Mullen, C. D. et al., "Saturn Base Heating Handbook," NASA CR-61390, The
   Boeing Company, Huntsville, Alabama, May 1972.

PAYLOAD

IU

S-IVB STAGE

233 FT

S-1B STAGE

Sta
935.304

Reference Diameter
(257° Full Scale)

Gimbal
Sta
100.000

Sta
-1.000

S-IB-1 EIGHT (8) 200K THRUST - H-1 ENGINES

Fig. A-72 - Body Configuration: S-1B

AIR SCOOP

HEAT SHIELD
OUTER REGION

FIN TRAILING EDGE

FLAME SHIELD

HEAT SHIELD
INNER REGION
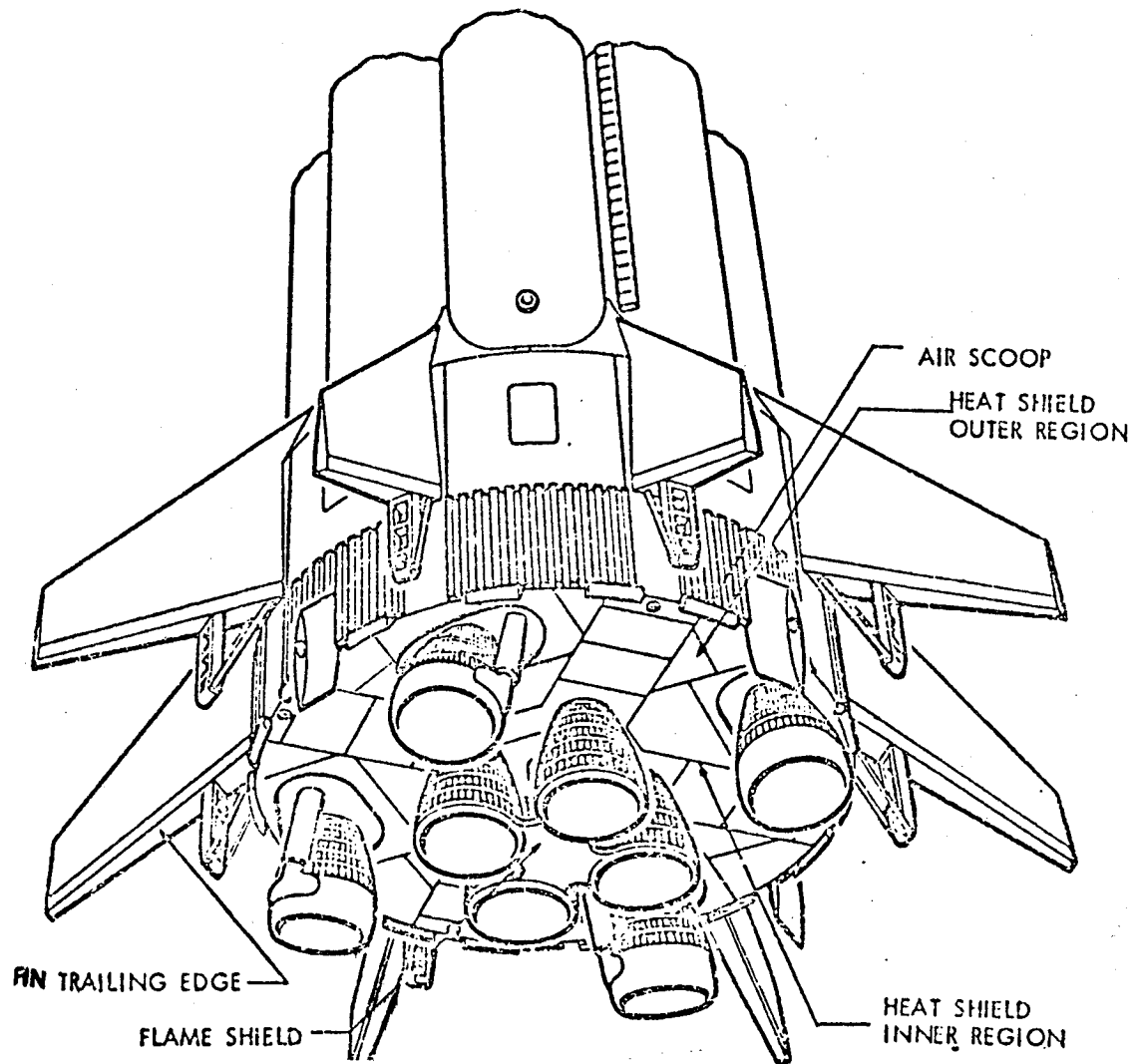
Fig. A-73 - Base View Saturn S-1B

LOCKHEED-HUNTSVILLE RESEARCH & ENGINEERING CENTER

$A_c = 360$

$D_c = 257_{REF}$

$D_B = 284 \text{ in}$

$D_N = 45.7$

$X_j = 58 \text{ in.}$

$\Theta_L = 5°$

$L_S = 174 \text{ in.}$

$\Theta_S = 4.4°$

$A_B = 439.5 \text{ Ft}^2$

$A_N = 57.0 \text{ Ft}^2 \text{ EQ.}$

$\dfrac{A_N}{A_B} = .13$

$\dfrac{A_B}{A_c} = 1.22$

$\dfrac{X_j}{D_B} = .2$

$\dfrac{L_S}{D_c} = .67$

Fig. A-74 Base Configuraton: S-1B, 201 Only

LOCKHEED-HUNTSVILLE RESEARCH & ENGINEERING CENTER

$D_c = 257 \text{ in}$

$D_B = 270 \text{ in}$

$D_N = 45.7 \text{ (i)}$

$X_j = 58 \text{ in}$

$\Theta_L = 5°$

$L_s = 174 \text{ in}$

$\Theta_s = 2°$

$A_B = 397.5 \text{ Ft.}^2$

$A_N = 57.0 \text{ Ft.}^2$

$\dfrac{A_N}{A_B} = .143$

$\dfrac{A_B}{A_c} = 1.1$

$\dfrac{X_j}{D_B} = .214$

$\dfrac{L_s}{D_c} = .66$
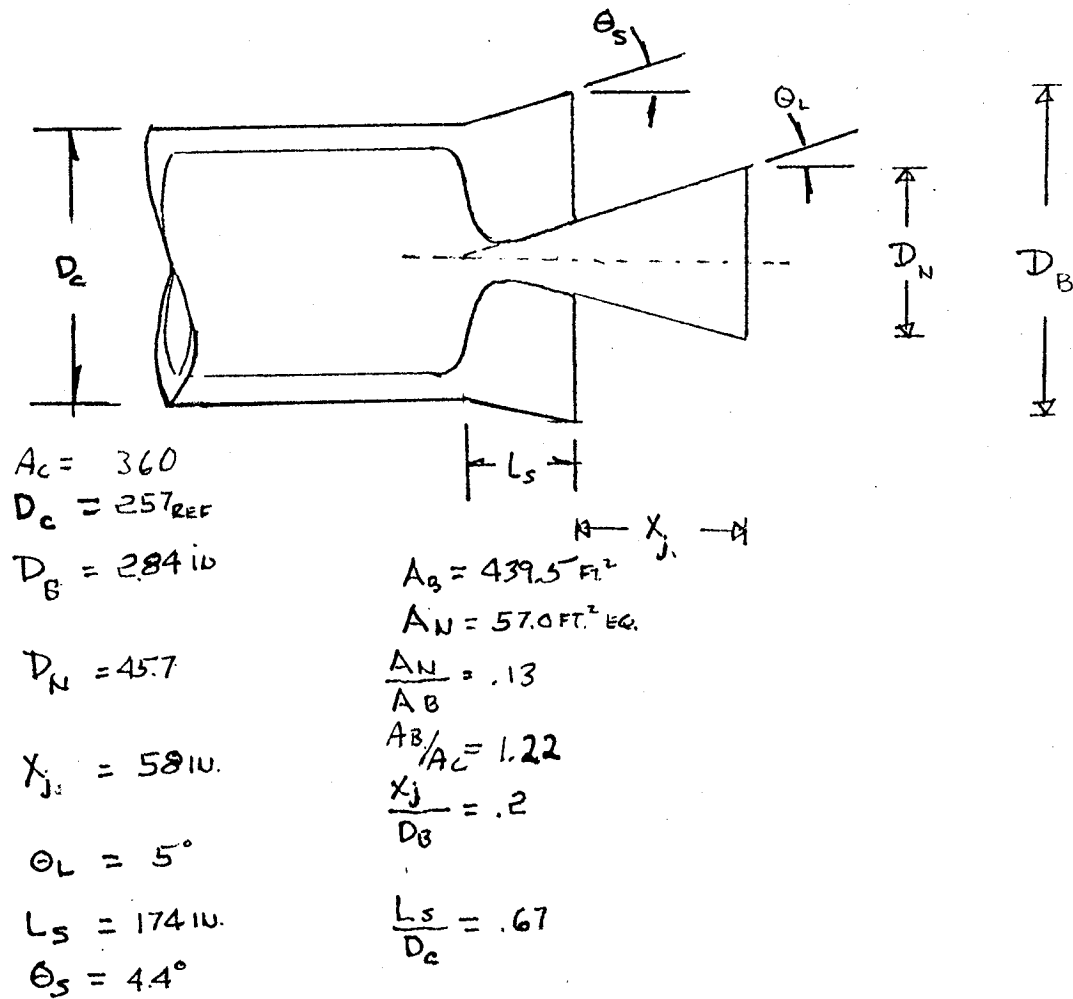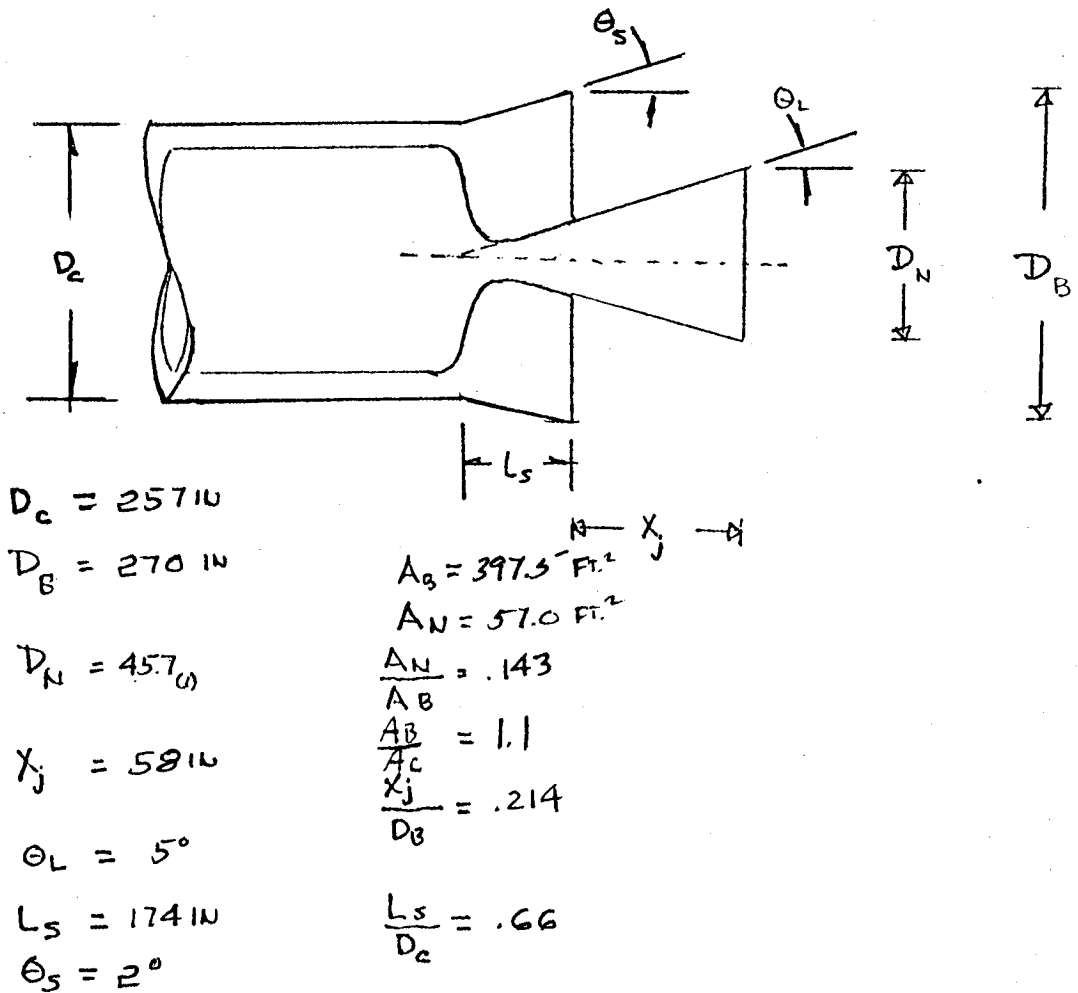
Fig. A-75 - Base Configuration: S-1B, 202, 203, 204

ENGINE OPERATING CHARACTERISTICS

P_C = 689 psi

P_E = 12.2 psi

γ_E = 1.3

M_E = 3.14

DIA_E = 45.7 in

θ_L = 5°

ϵ = 8
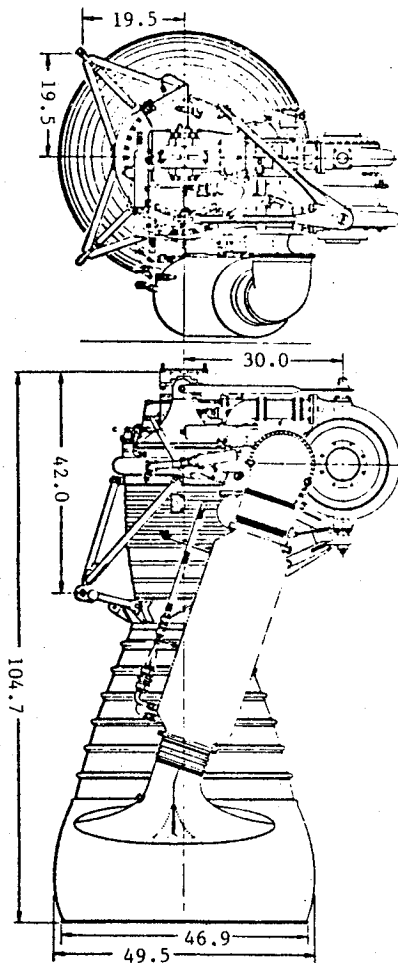
SPECIFICATIONS

Thrust (sea level): 205,000 lb.

Type: Liquid bipropellant, pump-fed

Propellants:

Fuel RP-1 (kerosene)
Oxidizer Liquid Oxygen
Mixture Ratio (o/f) 2.23:1

COMPONENTS

Thrust Chamber: Nozzle Area Ratio 8:1
Regeneratively cooled, tubular wall nozzle.

ESTIMATED ENGINE PERFORMANCE FOR 205K ENGINES
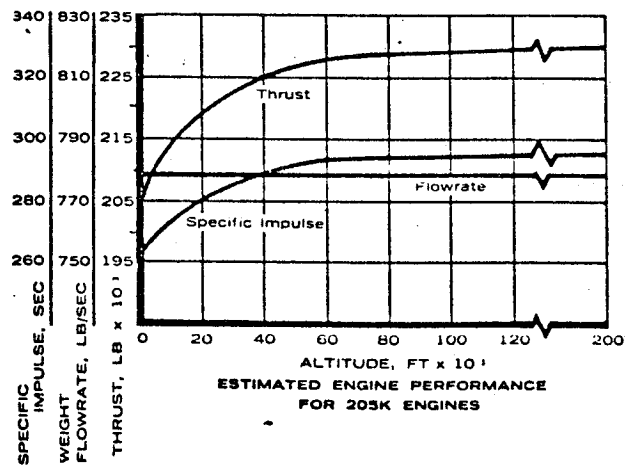
Fig. A-76 - Engine Characteristics: Saturn S-1B

A-128
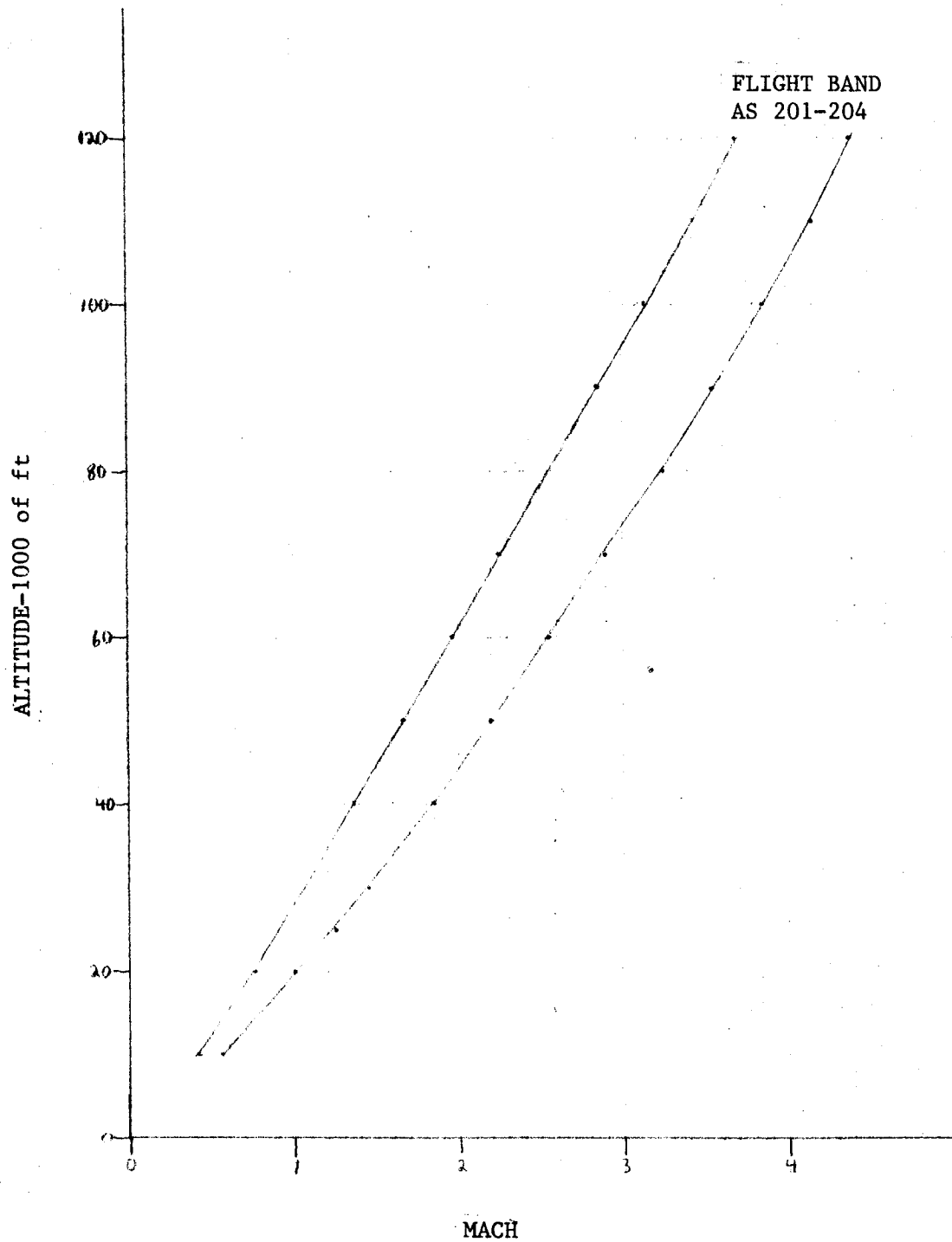
Fig. A-77 – Flight Altitude versus Mach Number: S-1B
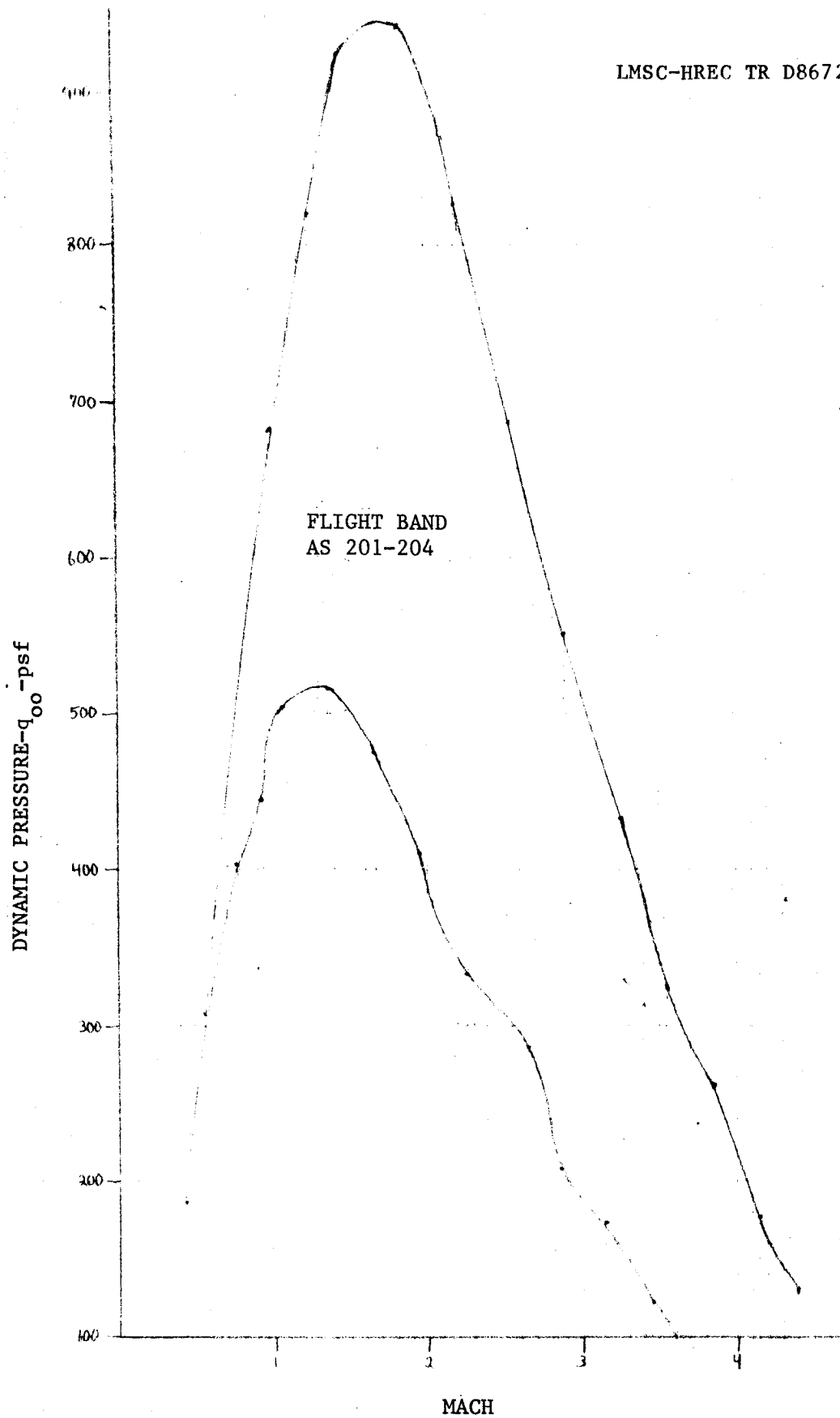
Fig. A-78 - Flight Dynamic Pressure versus Mach Number: S-1B
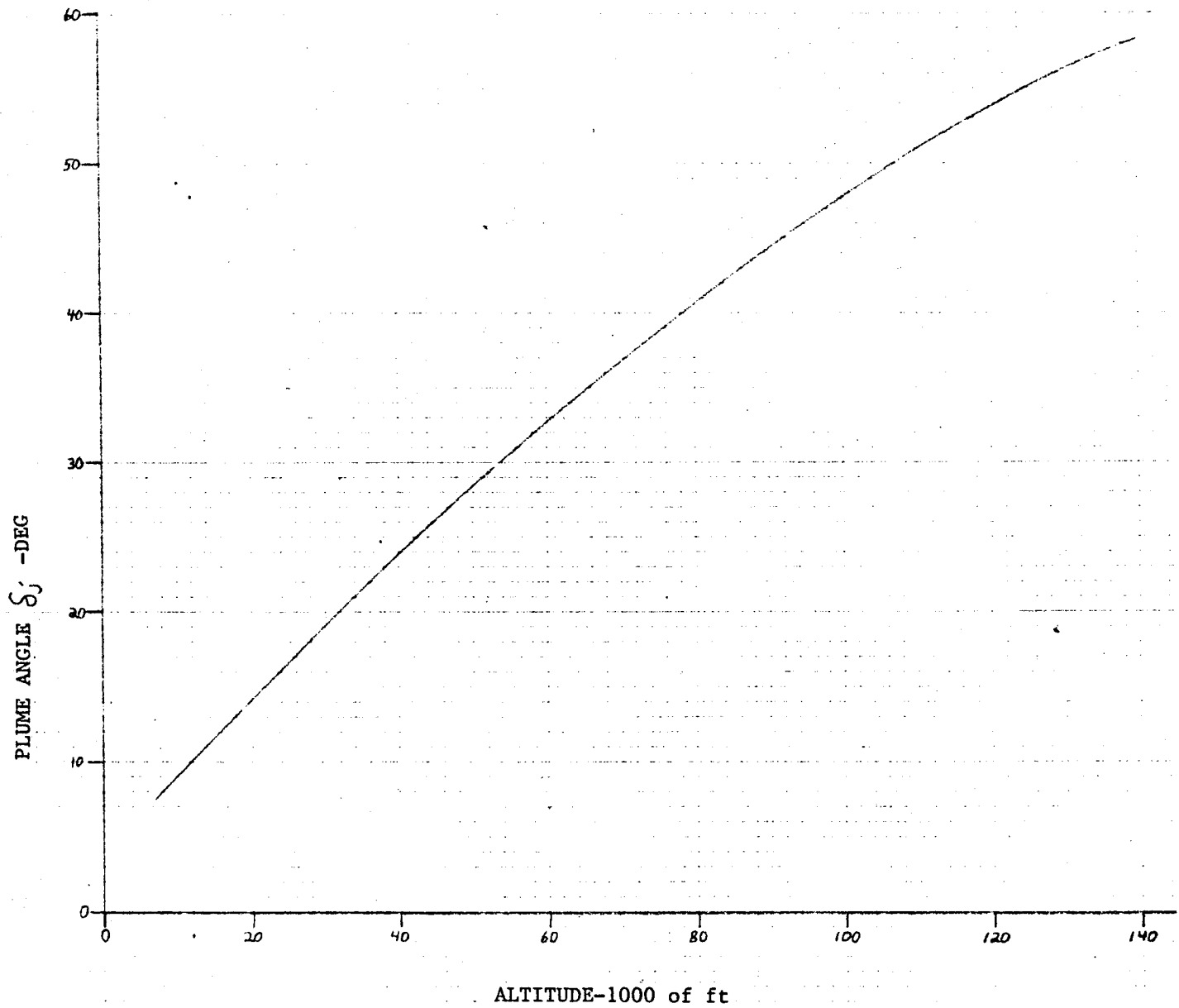
Fig. A-79 - Plume Angle versus Altitude: S-1B

LOCKHEED-HUNTSVILLE RESEARCH & ENGINEERING CENTER
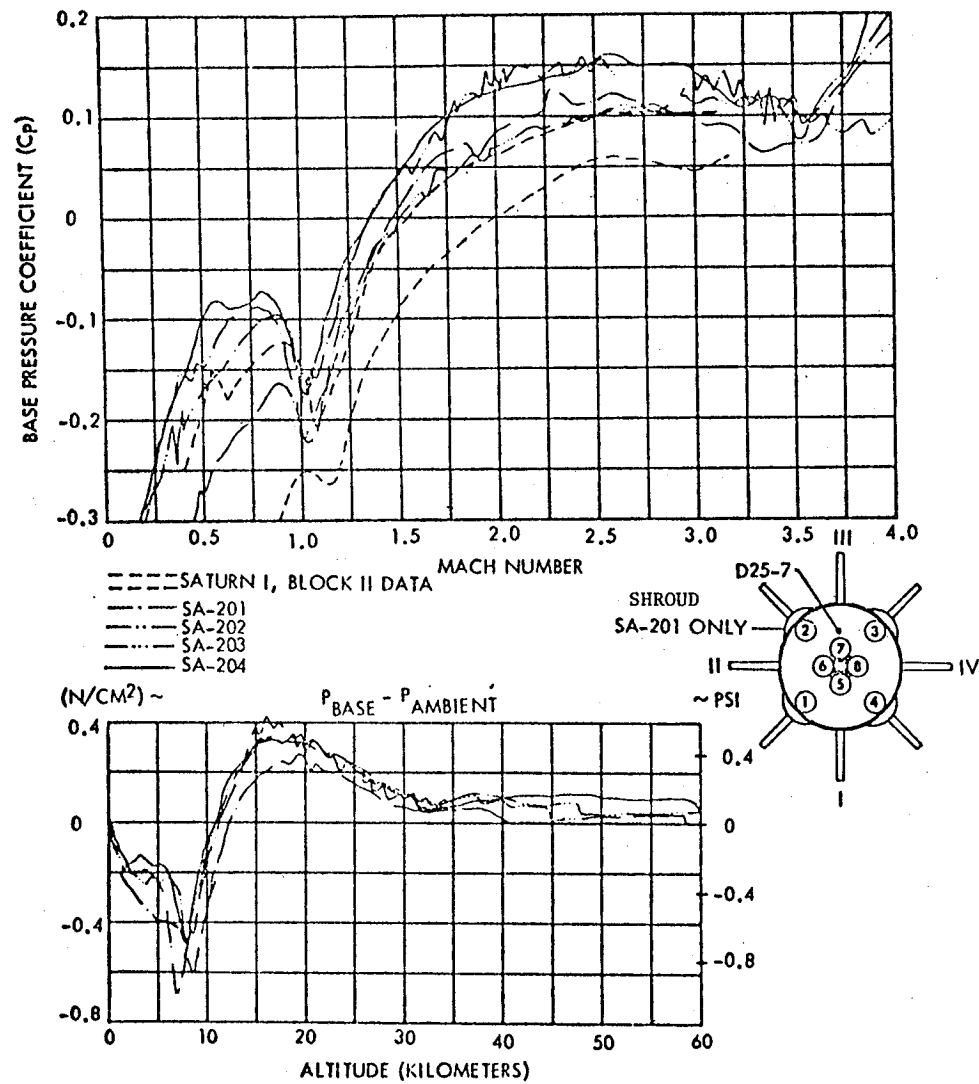
Fig. A-80 - Saturn I S-1B Stage Base Pressure Source Data

Table A-30   SATURN 1B – AS 201

$$A_B = 439.5 \ ft^2$$

Mach	Alt ft	P_{oo} Psf	q_{oo} Psf	Thrust lb	C_T
.43	10000	1455.60	188.40	1676000	20.00
.77	20000	973.60	404.07	1720000	9.50
.92	25000	750.00	444.36	1732000	8.80
1.07	30000	629.66	504.63	1744000	7.80
1.37	40000	393.12	516.49	1760000	7.70
1.67	50000	243.61	475.58	1774400	8.40
1.97	60000	151.03	410.29	1784000	9.89
2.25	70000	93.73	332.16	1789600	12.26
2.65	80000	58.51	287.62	1793600.	14.20
2.85	90000	36.78	209.12	1798400	19.50
3.13	100000	25.20	172.82	1800000	23.70
3.42	110000	14.84	121.50	1801000	33.72
3.70	120000	9.60	92.00	1802000	44.60

LOCKHEED–HUNTSVILLE RESEARCH & ENGINEERING CENTER

Table A-31 - SATURN 1B - AS 201

Mach	C_{PB}	C_{PB}Max	C_{PB}Min	P_B/P_{oo}	P_B/P_{oo}Max	P_B/P_{oo}Min
.43	-.300	-.35	-.25	.961	.955	.967
.77	-.190	-.24	-.15	.921	.900	.938
.92	-.179	-.229	-.129	.894	.864	.924
1.07	-.220	-.27	-.17	.823	.784	.864
1.37	-.050	-.10	-0-	.934	.868	1.0
1.67	.050	-0-	.10	1.09	1.0	1.19
1.97	.080	.03	.13	1.22	1.08	1.35
2.25	.115	.065	.165	1.41	1.23	1.59
2.65	.121	.071	.171	1.59	1.35	1.84
2.85	.10	.05	.15	1.57	1.28	1.85
3.13	.09	.04	.14	1.62	1.27	1.96
3.42	.07	.02	.12	1.57	1.16	1.98
3.70	.10	.05	.15	1.96	1.48	2.44

LOCKHEED-HUNTSVILLE RESEARCH & ENGINEERING CENTER

Table A-32 – SATURN 1B – AS 202

A_B= 397.7 ft^2

Mach	Alt ft	P_{oo} Psf	q_{oo} Psf	Thrust lb	C_T
.40	10000	1455.6	163.03	1676000	25.85
.64	20000	973.26	279.05	1720000	15.50 .
.92	25000	750.0	444.36	1732000	9.80
1.07	30000	629.66	504.63	1744000	8.69
1.40	40000	393.12	539.36	1760000	8.20
1.72	50000	243.61	504.49	1774400	8.84
2.03	60000	151.03	435.67	1784000	10.30
2.32	70000	93.73	353.14	1789600	12.74
2.62	80000	58.51	281.15	1793600	16.04
2.90	90000	36.78	216.52	1798400	20.88
3.20	100000	25.20	180.63	1800000	25.06
3.50	110000	14.84	127.25	1801000	35.59
3.85	120000	9.60	99.61	1802000	45.49

Table A-33 – SATURN 1B – AS 202

Mach	C_{PB}	C_{PB}Max	C_{PB}Min	P_B/P_{oo}	P_B/P_{oo} Max	P_B/P_{oo} Min
.40	-.2	-.25	-.15	.978	.972	.983
.64	-.135	-.185	-.085	.961	.946	.976
.92	-.1	-.15	-.05	.941	.911	.970
1.07	-.16	-.21	-.11	.872	.832	.912
1.40	.015	-.035	.065	1.02	.952	1.09
1.72	.085	.035	.135	1.18	1.07	1.28
2.03	.14	.09	.19	1.40	1.26	1.55
2.32	.15	.10	.20	1.57	1.38	1.75
2.62	.14	.09	.19	1.67	1.43	1.91
2.90	.15	.10	.20	1.88	1.59	2.18
3.20	.11	.06	.16	1.79	1.43	2.15
3.50	.11	.06	.16	1.94	1.51	2.37
3.85	.15	.10	.20	2.55	2.04	3.08

Table A-34   SATURN IB - AS 203

$A_B = 397.7 \text{ ft}^2$

Mach	Alt ft	P_{oo} Psf	q_{oo} Psf	Thrust lb	C_T
.55	10000	1455.6	308.22	1676000	13.67
1.00	20000	973.26	681.28	1720000	6.35
1.25	25000	750.0	820.31	1732000	5.31
1.45	30000	629.66	926.70	1744000	4.73
1.85	40000	393.12	941.82	1760000	4.70
2.20	50000	243.61	825.35	1774400	5.41
2.55	60000	151.03	687.45	1784000	6.53
2.90	70000	93.73	551.79	1789600	8.16
3.25	80000	58.51	432.61	1793600	10.42
3.55	90000	36.78	324.46	1798400	13.94
3.85	100000	25.20	261.47	1800000	17.31
4.15	110000	14.84	178.91	1801000	25.31
4.4	120000	9.60	130.10	1802000	34.83

Table A-35   SATURN 1B - AS 203

Mach	C_{PB}	$C_{PB}Max$	$C_{PB}Min$	P_B/P_{oo}	$P_B/P_{oo}Max$	$P_B/P_{oo}Min$
.55	-.13	-.18	-.08	.972	.962	.983
1.0	-.2	-.25	-.15	.860	.825	.895
1.25	-.085	-.135	-.035	.907	.852	.962
1.45	-.015	-.065	+.035	.978	.904	1.05
1.85	+.01	-.04	+.06	1.02	.904	1.14
2.20	.09	.04	.14	1.30	1.14	1.47
2.55	.10	.05	.15	1.46	1.23	1.68
2.90	.11	.06	.16	1.65	1.35	1.94
3.25	.12	.07	.17	1.89	1.52	2.26.
3.55	.10	.05	.15	1.88	1.44	2.32
3.85	.09	.04	.14	1.93	1.42	2.45

LOCKHEED-HUNTSVILLE RESEARCH & ENGINEERING CENTER

Table A-36   SATURN 1B - AS204

A_B = 397.7 ft^2

Mach	Alt ft	P_{oo} Psf	q_{oo} Psf	Thrust lb	C_T
.43	10000	1455.6	188.40	1676000	22.37
.82	20000	973.26	458.09	1720000	9.44
1.02	25000	750.0	546.21	1732000	7.97
1.22	30000	629.66	656.03	1744000	6.68
1.60	40000	393.12	704.47	1760000	6.28
1.94	50000	243.61	641.80	1774400	6.95
2.26	60000	151.03	540.0	1784000	8.31
2.56	70000	93.73	429.99	1789600	10.47
2.85	80000	58.51	332.67	1793600	13.56
3.15	90000	36.78	255.46	1798400	17.70
3.42	100000	25.40	206.32	1800000	21.94
3.67	110000	14.84	139.91	1801000	32.37
3.93	120000	9.60	103.79	1802000	43.66

LOCKHEED-HUNTSVILLE RESEARCH & ENGINEERING CENTER

Table A-37   SATURN 1B - AS 204

Mach	C_{PB}	C_{PB}Max	C_{PB}Min	P_B/P_{oo}	P_B/P_{oo}Max	P_B/P_{oo}Min
.43	-.15	-.10	-.20	.980	.987	.974
.82	-.07	-.12	-.02	.967	.944	.990
1.02	-.17	-.22	-.12	.876	.839	.913
1.22	-.05	-.10	-0-	.948	.896	1.0
1.60	.06	.01	.11	1.11	1.02	1.20
1.94	.12	.07	.17	1.32	1.18	1.45
2.26	.138	.088	.188	1.49	1.31	1.67
2.56	.16	.11	.21	1.73	1.50	1.96
2.85	.15	.10	.20	1.85	1.57	2.13
3.15	.12	.07	.17	1.83	1.49	2.18
3.42	.115	.065	.165	1.94	1.53	2.35
3.67	.13	.08	.18	2.23	1.75	2.70
3.93	.20	.15	.25	3.16	2.62	3.70

SATURN V

SATURN V

The Saturn V S-1C (first stage) booster is powered by five Rocketdyne F-1 engines capable of a total thrust of 7,500,000 lb at sea level. The second stage (S-2) is powered by five J-2 engines for a total thrust of 1,000,000 lb. The J-2 was also used in the second stage of the S-1B launch vehicle which was designed to test the Rocketdyne engines. The third stage uses a single J-2 engine to thrust the Apollo command module on its final ascent leg of its mission. The Saturn V S-1C stage was equipped with scoops on the base for the 501 flight, however, the 502 and later flights did away with the scoops. The design changes developed in the previous Saturn missions and used in the Saturn V vehicle were mainly in propulsion and materials substitution to achieve a larger, lighter, higher performance launch vehicle capable of lifting a much heavier payload to the moon and beyond.

The Saturn V vehicle and S-1c stage base description is presented in Figs. A-81 through A-86. The F-1 engine description and operating characteristics are presented in Fig. A-87. The Saturn V ascent trajectory data are presented in Figs. A-88 and A-89. The engine thrust for the F-1 engines is presented in Fig. A-90. The F-1 engine plume angle is presented in Fig. A-91. The Saturn V S-1C stage base pressure source data was taken directly from Reference 1 and is presented in Tables A-38 through A-47. The flight base instrumentation locations and the corresponding base pressure data were selected as the most representative of the measured data.

A-141

SATURN V REFERENCES

1. Lott, R.A., L.R. Baker, W.H. Sims, and R.W. McCanna, "Power-On Base Pressure for Space Shuttle Launch Configurations," LMSC-HREC D225152, Lockheed Missiles & Space Company, Huntsville, Ala., June 1971.

2. Mullen, C. R. et al., Saturn Base Heating Handbook," NASA CR-61390, The Boeing Company, Huntsville, Alabama, May 1972.
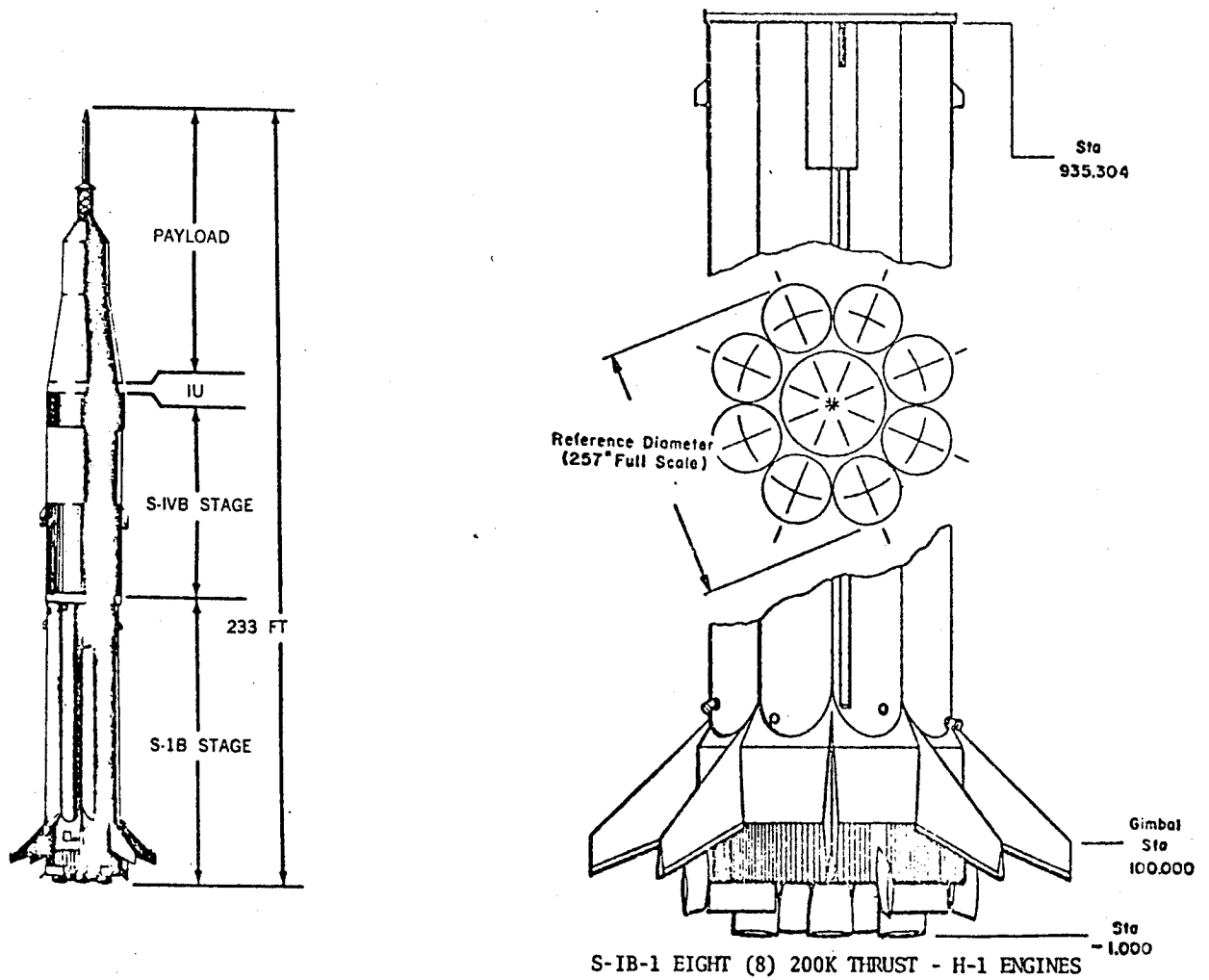
LOCKHEED-HUNTSVILLE RESEARCH & ENGINEERING CENTER
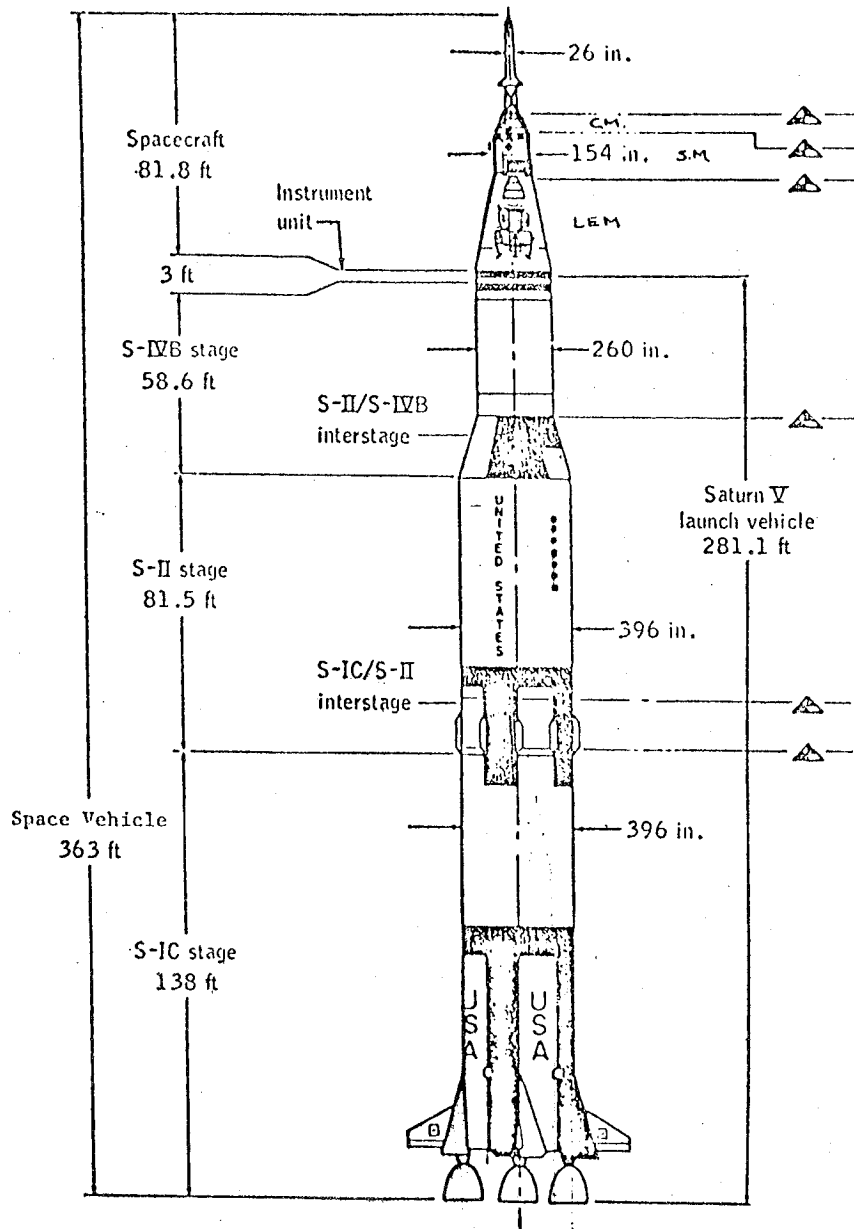
Fig. A-81 - Apollo Launch Vehicle Configuration
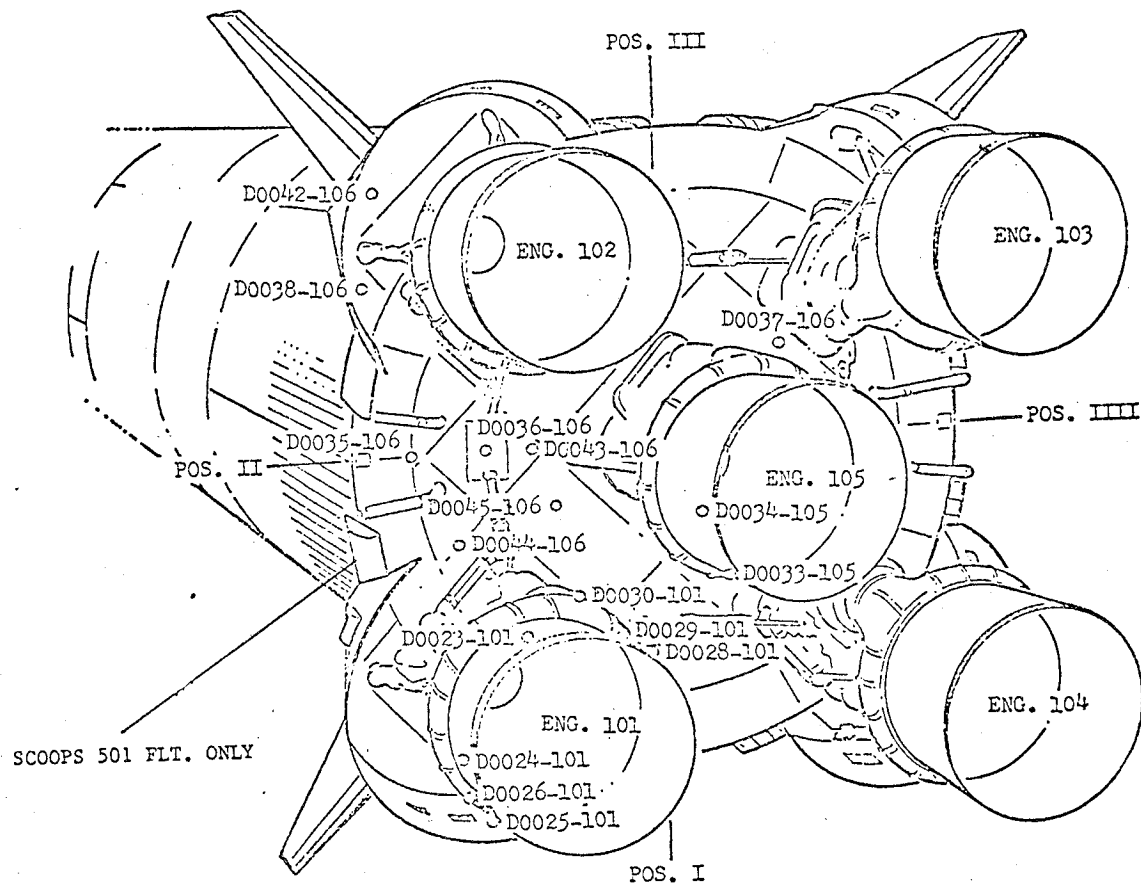
Fig. A-82 - Base Pressure Transducer Locations for Saturn 501

STA
112.0

81.3
48.5

227.4"

-115.4

FIN A

F IN C

ENG 101   ENG 105   ENG 103

228"   182"

FIN B

FIN C

ENG 102   ENG 103

198"R   ENG 105

ENG 101   ENG 104

70"R

FIN A   FIN D

X/D=227.4/396=.574

$A_N/A_B=.414$

VEHICLE LENGTH = 363 FEET
VEHICAL DIAMETER = 33 FEET
PROPELLANT = LOX/RP–1
TOTAL OF 29 STATIC, DIFFERENTIAL,
  PITOT, & PITOT-STATIC S-IC BASE
  PRESSURE MEASUREMENTS
O/F (NOM) = 2.30
P_{CH} = 965 PSIA
T_{CH} = 6510 ºR
γ = 1.22
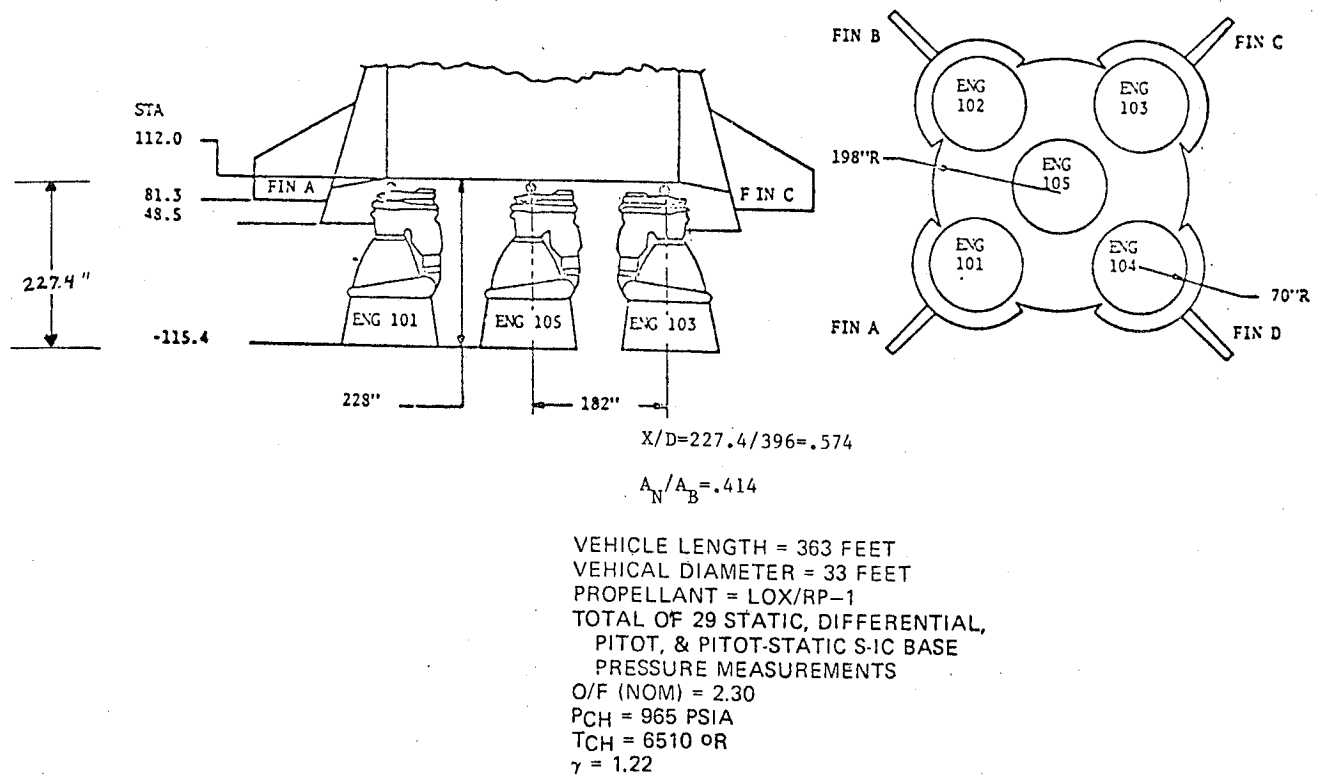
Fig. A-83 – Engine Configuration – Saturn V

NOTES:
1. All vehicle stations in inches.
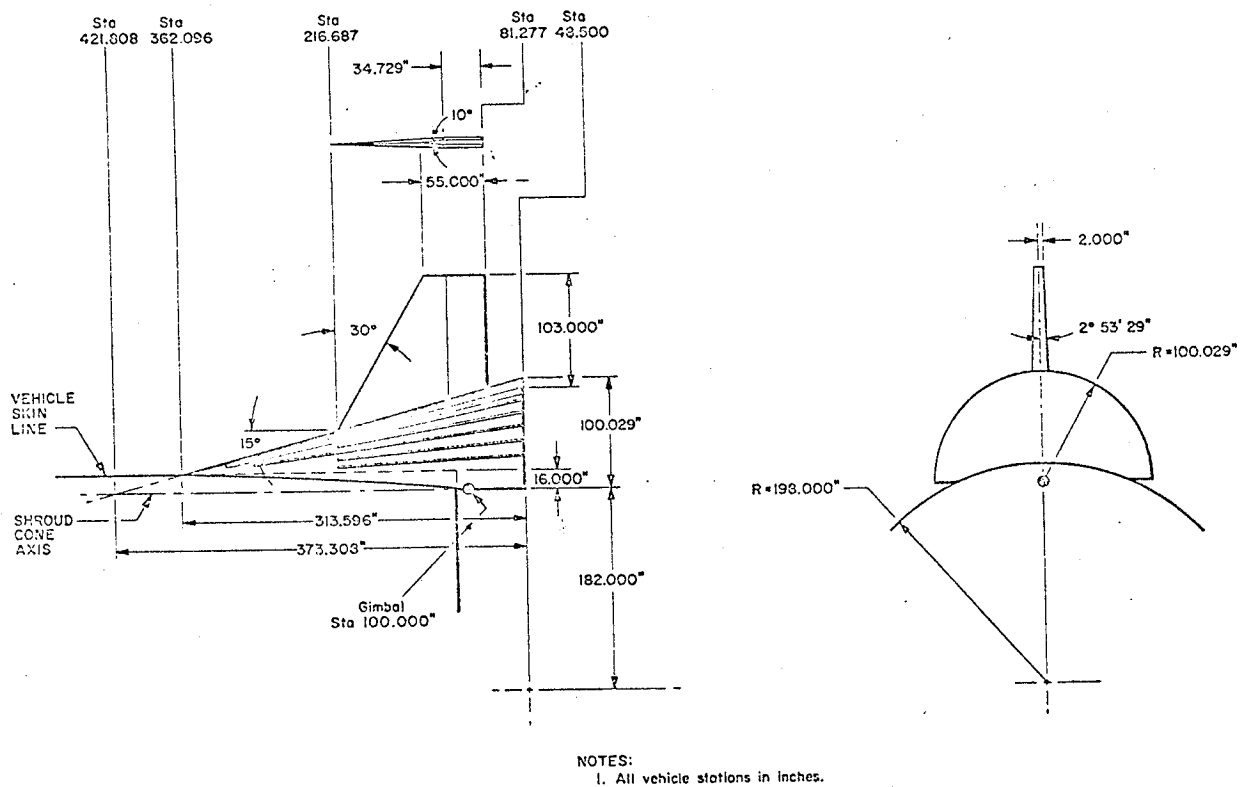
Fig. A-84 – Geometry of the Apollo Saturn V S-1C
Stage Engine Shroud and Fin

LOCKHEED-HUNTSVILLE RESEARCH & ENGINEERING CENTER

$A_B = 855 + 436.1 = 1291$ ft^2

$A_B/A_{cyl} = 1.5$

$D_B/D_{cyl} = 1.225$

1. All vehicle stations in inches.
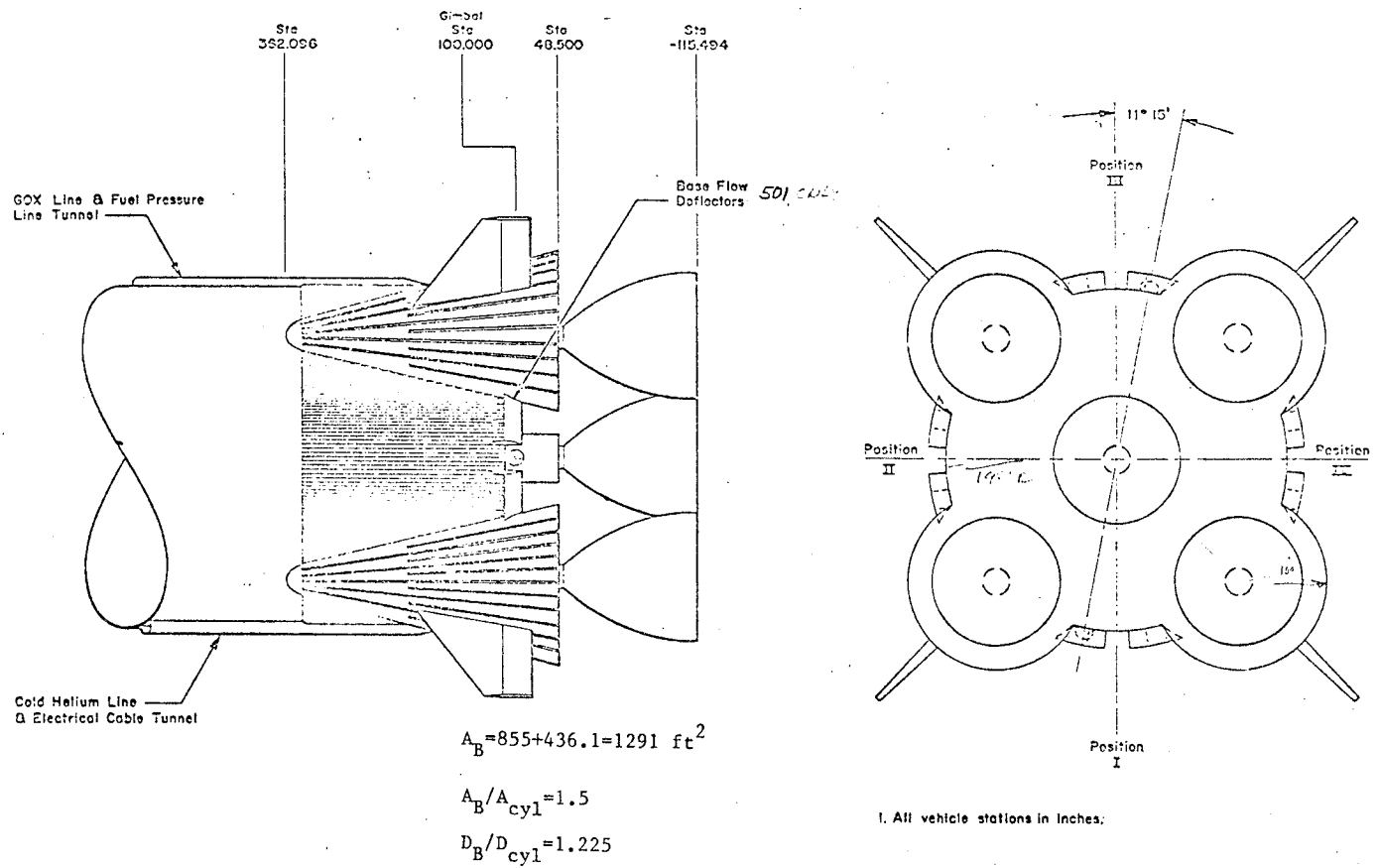
Fig. A-85 - Geometry of the Saturn V, S-1C Stage, Base Area

A-147

F-1 engine dimensions

NOZZLE AREA RATIO $\epsilon = 16:1$

FUEL INLET
11.8 I.D.

OXIDIZER INLET
16.1 I.D.

11.8 I.D. FUEL INLET

25.9   25.9

50.0

35.4

NO. 1 ACTUATOR
ATTACH POINT

NO. 2 ACTUATOR
ATTACH POINT

NO. 2 GIMBAL AXIS

35.4   35.4

$P_C = 965$ psi

$P_E = 6.17$ psi

$\gamma_E = 1.22$

$M_E = 3.68$

$DIA_E = 140$ in

$\theta_L = 5^o$

$\epsilon = 16$

NO. 1
GIMBAL AXIS

143.5"

INTERFACE PANEL

GIMBAL INTERFACE

5"

43.9

220.4"

64.8

NOZZLE EXTENSION
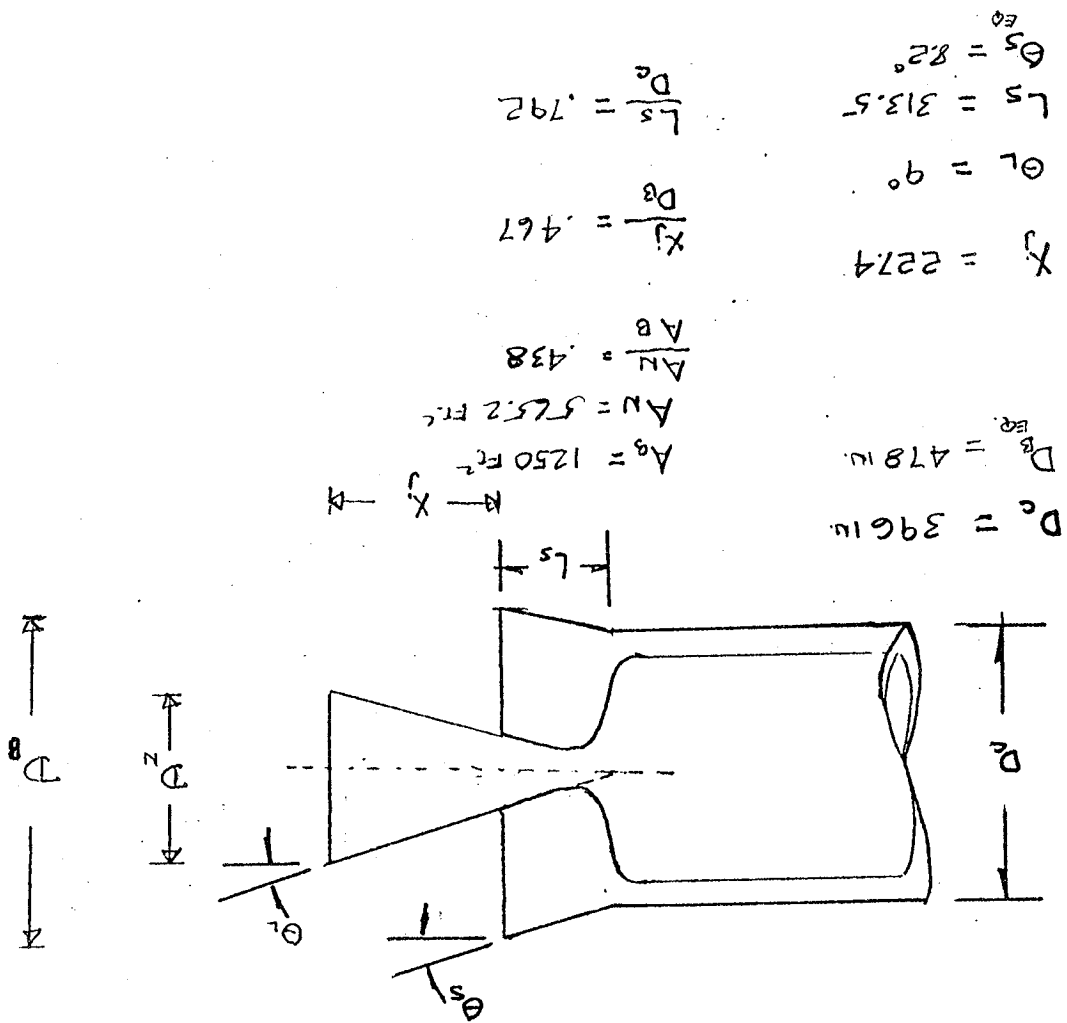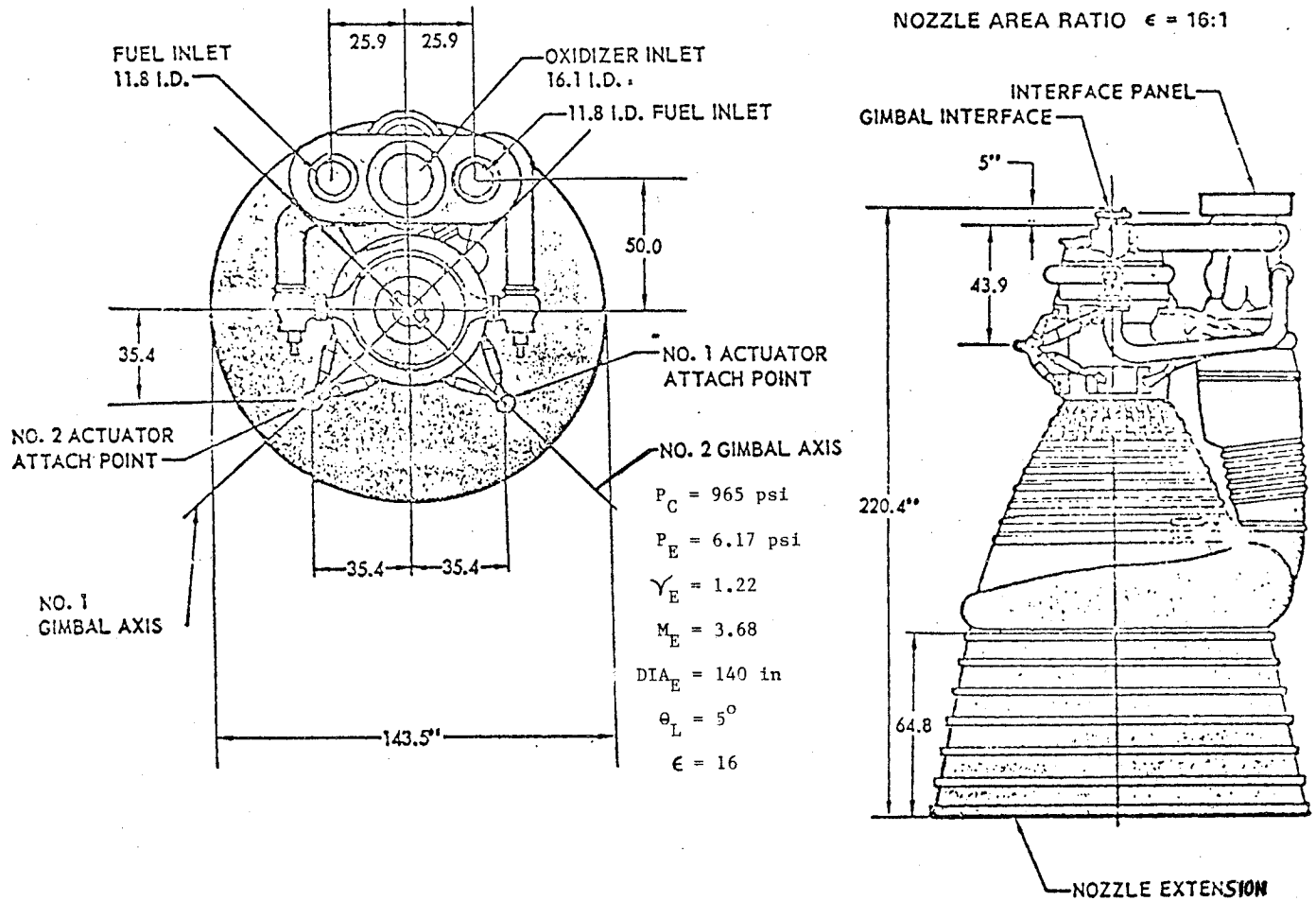
Fig. A-87 – Saturn V, F-1, Engine Dimensions
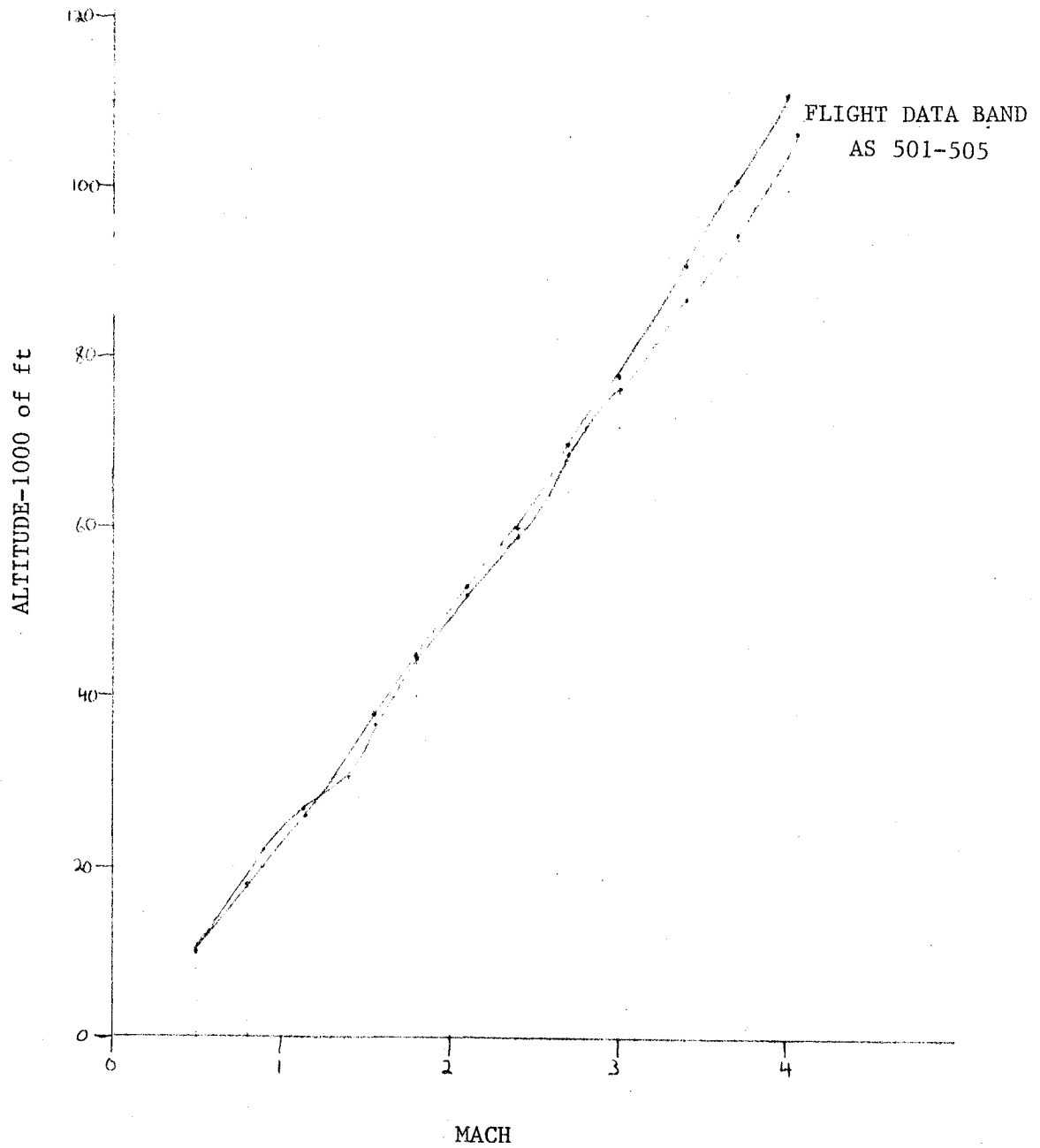
Fig. A-88 - Flight Altitude versus Mach Number - Saturn V

LOCKHEED-HUNTSVILLE RESEARCH & ENGINEERING CENTER

Fig. A-89 - Flight Dynamic Pressure versus Mach Number - Saturn V

LOCKHEED-HUNTSVILLE RESEARCH & ENGINEERING CENTER
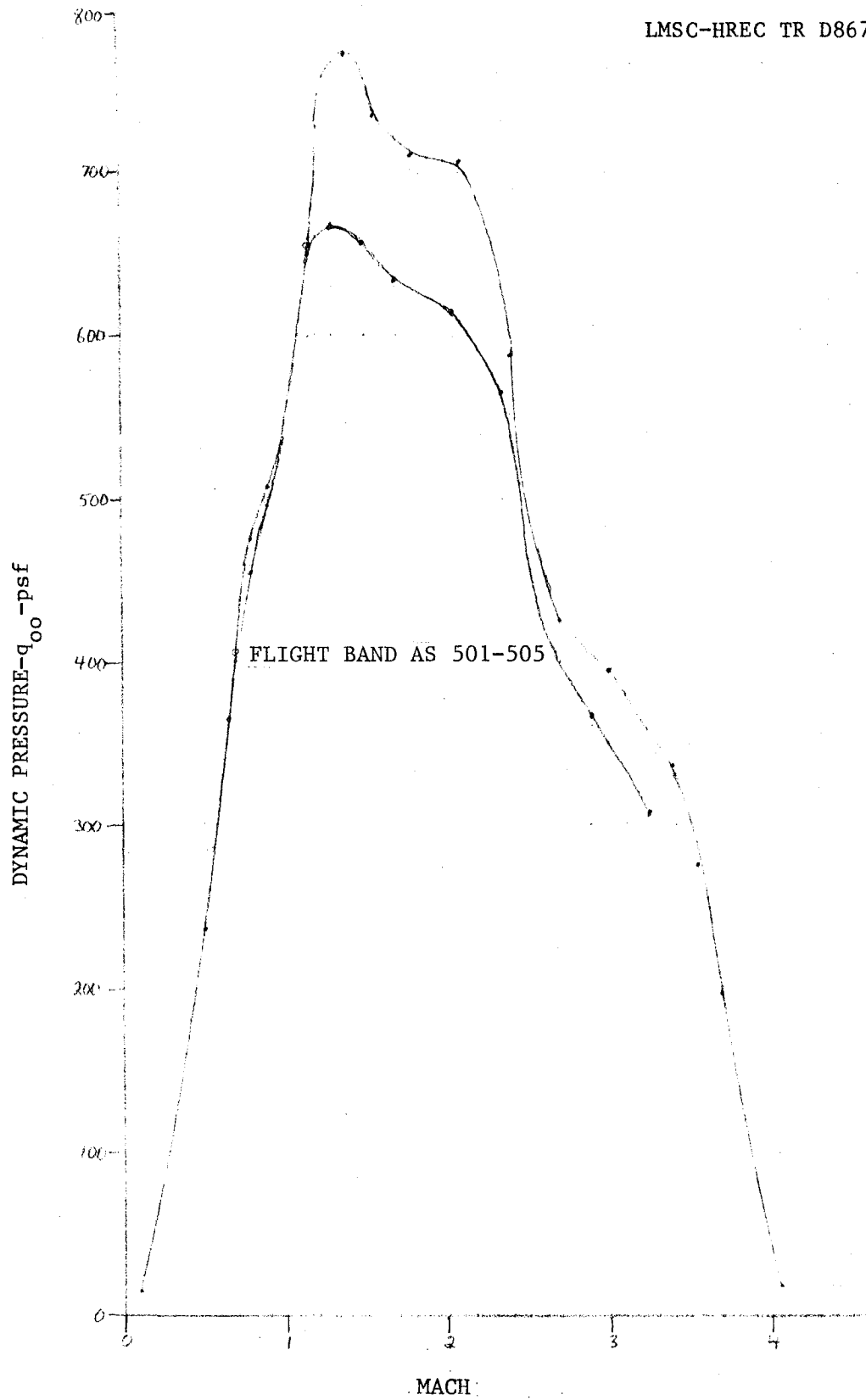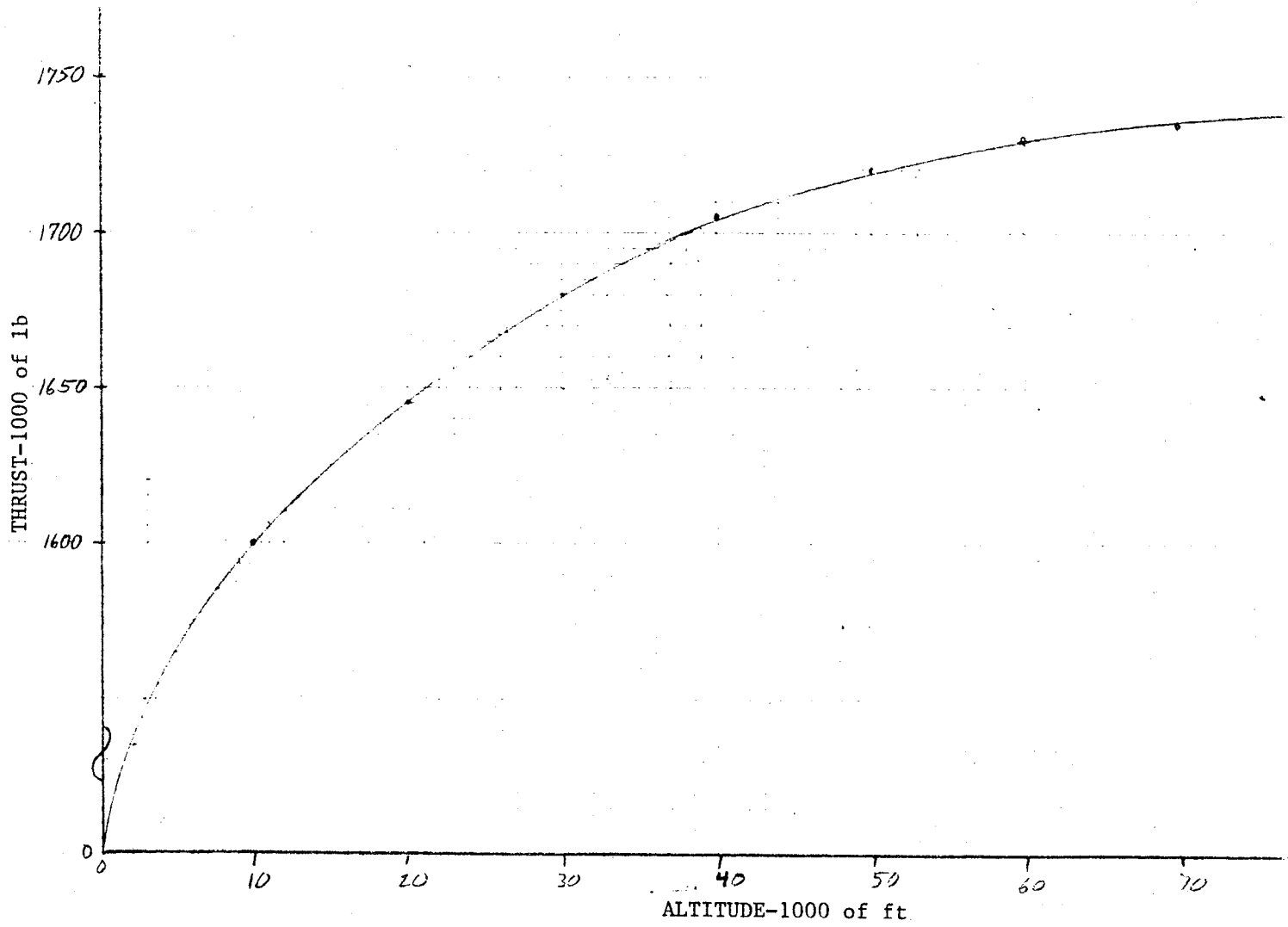
Fig. A-90 – Thrust versus Altitude – Saturn V
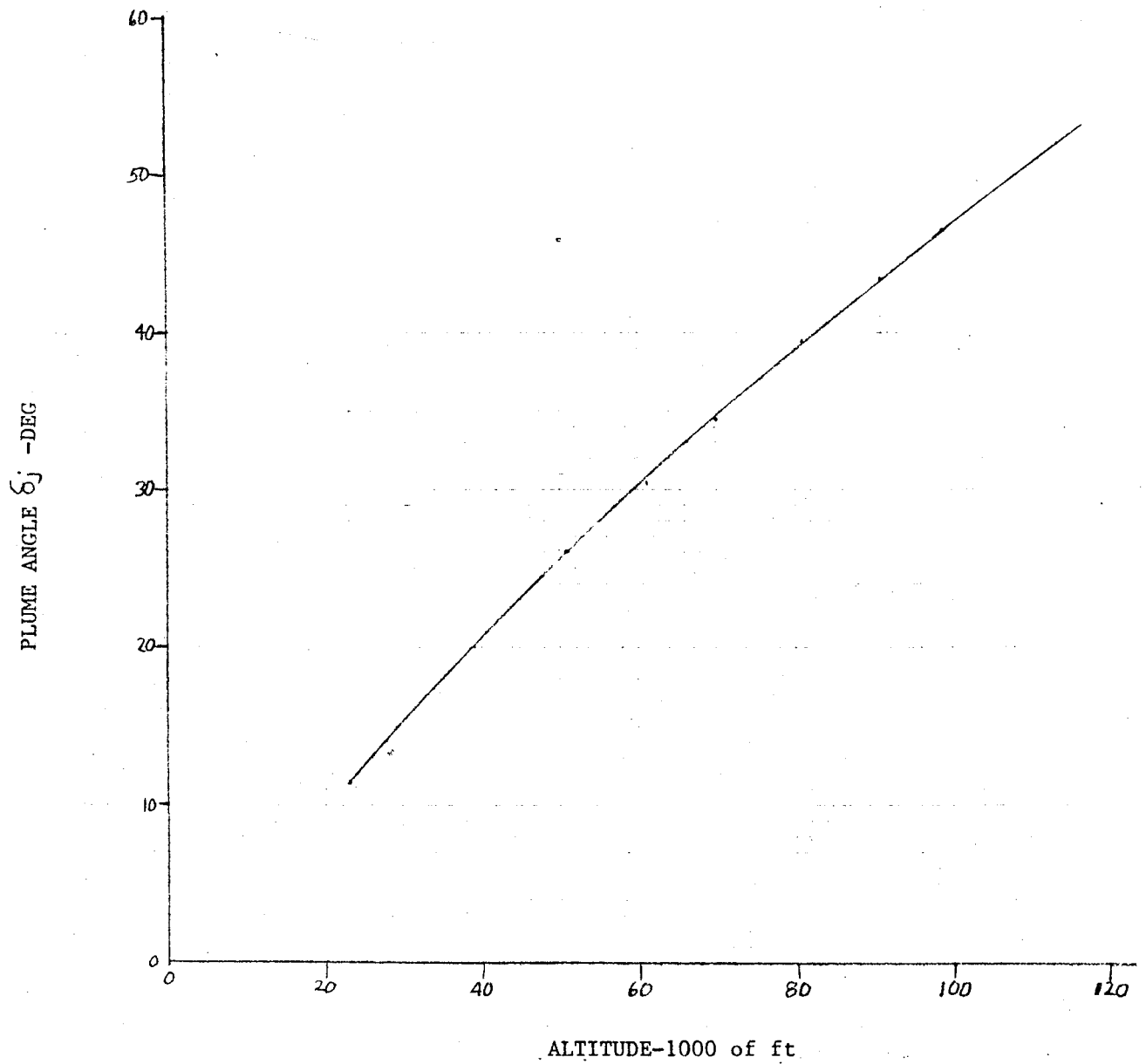
Fig. A-91 – Plume Angle versus Altitude: Saturn V

Table A-38   SATURN V AS 501

Mach	Alt ft	P_{oo} Psf	q_{oo} psf	Thrust 1b	AB=855 ft^2 C_T
.05	1312	2119.3	3.71	7625000	2403.81
.10	2625	2108.8	14.76	7720000	611.74
.12	3609	2046.2	20.63	7775000	440.79
.18	4922	2004.4	45.46	7825000	201.32
.22	5906	1920.9	65.08	7870000	141.44
.25	6562	1816.5	79.47	7890000	116.12
.35	7874	1691.2	145.02	7935000	63.99
.40	9187	1545.1	173.05	7975000	53.90
.50	10499	1357.2	237.51	8025000	39.52
.65	12795	1231.9	364.33	8050000	25.84
.80	18373	1064.8	477.03	8190000	20.08
.90	22967	897.8	509.05	8265000	18.99
1.15	26576	709.9	657.19	8340000	14.84
1.40	31169	563.7	773.40	8400000	12.70
1.55	38059	438.4	737.28	8500000	13.48
1.80	45277	313.2	710.34	8560000	14.09
2.10	53152	229.6	708.78	8610000	14.21
2.40	60042	146.1	589.08	8650000	17.17
2.70	70213	83.5	426.10	8680000	23.83
3.00	78087	62.6	394.38	8690000	25.77
3.40	91868	41.7	337.44	8710000	30.19
3.70	101054	20.8	199.33	8715000	51.36
4.00	111225	10.4	116.48	8715000	87.51

Table A-39 SATURN V AS 501 BASE PRESSURE DATA

	D0035		D0042	
Mach	C_{PB}	P_B/P_{oo}	C_{PB}	P_B/P_{oo}
.05	− .600	.997	−1.400	.993
.10	− .600	.994	−1.200	.988
.12	− .533	.992	− .933	.986
.18	− .550	.987	− .900	.981
.22	− .500	.984	− .700	.977
.25	− .340	.980	− .440	.975
.35	− .300	.974	− .400	.965
.40	− .227	.966	− .272	.960
.50	− .180	.958	− .206	.952
.65	− .130	.956	− .200	.932
.80	− .191	.910	− .175	.918
.90	− .159	.900	− .152	.905
1.15	− .124	.889	− .104	.907
1.40	− .049	.941	.009	1.010
1.55	.035	1.056	.064	1.103
1.80	.071	1.158	.101	1.225
2.10	.081	1.235	.128	1.372
2.40	.100	1.385	.159	1.613
2.70	.120	1.645	.144	1.774
3.00	.123	1.697	.176	1.997
3.40	.074	1.500	.140	1.946
3.70	.030	1.301	.080	1.802
4.00	− .042	.530	.057	1.800

Table A-40   SATURN V AS 502

Mach	Alt ft	P_{oo} Psf	q_{oo} psf	Thrust lb	$AB=855$ ft^2 C_T
.05	1312	2119.3	3.71	7625000	2403.81
.10	2625	2108.8	14.76	7720000	611.74
.12	3609	2046.2	20.63	7775000	440.79
.18	4922	2004.4	45.46	7825000	201.32
.22	5906	1920.9	65.08	7870000	141.44
.28	6562	1816.5	79.47	7890000	116.12
.35	7874	1691.2	145.02	7935000	63.99
.40	9187	1545.1	173.05	7975000	53.90
.50	10499	1357.2	237.51	8025000	39.52
.65	12795	1231.9	364.33	8050000	25.84
.80	18373	1064.8	477.03	8190000	20.08
.90	22967	897.8	509.05	8265000	18.99
1.15	26248	699.4	647.47	8340000	15.07
1.40	30841	563.7	773.40	8400000	12.70
1.55	37731	438.4	737.28	8485000	13.46
1.80	44949	313.2	710.34	8550000	14.07
2.10	52496	229.6	708.78	8610000	14.21
2.40	59058	146.1	589.08	8645000	17.16
2.70	69229	83.5	426.10	8675000	23.81
3.00	76775	62.6	394.38	8685000	25.76
3.40	87930	41.7	337.44	8700000	30.15
3.70	94492	20.8	199.33	8710000	51.11
4.05	106960	10.4	119.41	8715000	85.36

Table A-41   SATURN V AS 502 BASE PRESSURE DATA

	D0035		D0042	
Mach	C_{PB}	P_B/P_{oo}	C_{PB}	P_B/P_{oo}
.05	−2.000	.990	−1.200	.994
.10	−1.400	.986	−1.100	.989
.12	−1.132	.983	− .933	.986
.18	−1.050	.978	− .900	.981
.22	− .733	.976	− .667	.978
.28	− .460	.973	− .440	.974
.35	− .372	.967	− .400	.965
.40	− .245	.963	− .264	.960
.50	− .180	.958	− .206	.952
.65	− .135	.953	− .210	.928
.80	− .129	.937	− .191	.907
.90	− .115	.919	− .159	.888
1.15	− .097	.904	− .136	.866
1.40	− .002	.997	− .050	.933
1.55	.097	1.170	.010	1.107
1.80	.127	1.304	.050	1.119
2.10	.135	1.417	.073	1.225
2.40	.150	1.643	.093	1.398
2.70	.166	1.996	.116	1.696
3.00	.185	2.234	.130	1.867
3.40	.213	2.599	.146	2.096
3.70	.225	2.709	.150	1.806
4.05	.200	4.411	.129	3.200

Table A-42   SATURN V AS 503

Mach	Alt ft	P_{oo}Psf	q_{oo}psf	Thrust lb	AB=855 ft^2 C_T
.05	1312	2119.3	3.71	7625000	2403.81
.10	2625	2108.8	14.76	7720000	611.74
.12	3609	2046.2	20.63	7775000	440.79
.18	4922	2004.4	45.46	7825000	201.32
.22	5906	1920.9	65.08	7870000	141.44
.28	6562	1816.5	79.47	7890000	116.12
.35	7874	1691.2	145.02	7935000	63.99
.40	9187	1545.1	173.05	7975000	53.90
.50	10499	1357.2	237.51	8025000	39.52
.65	12795	1231.9	364.33	8050000	25.84
.80	18373	1064.8	477.03	8190000	20.08
.90	22967	897.8	509.05	8205000	18.99
1.15	26576	709.9	657.19	8340000	14.84
1.40	31169	563.7	773.40	8400000	12.70
1.55	38059	438.4	737.28	8500000	13.48
1.80	45277	313.2	710.34	8560000	14.09
2.10	53152	229.6	708.78	8610000	14.21
2.40	60042	146.1	589.08	8650000	17.17
2.70	70213	83.5	426.10	8680000	23.83
3.00	78087	62.6	394.38	8690000	25.77
3.40	91868	41.7	337.44	8710000	30.19
3.70	101054	20.8	199.33	8715000	51.36
4.05	111225	10.4	119.41	8715000	85.36

Table A-43   SATURN V AS 503 BASE PRESSURE DATA

	D0035		D0042	
Mach	C_{PB}	P_B/P_{oo}	C_{PB}	P_B/P_{oo}
.05	−.600	.997	−1.600	.992
.10	−.600	.994	−1.100	.989
.12	−.533	.992	− .933	.986
.18	−.600	.987	−1.000	.979
.22	−.467	.985	− .800	.973
.28	−.320	.981	− .520	.969
.35	−.300	.974	− .457	.960
.40	−.218	.967	− .318	.952
.50	−.193	.955	− .247	.943
.65	−.175	.940	− .195	.933
.80	−.183	.913	− .170	.919
.90	−.157	.895	− .139	.907
1.15	−.128	.878	− .093	.911
1.40	−.051	.934	− .020	.974
1.55	.081	1.142	.029	1.051
1.80	.092	1.226	.064	1.157
2.10	.108	1.333	.094	1.290
2.40	.124	1.513	.120	1.497
2.70	.147	1.845	.139	1.799
3.00	.166	1.996	.150	1.900
3.40	.128	1.897	.143	2.002
3.70	.114	2.200	.133	2.401
4.05	.009	1.135	.120	2.806

LOCKHEED-HUNTSVILLE RESEARCH & ENGINEERING CENTER

Table A-44   SATURN V AS 504

Mach	Alt ft	P_{oo}Psf	q_{oo}psf	Thrust lb	AB= $855ft^2$ C_T
.05	2297	2056.6	3.60	7675000	2493.50
.08	2953	2046.2	9.17	7750000	988.48
.12	3609	2004.4	20.20	7750000	448.73
.18	4265	1941.8	44.04	7800000	207.15
.24	5250	1837.4	74.08	7825000	123.54
.30	5906	1733.0	109.18	7875000	84.36
.35	7218	1607.7	137.86	7900000	67.02
.45	8531	1482.4	210.13	7950000	44.25
.55	10827	1336.3	282.96	8025000	33.17
.65	13780	1200.6	355.08	8075000	26.60
.75	17389	1033.5	406.94	8175000	23.50
.90	21654	897.8	509.05	8235000	18.92
1.05	26248	730.8	563.99	8335000	17.28
1.25	32810	584.6	639.41	8475000	15.50
1.45	38059	459.3	675.97	8500000	14.70
1.70	43309	334.0	675.68	8550000	14.80
1.95	50855	250.5	666.77	8600000	15.09
2.30	59058	156.6	579.89	8645000	17.44
2.55	67260	104.4	475.20	8675000	21.35
2.80	75134	62.6	343.55	8685000	29.57
3.15	84321	41.7	289.64	8700000	35.13
3.50	92524	31.3	268.39	8705000	37.93

Table A-45 SATURN V AS 504 BASDE PRESSURE DATA

Mach	D0035		D0037	
	C_{PB}	P_B/P_{oo}	C_{PB}	P_B/P_{oo}
.05	-.857	.994	-1.285	.994
.08	-.750	.991	-.833	.990
.12	-.667	.990	-.667	.990
.18	-.600	.987	-.550	.988
.24	-.467	.984	-.367	.987
.30	-.309	.980	-.218	.986
.35	-.237	.975	-.163	.983
.45	-.200	.969	-.145	.978
.55	-.193	.958	-.142	.969
.65	-.188	.944	-.153	.955
.75	-.180	.927	-.170	.931
.90	-.163	.907	-.130	.926
1.05	-.109	.914	-.047	.963
1.25	-.017	.982	.034	1.035
1.45	.043	1.058	.073	1.099
1.70	.084	1.154	.122	1.224
1.95	.095	1.241	.111	1.282
2.30	.110	1.410	.121	1.451
2.55	.108	1.518	.116	1.556
2.80	.110	1.733	.120	1.800
3.15	.133	1.998	.140	2.051
3.50	.108	1.864	.141	2.128

Table A-46 ' SATURN V AS 505

Mach	Alt ft	P_{oo} Psf	q_{oo} psf	Thrust lb	AB=855 ft^2 C_T
.04	1312	2119.3	2.37	7625000	3762.92
.08	2297	2056.6	9.21	7675000	974.66
.10	2953	2050.1	14.35	7750000	631.66
.15	3610	2046.2	32.23	7750000	281.24
.18	4265	1941.8	44.04	7800000	207.15
.25	5250	1837.4	80.39	7825000	113.85
.30	5906	1733.0	109.18	7875000	84.36
.35	7218	1607.7	137.86	7900000	67.02
.45	8531	1482.4	213.13	7950000	44.25
.55	11155	1346.7	285.16	8025000	32.91
.70	15420	1190.1	408.20	8125000	23.28
.80	19686	1012.6	453.64	8200000	21.14
.90	23623	876.9	497.20	8275000	19.47
1.15	27232	709.9	657.18	8350000	14.86
1.30	33466	563.7	666.86	8440000	14.80
1.50	39372	417.6	657.72	8510000	15.13
1.70	46262	313.2	633.60	8575000	15.83
2.05	52824	208.8	614.24	8615000	16.40
2.35	61354	146.1	564.79	8650000	17.91
2.65	69885	83.5	410.47	8675000	24.72
2.90	76775	62.6	368.53	8690000	27.58
3.25	87930	41.7	308.32	8700000	33.00
3.55	96461	31.3	276.12	8710000	36.89

Table A-47   SATURN V AS 505

Mach	D0035		D0037	
	C_{PB}	P_B/P_{oo}	C_{PB}	P_B/P_{oo}
.04	-2.600	.987	-2.200	.989
.08	-1.750	.986	-1.626	.987
.10	-1.250	.985	-1.250	.985
.15	-1.066	.983	-1.133	.982
.18	- .566	.982	- .600	.981
.25	- .450	.980	- .500	.977
.30	- .333	.976	- .367	.974
.35	- .275	.972	- .300	.969
.45	- .217	.966	- .226	.964
.55	- .193	.955	- .200	.953
.70	- .173	.944	- .183	.941
.80	- .133	.938	- .155	.928
.90	- .105	.936	- .121	.927
1.15	- .064	.944	- .061	.947
1.30	.036	1.043	.009	1.010
1.50	.084	1.138	.051	1.084
1.70	.109	1.238	.079	1.172
2.05	.139	1.437	.098	1.308
2.35	.152	1.597	.112	1.440
2.65	.153	1.898	.110	1.646
2.90	.167	2.030	.124	1.764
3.25	.166	2.246	.126	1.946
3.55	.173	2.326	.069	1.529

THOR DELTA

THOR DELTA - SOLID MOTOR STRAP ON CONFIGURATION

The Thor Delta configuration is an extension of the original Thor project but using solid rocket boosters to augment the thrust of the initial 1st stage vehicle.

The vehicle configuration is similar to the Thor except for the three strap-on Castor I solid rocket motors. The Castor I motors were used to augment the original Rocketdyne LR79-NA-11 main engine. The main engine developed a thrust of 170,000 lb at sea level and burned for approximately 146 sec. The Castor I motors were fired simulataneously with the core vehicle engine and burned for approximately 42 sec developing 63,500 lb of thrust at sea level. The Castor I motorcases were jettisoned after approximately 90 sec of flight.

The Thor Delta configuration with three strap-on solid motors is presented in Fig. A-92. Ascent trajectory data are presented in Figs. A-93 and A-94. The solid rocket motor thrust versus time curve is presented in Fig. A-95. The flight base pressure source data from Reference 1 is presented in Fig. A-96. Ascent flight trajectory data, thrust data and base pressure characteristics are presented in Tables A-48 and A-49.

THOR DELTA REFERENCES

1. Jackson, R.H., "Base Region Environmental Results Obtained from Three Thor Boosters," REport No. SM-46507, Douglas Missile & Space Division, June 1965.

2. "Solid Motor, Main Engine, and Vernier Engine Exhaust Plume Contours for the Six-Solid Retrofit Boosters," Memorandum A2-260-AAA5-D9442, McDonnell Douglas Aircraft Corp., 8 September 1969.

3. Greenwald, G.F., "Base Thermal Environment of Delta Vehicle with Six Strap-On Motors," McDonnell Douglas Aircraft Corp., California.
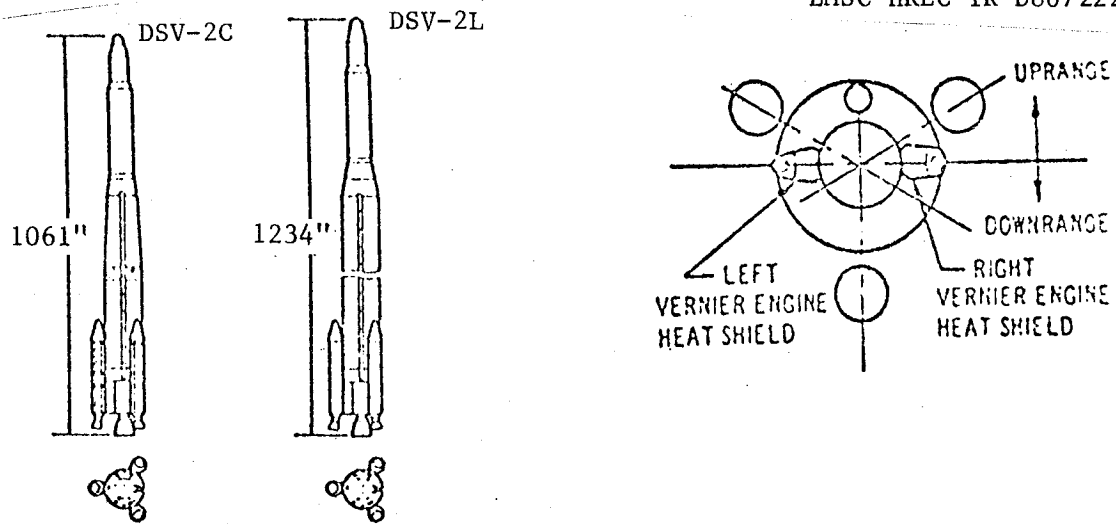
ENGINE PARAMETERS

ENGINE	MAIN ENG.	VERNIER ENGINE	CASTOR I
Fuel	RJ-1	RJ-1	TP-H8038
Oxidizer	LOX	LOX	--
Fuel/Oxidizer Ratio (By Weight)	2.269	1.81	--
Chamber Pressure (psia)	595	364	515 at 5 sec. 515 at Max Thrust
Chamber Temp (°R)	5840	5500	5860
Expansion Ratio	8.00	5.60	5.90
Exit Diameter (in.)	45.6	3.61	23.750
Nozzle Exit Half Angle (deg)	4.72	13.00	15.0
Nozzle Cant Angle (deg)	--	--	11.0
Maximum Thrust (lb$_f$)	--	--	63,500

THRUST CHARACTERISTICS: PERCENT MAX THRUST
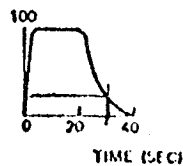
Fig. A-92 - Vehicle Configuration - THOR Delta
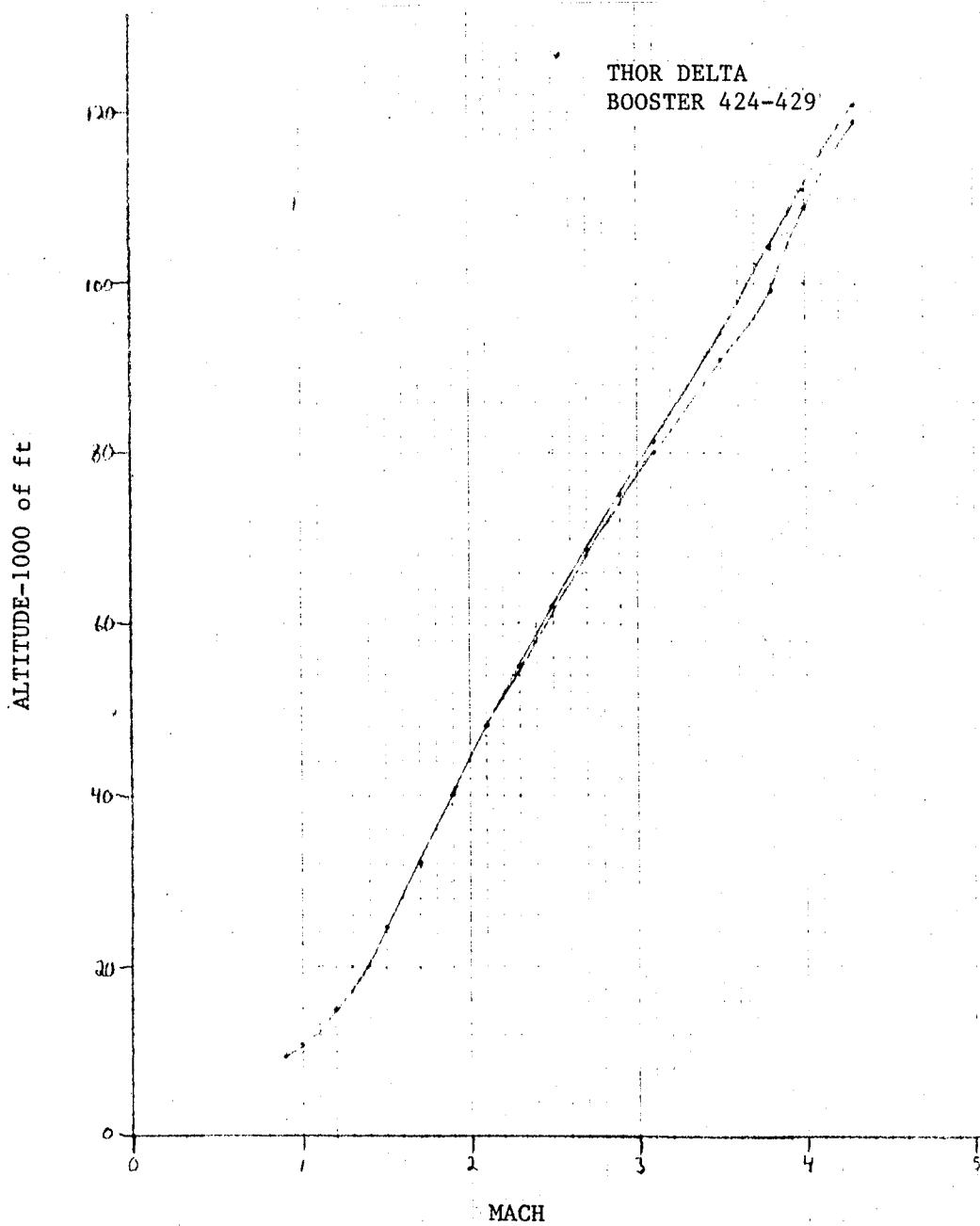
Fig. A-93 – Flight Altitude versus Mach Number – THOR Delta

LOCKHEED-HUNTSVILLE RESEARCH & ENGINEERING CENTER

Fig. A-94 — Flight Dynamic Pressure versus Mach Number — THOR Delta

DYNAMIC PRESSURE-q_{oo}-psf

MACH

THOR DELTA
BOOSTER 424-429

LOCKHEED-HUNTSVILLE RESEARCH & ENGINEERING CENTER

LMSC-HREC TR D867222
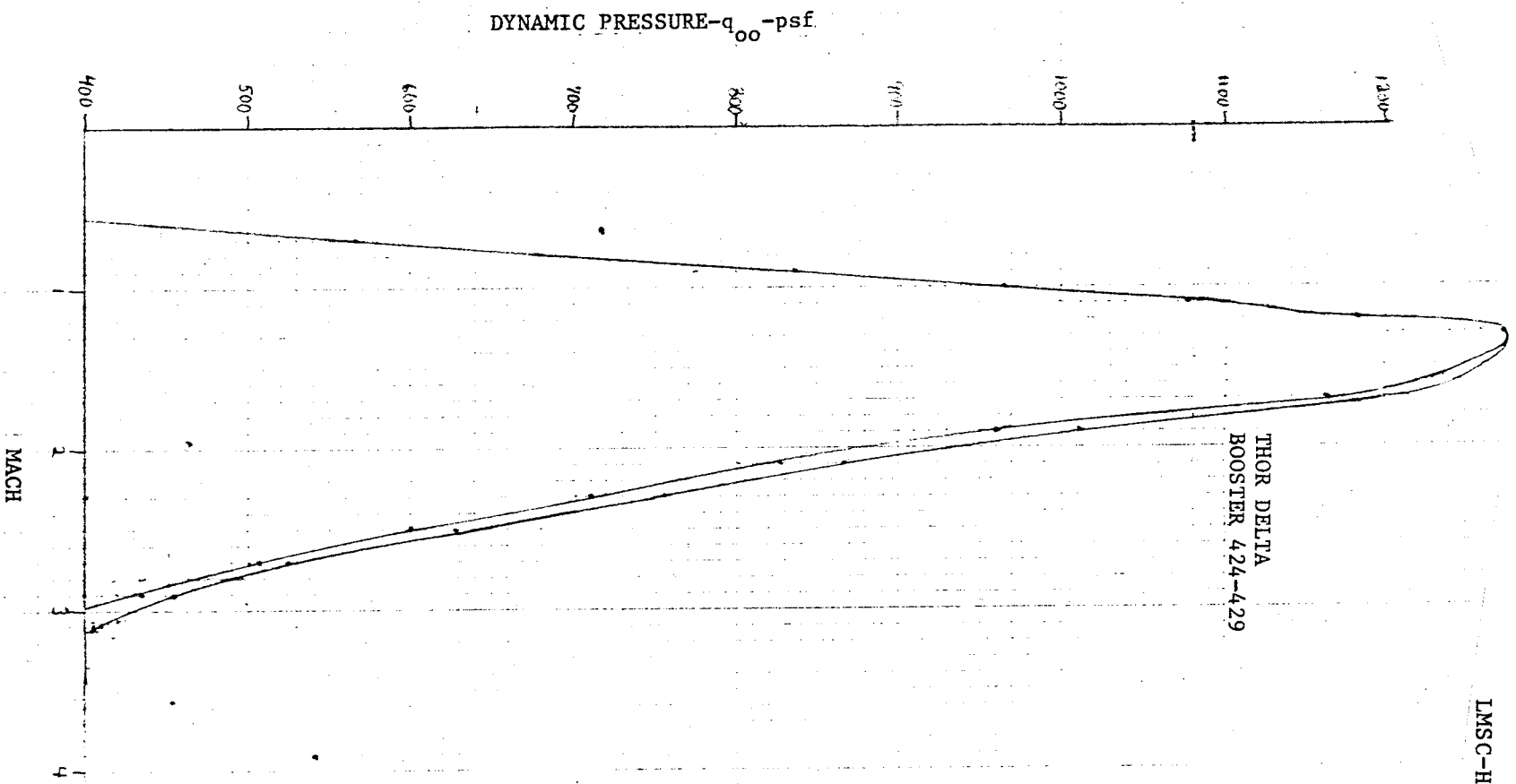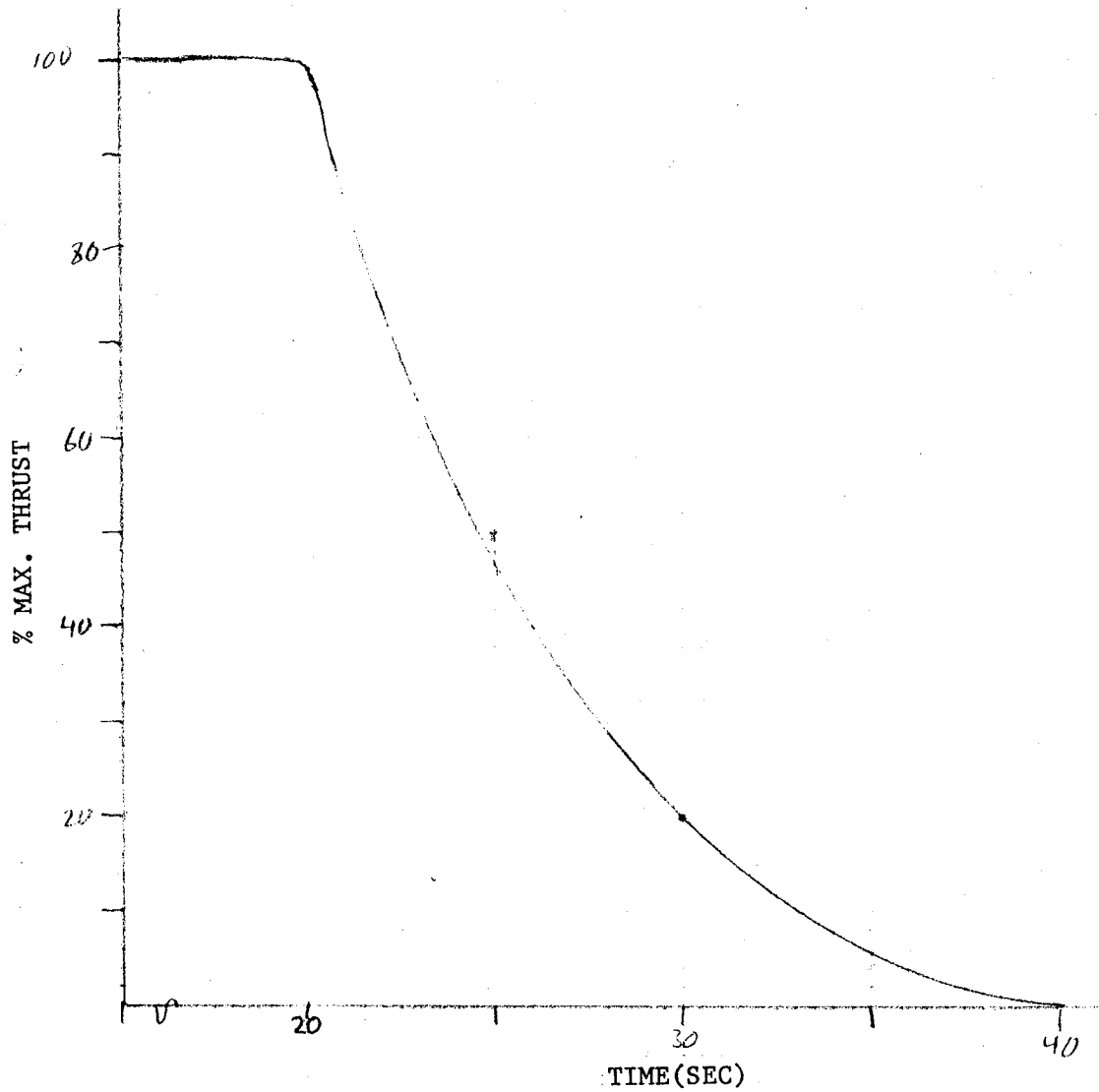
Fig. A-95 - Thrust versus Time - THOR Delta

LOCKHEED-HUNTSVILLE RESEARCH & ENGINEERING CENTER
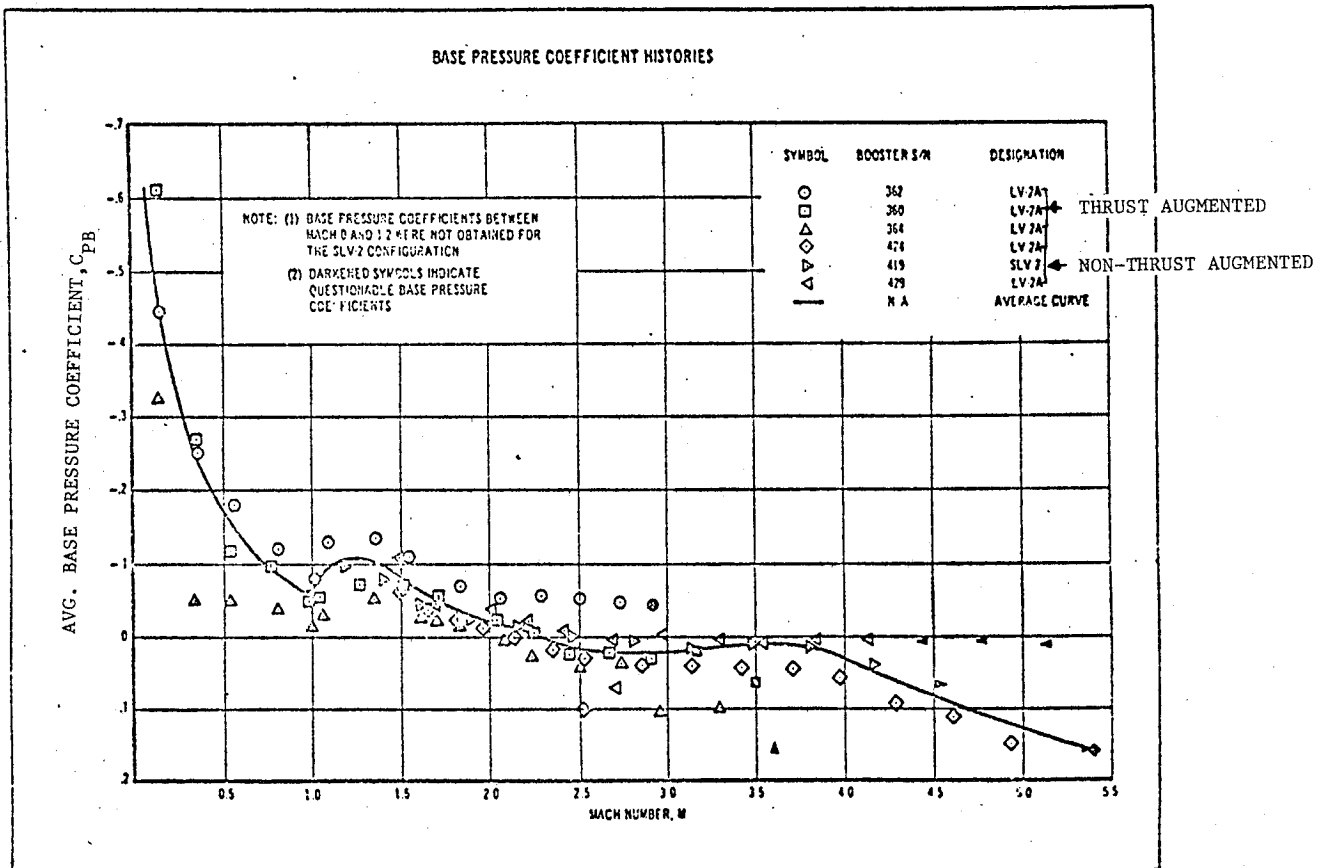
Fig. A-96 - THOR Delta Base Pressure Source Data

LOCKHEED-HUNTSVILLE RESEARCH & ENGINEERING CENTER

Table A-48   THOR DELTA BOOSTER 424

Mach	Alt ft	P_{oo}psf	q_{oo}psf	Thrust lb Core	Thrust lb SRB'S	AB=50.27 ft^2 CT	C_{Pb}	P_b/P_{oo}
.20	1200	2000.00	56.00	170000	190500	128.06	-.300	.992
.50	3800	1840.19	322.03	173000	190500	22.45	-.130	.977
.70	6500	1660.80	569.65	174000	190500	12.73	-.080	.973
.90	9500	1480.07	839.20	177000	190500	8.71	-.050	.969
1.00	11200	1380.00	966.00	178000	85725	5.43	-.050	.965
1.10	13200	1274.41	1079.43	180000	57150	4.37	-.060	.949
1.20	15200	1174.30	1183.69	183000	28575	3.56	-.078	.921
1.30	17500	1080.00	1277.64	185000	15240	3.12	-.085	.899
1.50	24500	801.05	1261.65	187000	3810	3.01	-.060	.906
1.70	32000	574.58	1162.38	189000	-0-	3.23	-.035	.929
1.90	40500	380.00	960.26	189600	-0-	3.93	-.020	.940
2.10	48000	268.05	827.47	190900	-0-	4.59	-0-	1.000
2.30	55000	191.80	710.24	191500	-0-	5.36	.015	1.056
2.50	62000	137.26	600.51	192600	-0-	6.38	.030	1.131
2.70	68800	99.90	509.79	192900	-0-	7.53	.040	1.204
2.90	75000	73.99	435.58	193200	-0-	8.82	.040	1.235
3.10	81500	54.00	363.26	193500	-0-	10.60	.038	1.256
3.50	93500	31.00	265.83	194000	-0-	14.52	.040	1.343
3.80	104700	18.90	191.04	194200	-0-	20.22	.050	1.505
4.00	111500	13.70	153.44	194600	-0-	25.23	.060	1.672
4.30	121000	9.20	119.08	194900	-0-	32.56	.090	2.165
4.50	127200	6.95	98.52	195000	-0-	39.37	.105	2.488
5.00	141900	3.90	68.25	195000	-0-	56.84	.160	3.800

Table A-49   THOR DELTA BOOSTER 429

Mach	Alt ft	P_{oo} psf	q_{oo} psf	Thrust lb Core	Thrust lb SRB'S	AB=50.27 ft^2 Ct	C_{Pb}	P_b/P_{oo}
.20	1200	2000.00	56.00	170000	190500	128.06	-.500	.986
.50	3800	1840.19	322.03	173000	190500	22.45	-.200	.965
.70	6500	1660.80	569.65	174000	190500	12.73	-.130	.955
.90	9500	1480.07	839.20	177000	190500	8.71	-.099	.944
1.00	11200	1380.00	966.00	178000	85725	5.43	-.099	.931
1.10	13200	1274.41	1079.43	180000	57150	4.37	-.110	.907
1.20	15200	1174.30	1183.69	183000	28575	3.56	-.118	.881
1.30	17500	1080.00	1277.64	185000	15240	3.12	-.120	.858
1.50	24500	801.05	1261.65	187000	3810	3.01	-.100	.843
1.70	31200	600.00	1213.80	189000	-0-	3.10	-.074	.850
1.90	39500	400.00	1010.80	189600	-0-	3.73	-.050	.874
2.10	47000	281.20	868.06	190900	-0-	4.37	-.035	.892
2.30	54000	201.19	745.01	191500	-0-	5.11	-.020	.926
2.50	61000	143.98	629.91	192600	-0-	6.08	-.008	.965
2.70	68000	103.07	525.97	192900	-0-	7.30	-0-	1.000
2.90	74000	77.56	456.60	193200	-0-	8.42	-.004	.976
10	80000	58.51	393.60	193500	-0-	9.78	-.004	.973
50	91200	34.90	299.27	194000	-0-	12.90	.005	1.043
3.80	99000	24.35	246.13	194200	-0-	15.70	.001	1.010
4.00	109000	15.51	173.71	194600	-0-	22.28	.001	1.011
4.30	119000	10.02	129.69	194900	-0-	29.89	.001	1.013
4.50	125000	7.77	110.14	195000	-0-	35.22	.001	1.014
5.00	139300	4.30	75.25	195000	-0-	51.55	.001	1.018

LOCKHEED-HUNTSVILLE RESEARCH & ENGINEERING CENTER

SPACE SHUTTLE - ORBITER

SPACE SHUTTLE - ORBITER

The Space Shuttle vehicle consists of an Orbiter with Space Shuttle Main Engine (SSME), an External Tank (ET), and two solid rocket boosters (SRB). The Orbiter with SSMEs and the SRBs are reusable elements while the ET is expended after each launch. The three SSMEs produce a total sea level thrust of 1.125 million lb. They are fueled with LOX and liquid hydrogen stored in the external tank. The engines are bearing mounted and capable of gimbaling for Orbite steering control. The External Tank reacts the SRB thrust through its intertank structure and provides attach structure to the Orbiter to react the SSME thrust. At liftoff the ET contains approximately 1.5 million lb of fuel. At main engine cutoff, the ET is separated from the Orbiter before orbital velocity is achieved. The ET then proceeds on a ballistic reentry path and breaks up prior to impact in the ocean. Each SRB produces approximately 2.65 million lb of thrust at sea level, and after about 55 sec they reduce thrust about one-third to prevent overstressing the vehicle during the period of maximum dynamic pressure. Two lateral sway braces and a diagonal attachment at the aft frame provide the structural attachment between the SRB and ET. The SRB forward attachment to the ET is by a single thrust attachment at the forward end of the forward skirt. The same forward skirt is used for attaching the main parachute riser attach-ments. The SRBs are released from the ET by pyrotechnic separation devices at the forward thrust attachment and aft sway braces. Eight separation motors on each SRB, four aft and four forward, separate the SRB from the Orbiter and ET.

The Space Shuttle Orbiter configuration and SSME engine characteristics are presented in Figs. A-97 through A-104. Ascent trajectory data are presented in Figs. A-105 and A-106. The SSME thrust versus altitude and plume angles are presented in Figs. A-107 and A-108, respectively. Ascent trajectory data, thrust data and base pressure characteristics are presented in Tables A-50 through A-59.

SPACE SHUTTLE REFERENCES

1. "Space Shuttle System Summary," Report SSV80-1, Rockwell International Space Systems Group, May 1980.

2. "STS-5 Postflight Report on Ascent External Aerodynamic Loads," Report SAS/AERO/83-094, Rockwell International, 1 March 1983.

LOCKHEED-HUNTSVILLE RESEARCH & ENGINEERING CENTER

$X_T = 325.15$

X_0 1702.066

NRP
$X_T = 976.0$
$Y_T = 0$
$Z_T = 400$

1467.066

X_0 235

650.85

Z_0 400

336.5

Z_T 400

Z_3 0

415.85

X_B 200

1789.60

X_B 1989.60

1847.875

250.5

X_T 2173.025
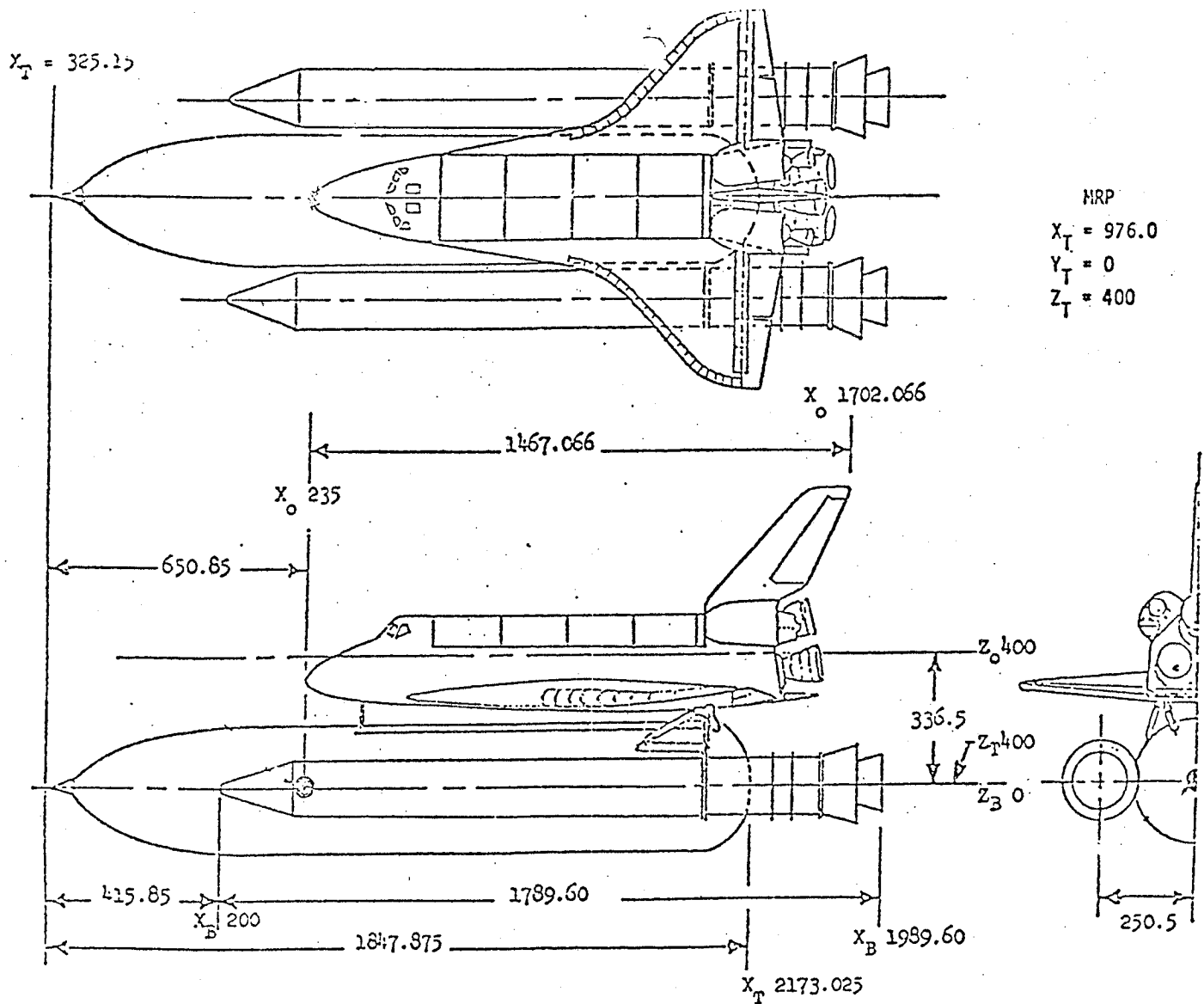
Fig. A-97 - Space Shuttle Launch Vehicle and Elements

AFT FUSELAGE
- ALUMINUM SKIN/STR SHELL (2124-T851)
- TITANIUM/BORON THRUST STRUCTURE

OMS POD
- GRAPHITE/EPOXY SKIN PANELS

VERTICAL TAIL
- ALUMINUM MACHINED SKINS 2124-T851
- ALUMINUM HONEYCOMB 2124-T81 RUDDER COVERS 2024-T81

MID FUSELAGE
- ALUMINUM SKIN/STR (2124-T851)
- ALUMINUM HONEYCOMB PANELS (2124)
- MISC - 2024-T6

X_O 1307

X_O 1528

RSI

X_O 576

X_O 236

FORWARD FUSELAGE (2024-T81) & CREW CABIN (2219-T851)
- ALUMINUM SKIN/STR

PAYLOAD BAY DOORS
- GRAPHITE/EPOXY HONEYCOMB PANELS
- GRAPHITE/EPOXY FRAME W/Ti FTG's
- INCONEL HINGES

WING
- ALUMINUM SKIN/STR & HONEYCOMB COVERS (2024-T81)
- ALUMINUM HONEYCOMB ELEVON COVERS 2024-T81
- ALUMINUM SPAR WEBS 2024-T62
- ALUMINUM RIB (TRUSS TUBES) 2024-T62

BODY FLAP
- ALUMINUM HONEYCOMB COVERS (2024)

- CONVENTIONAL ALUMINUM STRUCTURE
- MAXIMUM TEMPERATURE 350°F
- PROTECTED BY REUSABLE SURFACE INSULATION

Fig. A-98 - Orbiter Structure

A-176

GLOVE-WING
INTERSECTION
Y_o 188, X_o 1024

X_o 236 OUTER ML

GEOMETRY	WING	VERTICAL STAB.
AREA	2690 FT^2	413.25 FT^2
ASPECT RATIO	2.265	1.675
AIRFOIL Y_o 199	0010 MOD	WEDGE
SWEEP (LEADING EDGE)	45 DEG	45 DEG
(WING GLOVE)	81 DEG	
M.A.C.	474.81 IN.	199.81 IN.
DIHEDRAL (TRAILING EDGE)	3 DEG 30 MIN	

CONTROL SURFACE AREA & MAX DEFLECTION

AREA		MAX DEFLECTION
ELEVON (ONE SIDE)	206.57 FT^2	-35 TO +20 DEG
RUDDER	97.15 FT^2	±22.8 DEG
SPEED BRAKE	97.15 FT^2	0 TO 87.2 DEG (TOTAL)
BODY FLAP	135.75 FT^2	-11.7 TO +22.55 DEG

1458.245 IN.
121.52 FT

Z_o 400

556 IN.
46.33 FT

679 IN.
56.58 FT

FRP ———— Z_o 400

1292.3 IN.
107.69 FT
REF BODY LENGTH

X_o 236
(REF)

X_o 1528.3   STATIC GROUND
LINE

936.68 IN.
78.06 FT

Fig. A-99 – Orbiter Vehicle Dimensions
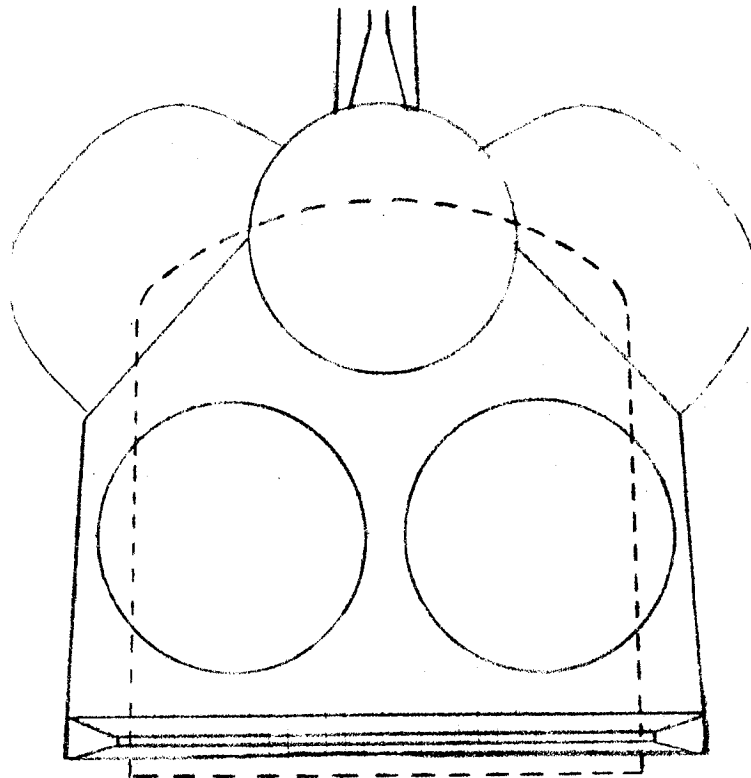
FUSELAGE AREA=295 ft^2

BASE AREA=436.66 ft^2

Fig. A-100 - Fuselage and Base Area - Orbiter

A-178

ENGINE
NUMBER

MAIN ENGINES (3);
470 KLB VACUUM THRUST;
375 KLB SEA-LEVEL THRUST

LH$_2$
PREVALVE

LH$_2$ FILL/DRAIN
DISCONNECT

ORBITER/ET
LO$_2$ DISC

ORBITER/ET
LH$_2$ DISC

LO$_2$ PREVALVE

12 IN. FEED

8 IN. LO$_2$
FILL & DRAIN

17 IN. FEED

ORBITER LOWER SURFACE

MAIN
ENGINES

8 IN. LH$_2$
FILL & DRAIN

LO$_2$

LH$_2$

EXTERNAL TANK
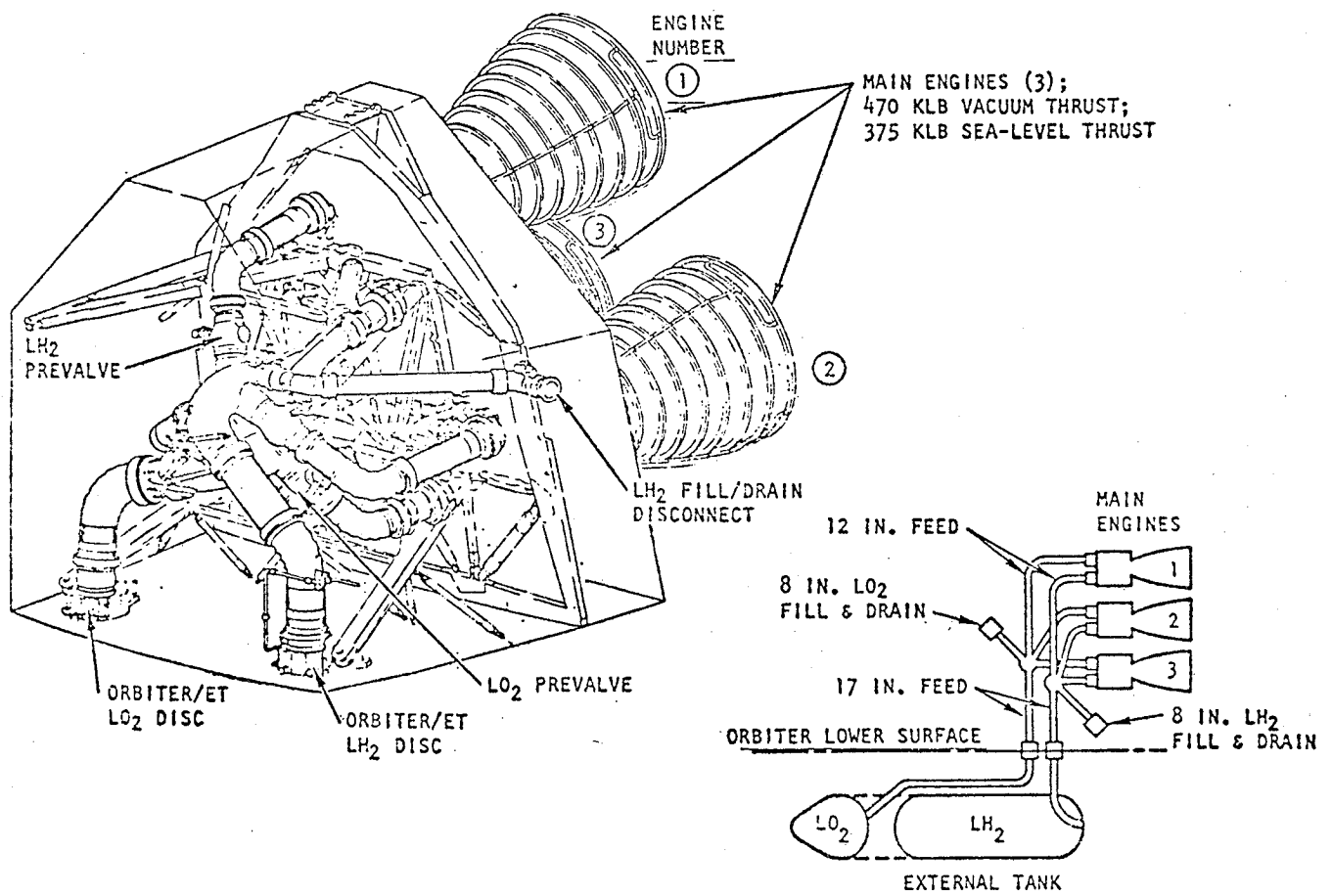
Fig. A-101 - Main Propulsion Subsystem - Orbiter
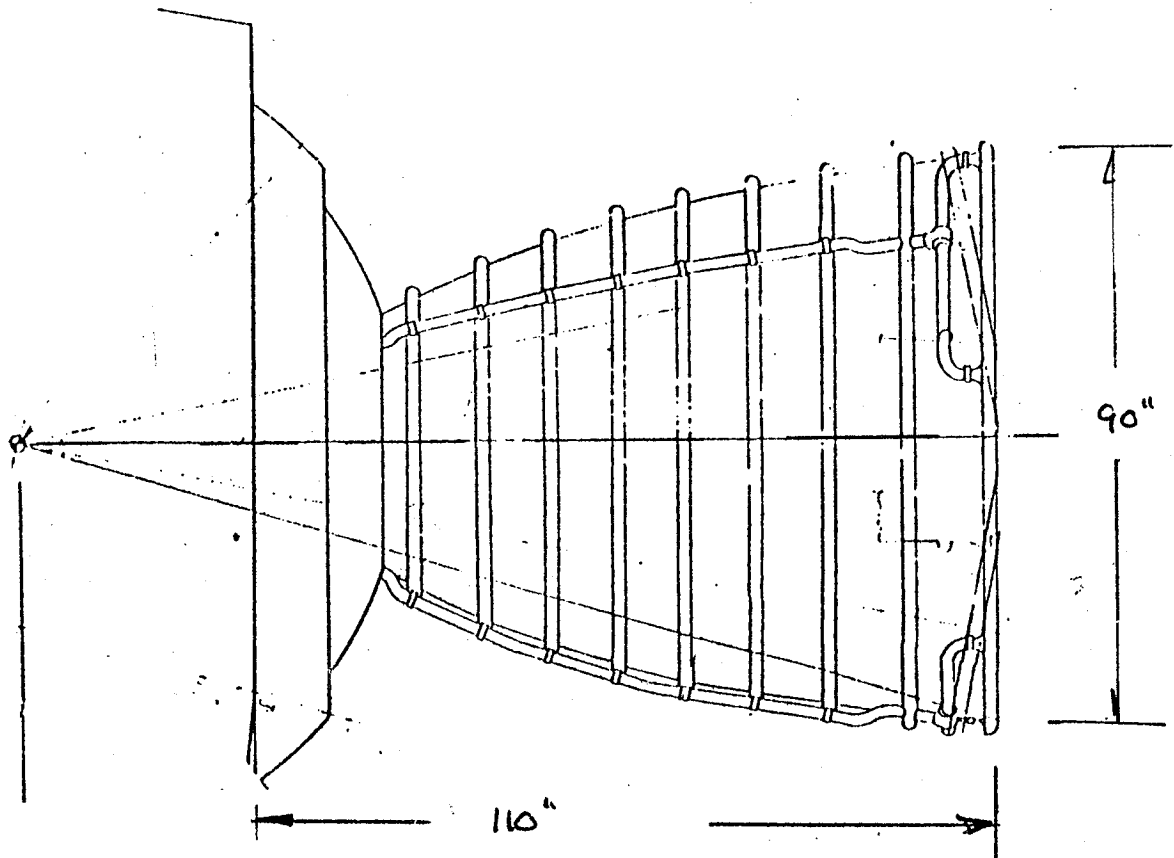
Fig. A-102 - Nozzle Dimensions - Orbiter

LOCKHEED-HUNTSVILLE RESEARCH & ENGINEERING CENTER
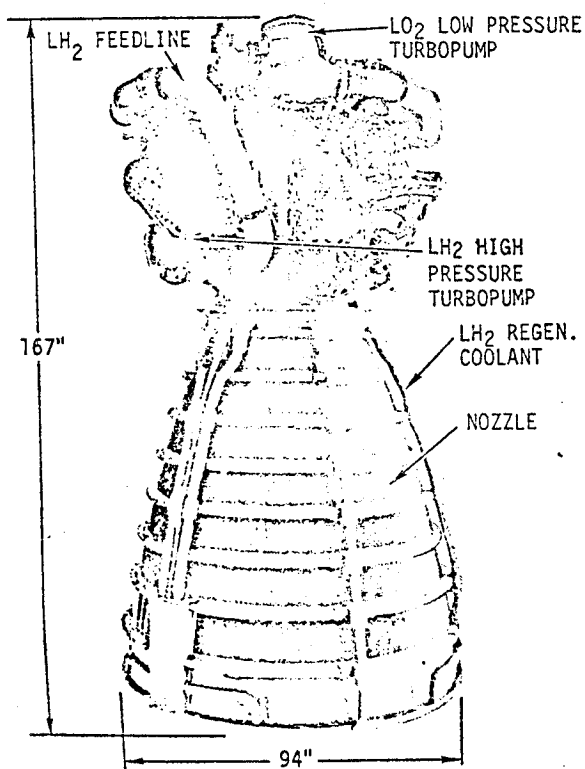
• THRUST (RATED POWER LEVEL)	
• SEA LEVEL	375,000 LBS
• VACUUM	470,000 LBS
• THROTTLING	65% - 109% RPL
• CHAMBER PRESSURE (RPL)	2970 PSIA
• AREA RATIO	77.5:1
• SPECIFIC IMPULSE (RPL)	
• SEA LEVEL	363.2
• VACUUM	455.2
• MIXTURE RATIO (OXYGEN/HYDROGEN)	6.0:1
• HI PRESS. LH2/LO2 PUMP TURBINE HP	62,000/24,000
• ENGINE FLOWRATE	1030 LBM/S
	19,600 GPM
• TOTAL ENGINE HORSEPOWER (RPL)	6,500,000 HP
• WEIGHT	6668 LBS
• LIFE	7.5 HRS/55 STARTS

Fig. A-103 - Space Shuttle Main Engines

$D_c = 232.6$ in.

$D_{B_{EQ.}} = 271.0$ in.

$A_B = 400$ FT^2

$A_N = 240$ FT^2

$\dfrac{A_N}{A_B} = .56$

$X_j = 110$ in.

$\dfrac{X_j}{D_B} = .39$

$\Theta_L = 5°$

$L_s = 155$ in.

$\dfrac{L_s}{D_c} = .494$

$\Theta_s = 9°$
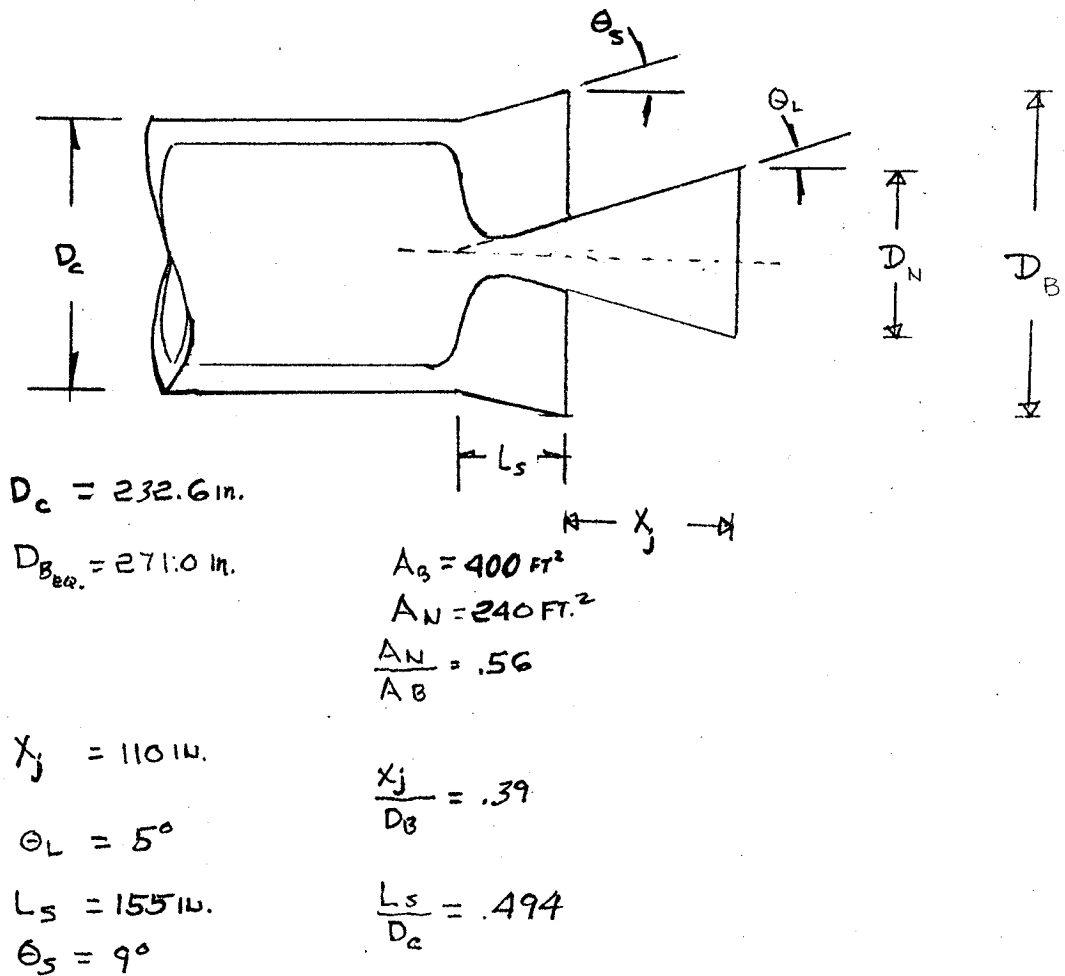
Fig. A-104 - Base Configuration - Orbiter

A-182
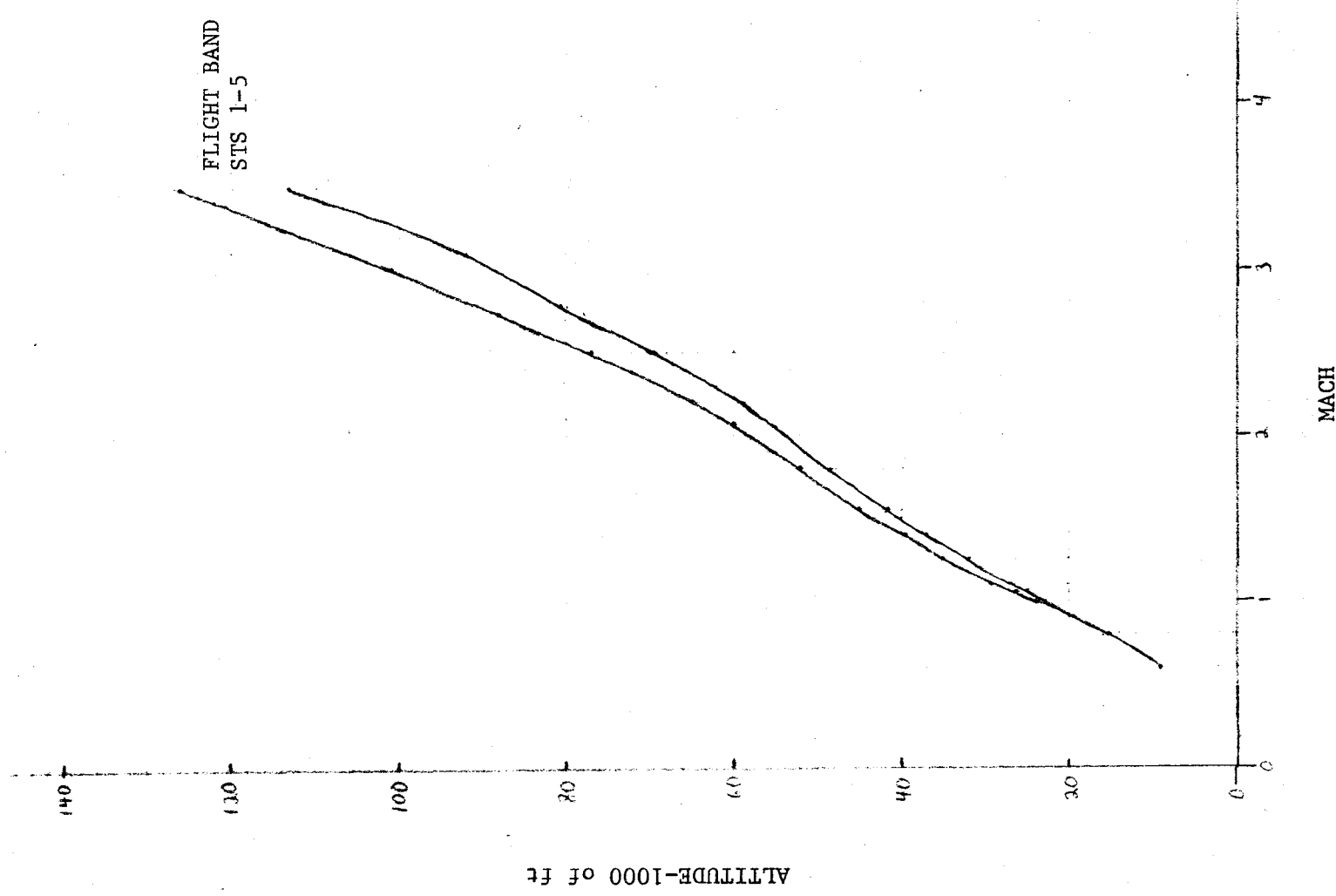
Fig. A-105 — Flight Altitude versus Mach Number — Orbiter

A-183
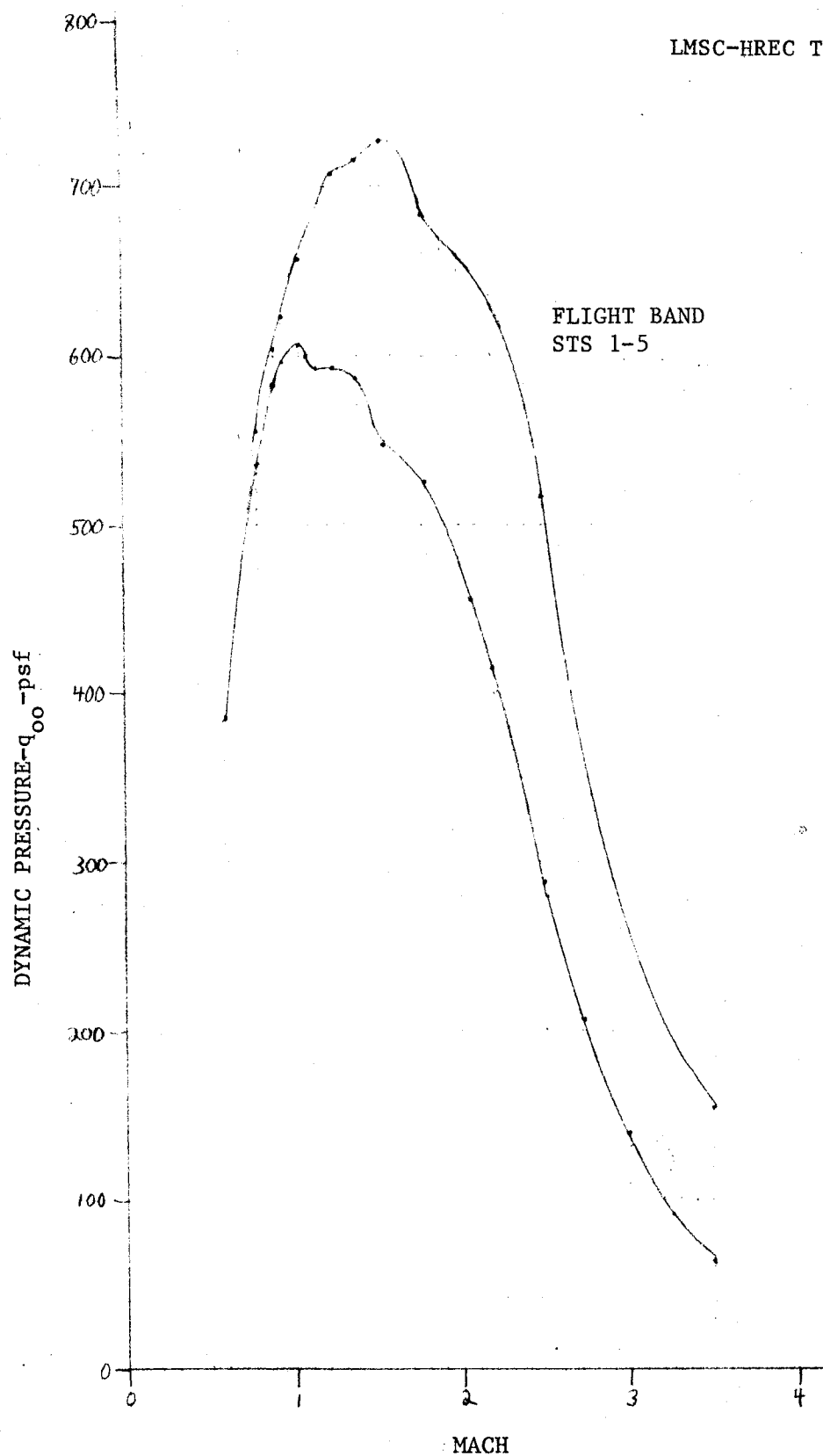
Fig. A-106 Flight Dynamic Pressure versus Mach Number - Orbiter

LOCKHEED-HUNTSVILLE RESEARCH & ENGINEERING CENTER
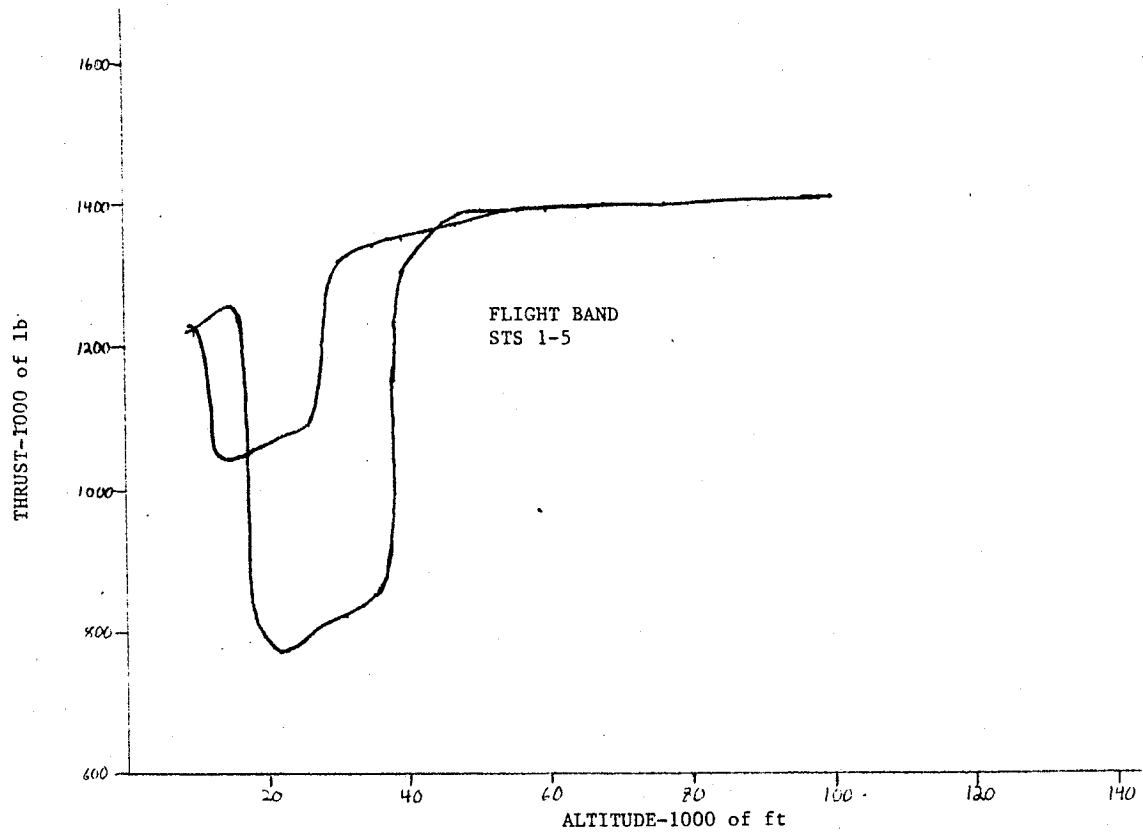
Fig. A-107 – Thrust versus Altitude: Space Shuttle Orbiter
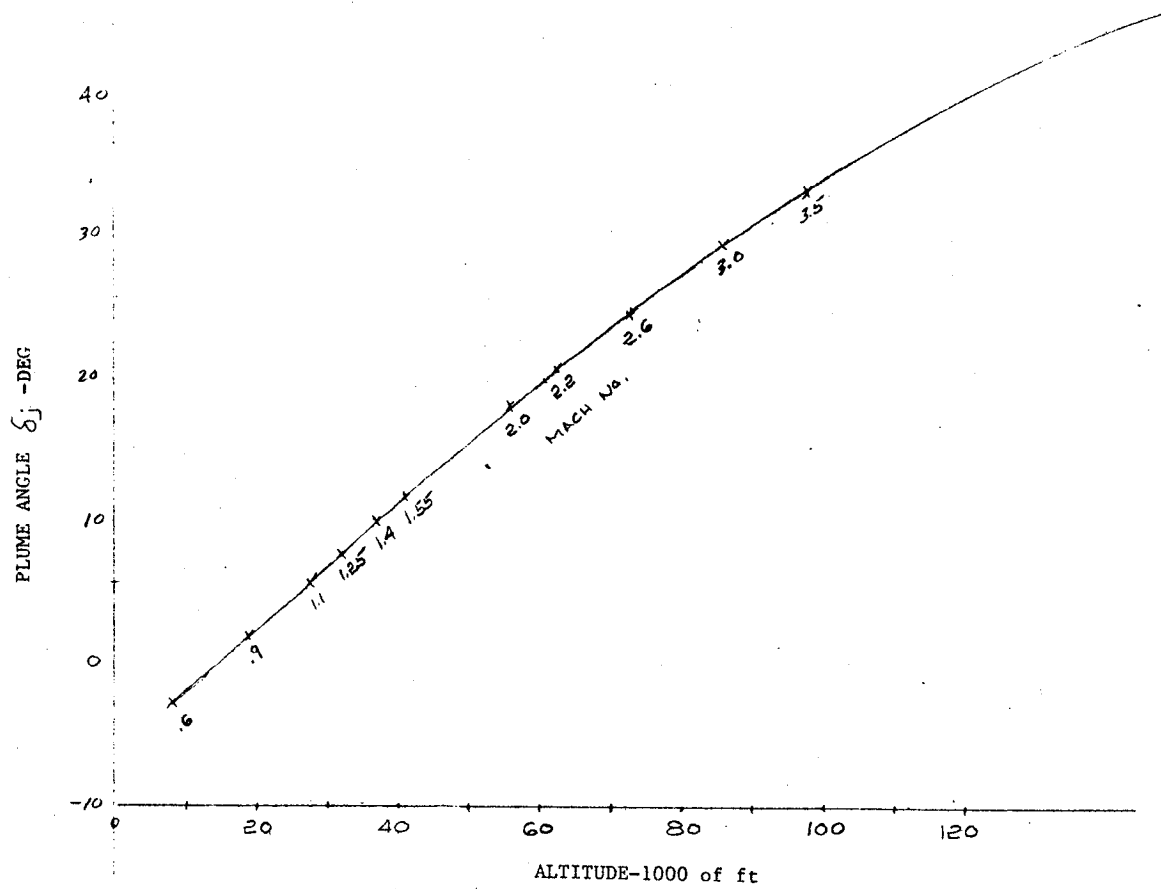
Fig. A-108 - Plume Angle versus Altitude - Orbiter

Table A-50   STS-1 ORBITER ELEMENT

Mach	ALT ft	P_{oo} Psf	q_{oo} psf	Orbiter Thrust lb	$A_B = 400$ ft^2 C_T (orb)
.60	9387	1527.84	385.02	1222000	7.93
.80	15879	1198.10	536.75	1258000	5.86
.90	19861	1026.72	582.15	798000	3.43
.95	21904	946.10	597.69	778000	3.25
1.05	26410	786.24	606.78	801000	3.30
1.10	28889	708.48	600.08	812000	3.38
1.15	31247	639.36	591.89	822000	3.47
1.25	35115	541.44	592.20	851000	3.59
1.40	39953	429.12	588.75	1309000	5.56
1.55	45512	326.88	549.73	1377000	6.26
1.80	52390	231.84	525.81	1382000	6.57
2.08	60000	151.03	457.39	1392000	7.61
2.20	64909	122.40	414.69	1395000	8.41
2.50	77556	66.24	289.80	1402000	12.09
2.72	88080	40.33	208.86	1407000	16.84
3.00	101000	22.25	140.18	1411000	25.16
3.25	114800	12.44	91.98	1411000	38.35
3.50	126037	7.45	63.88	1411000	55.22

LOCKHEED-HUNTSVILLE RESEARCH & ENGINEERING CENTER

Table A-51 – STS-1 ORBITER ELEMENT

Mach	C_{PB}	C_{PB}Max	C_{PB}Min	P_B/P_{oo}	P_B/P_{oo}Max	P_B/P_{oo}Min
.60	-.160	-.215	-.115	.959	.946	.971
.80	-.120	-.150	-.095	.946	.933	.957
.90	-.105	-.150	-.060	.940	.915	.966
.95	-.113	-.150	-.070	.929	.905	.956
1.05	-.135	-.165	-.105	.896	.873	.919
1.10	-.125	-.168	-.095	.894	.857	.920
1.15	-.100	-.120	-.080	.907	.889	.926
1.25	-.080	-.100	-.062	.913	.891	.932
1.40	-.045	-.080	-.030	.938	.890	.959
1.55	-.020	-.035	0	.966	.941	0
1.80	.025	.012	.040	1.060	1.030	1.090
2.08	.050	.020	.072	1.150	1.060	1.220
2.20	.060	.030	.080	1.200	1.100	1.270
2.50	.088	.055	.110	1.390	1.240	1.480
2.72	.100	.070	.122	1.520	1.360	1.630
3.00	.115	.090	.135	1.720	1.570	1.850
3.25	.122	.100	.145	1.900	1.740	2.070
3.50	.130	.105	.150	2.110	1.900	2.290

Table A-52   STS-2 ORBITER ELEMENT

Mach	Alt ft	P_{oo}psf	q_{oo} psf	Thrust	$A_B = 400$ ft^2 C_T
.60	8975	1523.52	383.93	1223000	7.96
.80	14925	1215.36	544.48	1260000	5.79
.90	18306	1064.16	603.38	1277000	5.29
.95	20118	989.28	624.98	1120000	4.48
1.05	24520	825.12	636.79	845000	3.32
1.10	26847	747.36	633.01	851000	3.36
1.15	28647	691.20	639.88	861000	3.36
1.25	33043	568.80	622.13	876000	3.52
1.40	38810	434.88	596.66	970000	4.06
1.55	43995	339.84	571.53	1367000	5.98
1.80	51400	236.16	535.61	1383000	6.46
1.94	55397	191.00	503.19	1390000	6.91
2.20	64169	125.28	424.45	1401000	8.25
2.50	74260	77.76	340.20	1407000	10.34
2.69	81603	53.00	268.46	1405000	13.08
3.00	93710	31.00	195.30	1410000	18.05
3.29	106615	17.00	128.81	1410200	27.37
3.50	122428	8.64	74.09	1412000	47.64

Table A-53 STS-2 ORBITER ELEMENT

Mach	C_{PB}	C_{PB} Max	C_{PB} Min	P_B/P_{oo}	P_B/P_{oo} Max	P_B/P_{oo} Min
.60	-.160	-.175	-.140	.959	.956	.965
.80	-.115	-.135	-.105	.948	.939	.953
.90	-.115	-.135	-.095	.935	.923	.946
.95	-.120	-.145	-.095	.924	.908	.940
1.05	-.142	-.155	-.130	.889	.880	.899
1.10	-.140	-.145	-.130	.881	.877	.889
1.15	-.125	-.135	-.115	.884	.875	.894
1.25	-.09	-.105	-.080	.902	.885	.912
1.40	-.045	-.077	-.027	.938	.894	.963
1.55	-.032	-.045	-.015	.946	.924	.975
1.80	-.008	-.018	.015	.982	.959	1.030
1.94	.004	-.006	.030	1.010	.984	1.080
2.20	.035	.020	.052	1.120	1.070	1.180
2.50	.055	.035	.076	1.240	1.150	1.330
2.69	.067	.040	.090	1.340	1.200	1.460
3.00	.085	.050	.110	1.540	1.320	1.690
3.29	.100	.060	.132	1.760	1.450	2.000
3.50	.125	.080	.165	2.070	1.690	2.410

Table A-54   STS-3 ORBITER ELEMENT

Mach	Alt ft	P_{oo} Psf	q_{oo} psf	Orbiter Thrust lbs	$A_B = 400$ ft^2 C_T orb
.60	9051	1522.08	383.56	1222000	7.96
.80	16144	1166.40	522.55	803000	3.84
.90	20043	1000.80	567.45	821000	3.62
.95	21771	934.56	490.41	825000	3.49
1.05	25781	792.00	611.23	841000	3.44
1.10	27697	730.08	618.38	1010000	4.08
1.15	29376	676.80	626.55	1154000	4.60
1.25	32473	591.84	647.33	1326000	5.12
1.40	37832	463.68	636.17	1348000	5.30
1.55	41969	380.16	639.33	1360000	5.32
1.80	48716	275.04	623.79	1377000	5.52
2.06	55020	191.70	569.45	1385000	6.08
2.20	59118	174.24	590.33	1389000	5.88
2.50	69861	93.72	410.03	1398000	8.52
2.79	80821	55.80	304.05	1402000	11.53
3.10	92684	33.00	221.99	1406000	15.83
3.50	113210	12.96	111.13	1406000	31.63

LOCKHEED–HUNTSVILLE RESEARCH & ENGINEERING CENTER

Table A-55 STS-3 ORBITER ELEMENT

Mach	C_{PB}	C_{PB}Max	C_{PB}Min	P_B/P_{oo}	P_B/P_{oo}Max	P_B/P_{oo}Min
.60	-.155	-.165	-.150	.961	.958	.963
.80	-.112	-.135	-.090	.949	.939	.959
.90	-.102	-.118	-.090	.942	.933	.949
.95	-.105	-.120	-.090	.934	.924	.943
1.05	-.110	-.135	-.090	.915	.896	.931
1.10	-.115	-.142	-.090	.903	.879	.924
1.15	-.115	-.135	-.090	.894	.875	.916
1.25	-.090	-.115	-.065	.902	.874	.929
1.40	-.050	-.080	-.035	.931	.890	.952
1.55	-.039	-.055	-.020	.934	.908	.966
1.80	-.020	-.035	-0-	.955	.921	1.000
2.06	-.005	-.020	.015	.985	.941	1.040
2.20	.008	-.010	.025	1.030	.966	1.080
2.50	.030	.015	.050	1.130	1.070	1.220
2.79	.050	.030	.070	1.270	1.160	1.380
3.10	.056	.042	.080	1.380	1.280	1.540
3.50	.080	.060	.110	1.690	1.510	1.940

Table A-56   STS-4 ORBITER ELEMENT

Mach	Alt ft	P_{oo}	q_{oo}	Orb Thrust	$A_B = 400 \text{ ft}^2$ C_T orb
.60	9672	1501.92	378.48	1228000	8.11
.80	16508	1159.2	519.32	764000	3.68
.90	20785	984.96	558.47	786000	3.52
.95	22668	914.4	577.67	794000	3.44
1.05	26390	786.24	606.78	1227000	5.06
1.10	28210	728.64	617.16	1316000	5.33
1.15	29540	686.88	635.88	1322000	5.20
1.25	32605	603.36	659.93	1334000	5.05
1.40	36755	501.12	687.54	1350000	4.91
1.55	40683	418.16	699.88	1361000	4.86
1.80	47018	305.28	692.38	1376000	4.97
2.01	53585	205.98	582.53	1386000	5.95
2.20	58680	168.48	570.81	1391000	6.09
2.50	68988	102.24	447.30	1399000	7.82
2.75	77649	66.02	349.49	1404000	10.04
3.07	88627	38.00	250.70	1407000	14.03
3.50	104291	20.16	172.87	1408000	20.36

Table A-57 STS-4 ORBITER ELEMENT

Mach	C_{PB}	$C_{PB}Max$	$C_{PB}Min$	P_B/P_{oo}	$P_B/P_{oo}Max$	$P_B/P_{oo}Min$
.60	-.138	-.150	-.125	.965	.962	.969
.80	-.125	-.140	-.110	.930	.922	.938
.90	-.110	-.123	-.095	.938	.930	.946
.95	-.112	-.138	-.080	.929	.913	.949
1.05	-.130	-.160	-.105	.899	.877	.919
1.10	-.130	-.150	-.110	.889	.873	.907
1.15	-.115	-.135	-.100	.894	.875	.907
1.25	-.090	-.115	-.080	.902	.874	.913
1.40	-.070	-.100	-.050	.904	.863	.931
1.55	-.060	-.080	-.038	.899	.865	.936
1.80	-.040	-.062	-.010	.909	.859	.977
2.01	-.032	-.050	.003	.910	.859	1.010
2.20	-.003	-.030	.020	.989	.898	1.070
2.50	.020	-.005	.040	1.080	.978	1.170
2.75	.036	.010	.060	1.190	1.050	1.320
3.07	.038	.020	.070	1.250	1.130	1.460
3.50	.055	.035	.090	1.470	1.300	1.770

Table A–58 STS–5 ORBITER ELEMENT

Mach	Alt ft	P_{oo} Psf	q_{oo} psf	Orb Thrust	$A_B = 400$ ft^2 C_T orb
.60	9169	1523.01	383.80	1225000	7.98
.80	14911	1239.51	555.30	1040000	4.68
.90	18999	1063.79	603.17	1061000	4.40
.95	20500	986.92	623.49	1068000	4.28
1.05	24388	852.91	658.23	1087000	4.13
1.10	26079	798.63	676.44	1092000	4.04
1.15	27753	739.81	684.88	1145000	4.18
1.25	31181	648.47	709.26	1325000	4.67
1.40	35703	523.02	717.58	1346000	4.69
1.55	39883	433.86	729.64	1357000	4.65
1.80	47021	301.28	683.30	1375000	5.03
2.20	56554	188.79	639.62	1391000	5.44
2.50	64726	118.36	517.83	1398000	6.75
3.50	108012	18.06	154.86	1409000	22.75

LOCKHEED–HUNTSVILLE RESEARCH & ENGINEERING CENTER

Table A-59 STS-5 ORBITER ELEMENT

Mach	C_{PB}	C_{PB} Max	C_{PB} Min	P_B/P_{oo}	P_B/P_{oo} Max	P_B/P_{oo} Min
.60	-.160	-.170	-.140	.959	.957	.965
.80	-.125	-.145	-.105	.944	.935	.953
.90	-.120	-.135	-.095	.932	.923	.946
.95	-.125	-.135	-.115	.921	.915	.928
1.05	-.117	-.130	-.100	.909	.899	.922
1.10	-.155	-.170	-.135	.869	.856	.886
1.15	-.145	-.156	-.122	.866	.856	.887
1.25	-.120	-.135	-.110	.869	.852	.879
1.40	-.087	-.105	-.070	.881	.856	.904
1.55	-.090	-.105	-.070	.849	.823	.882
1.80	-.040	-.075	-.025	.909	.829	.943
2.20	-.009	-.030	.010	.969	.898	1.030
2.50	.018	-.003	.040	1.080	.987	1.180
3.50	.060	.040	.085	1.510	1.340	1.730

SPACE SHUTTLE - EXTERNAL TANK

SPACE SHUTTLE - EXTERNAL TANK (ET)

The Space Shuttle vehicle consists of an Orbiter with Space Shuttle Main Engine (SSME), an External Tank (ET), and two solid rocket boosters (SRB). The Orbiter with SSMEs and the SRBs are reusable elements while the ET is expended after each launch. The three SSMEs produce a total sea level thrust of 1.125 million lb. They are fueled with LOX and liquid hydrogen stored in the external tank. The engines are bearing mounted and capable of gimbaling for Orbite steering control. The External Tank reacts the SRB thrust through its intertank structure and provides attach structure to the Orbiter to react the SSME thrust. At liftoff the ET contains approximately 1.5 million lb of fuel. At main engine cutoff, the ET is separated from the Orbiter before orbital velocity is achieved. The ET then proceeds on a ballistic reentry path and breaks up prior to impact in the ocean. Each SRB produces approximately 2.65 million lb of thrust at sea level, and after about 55 sec they reduce thrust about one-third to prevent overstressing the vehicle during the period of maximum dynamic pressure. Two lateral sway braces and a diagonal attachment at the aft frame provide the structural attachment between the SRB and ET. The SRB forward attachment to the ET is by a single thrust attachment at the forward end of the forward skirt. The same forward skirt is used for attaching the main parachute riser attachments. The SRBs are released from the ET by pyrotechnic separation devices at the forward thrust attachment and aft sway braces. Eight separation motors on each SRB, four aft and four forward, separate the SRB from the Orbiter and ET.

The Space Shuttle ET configuration is presented in Figs. A-109 through A-111. The ascent trajectory data are presented in Figs. A-112 and A-113. The ascent trajectory data, SSME and SRB thrust characteristics and base pressure characteristics are presented in Tables A-60 through A-69.

SPACE SHUTTLE REFERENCES

1. "Space Shuttle System Summary," Report SSV80-1, Rockwell International Space Systems Group, May 1980.

2. "STS-5 Postflight Report on Ascent External Aerodynamic Loads," Report SAS/AERO/83-094, Rockwell International, 1 March 1983.
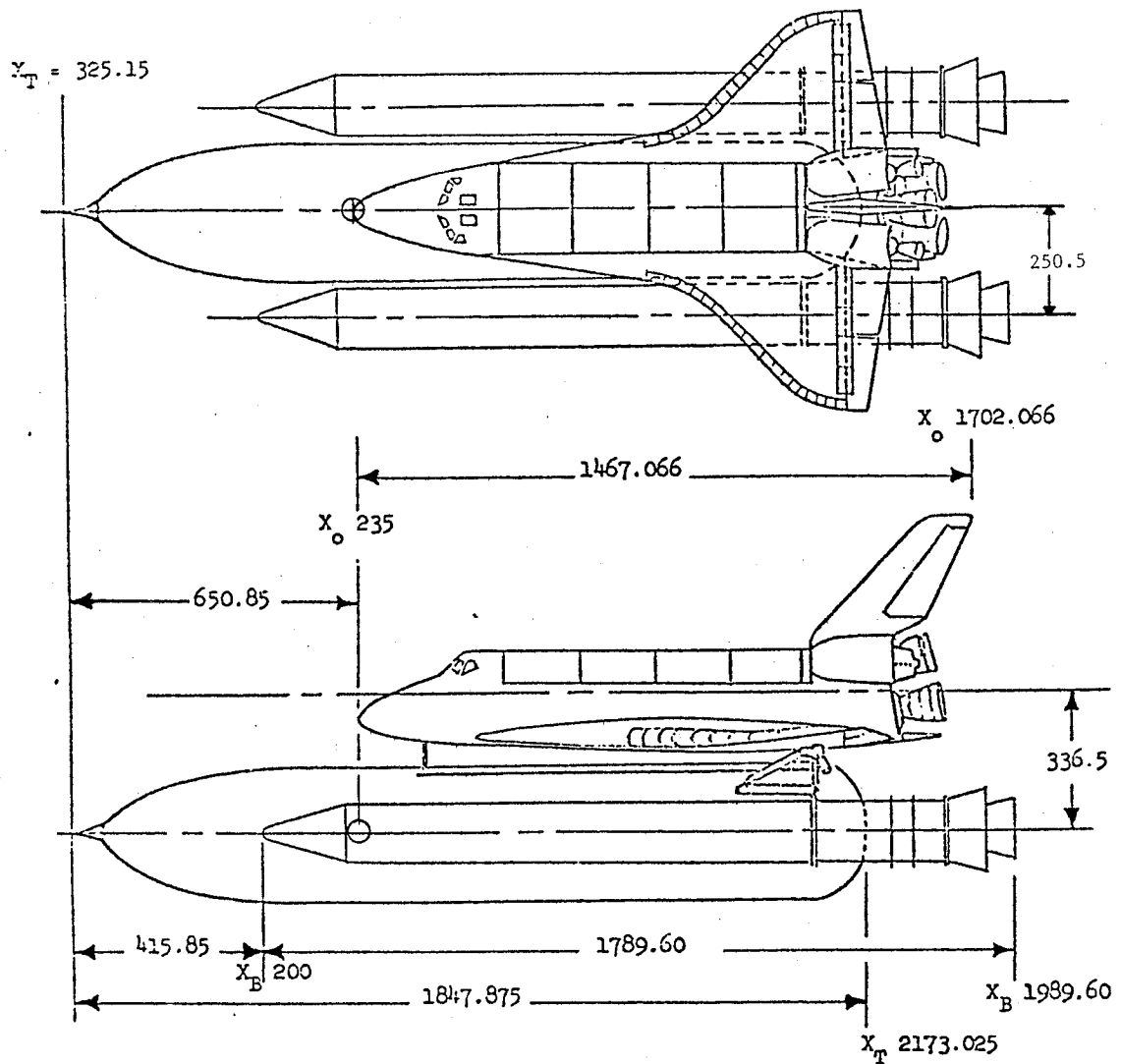
Fig. A-109 - Space Shuttle Launch Vehicle Configuration

EO-1

Fwd ET/ORB
Attach

Aft Right ET/ORB Attach (EO-3)

ET/ORB Right Umbilical (EO-5)

ET/ORB Left
Umbilical
EO-4

Aft Left
ET/ORB Attach
(EO-2)

ET Interface Locations
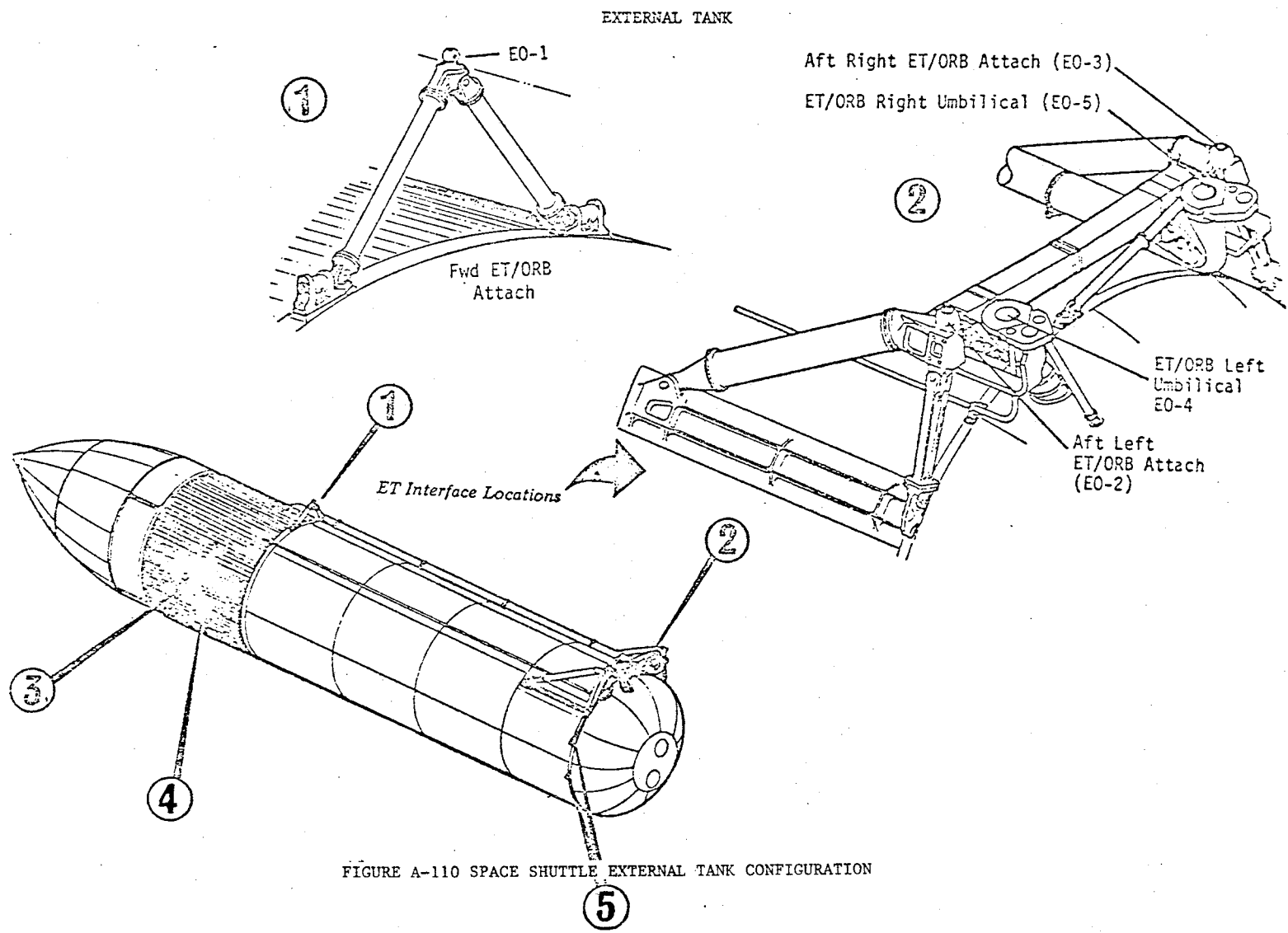
FIGURE A-110 SPACE SHUTTLE EXTERNAL TANK CONFIGURATION
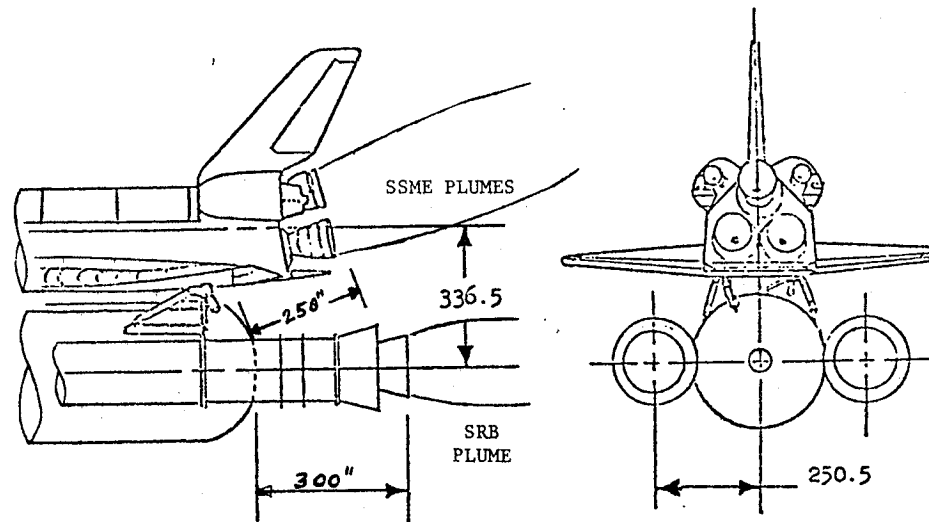
TOTAL BASE AREA = 1500 FT.^{2} = $A_{Borb} + A_{Bet} + A_{B2srb's}$

D_{BASE} $\doteq$ $\sqrt{A_{BASE}/\pi/4}$ = 43.7 FT. = 524.5 in.
EQUIVALENT

X_j/D_B = 300/524.5 = .572

SSME'S
D_{EXIT} = 90"
$D_{EQ.}$ = $\sqrt{3 \times 90^2}$
= 156 in.
X_j/D_B = .297

Fig. A-111 Base Configuration: External Tank

LOCKHEED–HUNTSVILLE RESEARCH & ENGINEERING CENTER
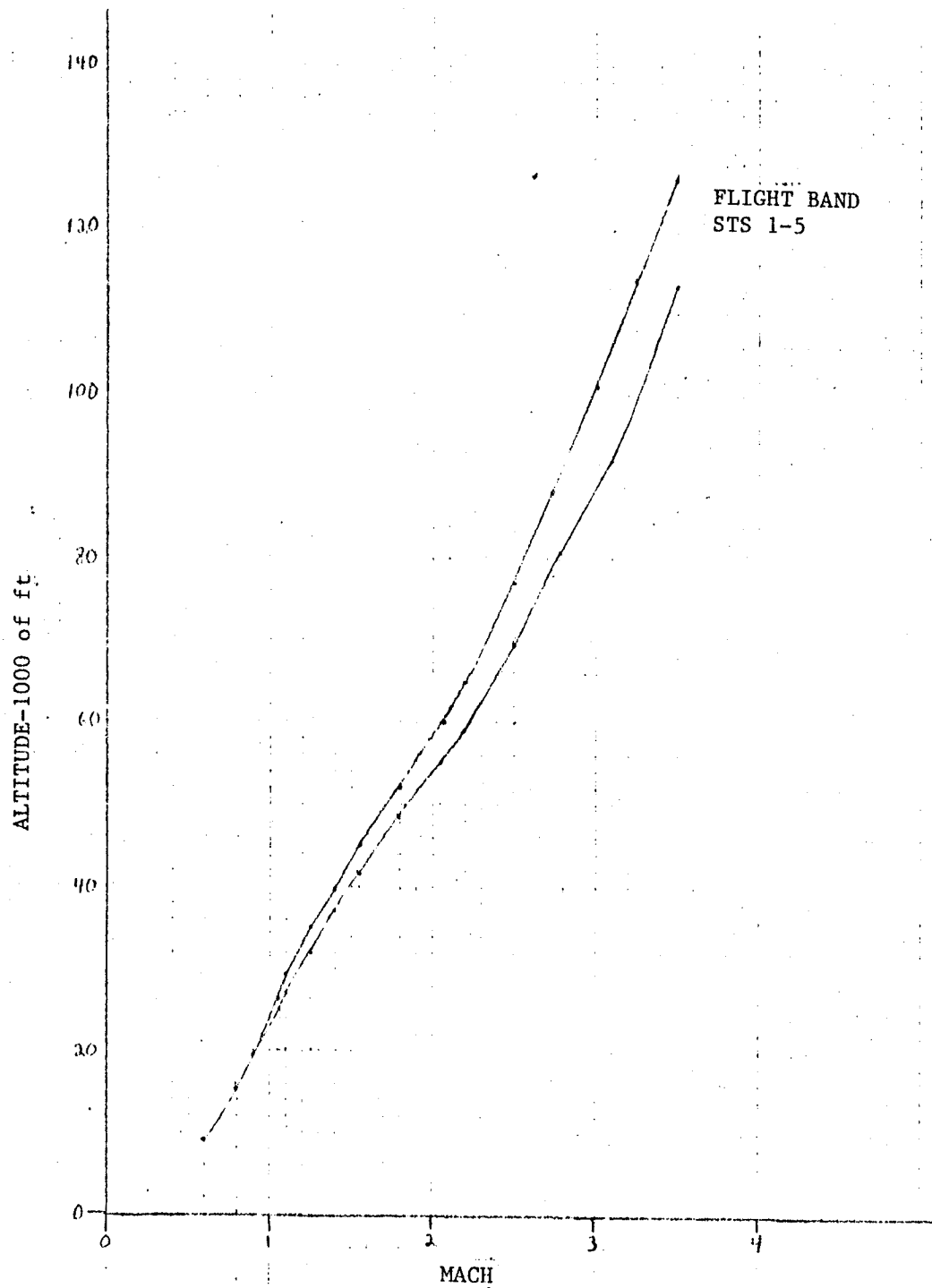
Fig. A-112 - Flight Altitude versus Mach Number: External Tank
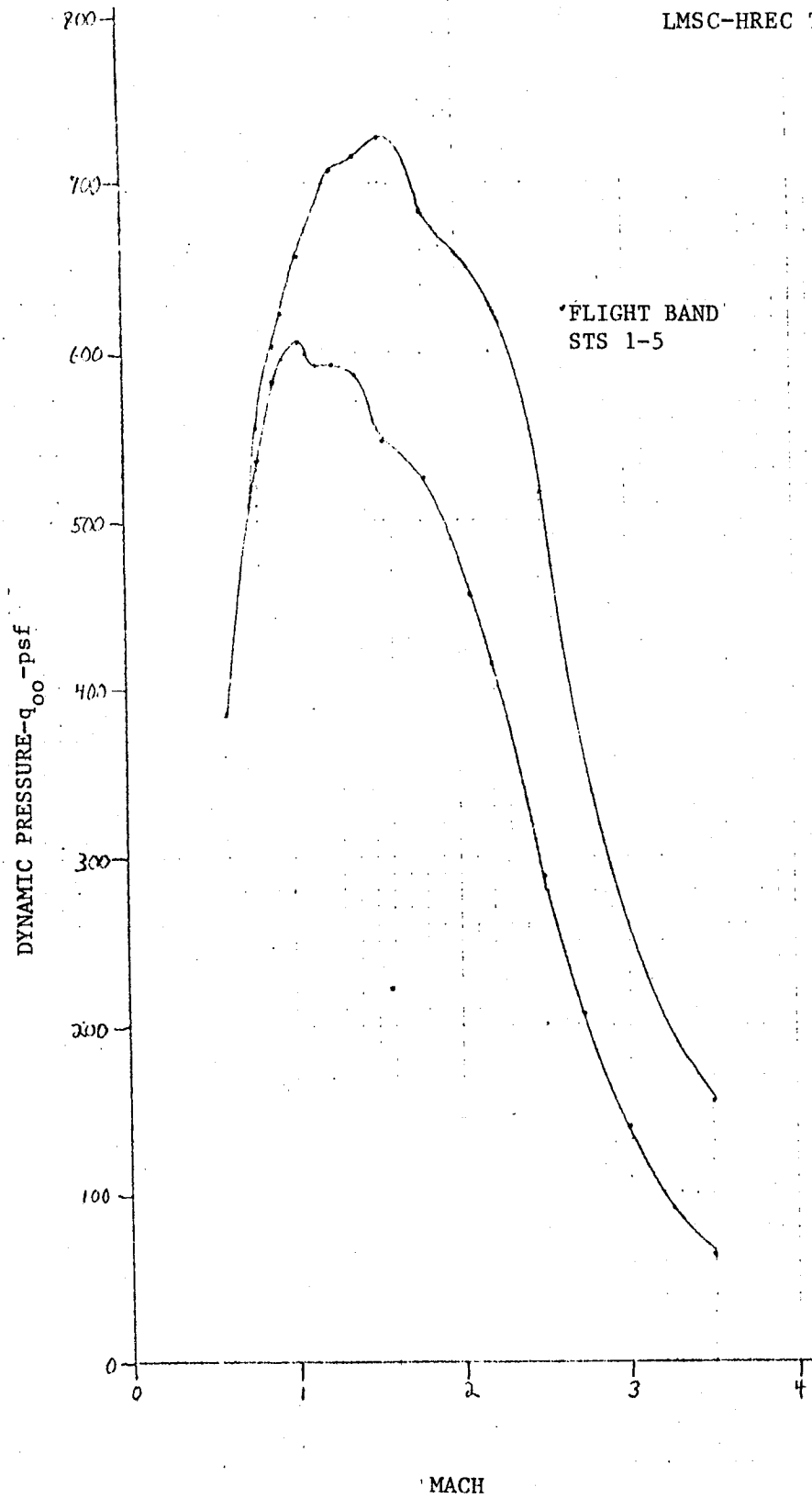
A-113 — Flight Dynamic Pressure versus Mach Number: External Tank

Table A-60   STS-1 EXTERNAL TANK

$A_B = 604$ ft^2

Mach	Alt ft	P_{oo} psf	q_{oo} psf	Thrust lb SSME+SRB	C_T
.60	9387	1527.84	385.02	5084000	21.86
.80	15879	1198.10	536.75	4694000	14.48
.90	19861	1026.72	582.15	4550000	12.94
.95	21904	946.10	597.69	4538000	12.57
1.05	26410	786.24	606.78	4458000	12.16
1.10	28889	708.48	600.08	4460000	12.31
1.15	31247	639.36	591.89	4564000	12.77
1.25	35115	541.44	592.20	4666000	13.04
1.40	39953	429.12	588.75	4770000	13.41
1.55	45512	326.88	549.73	5006000	15.08
1.80	52390	231.84	525.81	5048000	15.89
2.08	60000	151.03	457.39	5088000	18.42
2.20	64909	122.40	414.69	5004000	20.00
2.50	77556	66.24	289.80	4722000	26.98
2.72	88080	40.33	208.86	4414000	35.00
3.00	101000	22.25	140.18	4080000	48.19
3.25	114800	12.44	91.98	3702000	66.64
3.50	126037	7.45	63.88	3382000	87.65

LOCKHEED-HUNTSVILLE RESEARCH & ENGINEERING CENTER

Table A-61 STS-1 EXTERNAL TANK

Mach	C_{PB}	C_{PB} max	C_{PB} min	P_B/P_{oo}	P_B/P_{oo} max	P_B/P_{oo} min
.60	−.301	−.370	−.230	.924	.907	.942
.80	−.234	−.300	−.160	.895	.866	.928
.90	−.216	−.280	−.140	.878	.841	.920
.95	−.199	−.260	−.130	.874	.835	.918
1.05	−.207	−.270	−.130	.840	.792	.899
1.10	−.193	−.260	−.130	.837	.780	.890
1.15	−.173	−.240	−.100	.840	.778	.907
1.25	−.115	−.180	−.045	.874	.803	.951
1.40	−.062	−.130	−.010	.915	.822	1.014
1.55	−.060	−.130	−.010	.899	.781	1.017
1.80	+.041	−.030	−.110	1.093	.932	1.249
2.08	+.087	.010	.150	1.263	1.030	1.454
2.20	+.116	.040	.180	1.393	1.136	1.610
2.50	+.170	.100	.240	1.744	1.438	2.050
2.72	+.207	.130	.270	2.072	1.673	2.398
3.00	+.331	.261	.400	3.085	2.644	3.520
3.25	+.396	.320	.460	3.928	3.366	4.401
3.50	+.518	.440	.580	5.442	4.773	5.974

LOCKHEED-HUNTSVILLE RESEARCH & ENGINEERING CENTER

Table A-62 STS-2 EXTERNAL TANK

A_B=604 ft^2

Mach	Alt ft	P_{oo} psf	q_{oo} psf	Thrust lb SSME+SRB	C_T
.60	8975	1523.52	383.93	5194000	22.40
.80	14925	1215.36	544.48	4804000	14.61
.90	18306	1064.16	603.38	4684000	12.85
.95	20118	989.28	624.98	4642000	12.29
1.05	24520	825.12	636.79	4562000	11.86
1.10	26847	747.36	633.01	4508000	11.79
1.15	28647	691.20	639.88	4540000	11.75
1.25	33043	568.80	622.13	4680000	12.45
1.40	38810	434.88	596.66	4850000	13.46
1.55	43995	339.84	571.53	4968000	14.39
1.80	51400	236.16	535.61	5046000	15.60
1.94	55397	191.00	503.19	5084000	16.73
2.20	64169	125.28	424.45	5086000	19.84
2.50	74260	77.76	340.20	4744000	23.09
2.69	81603	53.00	268.46	4468000	27.55
3.00	93710	31.00	195.30	4252000	36.05
3.29	106615	17.00	128.81	3884000	49.92
3.50	122428	8.64	74.09	3428000	76.60

Table A-63 STS-2 EXTERNAL TANK

Mach	C_{PB}	C_{PB} max	C_{PB} min	P_B/P_{oo}	P_B/P_{oo} max	P_B/P_{oo} min
.60	−.212	−.280	−.138	.947	.929	.965
.80	−.187	−.225	−.152	.916	.899	.932
.90	−.167	−.195	−.145	.905	.889	.918
.95	−.178	−.201	−.145	.888	.873	.908
1.05	−.185	−.210	−.131	.857	.838	.899
1.10	−.180	−.245	−.122	.848	.792	.897
1.15	−.174	−.255	−.111	.839	.764	.897
1.25	−.138	−.195	−.070	.849	.787	.923
1.40	−.058	−.126	−.012	.920	.827	.984
1.55	−.017	−.062	−.037	.971	.896	1.062
1.80	.031	−.018	.072	1.070	.959	1.163
1.94	.059	.025	.090	1.155	1.066	1.237
2.20	.101	.050	.141	1.342	1.169	1.478
2.50	.134	.084	.184	1.586	1.368	1.805
2.69	.173	.153	.223	1.876	1.775	2.130
3.00	.234	.184	.284	2.474	].159	2.789
3.29	.334	.283	.384	3.531	3.144	3.910
3.50	.525	.475	.575	5.502	5.073	5.931

LOCKHEED-HUNTSVILLE RESEARCH & ENGINEERING CENTER

Table A-64 STS-3 EXTERNAL TANK

$A_B = 604 \ ft^2$

Mach	Alt ft	P_{oo} psf	q_{oo} psf	Thrust lb SSME+SRB	C_T
.60	9051	1522.08	383.56	5236000	22.60
.80	16155	1166.40	522.55	4826000	15.29
.90	20043	1000.80	567.45	4696000	13.70
.95	21771	934.56	490.41	4692000	15.84
1.05	25781	792.00	611.23	4588000	12.43
1.10	27697	730.08	618.38	4576000	12.25
1.15	29376	676.80	626.55	4612000	12.19
1.25	32473	591.84	647.33	4724000	12.08
1.40	37832	463.68	636.17	4898000	12.75
1.55	41969	380.16	639.33	5004000	12.96
1.80	48617	275.04	623.79	5126000	13.61
2.06	55020	191.70	569.45	5176000	15.05
2.20	59118	174.24	590.33	5176000	14.52
2.50	69861	93.72	410.03	4812000	19.43
2.79	80821	55.80	304.05	4518000	24.60
3.10	92684	33.00	221.99	4216000	31.44
3.50	113210	12.96	111.13	3562000	53.07

Table A-65 STS-3 EXTERNAL TANK

Mach	C_{PB}	C_{PB} max	C_{PB} min	P_B/P_{oo}	P_B/P_{oo} max	P_B/P_{oo} min
.60	-.182	-.281	-.098	.954	.929	.975
.80	-.159	-.248	-.105	.929	.889	.953
.90	-.154	-.240	-.105	.913	.864	.940
.95	-.149	-.250	-.072	.906	.842	.954
1.05	-.155	-.209	-.103	.880	.839	.921
1.10	-.163	-.238	-.099	.862	.798	.916
1.15	-.132	-.201	-.082	.878	.814	.924
1.25	-.107	-.152	-.061	.883	.834	.933
1.40	-.054	-.099	-.016	.926	.864	.978
1.55	-.031	-.072	-.010	.948	.879	1.017
1.80	.006	-.025	.032	1.014	.943	1.073
2.06	.041	-.005	.055	1.122	.985	1.163
2.20	.057	-.018	.063	1.193	1.061	1.213
2.50	.101	.041	.121	1.442	1.179	1.529
2.79	.136	.076	.166	1.741	1.414	1.905
3.10	.179	.119	.230	2.204	1.801	2.547
3.50	.320	.260	.350	3.744	3.229	4.001

LOCKHEED-HUNTSVILLE RESEARCH & ENGINEERING CENTER

Table A-66   STS-4 EXTERNAL TANK

$A_B = 604$ ft^2

Mach	Alt ft	P_{OO} psf	q_{OO} psf	Thrust lb SSME+SRB	C_T
.60	9672	1501.92	378.48	5200000	22.75
.80	16508	1159.20	519.32	4700000	14.98
.90	20785	984.96	558.47	4682000	13.88
.95	22668	914.40	577.67	4702000	13.48
1.05	26390	786.24	606.78	4856000	13.25
1.10	28210	728.64	617.16	4890000	13.11
1.15	29540	686.88	635.88	4896000	12.75
1.25	32605	603.36	659.93	4910000	12.32
1.40	36755	501.12	687.54	5150000	12.40
1.55	40683	418.16	699.88	5260000	12.44
1.80	47018	305.28	692.38	5350000	12.79
2.01	53585	205.98	582.53	5380000	15.29
2.20	58680	168.48	570.81	5400000	15.66
2.50	68988	102.24	447.30	5180000	19.17
2.75	77649	66.02	349.49	4910000	23.26
3.07	88627	38.00	250.70	4823000	31.85
3.50	104291	20.16	172.87	4740000	45.39

Table A-67   STS-4 EXTERNAL TANK

Mach	C_{PB}	C_{PB} max	C_{PB} min	P_B/P_{oo}	P_B/P_{oo} max	P_B/P_{oo} min
.60	-.139	-.200	-.102	.965	.950	.974
.80	-.123	-.200	-.091	.945	.910	.959
.90	-.110	-.225	-.082	.938	.872	.954
.95	-.118	-.200	-.099	.925	.874	.937
1.05	-.125	-.200	-.082	.904	.846	.937
1.10	-.143	-.220	-.091	.879	.814	.923
1.15	-.109	-.200	-.080	.899	.815	.926
1.25	-.079	-.162	-.040	.914	.823	.956
1.40	-.045	-.110	.005	.938	.849	1.007
1.55	-.024	-.082	.025	.960	.862	1.042
1.80	.012	-.037	.055	1.027	.916	1.125
2.01	.047	.001	.080	1.133	1.003	1.226
2.20	.075	.022	.101	1.254	1.075	1.342
2.50	.126	.076	.151	1.551	1.333	1.661
2.75	.171	.126	.231	1.905	1.667	2.223
3.07	.241	.191	.266	2.590	2.011	2.408
3.50	.316	.266	.341	3.710	3.281	3.924

LOCKHEED-HUNTSVILLE RESEARCH & ENGINEERING CENTER

Table A-68 STS-5 EXTERNAL TANK

$A_B = 604$ ft^2

Mach	Alt ft	P_{oo} psf	q_{oo} psf	Thrust lb SSME+SRB	C_T
.60	9169	1523.01	383.80	5212000	22.48
.80	14911	1239.51	555.30	4872000	14.53
.90	18999	1063.79	603.17	4716000	12.94
.95	20500	986.92	623.49	4688000	12.45
1.05	24388	852.91	658.23	4568000	11.49
1.10	26079	798.63	676.44	4530000	11.09
1.15	27753	739.81	684.88	4568000	11.04
1.25	31181	648.47	709.26	4672000	10.91
1.40	35703	523.02	717.58	4850000	11.19
1.55	39883	433.86	729.64	4948000	11.23
1.80	47021	301.28	683.30	5082000	12.31
2.20	56554	188.79	639.62	5154000	13.34
2.50	65726	118.36	517.83	4950000	15.83
3.50	108012	18.06	154.86	3642000	38.94

LOCKHEED-HUNTSVILLE RESEARCH & ENGINEERING CENTER

Table A-69 STS-5 EXTERNAL TANK

Mach	C_{PB}	C_{PB} max	C_{PB} min	P_B/P_{oo}	P_B/P_{oo} max	P_B/P_{oo} min
.60	-.194	-.260	-.120	.951	.934	.970
.80	-.167	-.230	-.090	.925	.897	.960
.90	-.152	-.220	-.080	.914	.875	.955
.95	-.159	-.220	-.080	.900	.861	.949
1.05	-.166	-.230	-.090	.872	.822	.931
1.10	-.186	-.250	-.100	.842	.788	.915
1.15	-.162	-.230	-.090	.850	.787	.917
1.25	-.137	-.200	-.060	.850	.781	.934
1.40	-.093	-.160	-.020	.872	.780	.973
1.55	-.061	-.130	.010	.897	.781	1.017
1.80	+.015	-.050	.80	1.034	.887	1.181
2.20	+.026	-.050	.090	1.088	.831	1.305
2.50	+.059	-.020	.120	1.258	.913	1.525
3.50	+.191	.120	.260	2.638	2.029	3.230

LOCKHEED-HUNTSVILLE RESEARCH & ENGINEERING CENTER

TITAN 3C

TITAN III-C

The Titan missile series was developed to be an economical means to launch payloads into an earth orbit using solid rocket boosters (SRB) to boost a main core rocket. The two (zero stage) 120 in. SRBs produce about 2.6 million lb of thrust at sea level. The two first stage Aerojet General engines produced about 237,000 lb of thrust each from the boattail base of the main core vehicle and burned approximately 140 sec. The core engines do not operate until burnout of the SRBs. The second stage is powered by one Aerojet engine producing 100,000 lb thrust for approximately 207 sec after which the transfer stage takes over to boost the payload into orbit. The Titan 3-C configuration was the main forerunner of the Space Shuttle configuration in use today.

The TITAN-3C configuration and engine characteristics are presented in Figs. A-114 through A-116. Ascent trajectory data are presented in Figs. A-117 and A-118. the 120 in solid motor thrust and nozzle plume angles are presented in Figs. A-119 and A-120. The TITAN 3-C trajectory, thrust and base pressure characteristics are presented in Tables A-70 and A-71.

TITAN III-C REFERENCES

The Titan IIIC flight data was obtained in unpublished form from the Martin Marietta Corporation.

LOCKHEED-HUNTSVILLE RESEARCH & ENGINEERING CENTER
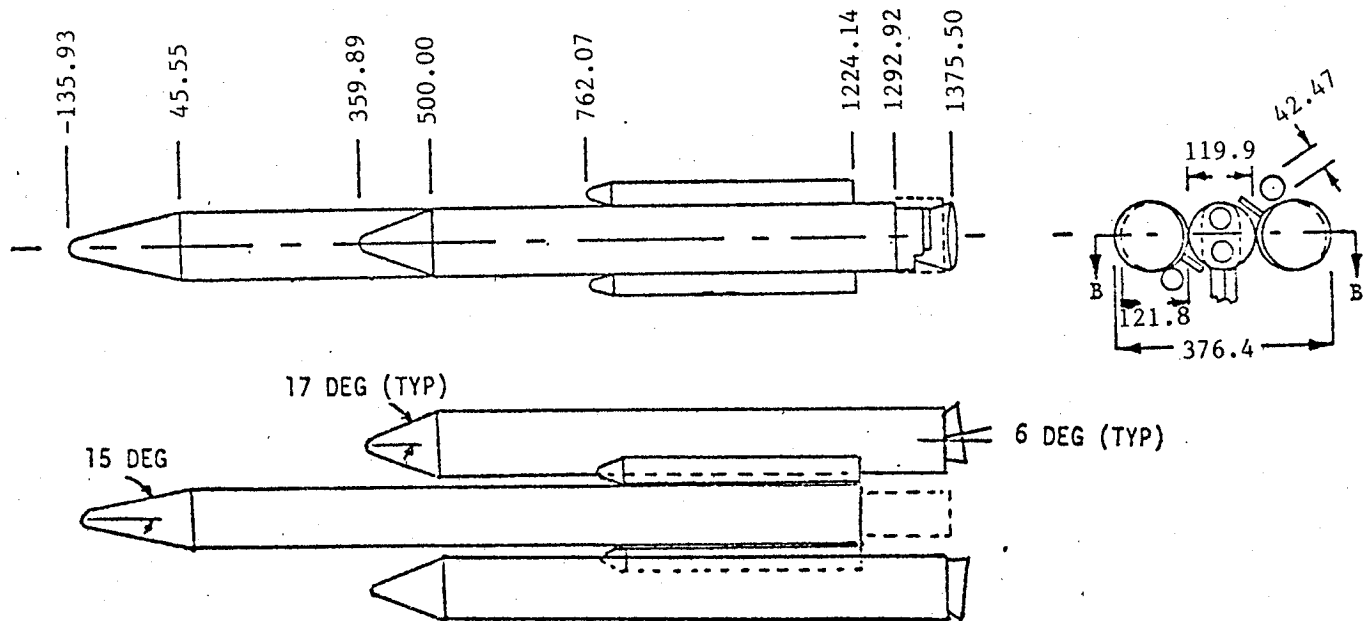
ENGINE DATA

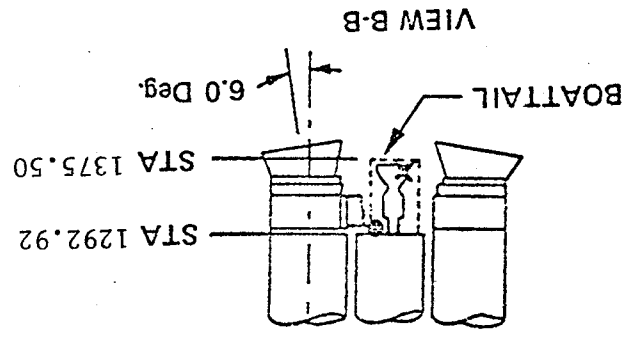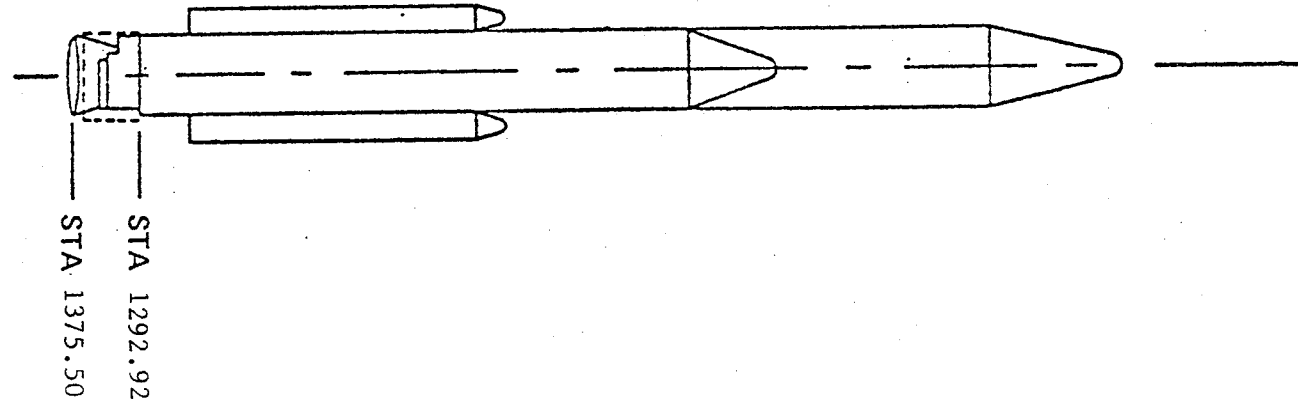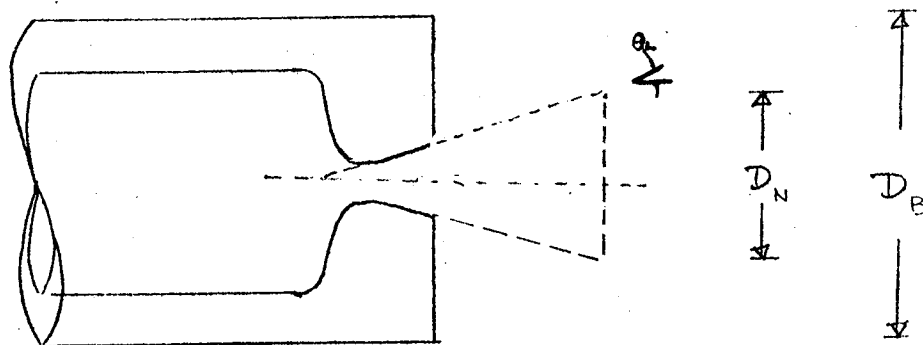|	
Nozzle Throat Diameter	37.57 in
Nozzle Exit Diameter	106.17
Nozzle Throat Area	61.07 in^2
Nozzle Area Ratio	8.0
Nozzle Exit Angle	15.0 deg
Exit Mach Number	3.12
Specific Heat Ratio	1.202
Gas Molecular Weight	28.59
Nozzle Contour	Conical

Fig. A-114 - Titan IIIC Geometry

LOCKHEED-HUNTSVILLE RESEARCH & ENGINEERING CENTER
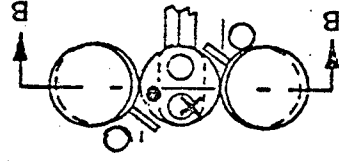
FIGURE A-115 BASE PRESSURE AND NOZZLE EXIT PRESSURE LOCATIONS: TITAN IIIC

X 2255

● 2244

VIEW B-B

6.0 Deg.

STA 1375.50

STA 1292.92

BOATTAIL

STA 1375.50

STA 1292.92

$$D_B = 10.0 \text{ FT} \qquad A_B = 78.5 \text{ FT}^2$$

$$D_N = 5.16 \text{ FT} \qquad \frac{A_N}{A_B} = .266$$

$$X_j = \qquad\qquad \frac{X_j}{D_B} =$$

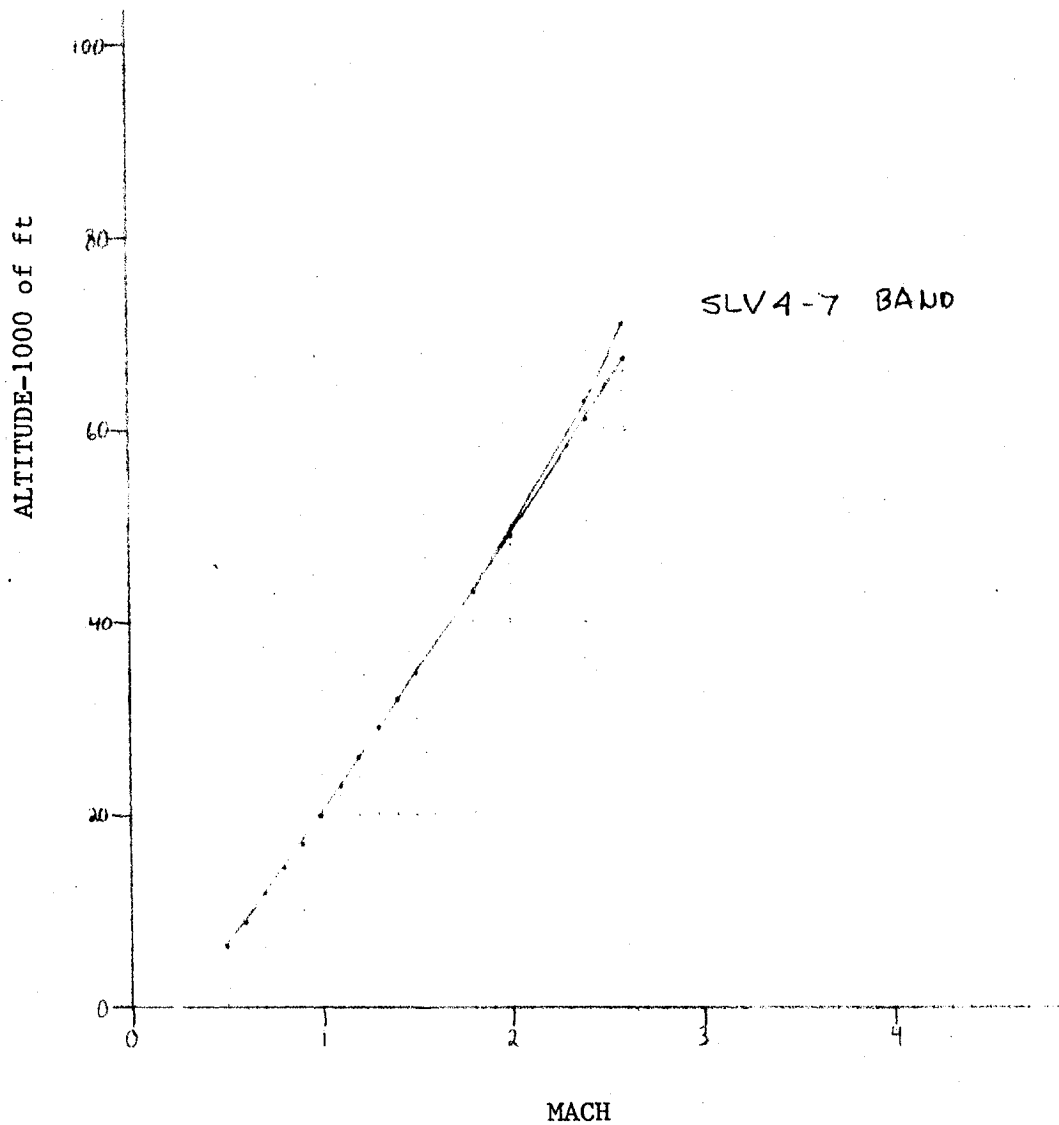$$\Theta_L =$$

Fig. A-116 – Nozzle Configuration: Titan IIIC

Fig. A-117 - Flight Altitude versus Mach Number: Titan IIIC

SLV1-7 BAUP

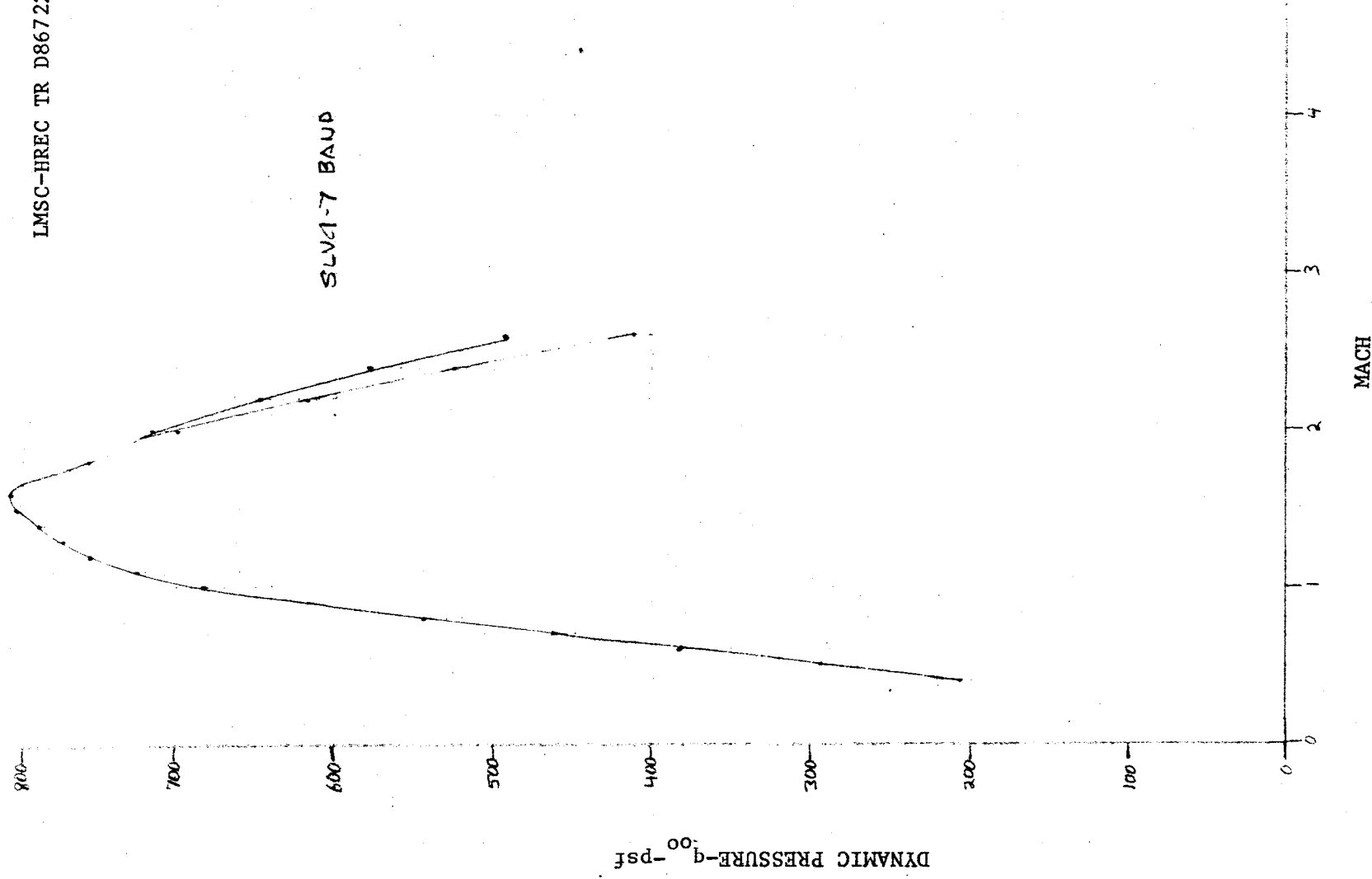Fig. A-118 - Flight Dynamic Pressure versus Mach Number: Titan IIIC

A-220

LOCKHEED-HUNTSVILLE RESEARCH & ENGINEERING CENTER
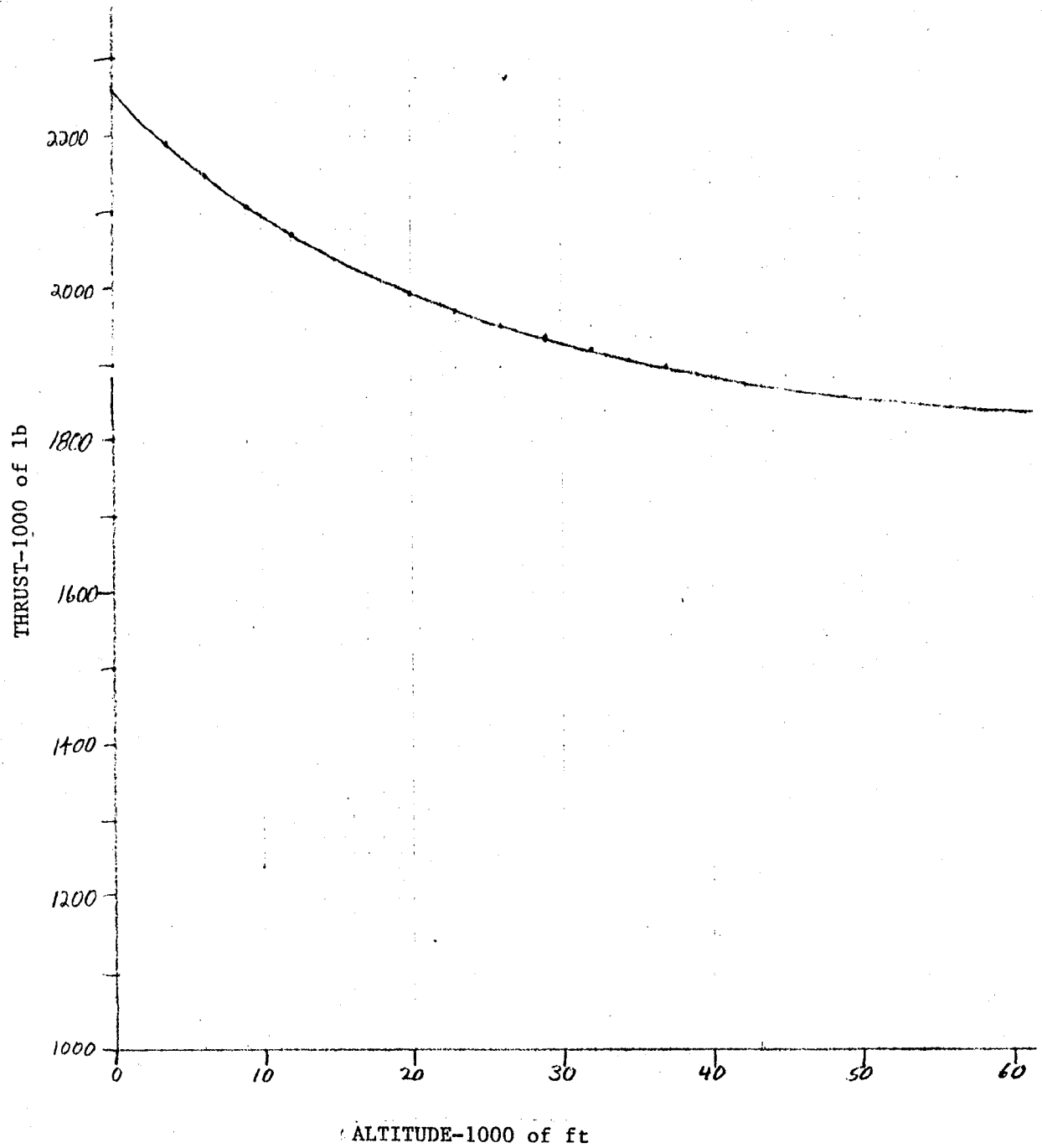
Fig. A-119 - Thrust versus Altitude: Titan IIIC
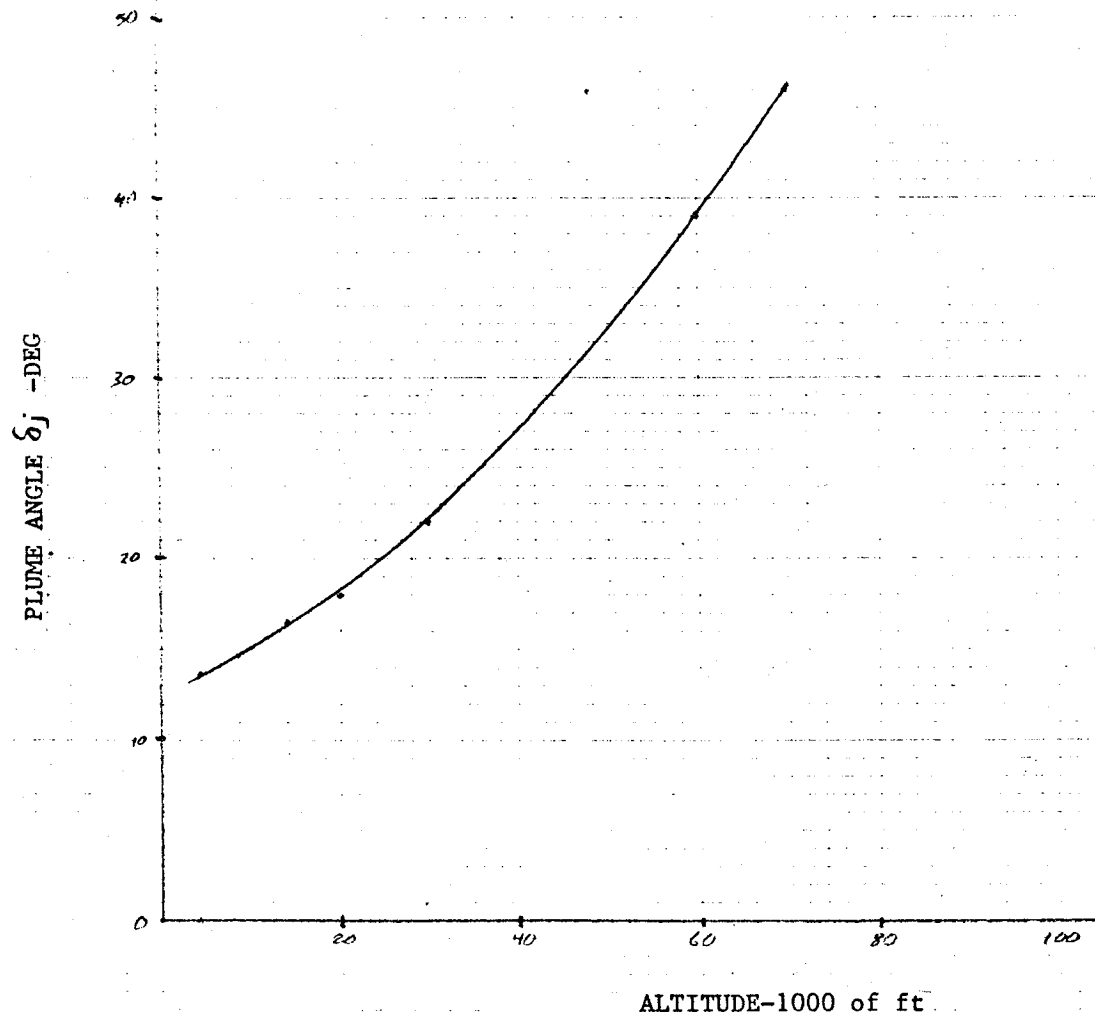
Fig. A-120 - Plume Angle versus Altitude: Titan IIIC

Table A-71   TITAN IIIC SLV4

Mach	Alt. Ft.	P_∞ psf	q_∞ psf	Thrust lb.	$A_B = 78.5$ ft^2 C_T	C_{PB}	P_B/P_∞
.4	3800	1840.00	206.08	2190000	135.37	−.714	.920
.5	6200	1670.00	292.25	2150000	93.72	−.474	.917
.6	9000	1512.91	381.25	2110000	70.50	−.373	.906
.7	12000	1346.23	461.76	2075000	57.24	−.315	.892
.8	14500	1215.00	544.32	2050000	47.98	−.268	.880
.9	17300	1080.00	612.36	2020000	42.02	−.220	.875
1.0	20000	973.26	681.28	1998000	37.36	−.186	.870
1.1	23000	857.24	726.08	1975000	34.65	−.163	.862
1.2	26000	752.70	758.72	1959000	32.89	−.139	.860
1.3	29000	658.76	779.31	1940000	31.71	−.123	.855
1.4	32000	574.58	788.32	1926000	31.12	−.109	.850
1.5	34500	510.00	803.25	1910000	30.29	−.097	.847
1.6	37100	450.00	806.40	1900000	30.01	−.084	.850
1.8	43200	335.00	759.78	1895000	31.77	−.051	.885
2.0	49200	250.00	700.00	1858000	33.81	−.018	.950
2.2	56000	182.84	619.46	1841000	37.86	.015	1.050
2.4	63000	130.85	527.59	1839000	44.46	.037	1.150
2.6	71100	87.00	411.68	1837000	56.84	.057	1.270

Table A-71   TITAN IIIC SLV7

Mach	Alt. Ft.	P_∞ psf	q_∞ psf	Thrust lb.	$A_B = 78.5$ ft^2 C_T	C_{PB}	P_B/P_∞
.4	3800	1840.00	206.08	2190000	135.37	-.446	.950
.5	6200	1670.00	292.25	2150000	93.72	-.280	.951
.6	9000	1512.91	381.25	2110000	70.50	-.179	.955
.7	12000	1346.23	461.76	2075000	57.24	-.146	.950
.8	14500	1215.00	544.32	2050000	47.98	-.134	.940
.9	17300	1080.00	612.36	2020000	42.02	-.115	.935
1.0	20000	973.26	681.28	1998000	37.36	-.100	.930
1.1	23000	857.24	726.08	1975000	34.65	-.089	.925
1.2	26000	752.70	758.72	1959000	32.89	-.061	.939
1.3	29000	658.76	779.31	1940000	31.71	-.042	.950
1.4	32000	574.58	788.32	1926000	31.12	-.022	.970
1.5	34500	510.00	803.25	1910000	30.29	-0-	1.000
1.6	37100	450.00	806.40	1900000	30.01	.011	1.020
1.8	43200	335.00	759.78	1895000	31.77	.053	1.120
2.0	49000	255.54	715.51	1860000	33.12	.079	1.220
2.2	55000	191.79	649.78	1843000	36.13	.103	1.350
2.4	61000	143.97	580.49	1839000	40.36	.112	1.450
2.6	67800	104.00	492.13	1838000	47.58	.125	1.590

LOCKHEED–HUNTSVILLE RESEARCH & ENGINEERING CENTER